Mechanistic Studies on Memory of Chirality Alkylations of 1,4-Benzodiazepin-2-ones
&
Structural-based Design of Insecticidal AChE Inhibitors for Malaria Mosquito, Anopheles gambiae

Danny Chung Hsu

Dissertation submitted to the Faculty of the
Virginia Polytechnic Institute and State University
in partial fulfillment of the requirements for the degree of

Doctor of Philosophy

in

Chemistry

Dr. Paul R. Carlier, Chairman

Dr. Felicia Etzkorn

Dr. Paul A. Deck

Dr. David G.I. Kingston

Dr. James M. Tanko

Dr. Larry T. Taylor

September 18th, 2007
Blacksburg, Virginia

Keywords: Memory of Chirality, Asymmetric Synthesis, 1,4-Benzodiazepin-2-one, Density Functional Theory, Enolate Chemistry, Freeze Frame Observation, Kinetics, Acetylcholinesterase, Free Cysteine Targeting, Sulfhydryl Reagents, Anopheles gambiae

Mechanistic Studies on Memory of Chirality Alkylations of 1,4-Benzodiazepin-2-ones & Structural-based Design of Insecticidal AChE Inhibitors for Malaria Mosquito, *Anopheles gambiae*

Danny Chung Hsu

ABSTRACT

Memory of chirality (MOC) is an emerging strategy for asymmetric synthesis which relies upon the intermediacy of *transiently* non-racemic reactive species. In these reactions the configuration of the sole stereogenic center of the enantiopure starting material is "memorized" by a chiral non-racemic conformation in the intermediate; trapping then captures the stereochemical information, and generates a new stereogenic center with high fidelity. We experimentally and computationally studied the highly retentive deprotonation/alkylations of 1,4-benzodiazepin-2-ones (BZDs) that rely upon this strategy. We captured a transiently non-racemic BZD enolate intermediate in enantiopure form, then released the enolate and observed its subsequent reaction. This approach allowed the first ever step-wise observation of the stereochemical course of such a MOC process.

Approximately 2 million deaths are caused by malaria every year in the world. In total roughly 3.2 billion people are living under the risk of malaria transmission. Current use of anticholinesterase insecticides has been limited by their toxicity to human beings. A major African malaria insect vector, Anopheles gambiae (*Ag*), was targeted. Based on sequence alignment and homology models of *Ag*AChE, a strategy of dual-site binding was adopted that targets Trp84 in the active site and Cys286 at the peripheral site. Selective AChE inhibitors have been designed and synthesized.

Acknowledgements

I would like to express my heartfelt gratitude to my advisor Dr. Paul R. Carlier for his guidance, encouragement, and continuous support. He has inspired and advised me to grow intellectually and technically in multidisciplinary research areas. I am very honored and deeply indebted to be his student. I am grateful to my advisory committee, Dr. Felicia Etzkorn, Dr. Paul A. Deck, Dr. David G. I. Kingston, Dr. James M. Tanko, and Dr. Larry T. Taylor for their advice, patience, and kindness.

I am obliged to Dr. Jeff R. Bloomquist and Dr. Troy D. Anderson of the Department of Entomology for conducting AChE bioassay. I thank Dr. Eric A. Wong and Dr. Ranginee Choudhury of the Department of Animal and Poultry Science for preparing recombinant enzymes. I also thank Dr. Larry T. Taylor for his HPLC thermostat.

I would like to thank the Carlier group members, past and present, for creating supportive and fun environment in our lab. Particularly I am indebted to Dr. Polo C.-H. Lam, Dr. Dawn M. Wong, and Dr. Hongwu Zhao for sharing their knowledge and expertise, and for valuable discussions. I thank Nipa Deora, Yiqun Zhang, Yang-Sheng Sun, Larry Williams, Dr. Ming Ma, Jason Harmon, and Joe DeGuzman, Josh Hartsel, Chris Monceaux for their friendship.

I would also like to thank Mr. Tom Glass (NMR), Mr. Bill Bebout (Mass Spectroscopy), Mr. Kim Harich (Mass Spectroscopy), and Ms. Carla Slebodnick (X-ray) for their help and support. I acknowledge the financial support of the Department of Chemistry at Virginia Tech.

I am grateful to my parents, grandma, and brother for their everlasting love and encouragement. Without their unconditional support I could not come this far.

Dedication

To my parents

List of Figures

List of Schemes

List of Tables

List of Abbreviations

BZD	1,4-benzodiazepin-2-one
TBAF	Tetra-*n*-butylammonium fluoride
TASF	Tris(dimethylamino)sulfonium difluorotrimethylsilicate
Hmg	Homogenate
ACh	Acetylcholine
AChE	Acetylcholinesterase
BChE	Butyrylcholinesterase
WT	Wild type
Ag	*Anopheles gambiae*
Tc	*Torpedo californica*
Dm	*Drosophila melanogaster*
CAS	Catalytic anionic site
PAS	Peripheral anionic site
DTNB	5,5'-dithiobis(2-nitrobenzoic acid)
DTP	Dithiopyridine
DTT	Dithiothreitol
PCMB	p-Chloromercuribenzoate
NEM	N-ethylmaleimide
CM	Carbamate
OP	Organophosphate

Chapter 1. Memory of Chirality (MOC)[1]

1.1 Introduction

The term "memory of chirality" (MOC) was coined by Fuji, who was the first to successfully design a reaction to capitalize on this principle.[2] The proposal that MOC could underly reaction enantioselectivity was actually first offered by Seebach (vide infra).[3] MOC has attracted attention in part because it appears to do the impossible: *how can the memory of the sole chiral center of a substrate be retained in a process that destroys that center?* MOC has been described as a phenomenon in which:

> "central chirality at a carbon alpha to a carbonyl group is preserved as transient axial chirality of the intermediate enolate and is then regenerated as central chirality in the reaction product (memory of chirality)."[2]

> "the chirality of the starting material is preserved in a reactive intermediate for a limited time"[4]

> "the chirality of a starting material having a chiral sp^3-carbon is preserved in the reaction product even though the reaction proceeds at the chiral carbon as a reaction center through reactive intermediates such as carbanion, singlet monoradicals, biradicals, or carbenium ions"[5]

Although all these definitions capture the key concept of MOC, the last definition by Matsumura[5] best illustrates the scope of intermediates to which it has been applied. Yet for the purpose of this review we would offer our own definition:

A "memory of chirality" reaction can be defined as a formal substitution at a sp^3-stereogenic center that proceeds stereospecifically, even though the reaction proceeds by trigonalization of that center, and despite the fact that no other permanently chiral elements are present in the system.

As Fuji's 1991 definition[2] illustrates, the key to this phenomenon is the preservation of the static central chirality of the starting material in the form of *transient* (or "dynamic") conformational chirality of the reactive intermediate. Thus MOC methods offer a conceptually different approach to stereocontrol than Seebach's Self Regeneration of Stereocenters (SRS) strategy,[6] which relies upon the influence of a permanent chiral center in the reactive intermediate. The concept of dynamic chirality will be discussed below, as will additional requirements for successful MOC transformations. Fuji and Kawabata have published two excellent reviews on MOC,[4,7] and I was a co-author of a review that appeared in 2005.[1] In this chapter, I update and expand upon our published review.

1.2 Requirements for Memory of Chirality

Beginning students of organic chemistry learn that if a enantiopure sp^3-hybridized stereogenic center is trigonalized, any chiral products resulting from that intermediate will be largely racemic (Scheme 1.1). In some S_N1 reactions a slight preference of retentive substitution is seen, due to shielding of backside attack by the leaving group. However, these low stereoselectivities are not synthetically useful.

Scheme 1.1 Racemic products resulting from a planar, achiral intermediate

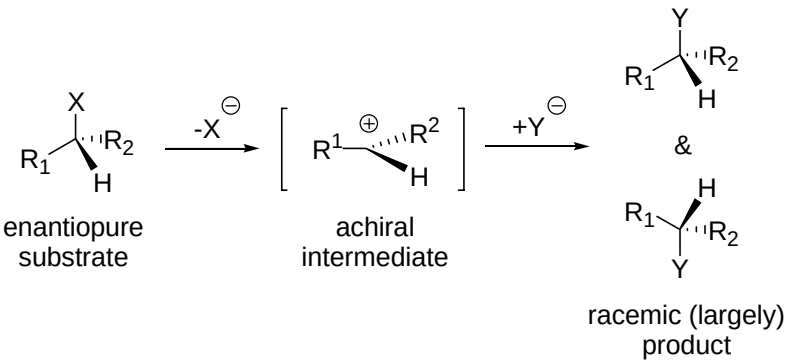

In the absence of any other chiral controllers, a substantially non-racemic outcome would only be possible if the intermediate possesses some form of *conformational* chirality.[2,3]

By its very nature, this conformational chirality will be short-lived; Fuji and Kawabata have termed this phenomenon "dynamic chirality,"[4] since the enantiopurity of this intermediate is dependent on time and temperature. To illustrate this concept, these authors contrast the chirality present in phenylalanine **1** and phenylpropionic acid **2** (Figure 1.1).

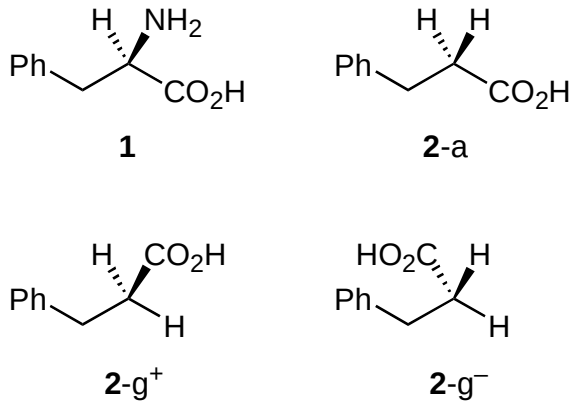

Figure 1.1 Static, central chirality in **1** vs dynamic, conformational chirality in **2**

Phenylalanine **1** possesses static, central chirality. Phenylpropionic acid **2** however is normally considered to be achiral. Closer consideration leads to the realization that in addition to the achiral anti-conformation **2**-a typically drawn for phenylpropionic acid, two chiral, enantiomeric gauche conformations **2**-g^+ and **2**-g^- exist. Of course, under normal conditions, these enantiomeric conformations interconvert rapidly by single bond rotation. Nevertheless, under appropriate circumstances, conformational chirality could influence the stereochemical fate of a reactive intermediate.

However, formation of a conformationally chiral intermediate is not a sufficient condition for MOC: this intermediate must be formed *enantioselectively*. The essential requirements for a MOC reaction are illustrated for a hypothetical deprotonation/methylation in Scheme 1.2.

Scheme 1.2 Essential requirements for a MOC reaction of hypothetical depronation/methylation

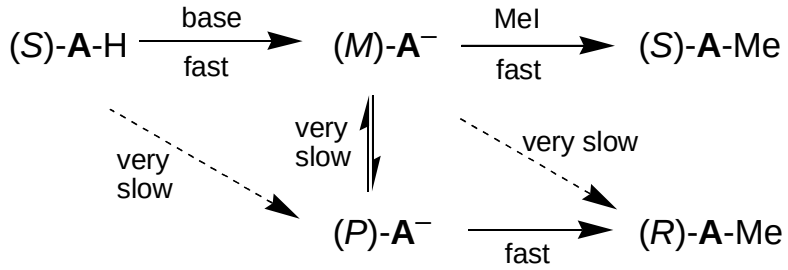

Firstly, deprotonation of the stereogenic center in the enantiopure reactant (*S*)-**A**-H must generate a conformationally chiral reactive intermediate (*M*)-**A**$^-$ with high enantioselectivity. We use the helical descriptors (*M*)- and (*P*)- to describe the chirality of the intermediates; the choice of (*M*)-helicity in this example is arbitrary. Secondly, this conformationally chiral intermediate (*M*)-**A**$^-$ must not readily racemize, at least not on the time scale of the desired subsequent reaction. Finally, the conformationally chiral intermediate must react with MeI with high stereopecificity to produce (*S*)-**A**-Me (again, the choice of (*S*)-configuration is arbitrary). Failure to meet all three of these requirements will result in zero or low enantioselectivity. Note that both steps of the MOC process involve transfer of chirality: from static, central chirality to transient, conformational chirality (1), and then back again (2). How to ensure efficient chirality transfer in both steps is not immediately clear, and represents the essential challenge of the MOC strategy.

1.3 Dynamic Chirality

Since conformational chirality is by definition transient, one question arises immediately: what kind of lifetime is needed for the conformationally chiral reactive intermediate? Assuming that racemization of this intermediate is a unimolecular process, the Eyring equation[8] provides a physical chemical foundation upon which to design MOC methods (Table 1.1).

Table 1.1 Dependence of Racemization $t_{1/2}$ on Barrier and Temperature

racemization barrier $\Delta G^{\ddagger}$(kcal/mol)	racemization $t_{1/2}$ at -78 °C[a]	racemization $t_{1/2}$ at 25 °C[a]
12	2.4 sec	3.5×10^{-5} sec
14	7 min	1.0×10^{-3} sec
16	20 h	3.0×10^{-2} sec
18	148 days	0.9 sec
20	70 years	26 sec

[a]Racemization $t_{1/2} = \ln 2/k_{rac}$, where k_{rac} =2*(kT/h)*exp(-$\Delta G^{\ddagger}$/RT)

As shown in Table 1, at –78 °C, a barrier of 16 kcal/mol would provide a reactive intermediate sufficient time to undergo a slow intermolecular reaction without significant racemization. However, at room temperature, racemization would proceed two million times faster, and intramolecular reaction or solvent trapping would appear to provide the only way to achieve enantioselective reaction of such an intermediate. From a design standpoint, therefore, successful intermolecular MOC reactions rarely depend upon hindered rotation around an sp^3-sp^3 bond, since such bonds typically have barriers to rotation of less than 7 kcal/mol.[9] In contrast, sp^2-sp^2 bonds have been used extensively as a source of conformational chirality in intermolecular reactions, since barriers in excess of 16 kcal/mol are easily achieved.[10]

1.4 Memory of Chirality in Enolate Chemistry

The MOC phenomenon was first demonstrated in the field of enolate chemistry,[2] and to date enolates have proven the most fertile ground for the application of the MOC principle.

1.4.1 α-Alkylation of an Aspartic Acid Ester Enolate

In the course of studying α-alkylation of diethyl malate **3** via its dilithiated derivative **4**, Seebach and Wasmuth turned their attention to the *N*-formyl aspartic acid ester analog **6** (Scheme 1.3).[3]

Scheme 1.3 First insight into the possible use of an axially chiral enolate in an α-alkylation of amino acid derivatives

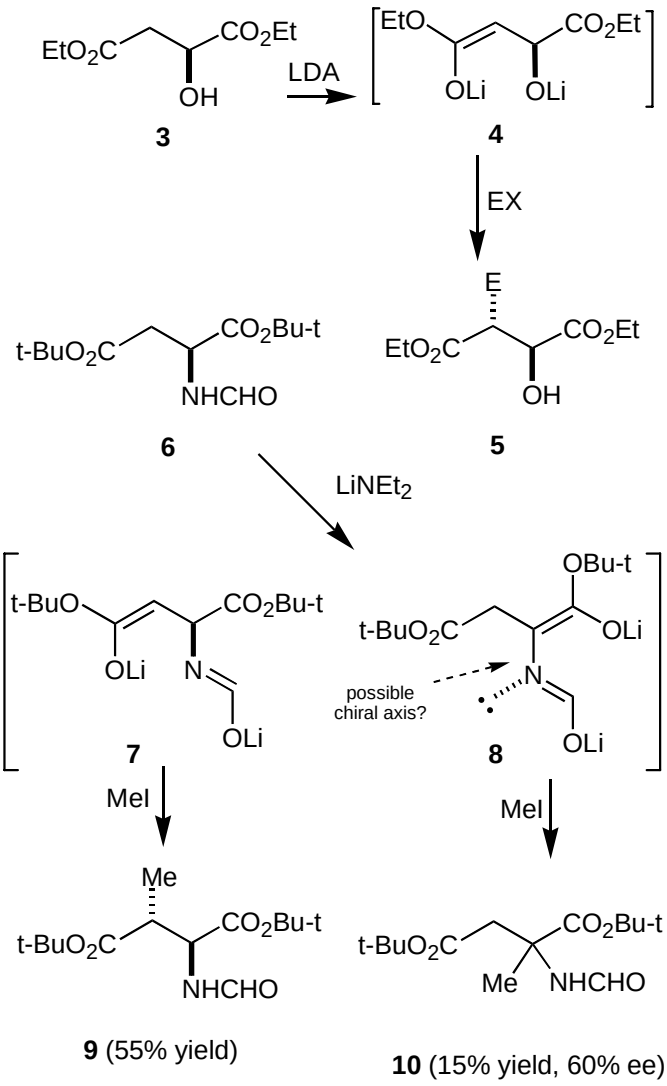

In addition to obtaining the expected α-alkylation product **9**, they obtained a 15% yield of the α-alkylation product **10**. Unexpectedly, **10** was isolated in 60% ee. To account for how **10** was obtained in enantiomerically enriched form from an intermediate **8** that possessed no chiral center, Seebach proposed two explanations. Firstly, reaction could proceed through a mixed aggregate of chiral enolate **7** and achiral enolate **8**. In this way, chiral enolate **7** would act as a chiral controller for alkylation of the achiral enolate **8**. A second possibility is that enolate **8** possessed axial chirality, due to a non-co-planar orientation of the enolate and imine moieties (as depicted in Scheme 1.3). Although the original paper did not record any

experiments to discriminate between these two mechanistic scenarios, Seebach later[6] suggested that the mixed aggregate scenario was operative. Thus, MOC (as defined in Section 1 above) may not be responsible for asymmetric induction in **10**. Nevertheless, as will become clear in the course of this review, amino acid derivatives have proven very fertile ground for MOC methods, and axial chirality along the N-C(2) bond of amino acid ester enolates has been shown to play a major role in many of these reactions.

1.4.2 Designed Asymmetric Alkylation of a Napthyl Ketone

Fuji was the first to intentionally design a reaction that would capitalize on the MOC phenomenon.[2] His key insight was that deprotonation of a stereogenic center α to a carbonyl in **11** need not always lead to an achiral enolate intermediate **12** (Scheme 1.4).

Scheme 1.4 Intentional design of conformationally chiral enolates

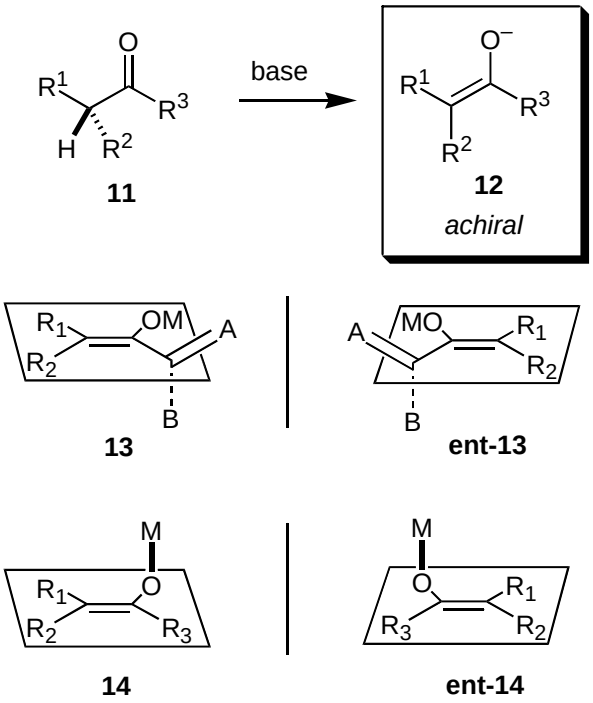

Under the appropriate circumstances, conformationally chiral enolates might be formed, such as axially chiral **13** or planar chiral **14**. Of course, for a successful MOC reaction, these

chiral enolates would need to be formed enantioselectively, and not racemize quickly on the alkylation reaction time scale.

To achieve a slowly racemizing, axially chiral enolate intermediate, Fuji and Kawabata chose to explore deprotonation of chiral 1-naphthylketone **15**. Deprotonation of **15** with KH/18-crown-6, followed by trapping with MeI gave the desired product **17** in 66% ee (Scheme 1.5).

Scheme 1.5 First intentional MOC reaction

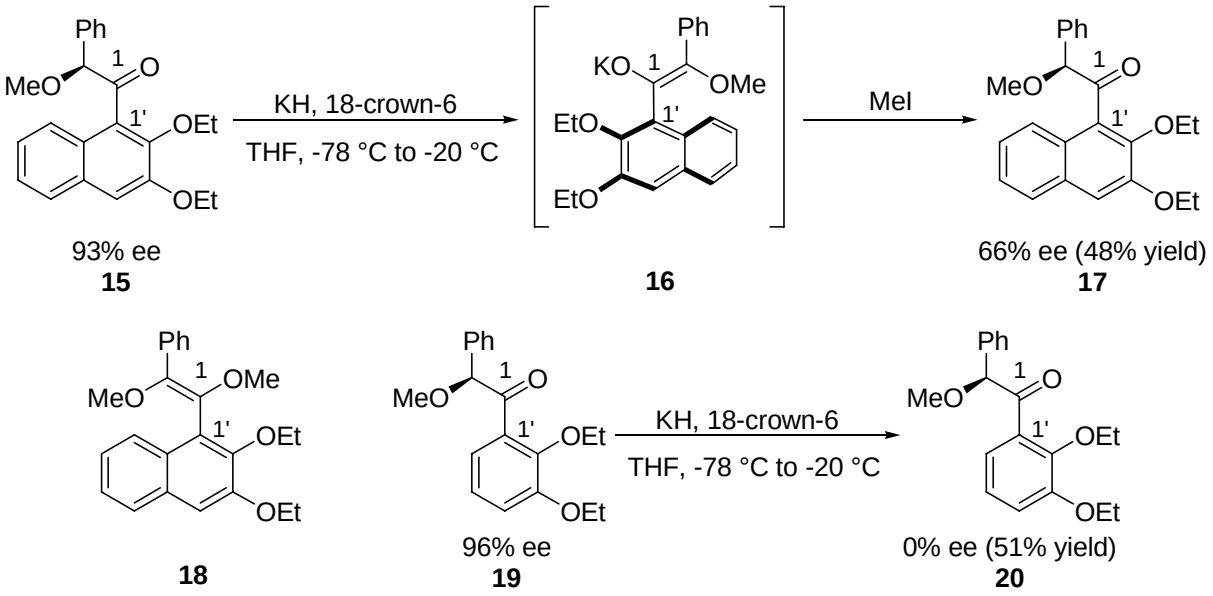

This stunning result clearly indicates the formation of a nonracemic chiral enolate intermediate. The authors proposed that reaction occurs via axially chiral enolate **16**, whose structure is reminscent of the atropisomeric 1,1-binapthyls. Support for an axially chiral enolate such as **16** came from two other observations. First, *O*-alkylation product **18** was also detected in the reaction mixture and HPLC immediately following reaction indicated 65% ee. At room temperature (21 °C), **18** was found to racemize with a half-life of 53 minutes, corresponding to a barrier of 22.6 kcal/mol.[7] Secondly, compound **19**, the phenyl analog of **15** was subjected to the same reaction conditions, but gave racemic **20**. This result is consistent

with the expectation that the enolate derived from **19** would possess a lower barrier for rotation along the 1,1' bond than would the 1-naphthyl analog **16**.

1.4.3 Enantioselective α-alkylation of Amino Acid Esters without External Chiral Sources.

Asymmetric synthesis of α-substituted α-amino acids has attracted considerable attention because of the biological and medicinal importance of these compounds.[6,11,12] Fuji and Kawabata realized that these compounds could potentially be obtained by a MOC deprotonation/alkylation of the appropriate amino acid derivative **21** (Scheme 1.6).

Scheme 1.6 Three types of enolate chirality: (A) axial, (B) planar, and (C) central

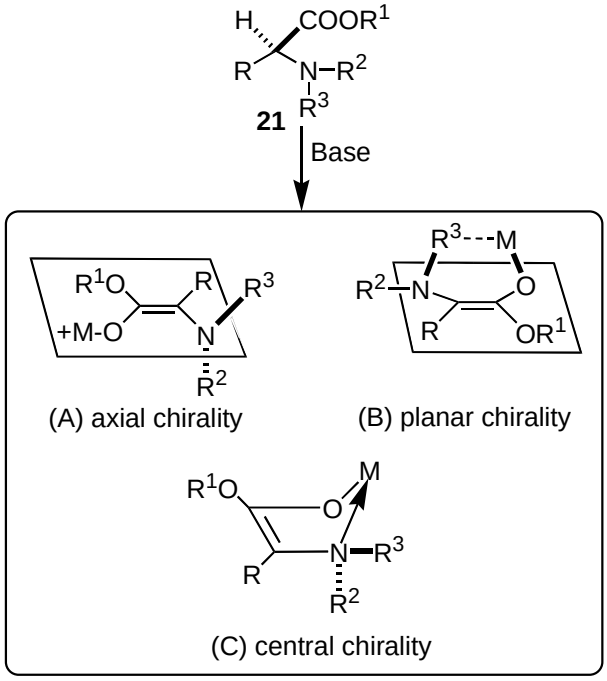

Three types of enolate chirality can be envisioned: axial (A), planar (B), and central (C). A key design feature of the authors is the use of two non-identical nitrogen protecting groups that differ widely in steric bulk. The authors' first published report relied upon *N*-Me,*N*-Boc amino acid esters (Table 1.2).[13]

Table 1.2 Asymmetric methylation of (*S*)-**22**

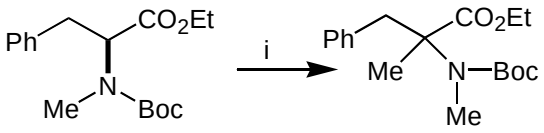

(*S*)-**22** i) 1. Base, -78°C 2. MeI, THF **23**

entry	Base (Equiv.)	%ee	%yield
1	LiTMP (1.0)	82 (*S*)	40
2	LDA (1.2)	22 (*S*)	57
3	KHMDS (1.2)	20 (*R*)	79

As hoped, non-racemic products were obtained, the best %ee being realized with LiTMP as base (entry 1). Interestingly, both lithium bases gave retention, but KHMDS gave a predominance of inversion (20 % ee). Although this work represents a major achievement, the yield under the most enantioselective conditions is clearly not acceptable, and the products are not easily demethylated. Six years later Kawabata and Fuji reported a greatly superior protocol that relies upon *N*-MOM,*N*-Boc amino acid esters (Table 1.3).[14]

As can be seen in Table 1.3, the *N*-MOM,*N*-Boc amino acid esters are alkylated in 76-93 % ee and 78-96 % yield. In addition to providing superior yields and enantioselection, the two protecting groups are easily removed during acidic ester hydrolysis (6M aq. HCl), affording the corresponding α-Me-α-amino acids in 51-86% yields. In each case where correlation was performed, the α-methylation was shown to proceed with retention of configuration.

The proposed mechanism for MOC in this reaction will be discussed below. However, at this point a question can be raised. Can the structural features that contribute to MOC successfully compete against the influence of a nearby chiral center? Fuji and Kawabata addressed this question by studying the α-alkylation of L-Isoleucine and D-allo-Isoleucine derivatives **26** and **29** (Scheme 1.7).[15]

Table 1.3 Asymmetric α-methylation of N-MOM-N-Boc α-amino acid derivatives

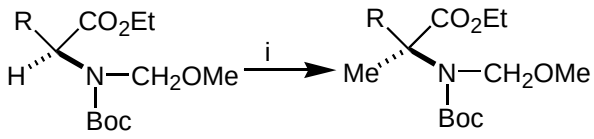

(*S*)-**24a**-**g** **25a**-**g**

i) 1. KHMDS, Toluene-THF (4:1), 30 m.
2. MeI, -78 °C.

Substrate	R	% Yield	% ee (configuration)
24a	$PHCH_2$	96	81 (*S*)
24b	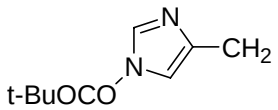	83	93
24c	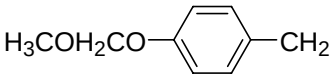	94	79 (*S*)
24d	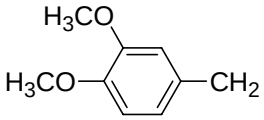	95	80 (*S*)
24e	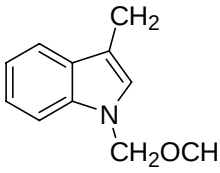	88	76
24f	Me_2CH	81	87 (*S*)
24g	Me_2CHCH_2	78	78 (*S*)

Scheme 1.7 MOC α-alkylation of Isoleucine derivatives

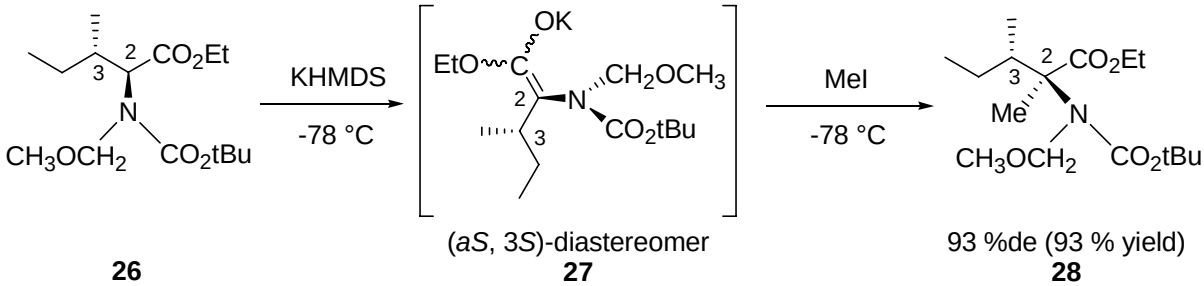

26 (*aS*, 3*S*)-diastereomer **27** 93 %de (93 % yield) **28**

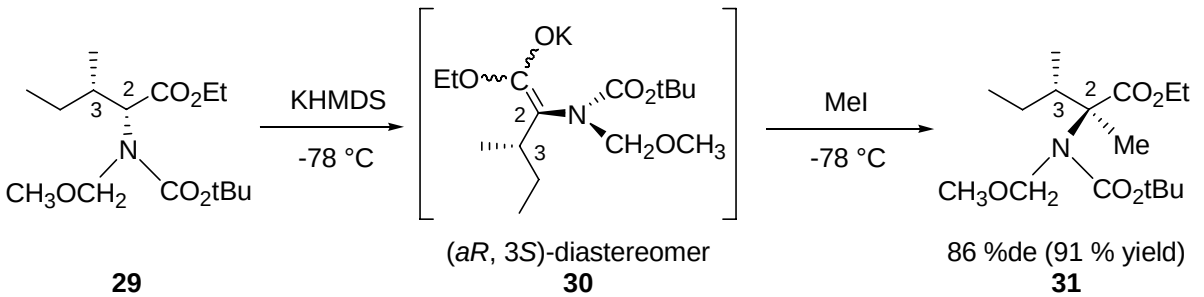

29 (*aR*, 3*S*)-diastereomer **30** 86 %de (91 % yield) **31**

These diastereomeric amino acid esters have the same absolute configuration at C(3), but opposite configurations at C(2). When the *N*-MOM,*N*-Boc ethyl esters **26** and **29** were subjected to the standard deprotonation/methylation protocol, a high degree of retention was observed in both cases, providing **28** and **31** in excellent diastereoselectivity (93% and 86% de respectively). Thus the stereochemical course of deprotonation/methylation of **26** and **29** appears to be controlled by the chirality at C(2). If the chiral information at C(2) had been lost during enolate formation, α-methylation would have given products with an identical diastereomeric composition via a common enolate intemediate. The fact that different diastereoselectivities were obtained from **26** and **29** suggests the intermediacy of diastereomeric enolate intermediates such as **27** (a*S*, 3*S*) and **30** (a*R*, 3*S*), respectively.

1.4.4 Enantioselective Synthesis of Aza-cyclic Amino Acids

Cyclic amino acids with a quaternary stereocenter constitute a valuable class of nonnatural amino acids with highly constrained conformations. The importance of these compounds has motivated the development of efficient methods for their asymmetric synthesis.[16] Kawabata et al. reported a simple and efficient protocol for asymmetric intramolecular cyclization of α-amino acids derivatives to afford a variety of quaternary aza-cyclic amino acids of high enantiomeric purity.[17] Knowing that the *N*-Boc group was critical to the intermolecular enantioselective α-methylation of α-amino acid esters via memory of chirality, Kawabata et al. designed a series of *N*-Boc-*N*-ω-bromoalkyl-α-amino acid derivatives **32a**-**h** as substrates for asymmetric intramolecular cyclization (Table 1.4).

Table 1.4. Enantioselective synthesis of aza-cyclic quaternary amino acid derivatives

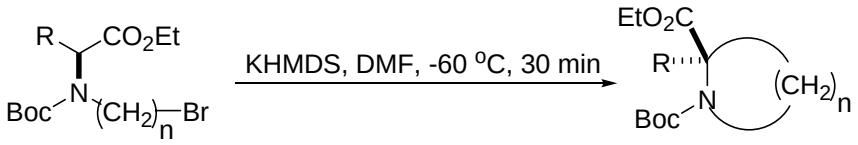

(*S*)-**32a-h** **33a-h**

Substrate	n	R	% yield	% ee
32a	3	$PhCH_2$	94	98(*S*)
32b	3	4-EtO-C_6H_4-CH_2	95	97
32c	3	$MeSCH_2CH_2$	92	97
32d	3	Me_2CH	78	94
32e	3	CH_3	91	95(*R*)
32f	2	$PhCH_2$	61	95
32g	4	$PhCH_2$	84	97
32h	5	$PhCH_2$	31	83 (*S*)

Treatment of **32a-h** with KHMDS in THF at –78 °C gave the corresponding optically active aza-cyclic amino acid derivatives **33a-h** in 31-95% yields and 83-98% ee (Table 1.4). Thus, by this protocol the enantioselective construction of four-, five,- six-, and seven-membered aza-cyclic amino acids was achieved. The chirality of the parent amino acids was almost completely preserved during enolate formation and subsequent cyclization, giving enantiomerically enriched aza-cyclic quaternary amino acids with retention of configuration.

Later on, Kawabata et al. further developed diastereomeric aza-cyclic amino acids derivatives by asymmetric intramolecular conjugate addition (table 1.5).[18] **34a-d** were treated with KHMDS in DMF-THF at –78 °C to afford the corresponding enantiomerically enriched aza-cyclic amino acid derivatives **35a-d** in 19-74% yields and 91-98% ee (Table 1.5). Similarly, five-, six-, seven-membered diastereomeric aza-cyclic amino acids were prepared in high enantioselectivities. This MOC cyclization by intramolecular conjugate addition also occurred with retention of configuration.

Table 1.5 MOC cyclization of **34**

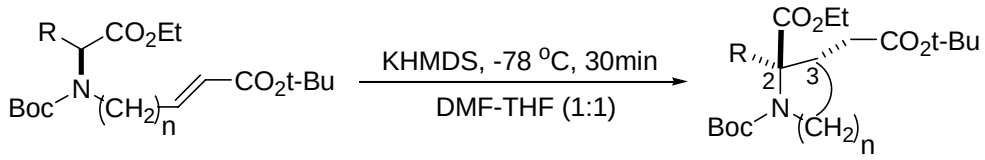

(*S*)-**34a-d** **35a-d**

Substrate	n	R	% yield	% ee
34a	2	$PhCH_2$	65	91 (2*R*, 3*S*)
34b	3	$PhCH_2$	66	97
34c	3	4-EtO-C_6H_4-CH_2	74	98
34d	4	$PhCH_2$	19	91

In 2006, Kawabata reported enantiodivergent asymmetric cyclization via MOC (table 1.6).[19] When a potassium amide base was used in DMF, the cyclization was carried out with retention of configuration; however, by applying a lithium amide base in THF, inversion of configuration was observed. As each conversion from natural (*L*)-amino acid derivatives resulted in high enantioselectivity, concise routes to both enantiomers of cyclic quaternary amino acids were provided.

Table 1.6 Stereochemical diversity in MOC cyclization of **32**

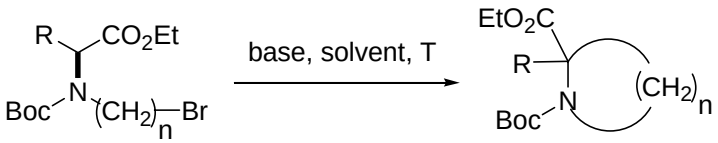

(*S*)-**32a,c,e,f,i** **32a,c,e,f,i**

Substrate	n	R	base	solvent	T	% yield	% ee
32a	3	$PhCH_2$	KHMDS	DMF	-60 °C	94	98 (*S*)
32a	3	$PhCH_2$	LTMP	THF	20 °C	93	91 (*R*)
32c	3	$MeSCH_2CH_2$	KHMDS	DMF	-60 °C	92	97 (*S*)
32c	3	$MeSCH_2CH_2$	LTMP	THF	20 °C	92	81 (*R*)
32e	3	CH_3	KHMDS	DMF	-60 °C	91	95 (*R*)
32e	3	CH_3	LTMP	THF	20 °C	91	87 (*S*)
32f	2	$PhCH_2$	KHMDS	DMF	-60 °C	61	95 (*R*)
32f	2	$PhCH_2$	LTMP	THF	20 °C	69	90 (*S*)
32i	2	$MeSCH_2CH_2$	KHMDS	DMF	-60 °C	98	97 (*S*)
32i	2	$MeSCH_2CH_2$	LTMP	THF	20 °C	66	83 (*R*)

1.4.5 Proposed Mechanisms of Asymmetric Induction in Deprotonation/Alkylation of Amino Acid Esters

Fuji and Kawabata have carried out a number of mechanistic investigations that support the role of MOC in stereochemical control. As discussed in 1.4.3 above, in the alkylation of naphthyl ketone **15**, axially chiral enol ether **18** was isolated (Scheme 1.5). For the enantioselective deprotonation/alkylation of *N*-Boc,*N*-Me amino acid esters **22**, the authors considered several mechanistic scenarios. (Figure 1.2)

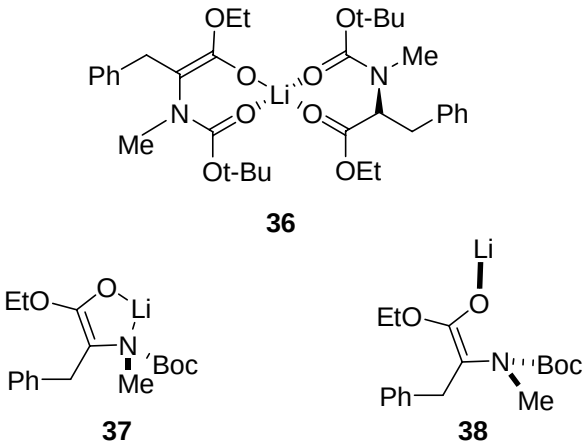

Figure 1.2 Three possible intermediates during asymmetric induction

Asymmetric induction could arise from a chiral enolate/starting material aggregate **36**, a species **37** with a chiral N atom, or an axially chiral enolate **38**. To rule out the intermediacy of a chiral enolate/starting material aggregate such as **36**, the authors conducted a crossover experiment (Scheme 1.8).[13]

Scheme 1.8 Crossover experiment to investigate the origin of chirality

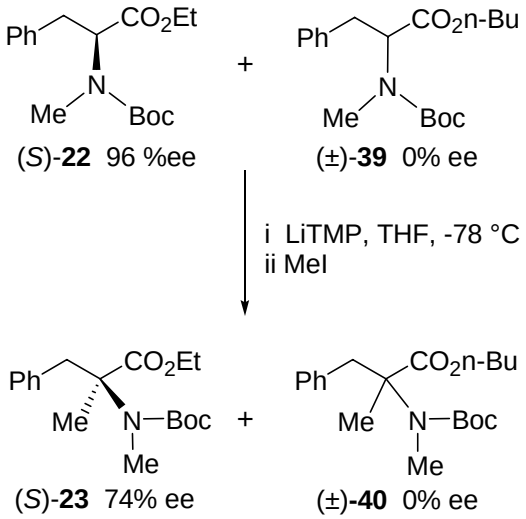

A 1:1 mixture of (*S*)-**22** and (±)-**39** were subjected to deprotonation with LiTMP at –78 °C followed by addition of methyl iodide, to afford optically active **23** (74% ee, 26% yield) and racemic **40** (30% yield). The same treatment of a 1:1 mixture of racemic **22** and optically active **39** (96% ee) afforded the racemic **23** (17% yield) and optically active **40** (71% ee, 24% yield). These results clearly demonstrate that transfer of chirality between the enolates derived from **22** and **39** does *not* occur. Thus asymmetric induction in these reactions is not due to formation of a chiral enolate/starting material aggregate such as **36**. Interestingly, however, in a subsequent study on deprotonation/methylation of *O*-methyl mandelic acid amides, Fuji and Kawabata did find support for a mixed aggregate mechanism for asymmetric induction.[20]

In support of the proposal that axially chiral enolates such as **38** underly the MOC deprotonation/alkylation of amino acid esters, Fuji and Kawabata reported isolation of the (*Z*)- and (*E*)-TBS ketene acetals **41** (Figure 1.3).[14]

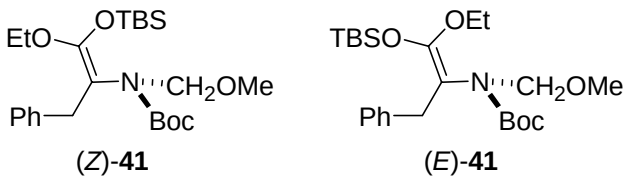

Figure 1.3 (*Z*)- and (*E*)-TBS ketene acetals **41**

The methylene protons of the MOM groups are diastereotopic in both isomers of **41**, indicating restricted rotation of the C(2)-N bond. The rotational barrier of the C(2)-N bond in major Z-isomer of **41** was determined to be 16.8 kcal/mol by variable–temperature ^{1}H NMR measurements in [d_8]toluene. This barrier corresponds to a racemization half-life of 7 days at –78 °C. Thus the formation of a slowly racemizing axially chiral potassium enolate appears feasible. The racemization barrier of the potassium enolate was then directly measured by periodic quenching of the enolate intermediate generated from **24a** at –78 °C with methyl iodide. The plot of the relative ee value of **25a** (ln ee_0/ee_t) versus deprotonation time (t) was linear, and the racemization rate was calculated from the slope ($2k = 5.34 \times 10^{-4}$ min^{-1}, corresponding to a racemization half-life of 22 h at –78 °C). Application of the Eyring equation indicates a barrier to racemization of 16.0 kcal/mol at –78 °C, similar to that of TBS ketene acetal (*Z*)-**41**.

Additional support for the intermediacy of an axially chiral enolate was found in deprotonation/alkylation of two cleverly designed substrates **42** and **43** (Figure 1.4).

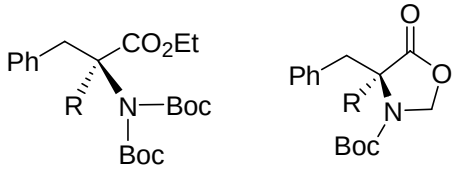

42: R = H
44: R = Me

43: R = H
45: R = Me

Figure 1.4 Examination of the intermediacy of axially chiral enolate in deprotonation/alkylation

Deprotonation/methylation of enantiopure (*S*)-**42** and (*S*)-**43** gave racemic **44** and racemic **45** respectively. These racemic results are consistent with the intermediacy of *achiral* enolates. For **42**, the presence of two identical Boc protecting groups removes the possibility of chirality on the N-C(2) axis. In the case of **43**, the 5-membered ring prevents the N substituents from rotating out of the enolate plane to attain axial dissymetry.

As mentioned in Section 1.2, the generation of conformationally chiral intermediates is not a sufficient condition for MOC. To achieve effective MOC, the conformationally chiral intermediate must be generated in enantiopure form. How does the deprotonation of enantiopure, centrally chiral esters (*S*)-**22**, **24**, and **32** generate nonracemic conformationally chiral enolates? Furthermore, how can the uniformly retentive transformation of the substrates be rationalized? Fuji and Kawabata proposed that deprotonation of (*S*)-**24a** occurs through **46**, which MM3 identified to be the most stable conformer (Scheme 1.9).[14] Deprotonation yields the axially chiral nonracemic enolate **47**. Steric control of the alkylation then leads to retentive methylation and formation of (*S*)-**25a**. Fuji and Kawabata proposed a similar mechanism to account for retentive cyclization of (*S*)-**32a** (Scheme 1.10).[19]

Scheme 1.9 Proposed mechanism of retentive methylation of (*S*)-**24a**

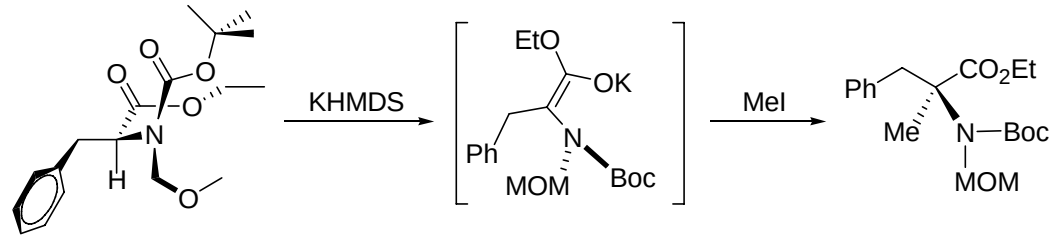

46
most stable conformer
of (*S*)-**24a**

axially chiral
nonracemic
enolate **47**

(*S*)-**25a**

In this case a conformational search identified two stable conformers **48a-b** of similar energy. The authors proposed that deprotonation of **48b** is disfavored due to a steric interaction between KHMDS and the *N*-Boc group (transition state **49b)**. Thus, deprotonation of **48a** is favored, to give axially chiral nonracemic enolate **49**, which then cyclizes to give (*S*)-**33a**. Furthermore, Kawabata investigated a similar hypothesis for the stereochemical control of MOC cyclization of (*S*)-**32a** (Scheme 1.10).[17,19] Chelation of the Boc-carbonyl oxygen to lithium cation in less coordinative solvent caused the transition state **49b** to be dominant over **49a**, and thus led to product with inversion of configuration.

Scheme 1.10 Proposed mechanism of MOC cyclization of (*S*)-**48a** and **48b**

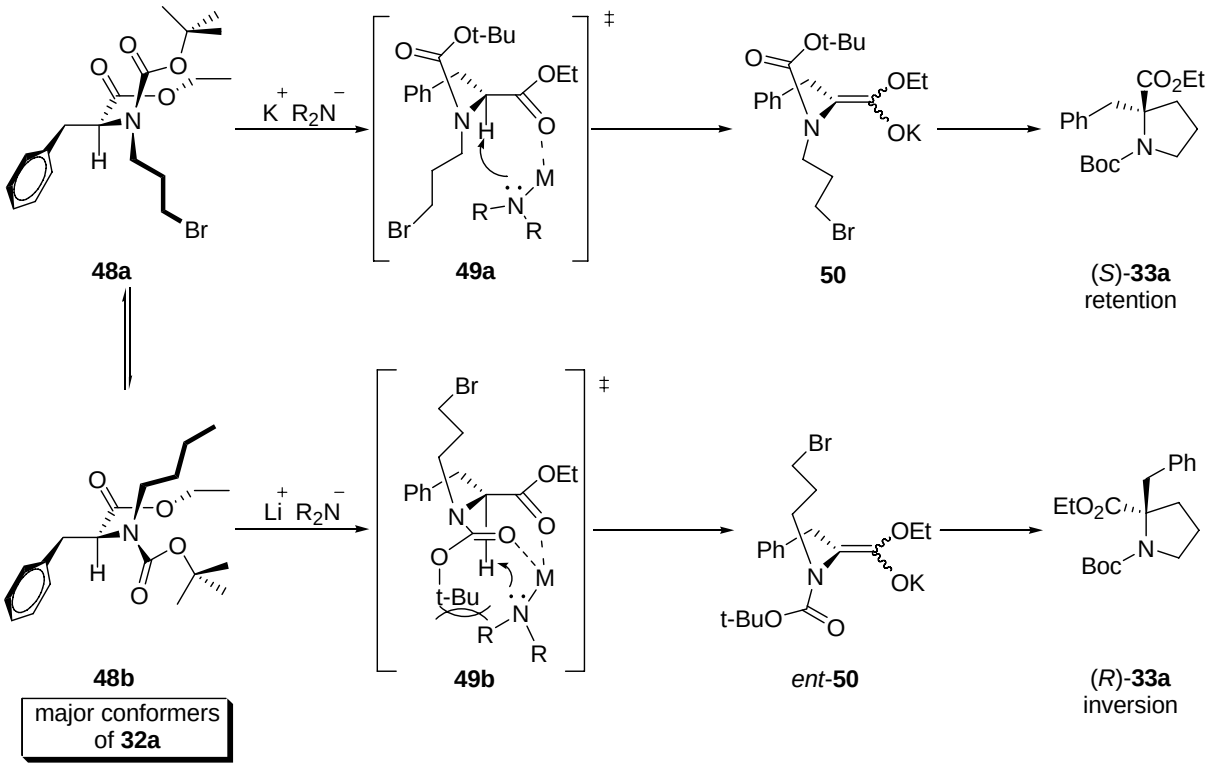

The mechanistic rationale offered by Fuji and Kawabata for retentive deprotonation/alkylation of amino acid esters **22**, **24**, and **32** is powerful in its simplicity. One experimental detail that is not accomodated by the model as laid out thus far is the lower enantioselectivity obtained with electrophiles other than MeI. To account for this variation, Fuji and Kawabata proposed that enolate aggregates exist in solution and possess differential reactivities and selectivities toward individual electrophiles. In support of this idea, the authors demonstrated superior allylation %ee with homo- and heterodimeric substrates designed to form intramolecular aggregates.[21,22]

1.4.6 Other Cyclization Reactions Involving Axially Chiral Enolate Intermediates

Concurrent with Fuji's early studies on MOC, Stoodley and his coworkers isolated a bicyclic side product **53** with complete retention of configuration as they attempted to transform **51** into **52** (Scheme 1.11).[23]

Scheme 1.11 MOC cyclization of **51**

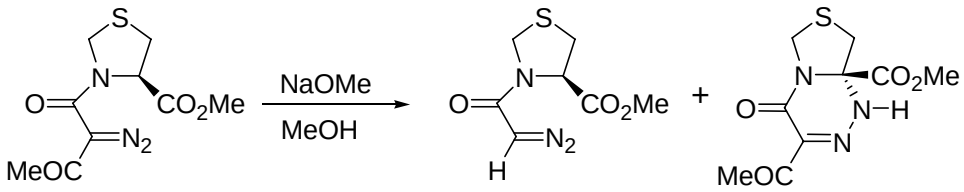

The best conditions devised for the preparation of bicyclic compound **53** involved the addition of triethylamine to a boiling solution of **51** in methanol (65% yield). To account for the stereochemistry of **53**, Stoodley et al. postulated the intermediacy of axially chiral enolate **54** with a sizeable energy barrier to racemization (Scheme 1.12).

Scheme 1.12 Racemization of axially chiral enolate **54**

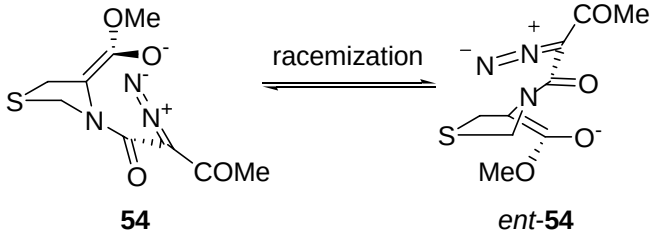

Restricted rotation about the amide bond of **51** was evidenced by ^{1}H NMR spectroscopy at –60 °C in $CDCl_3$, which demonstrated the presence of three rotamers in the ratio of 50: 32:18.[24] The kinetic preference for the deprotonation of **51** to give chiral enolate **54** rather than its enantiomer *ent*-**54** is attributable to the stability of conformation **55** relative to conformation **56** (Scheme 1.13).

Scheme 1.13 Kinetic preference for the deprotonation of **54**

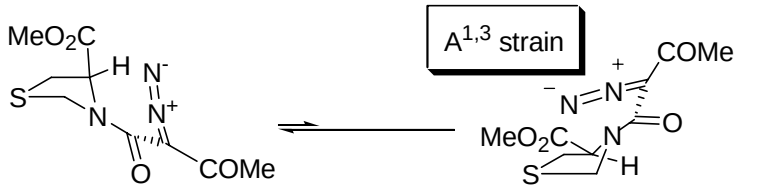

Although both **55** and **56** adopt the (*Z*)-amide geometry and an *anti*-relation between the keto and diazonium groups, significant $A^{1,3}$ interaction exists between the *N*-acyl substituent and CO_2Me group in geometry **56**. Thus deprotonation of major conformer **55** gives enolate **54** in preference to *ent*-**54**, which then cyclizes to **53**.

Stoodley and coworkers found that this reaction could be extended to thiazolidine dioxides **57**, giving the bicyclic sulfone **58** with complete retention of configuration (86% yield) (Scheme 1.14).[25]

Scheme 1.14 MOC cyclization of **57**

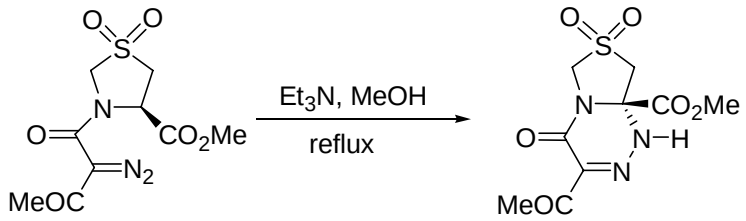

57 **58**

Finally, Stoodley and co-workers found that intramolecular aldol reaction of **59** gave two enantiopure, diastereomeric products **60** and **61** in a 72:28 ratio (Scheme 1.15).[26]

Scheme 1.15 Intramolecular aldol reaction of **59**

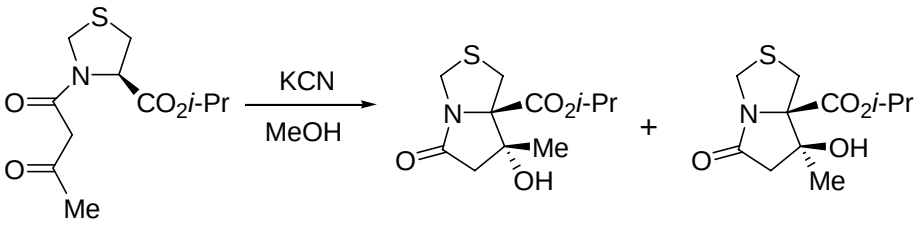

59 **60** **61**

60:**61** = 72:28 (combined yield 68%)

The retentive stereochemistry is again consistent with the conformation selection mechanism described above in Scheme 1.13. Stoodley and co-workers later extended this reaction with similar success to the oxaproline and proline analogs.[27]

After Fuji & Kawabata reported their first studies of deprotonation/alkylations of protected amino acid esters, González-Muñiz published a MOC route to conformationally constrained quaternary 4-alkyl-4-carboxy-2-azetidinones (Scheme 1.16).[28,29,30] The asymmetric induction proved sensitive to the identity of the nitrogen protecting group, the ester alkyl group, and the amino acid side chain. The optimum substrate **62** cyclized to **63** in 70% ee. The authors attributed asymmetric induction to the formation of an axially chiral enolate, a proposal that is strengthened by the structural similarity of **62** to Fuji and Kawabata's substrate **32**.

Scheme 1.16 MOC cyclization of **62**

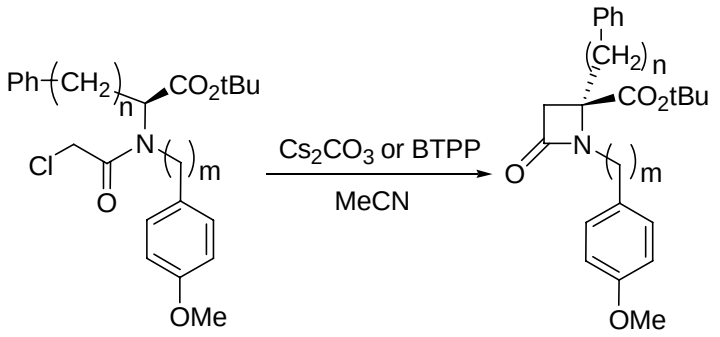

62 (n=0, m=1)

63 (n=0, m=1)
61% yield, 70% ee

In closing this section on enantioselective enolate cyclizations we must note a study by Seebach and coworkers on the retentive rearrangement of a lithiated *N*-acyl-tetrahydroquinoline **64**.[31] Although the mechanism of this reaction has not been firmly established, the authors proposed opening of the tetrahydroisoquinoline ring to a give an axially chiral enolate **65**, followed by enantioselective ring closure (Scheme 1.17).

Scheme 1.17 Retentive rearrangement of **64**

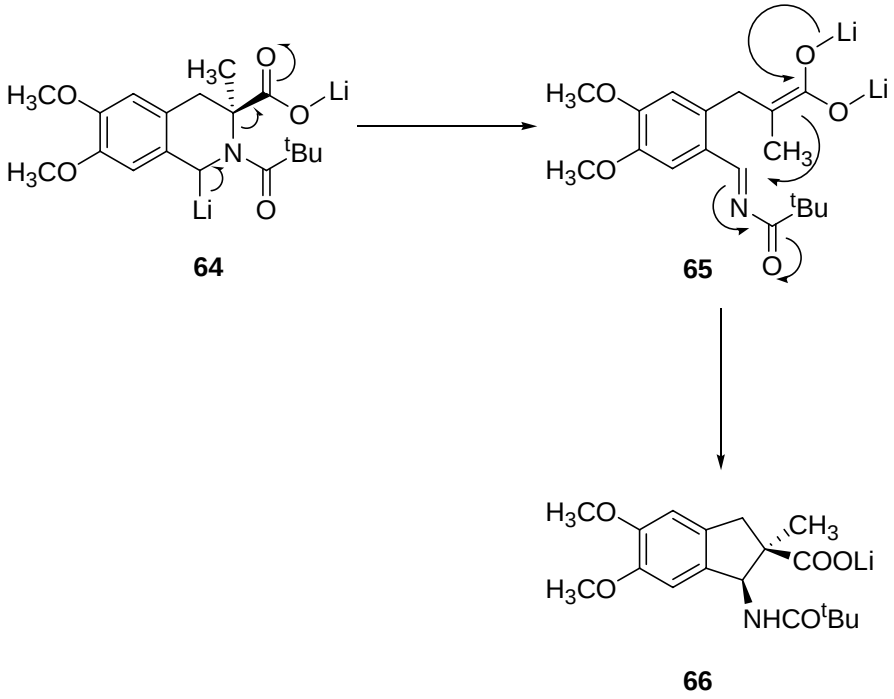

1.4.7 Enantioselective Synthesis of Quaternary 1,4-Benzodiazepin-2-ones

1,4-Benzodiazepin-2-ones are among the most important scaffolds in medicinal chemistry, representing the prototypical "privileged structure."[32,33] However, 1,4-benzodiazepin-2-ones possessing a quaternary center at C(3) have received very little attention from synthetic or medicinal chemists, possibly due to the limited commercial availability of the most obvious starting materials (enantiopure quaternary amino acids). Recently, Carlier and coworkers reported a MOC route to such "quaternary" 1,4-benzodiazepin-2-ones (Scheme 1.18).[34] Whereas sequential deprotonation/benzylation of enantiopure alanine derivative (*S*)-**67a** gave racemic **68a**, application of the same protocol to the *N*-*i*-Pr analog **67b** gave the desired product **68b** in 97% ee. These divergent results were attributed to the formation of a conformationally chiral enolate intermediate, whose racemization rate critically depends on the size of the N(1) substituent R^1. High levels of enantioselectivity for alkylation of **67b** were attained with other active electrophiles (Table 1.7). Enantioselectivities range from 94 to 99%, and are independent of the size of the electrophile. Methylation and allylation reactions

of the *N*-*i*-Pr phenylalanine analog (*S*)-**69b** are also highly enantioselective (95 and 86% ee respectively). Retentive stereochemistry was established by hydrolysing quaternary 1,4-benzodiazepin-2-one **68b** and **70b** to the known quaternary amino acids (8M HCl, 140 °C, 3 days, 50-62% yield), and by chiral stationary phase HPLC of deuteration product **73**.

Scheme 1.18 Size of R^1 as key determinant in MOC deprotonation/alkylation of 1,4-benzodiazepin-2-ones

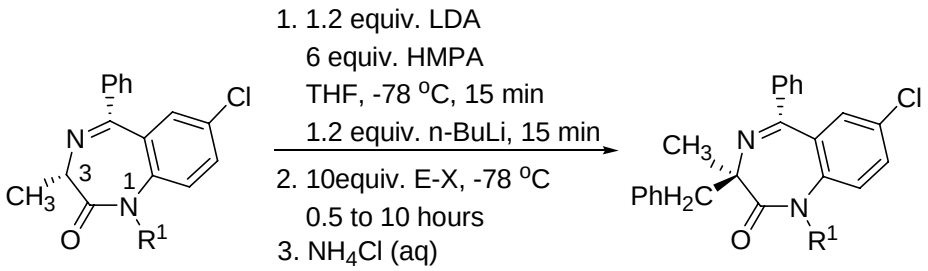

	R^1
(*S*)-**67a**	Me
(*S*)-**67b**	*i*-Pr

	% ee	% yield
(*R*)-**68a**	0	72
(*R*)-**68b**	97	74

Table 1.7 Enantioselective Synthesis of Quaternary 1,4-Benzodiazepin-2-ones via Memory of Chirality

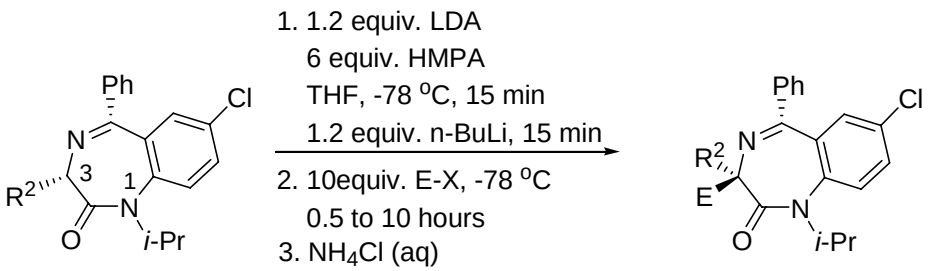

	R^2
(*S*)-**67b**	Me
(*S*)-**69b**	CH_2Ph

68b, **70b**-**74b**

R^2	E-X	product	%yield	%ee
Me	BnBr	(+)-**68b**	74	97 (3*R*)
Me	4-$MeC_6H_4CH_2Br$	(+)-**70b**	68	95 (3*R*)
Me	2-$PhC_6H_4CH_2Br$	(+)-**71b**	70	99
Me	Allyl-Br	(+)-**72b**	76	94
Me	D-OTFA	(+)-**73b**	85[a]	99 (3*S*)
Bn	MeI	(-)-**68b**	64	95 (3*S*)
Bn	Allyl-Br	(+)-**74b**	57	86

[a]Extent of deuteration: 96%.

As mentioned previously, enantioselectivity in these reactions is attributed to the formation of nonracemic, conformationally chiral enolates. To understand how these enolates are chiral, and how they are formed enantioselectively, one must appreciate the non-planar nature of the benzodiazepine ring. Despite the absence of a stereogenic center, glycine-derived 1,4-benzodiazepin-2-ones **75a-d** are chiral, existing as conformational enantiomers (Table 1.8). [35,36]

The helical descriptors (*M*)- and (*P*)- are used to describe the sense of ring chirality, based on the sign of the R^1-N(1)-C(10)-C(9) dihedral angle. As demonstrated in Table 1.8, the barrier to inversion in these compounds depends strongly upon the size of the N(1) substituent.[34,35,37,38] It is also well known that when a single substituent is present at C(3) (as in **67b**), it strongly prefers to be pseudoequatorial.[39] Thus the chirality at C(3) controls the helicity of the diazepine ring of **67b**. As shown in Scheme 1.19, a (3*S*)-center will induce the diazepine ring to adopt the (*M*)-conformation.

Table 1.8. Dynamic chirality of **75a-d** ($\Delta G^{\ddagger}$ values were determined by ^{1}H NMR spectroscopy (coalescence))

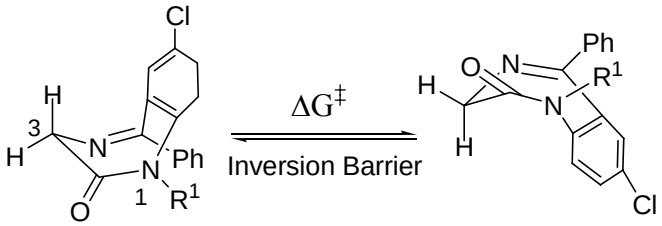

(*M*)-**75a-d** (*P*)-**75a-d**

	R_1	$\Delta G^{\ddagger}$ (kcal/mol)
75c	H	12.3[a]
75a	Me	18.0[b]
75b	*i*-Pr	21.1[b]
75d	*t*-Bu	> 24[c]

[a]Ref. 35. [b]Ref. 34, 38 [c]Ref. 37

Scheme 1.19 BZD in (*M*)-conformation induced by the central chirality at C3

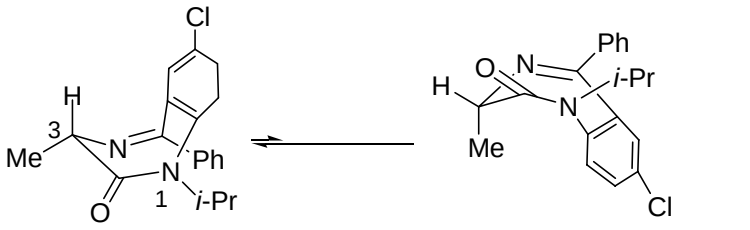

pseudoequatorial methyl in (*M*)-conformer of (3*S*)-**67b**

pseudoaxial methyl in (*P*)-conformer of (3*S*)-**67b**

Therefore, although deprotonation of (3*S*)-**67b** destroys the stereogenic center at C(3), the resulting enolate would remain chiral by virtue of the non-planar diazepine ring. Since the major (*M*)-conformer of (3*S*)-**67b** is stereoelectronically better disposed for deprotonation than is the minor (*P*)-conformer, deprotonation should preferentially yield the (*M*)-enolate.

To address the issues of enolate structure and racemization, DFT calculations were carried out on **76b**, the enolate ion derived from des-chloro analog of **67b** (Figure 1.5).

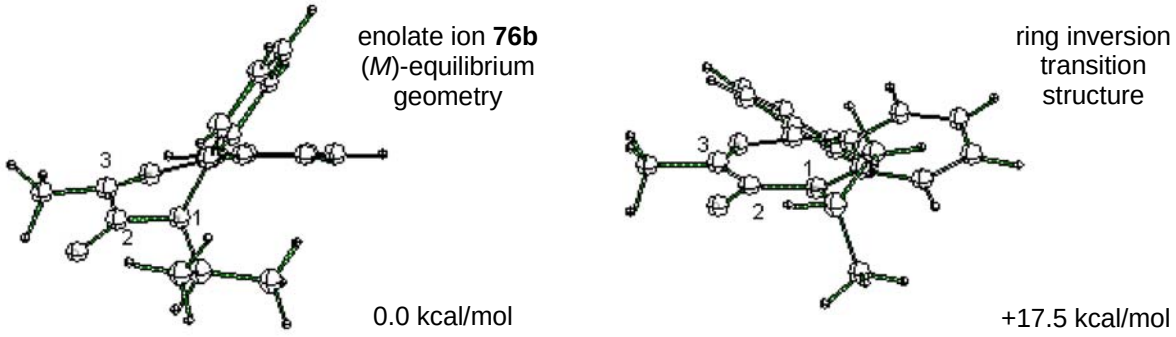

Figure 1.5. B3LYP/6-31G* equilibrium geometry and ring inversion transition structure of *N*-*i*-Pr enolate anion **76b** (relative free energies at B3LYP/6-31+G*//B3LYP/6-31G*).

Identical calculations were carried out on **76a**, the *N*-Me analog. The equilibrium geometries of enolates **76a-b** are chiral, and feature essentially flat C(3) carbons (sum of angles 358.5, 359.0°). Thus, at early time we believed that the retentive stereochemistry cannot be attributed to pyramidalization of C(3); however, now we are re-considering the issue as the sum of angles at C(3) is not a sensitive measure of slight pyramidalization. Detail will be discussed at section 2.9.

The calculated ring inversion transition structures of **76a**-**b** indicate near eclipsing of the N(1) substituent (R^1) and C(8) (dihedral angles 13.4°, 12.8°). B3LYP/6-31+G*//B3LYP/6-31G* activation free energies for ring inversion at –78 °C of **76a** (*N*-Me) and **76b** (*N*-*i*-Pr) are 12.4 and 17.5 kcal/mol, which correspond to racemization $t_{1/2}$(-78 °C) values of 0.11 minutes and 970 hours respectively. Thus the racemizing benzylation of **67a** and the enantioselective benzylation of **67b** (Scheme 1.18) may be rationalized. Finally, if the model proposed thus far is correct, retentive alkylation necessitates approach of the electrophile to the concave face of enolate. The factors that would favor this contra-steric alkylation will be thoroughly discussed in Chapter 2.

Carlier et al. also applied similar asymmetric induction in the enantioselective synthesis of quaternary proline-derived 1,4-benzodiazepine-2,5-diones via memory of chirality (Table 1.9).[40] In light of relatively low inversion barrier of 12.2 kcal/mol of the corresponding axially chiral enolate (B3LYP/6-31+G*//B3LYP/6-31G*), MOC deprotonation/alkylation was carried out in situ at -100 °C to attain excellent yield and enantioselectivities. This successful protocol allowed the enolate to trap electrophiles instantaneously; moreover the enolate was found to have sufficient conformational stability without significant racemization at 173K with reference to ring inversion half-life of 4 min. From the equilibrium structure of the calculated enolate, Carlier also noted that the reaction carbon was slightly pyramidalized toward the concave face, which correlated with the aforementioned contra-steric alkylation.[41]

Table 1.9 In situ MOC deprotonation/trapping of **77b**

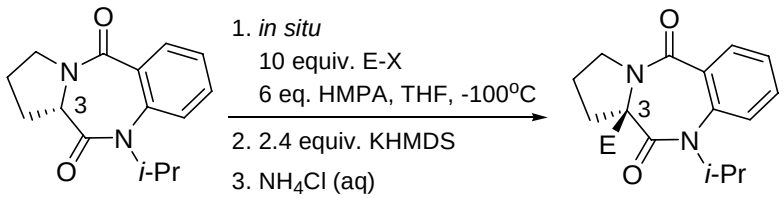

E-X	product	%yield	%ee
Allyl-Br	(+)-**78b**	75	98
BnBr	(+)-**79b**	92	96 (3*R*)
4-$MeC_6H_4CH_2Br$	(+)-**80b**	92	99 (3*R*)
2-$PhC_6H_4CH_2Br$	(+)-**81b**	82	95 (3*R*)
MeOTF	(+)-**82b**	24	>99.5 (3S)

In order to allow diverse functionalization at N(1), Carlier et al. reported an enantioselective deprotonation/alkylation of *N*-PMB 1,4-benzodiazepin-2-one (*S*)-**83e** due to the facile removal of the PMB group under mildly acidic condition.[42] Nevertheless, kinetic studies indicated that the corresponding enolate had a racemization barrier of 12.0 kcal/mol at 173K. Apart from the in situ protocol, the authors investigated MOC reactions at -109 °C (Table 1.10).

Table 1.10 MOC deprotonation/alkylation of **83e**

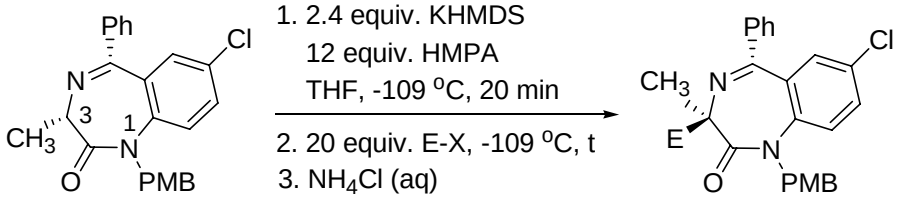

E-X	t (min)	product	%yield	%ee
BnI	10	**68e**	93	97
4-$MeC_6H_4CH_2Br$	10	**70e**	92	93
2-$PhC_6H_4CH_2Br$	60	**71e**	81	97
Allyl-I	5	**72e**	88	89
EtI	30	**83e**	8	46

The disadvantage of having the PMB substituent at N(1) was the requirement of undesirable, cryogenic reaction temperature to achieve adequate enantioselectivity. Subsequently, Carlier and co-workers found the secondary di-(*p*-anisyl)methyl (DAM) group to be bulkier and also easily removed.[43] Therefore, the large steric bulk of the DAM group at N(1) imparted a significant barrier to racemization of the axially chiral enolates, which led to excellent enantioselectivity from Ala-, Phe-, Abu-, and Met-derived 1,4-benzodiazepin-2-ones (*S*)-**67f, 69f, 84f and 85f** at -78 and -42 °C (Table 1.11) and from 1,4-benzodiazepine-2,5-diones (*S*)-**77f** and (*S*)-**93f** derived from proline and thioproline at -100 °C (Table 1.12). Compared to the deprotonation/alkylation results of *N*-*i*-Pr analogue of **67b**, product yields were significantly improved (Table 1.11, cf. **68**, **70** and **72**). The advantages of the DAM group are also evident in reaction with ethylbromoacetate and ethyl iodide (Table 1.11, **86** and **87**), where the corresponding alkylations of the *N*-*i*-Pr analogue (*S*)-**67b** failed. Moreover, it is important to note that addition of HMPA is not necessary to achieve high yields of the alkylated products of 1,4-benzodiazepine-2,5-diones **77f** and **93f** (Table 1.12, cf. entries 1 and 2, 3 and 4, and 5 and 6); in contrast, HMPA is required for acceptable yields in MOC reactions of 1,4-benzodiapin-2-ones.

Table 1.11 Enantioselective deprotonation/alkylation of Ala-, Phe-, Abu-, and Met-derived *N*-DAM-1,4-benzodiazepin-2-ones (*S*)-**67f, 69f, 84f and 85f**

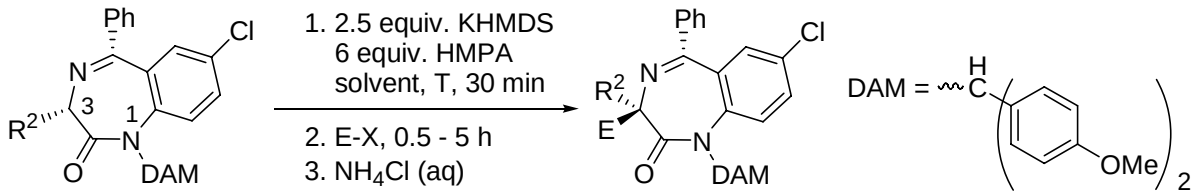

(*S*)-**67f, 69f, 84f, 85f** **68f, 70f, 72f, 74f, 86-92f**

Substrate	R^2	solvent	T (°C)	E[a]	Product	% yield[b]	% ee[b]
67f	CH_3	THF	-78	Bn	**68f**	80 (72)	99 (*97*) *R*
67f	CH_3	THF	-78	4-$MeC_6H_4CH_2$-	**70f**	82 (76)	>99.5 (94) *R*
67f	CH_3	THF	-78	Allyl	**71f**	88 (76)	99 (94)
67f	CH_3	THF	-78	-CH_2CO_2Et	**86f**	86 (0)	98 (na) *R*
67f	CH_3	THF	-78	Et	**87f**	65 (0)[c]	96 (na)
69f	$PhCH_2$	DME	-42	Allyl	**74f**	58	92
69f	$PhCH_2$	DME	-42	-CN	**88f**	68	96
84f	Et	DME	-42	Bn	**89f**	65	94 *R*
84f	Et	DME	-42	Allyl	**90f**	58	94
85f	$MeSCH_2CH_2$	DME	-42	Me	**91f**	67	87
85f	$MeSCH_2CH_2$	DME	-42	-CN	**92f**	80	87

[a] Electrophiles (equiv.) used: BnBr (10), 4-$MeC_6H_4CH_2Br$ (10), allyl bromide (10), $BrCH_2CO_2Et$ (10), EtI (20), tosyl cyanide (2.0), MeI (10). [b] Value in parenthesis corresponds to that of the N-*i*-Pr analogue obtained from **67b**. [c] LDA provided superior yields of 84f and was used in place of KHMDS.

Furthermore, the DAM group was shown to be deprotected by acidic hydrolysis with high yield and no decay in enantioselectivity (Table 1.13). Thus, this methodology could be used to prepare enantiopure quaternary benzodiazepines with diverse N(1)-functionalization.

Table 1.12 Enantioselective deprotonation/alkylation of N-DAM-1,4-benzodiazepine-2,5-diones (*S*)-**77f** and (*S*)-**93f** derived from Proline and Thioproline

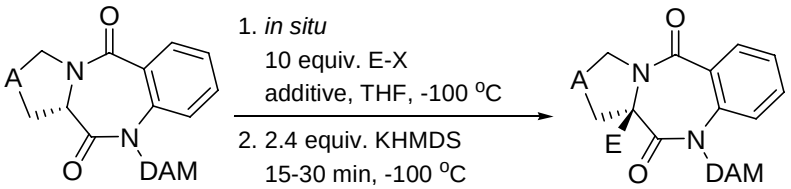

Entry	Substrate	A	Additive	E	Product	% yield	% ee
1	**77f**	CH_2	HMPA	Bn	**79f**	98	98 *R*
2	**77f**	CH_2	NA	Bn	**79f**	83	99 *R*
3	**77f**	CH_2	HMPA	4-$MeC_6H_4CH_2$-	**80f**	93	>99.5 R
4	**77f**	CH_2	NA	4-$MeC_6H_4CH_2$-	**80f**	83	99 *R*
5	**77f**	CH_2	HMPA	2-$PhC_6H_4CH_2$-	**81f**	94	99 R
6	**77f**	CH_2	NA	2-$PhC_6H_4CH_2$-	**81f**	87	94 R
7	**93f**	S	NA	Bn	**94f**	98	99
8	**93f**	S	NA	Allyl	**95f**	89	95

Table 1.13 Facile acidic removal of the *N*-DAM group

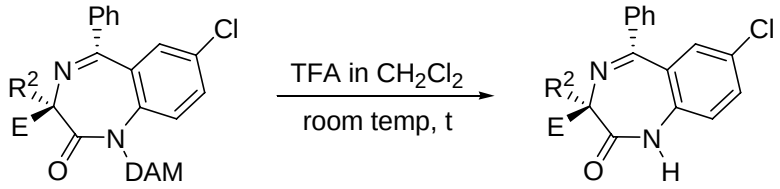

Substrate	R^2	E	% TFA-CH_2Cl_2 (v/v)	t (h)	Product	% yield	% ee
68f	Me	Bn	25	1	**68c**	96	>99.5 *R*
70f	Me	4-$MeC_6H_4CH_2$-	6.25	1.5	**70c**	98	99 *R*
72f	Me	Allyl	6.25	1	**72c**	97	98
86f	Me	-CH_2CO_2Et	6.25	1.5	**86c**	98	99 *R*
89f	Et	Bn	25	0.75	**89c**	94	98 R
90f	Et	Allyl	6.25	1.5	**90c**	99	94

1.5 Memory of Chirality in Radical Chemistry

1.5.1 Retentive Benzylic Substitution Induced by Dynamic Planar Chirality

Recently, Koning and co-workers developed a method for the stereospecific umpolung of arene-tricarbonylchromium complexes **96** derived from readily available chiral 1-arylalkanols. Calculations indicated that the benzylic radical **97** resulting from 1 electron reduction and fragmentation of **96** is actually better described as a 17-valence electron complex with an exocyclic C-C double bond (Scheme 1.20).[44]

Scheme. 1.20 17-valence electron complex **97** formed from 1 electron reduction of **96**

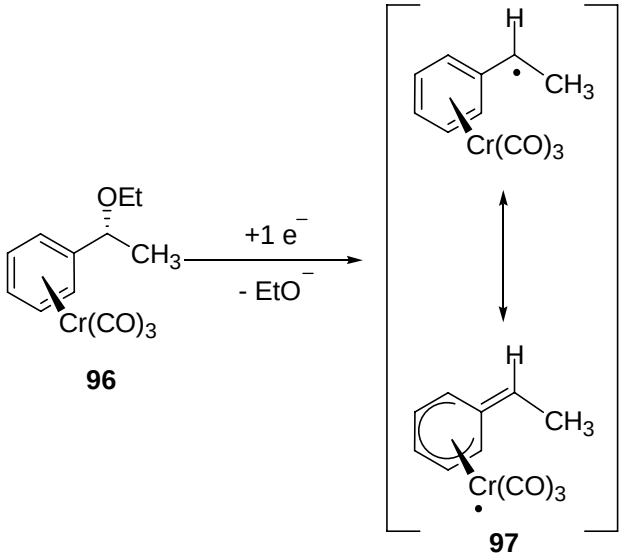

96 **97**

As such **97** would have a significant barrier to rotation along the benzylic bond; DFT calculations indicated a barrier of 13.2 kcal/mol for the racemization of **97**, corresponding to a half-life of about one minute at -78 °C (Scheme 1.21).

Scheme 1.21 Intermediate **97** with dynamic planar chirality

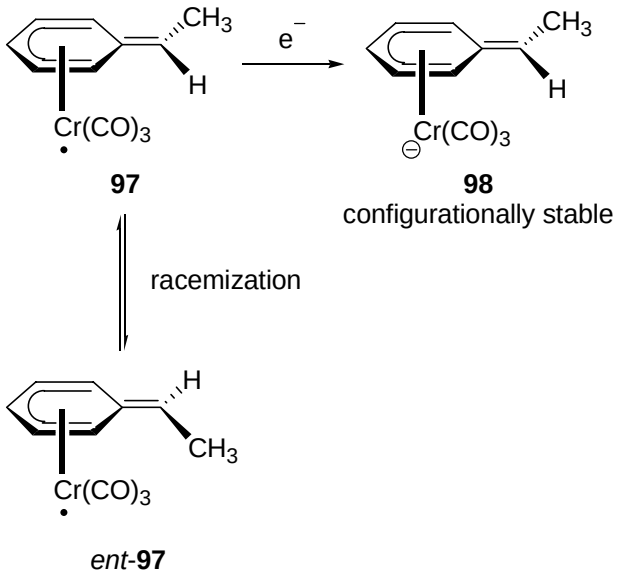

Koning et al. envisaged that if radical **97** could be generated enantioselectively from **96**, and rapidly reduced to the configurationally stable anion **98**, enantioselective alkylation at the benzylic carbon should be possible. Starting from readily available (*R*)-1-phenylethanol (91% ee), the complex **96** was obtained (91% ee). Treatment of **96** with 2.1 equivalents of lithium 4,4'-di-tert-butylbiphenyl (LiDBB) in THF at –78 °C afforded a solution of the anion **98**, which was treated with a variety of electrophiles to give rise to the desired products **99** in fair yields (37-72%) and with high degree of retention (87-99 %ee, Table 1.14).

Table 1.14 The enantioselective alkylation of **96**

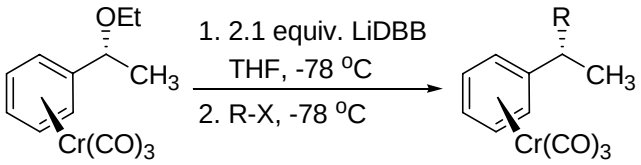

96 (91% ee) **99a-d**

Entry	RX	Product	% yield	% ee
1	TMSCl	**99a**	72	87
2	$PhCH_2Br$	**99b**	37	87
3	MeOC(O)Cl	**99c**	67	86
4	$Me_2NC(O)Cl$	**99d**	57	84

As no external chiral sources are present in these reactions, the origin of the stereoselectivity could only be ascribed to preservation of the chirality of the starting material in both radical and anionic intermediates. In this case it appears that the central chirality of the starting materials is retained in the form of the proposed planar chiral intermediate **97**.

1.5.2 Retentive Radical Trapping Controlled by a Slow Ring Inversion

It is a well-known that acyclic radicals invert rapidly, and the barrier to inversion has been estimated at less than 0.5 kcal/mol.[45] However, for a cyclic radical, the racemization and ring inversion processses would be coupled, possibly increasing the barrier. Since the barrier to chair-chair ring-inversion in the tetrahydropyranyl radical **100** is likely 5-10 kcal/mol, Rychnovsky and co-workers envisioned that if **100** could be generated in nonracemic form, stereoselective trapping might be be possible (Scheme 1.22).

Scheme 1.22 Radical intermediate **100** conformational chirality

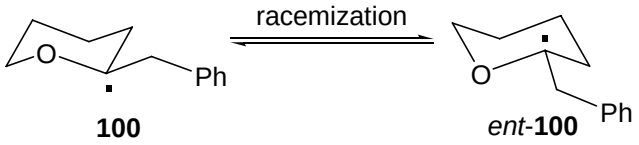

100 *ent*-**100**

Carboxylic acid **101** was prepared in optically pure form and converted to its corresponding *N*-hydroxypyridine-2-thione ester. Photolysis of the ester in toluene at -78 °C with 1 M PhSH as a hydrogen atom donor led to the expected product **102** in 86 %ee with retention of configuration (Scheme 1.23).[46] The enantiomeric excess of **102** was found to depend strongly upon the concentration of the PhSH quench, evidencing competition between ring inversion and intermolecular trapping. A similar conformational memory effect was also observed when enantiopure radical **100** was generated reductively (Scheme 1.24).

Scheme 1.23 MOC reduction of **101**

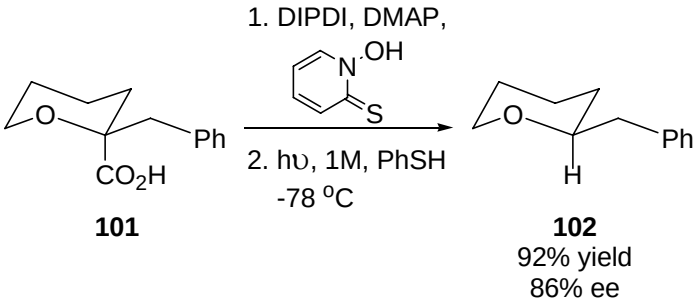

Scheme 1.24 Enantiomeric purity of **102** depended on the concentration of reducing agent

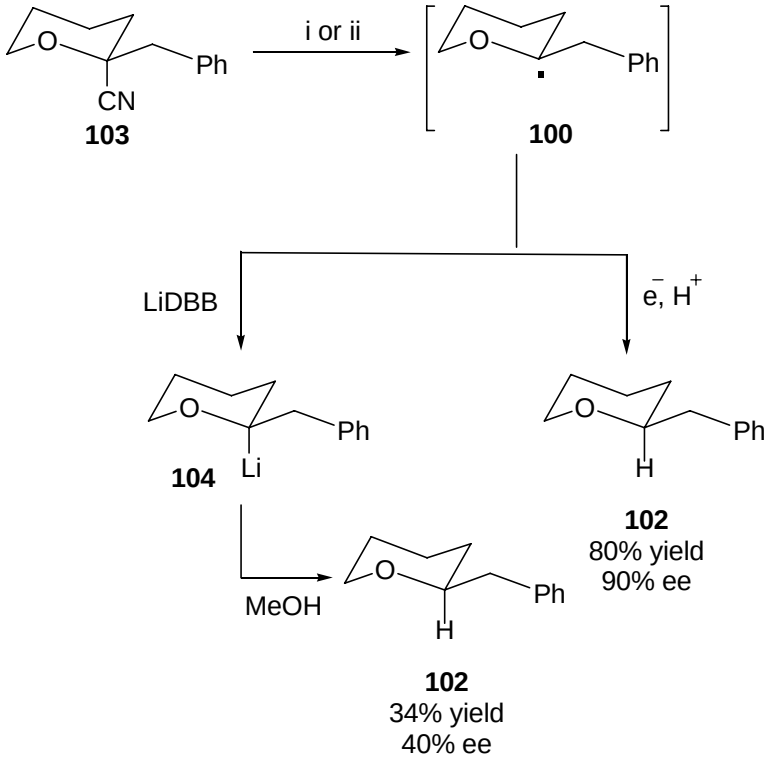

Reagents and conditions: i)LiDBB (0.63 M), THF, -78 °C; MeOH. ii)Li/NH_3 (6.4 M), THF, -78 °C.

The enantiomeric purity of the product **102** in these reactions was highly dependent upon the concentration of reducing agent, suggesting competition between reduction and racemization of radical **100**. In both the photolysis and reductive cleavage reactions, memory of the original chiral centers of **101** and **103** is proposed to be retained by the conformation of the tetrahydropyranyl ring (and not simply by the pyramidalization of a sp^3-hybridized radical). Therefore, these reactions constitute examples of memory of chirality.

1.5.3 Memory of Chirality in Radical Cyclization

Rychnovsky and co-workers have also exploited conformational chirality in the transannular cyclization of medium ring radicals (Scheme 1.25).[47]

Scheme 1.25 MOC transannular cyclization of **105**

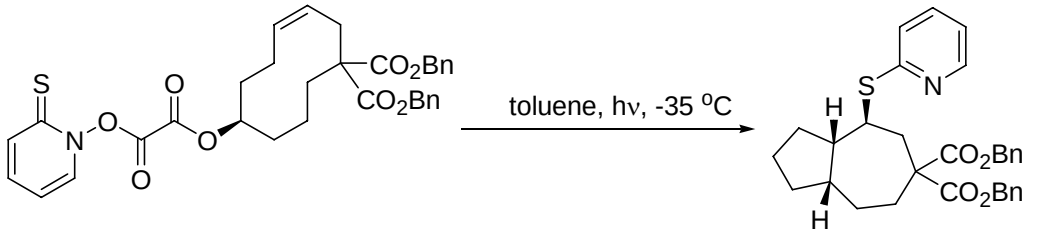

105 (86% ee) **106** (43% yield, 68% ee)

Enantiomerically enriched *N*-hydroxypyridine-2-thione mixed oxalate **105** was prepared in situ from the corresponding cyclodecenyl alcohol and photolysed in toluene at –35 °C; bicyclic product **106** was obtained in 68 %ee. The authors proposed that photolysis of **105** generated cyclodecenyl radical **107** (Scheme 1.26).

Scheme 1.26 Proposed mechanism of transannular cyclization of **105**

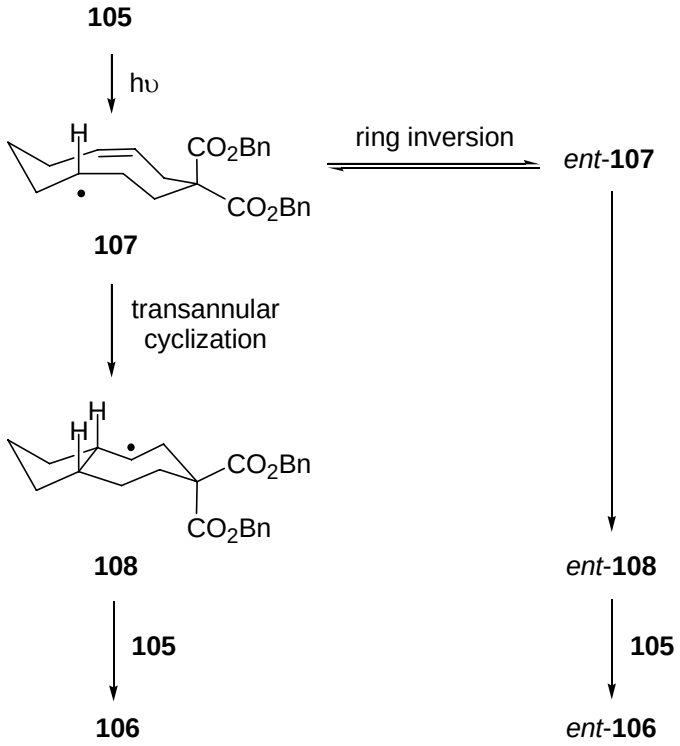

Radical **107** possesses conformational chirality and is generated in nonracemic form from the enantioenriched starting material. If transannular cyclization of **107** can compete effectively with inversion of the medium ring conformation to *ent*-**107**, bicyclic radical **108** will be formed in nonracemic form. Finally, transfer of the 2-thiopyridiyl moiety from the starting material (**105**) would generate optically enriched product **106** and propagate the radical chain.

Curran and coworkers have developed a series of highly enantioselective radical cyclization reactions that convert atropisomeric starting materials to centrally chiral products.[48-50] Although these reactions may best be considered as examples of "transfer of chirality," their success also depends upon the transient conformational chirality of a reactive intermediate. In this sense these reactions can also be considered as examples of memory of chirality. *o*-Iodoacrylanilides **109** are atropisomeric and the (*M*)- and (*P*)-enantiomers were prepared via a chiral pool route from lactic acid (Scheme 1.27). The barrier for interconversion of the enantiomers of **109** was estimated to be 30.8 kcal/mol. However, upon radical deiodination, a much more readily racemized radical **110** would be formed. Since oxindoles (*R*)-**111** and (*S*)-**111** were obtained in high enantiomeric excess from the antipodal starting materials, the authors concluded that cyclization of aryl radical **110** was much faster than racemization .

Scheme 1.27 MOC radical cyclization of **109**

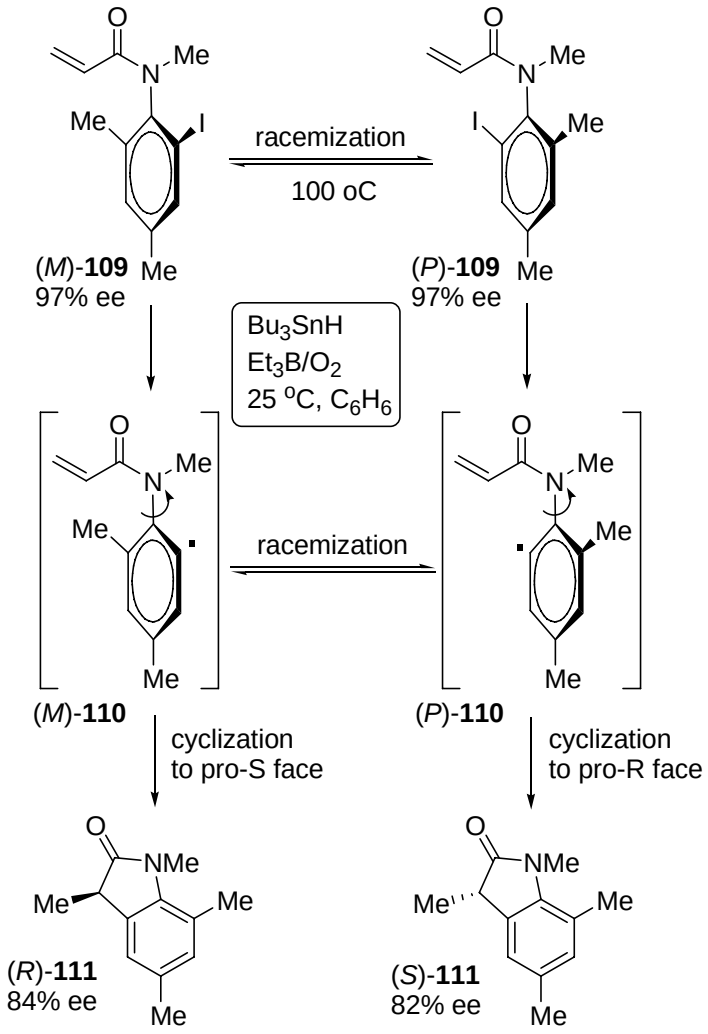

Note that the absolute configuration of the products indicates that radical cyclization of (*M*)-**110** occurs on the pro-*S* (i.e. β)-face of the alkene. Curran has described this process in terms of the alkene twisting toward the aryl radical.[50]

1.5.4. Memory of Chirality in the Cyclization of Photochemically-generated Diradicals.

In 1999, Giese and coworkers reported that an alanine derivative **112** underwent asymmetric photocyclization in the presence of naphthalene, a triplet quencher.[51] Two diastereomeric products **113** and **114** were formed in high enantiomeric excess (Scheme 1.28).

Scheme 1.28 MOC photocyclization of **112**

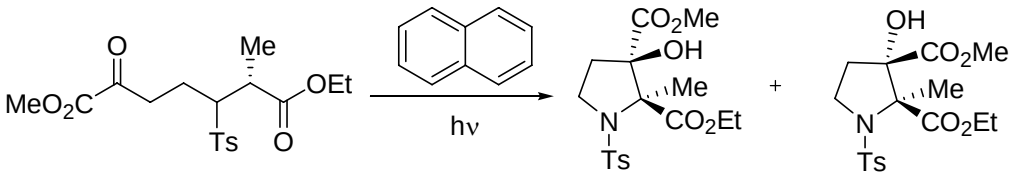

112

113
40% yield
96% ee

114
7% yield
94% ee

Note that **113** and **114** have identical configurations at the C(2). The authors proposed that asymmetric reaction occurred via a singlet diradical intermediate. Photochemical reaction in the absence of a triplet quencher gave significantly lower asymmetric induction, suggesting intervention of the longer lived (and thus racemizable) triplet diradical. The formation of major product **113** was rationalized to occur via formation of helically chiral singlet diradical (*M*)-**115** (Scheme 1.29).

Scheme 1.29 Helically chiral singlet diradical **115**

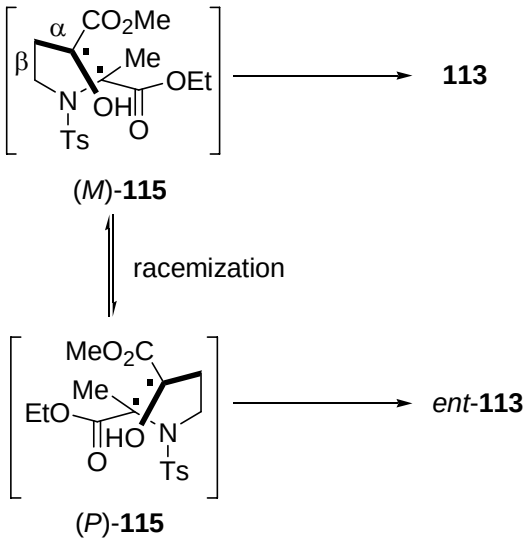

Unrestricted Hartree-Fock calculations on **115** indicated that rotation of the β-single bond would be the slow step of racemization, and would feature a barrier of 5 kcal/mol. This barrier, though quite low, is higher than the expected 2 kcal/mol barrier for cyclization of the singlet diradical. The enantiospecific formation of **115** in the (*M*)-conformation can be rationalized in terms of the (*S*)-configuration of starting material **112** and the intramolecular

nature of the hydrogen atom abstraction. Finally, the formation of the minor diastereomer **114** can be rationalized in terms of a singlet diradical intermediate that differs from (*M*)-**115** only in the orientation of the α-sigma bond.

An asymmetric cyclization of a diradical generated by photodecarboxylation was reported by Griesbeck and coworkers.[52] Upon irradiation L-proline derivative **116** formed benzodiazepine derivative **117** in 86% ee and greater than 98% de (Scheme 1.30).

Scheme 1.30 MOC photodecarboxylation of **116**

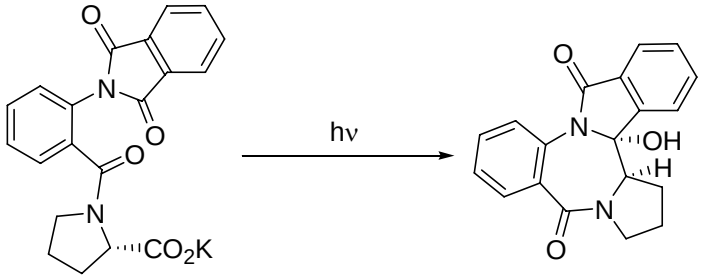

116 **117**
86% ee (>98% de)
45% yield

The high enantioselectivity was initially unexpected, because **117** results from the recombination of a 1,7-triplet diradical. As described above, the intervention of triplet diradicals proved deleterious to the enantioselectivity of reaction of alanine ester **112**, since it possesses only low rotation barrier single bonds. However, the authors proposed that the conformationally chiral 1,7-triplet diradical formed by photodecarboxylation of **116** exhibits a high barrier to rotation around the sp^2-sp^2 C-N(prolyl) bond. In suppport of this proposal, molecular mechanics calculations on **116** indicated a barrier of 13 kcal/mol about this bond. The authors did not speculate as to how the diradical intermediate was formed in enantiopure form, but a strong conformational preference in the starting material **116** is likely responsible.

1.5.5 Diastereoselective Photocycloaddition Controlled by Crystallization

Sakamoto and co-workers developed a methodology to control stereochemistry in photocycloaddition by using crystallization and memory effect of conformational chirality.[53]

Proline-derived 2-alkoxy-1-naphthamides existed in a mixture of conformational diastereomers in solution. Crystallization was applied to converge the mixture into single diastereomer (*M*)-(*S*)-**118** (Scheme 1.30). Then the crystal was dissolved at low temperature and followed by photocycloaddition of the amide with 9-cyanoathracene led to 4+4 adducts **119a-b** in near perfect diastereoselectivity at -20 °C (Scheme 1.32). Although this is not a true MOC reaction as there is a proline stereogenic center in **118**, it is still interesting to address the memory effect of the frozen conformation of the single diastereomer involved in the asymmetric synthesis.

Scheme 1.31 Convergence of conformational epimers into single diastereomer

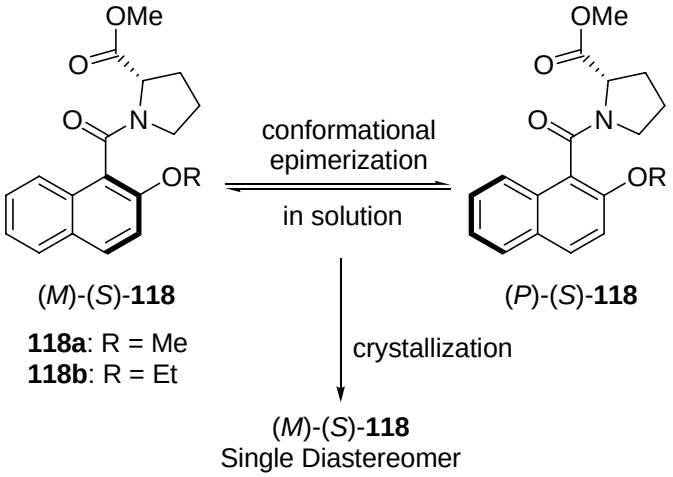

Scheme 1.32 Diastereoselective photocycloaddition of **118** with 9-cyanoathracene

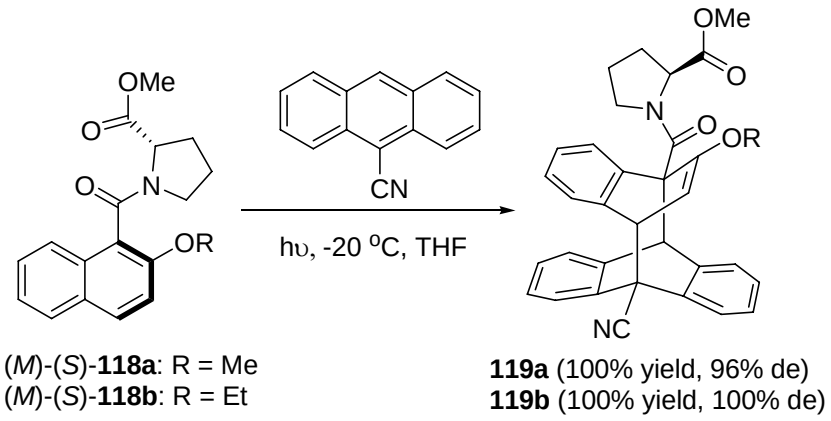

1.6 Memory of Chirality Involving Carbocation Intermediates

Matsumura and co-workers found the *N*-benzoylated serine derivative **120** was electrochemically oxidized to give **121** with inversion of configuration in 69% yield and 39% ee (Scheme 1.33).[54]

Scheme 1.33 MOC electrochemical oxidation of **120**

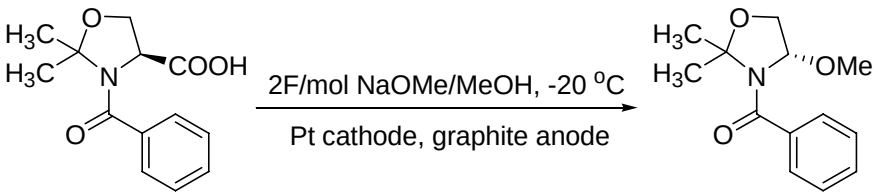

120 **121** (80% ee)

To increase the enantioselectivity, analog **122** bearing a bulky *o*-phenylbenzoyl as the *N*-protecting group was synthesized. Interestingly, electrolysis of **122** proceeded in retentive fashion, giving α-methoxylated serine derivative **123** in 80% ee (Scheme 1.34).[53]

Scheme 1.34 MOC electrochemical oxidation of **122**

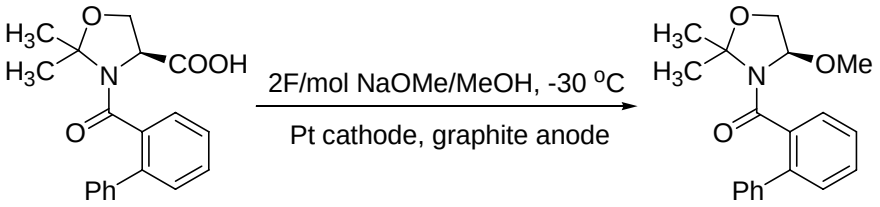

122 **123** (80% ee)

To account for the retentive stereochemistry, the authors proposed that reaction occurred via conformationally chiral iminium ion **124**. Since the *o*-phenyl group shields the bottom face of the iminium ion, methanol attacks from above, yielding **123** (Scheme 1.35). Formation of the conformationally chiral iminium **124** in the indicated enantiomeric form was rationalized in terms of oxidation of the most stable conformer (AM1) of the enantiopure starting material **122**. Racemization of **124** would be slowed by hindered rotation of the sp^2-sp^2 amide single bond, and thus capture by MeOH leads to **123** in high enantiomeric purity.

Scheme 1.35 Proposed mechanism for retentive stereochemistry in electrochemical oxidation of **122**

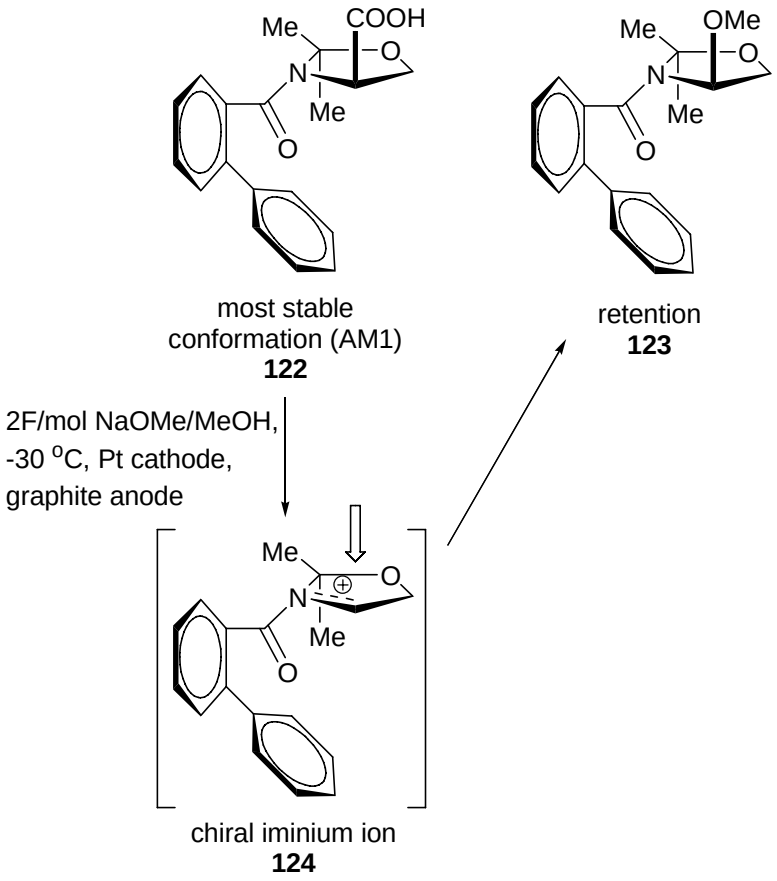

1.7 Memory of Chirality in Gold(I)-Catalyzed Reactions

1.7.1 Enantioselective Gold(I)-Catalyzed Rautenstrauch Rearrangement

Recently, Toste and co-workers developed enantioselective Au(I)-catalyzed cyclopentenone synthesis.[55] Enantioenriched propargyl pivaloates **125a-e** underwent Rautenstrauch rearrangement to deliver cyclopentenones **126a-e** in high yields and enantioselectivities (Table 1.15). The authors also proposed a non-MOC mechanism to account for the excellent chirality transfer (Scheme 1.36). The stereoselectivity was attributed to involve a transition state **128a** in which the C(1)-C(5) bond formed before the cleavage of the bond from O to stereogenic carbon C(3), where the leaving group occupied a position orthogonal to the alkene plane.

Table 1.15 Enantioselective Au(I)-catalyzed Rautenstrauch rearrangement

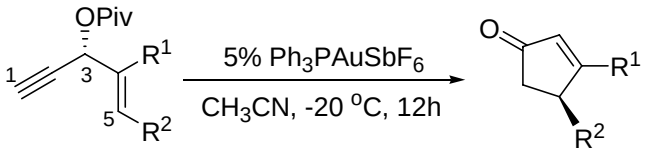

125a-e **126a-e**

Entry	Substrate	Product	% yield	% ee
1	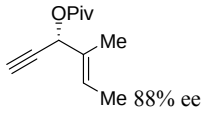	**126a**	84	82
2	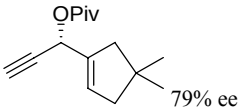	**126b**	80	77
3	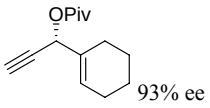	**126c**	86	91
4	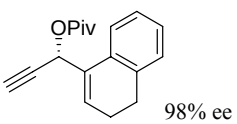	**126d**	88	96
5	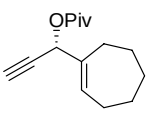	**126e**	82	83

Scheme 1.36 Toste's proposed non-MOC mechanism for the enantioselective Au(I)-catalyzed cyclopentenone synthesis

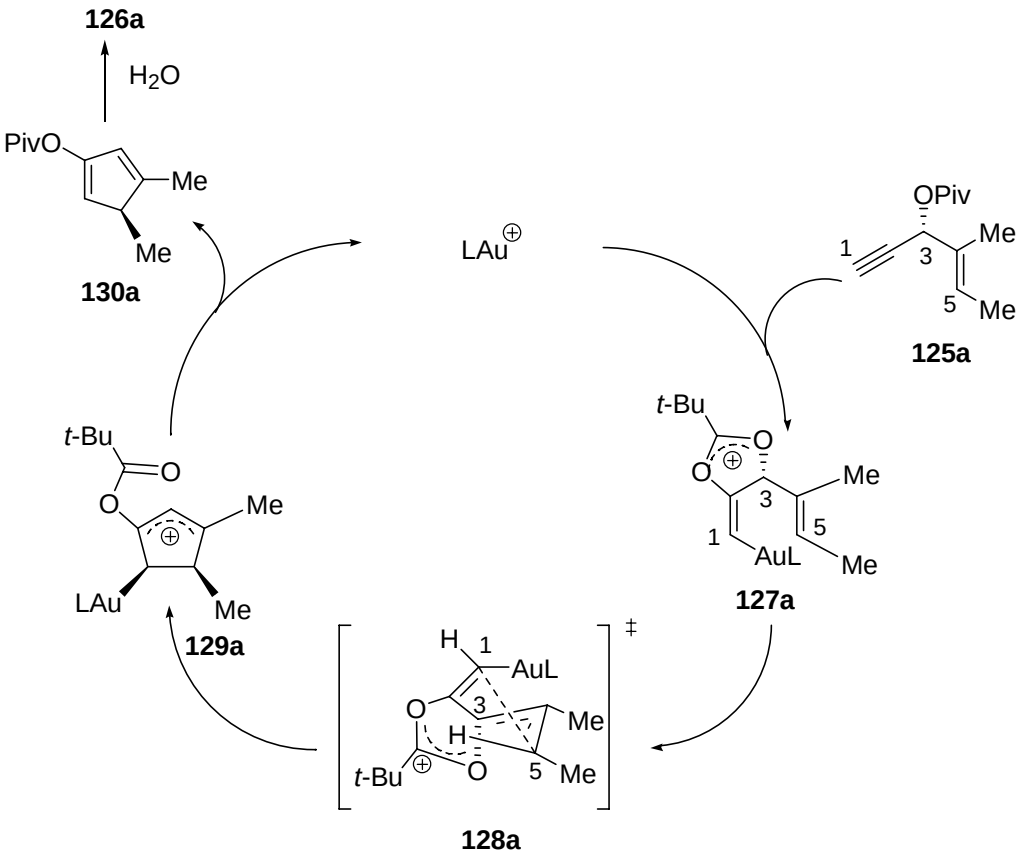

Subsequently, de Lera et al. studied this enantioselective Au(I)-catalyzed Rautenstrauch rearrangement by computation.[56] The calculations supported the proposal that the Au(I)-promoted pivaloyl transfer to C(2) preceded the formation of bond C(1)-C(5), and that the central chirality at C(3) was preserved as axial chirality along the C(3)-C(4) axis in the pentadienyl cation intermediate **134a** (Scheme 1.37). The helical descriptors (*M*)- and (*P*)- are used to describe the sense of ring chirality, based on the sign of the C(1)-C(2)-C(3)-C(4) dihedral angle. In order to undergo the chirality transfer efficiently, computation results predicted that the helix interconversion between (*M*)- and (*P*)-**134a** should be unfavorable. Furthermore, it should be noted that this MOC mechanism has been accepted by Toste as an alternative possibility in a recent review.[57]

Scheme 1.37 Mechanistic studies of the Au(I)-catalyzed Rautenstrauch rearrangement of **131a***

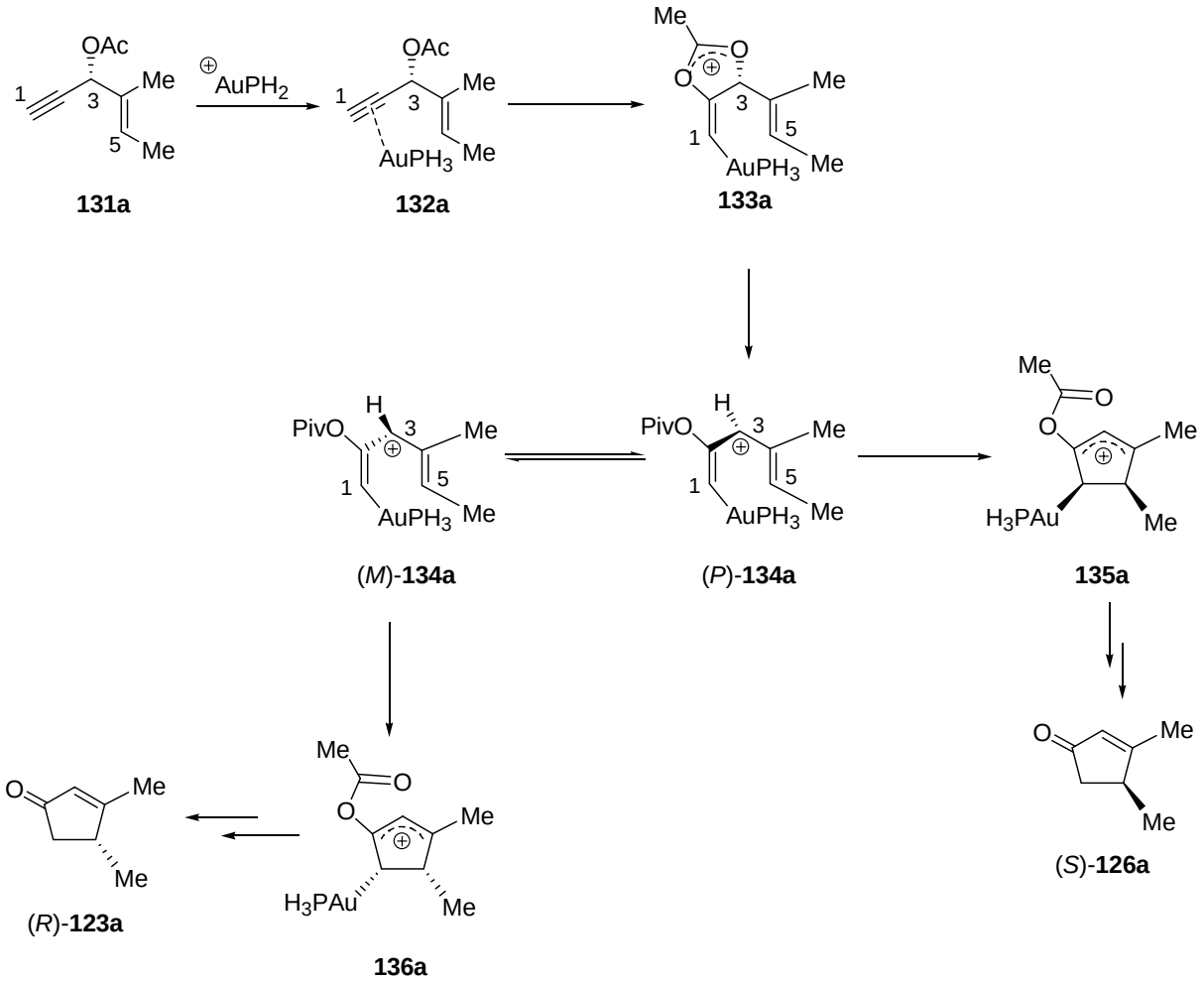

*In order to lower the computational cost, the original pivaloate and gold's ligand PPh_3 were replaced by acetate and respectively.

1.7.2 Memory of Chirality in the Gold(I)-Catalyzed Intramolecular Carboalkoxylation of Alkynes

Toste et al. reported another type of MOC Au(I)-catalyzed reaction.[58] Alkynes **137-139** underwent enantioselective Au(I)-promoted intramolecular carboalkoxylation to give enantioenriched indenyl ethers **140-142** with inversion of configuration (Table 1.16). The authors proposed that the central chirality at of the C-O bond was retained in the axial chirality of carbocation intermediate **145** (Scheme 1.38). The axial chirality was transferred

back to the chiral center when the vinylgold(I) intermediate **145** underwent intramolecular attack to the carbocation via transition state **146**.

Table 1.16 MOC Au(I)-catalyzed intramolecular carboalkoxylation

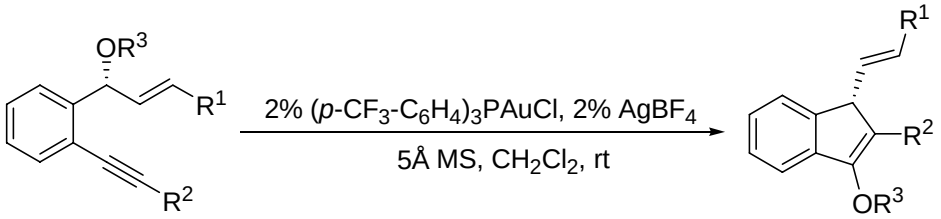

137-139 **140-142**

Substrate	R^1	R^2	R^3	Product	% yield	% ee
137 (82% ee)	Ph	CO_2CH_3	CH_3	**140**	99	81
138 (99% ee)	H	Ph	CH_3	**141**	92	95
139 (73% ee)	Ph	CO_2CH_3	Allyl	**142**	92	59

Scheme 1.38 Proposed mechanism of MOC Au(I)-catalyzed intramolecular carboalkoxylation

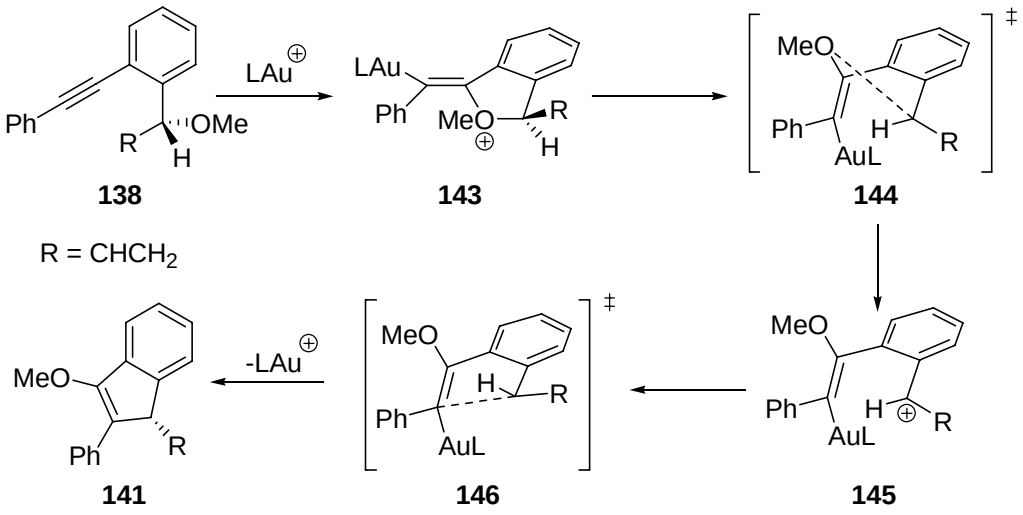

1.8 Summary

Memory of chirality is an emerging strategy for enantioselective synthesis. In general, MOC methods involve destruction of the sole original stereogenic center of a starting material, enantioselective generation of conformationally chiral intermediate, and subsequent enantioselective transformation into a centrally chiral product. For intramolecular or solvent-capture reactions, low barrier sp^3-sp^3 or sp^2-sp^3 bonds in the conformationally chiral intermediate can provide a sufficient barrier to racemization to permit enantioselective reaction. However, for intermolecular reactions, higher barrier sp^2-sp^2 bonds typically must be present to guarantee a sufficient racemization half-life for the reactive intermediate.

Successful MOC reactions must fulfill three conditions. First, the enantiopure centrally chiral starting materials must be enantioselectively transformed into a conformationally chiral intermediate. Second, this chiral intermediate must not racemize during the timescale of the reaction. Third, transformation of the conformationally chiral intermediate back to a centrally chiral product must occur with excellent enantioselectivity

To date, MOC has found most application in enolate chemistry, but the MOC principle has also been successfully applied in reactions involving radical, diradical, and carbocation intermediates. As chemists grow in their understanding of how to generate enantiopure, conformationally chiral reactive intermediates, further applications of the MOC principle will follow. Like the "self-regeneration of stereocenters" strategy,[6] successful MOC methods will use cheap, abundant members of the chiral pool as starting materials. Therefore, in certain cases, MOC methods may prove competitive with catalytic asymmetric synthesis for the preparation of enantiomerically pure compounds.

References for Chapter 1

1. Zhao, H.; Hsu, D. C.; Carlier, P. R., Memory of Chirality: an Emerging Strategy for Asymmetric Synthesis. *Synthesis* **2005**, 1-16.

2. Kawabata, T.; Yahiro, K.; Fuji, K., Memory of Chirality: Enantioselective Alkylation Reactions at an Asymmetric Carbon Adjacent to a Carbonyl Group. *Journal of the American Chemical Society* **1991,** 113, (25), 9694-9696.

3. Seebach, D.; Wasmuth, D., Alkylation of Amino Acids without Loss of Optical Activity: α- and β-Alkylation of an Aspartic Acid Derivative. *Angewandte Chemie-International Edition* **1981,** 20, 971.

4. Fuji, K.; Kawabata, T., Memory of chirality—A New Principle in Enolate Chemistry. *Chemistry: a European Journal* **1998,** 4, (3), 373-376.

5. Wanyoike, G. N.; Onomura, O.; Maki, T.; Matsumura, Y., Highly Enhanced Enantioselectivity in the Memory of Chirality via Acyliminium Ions. *Organic Letters* **2002,** 4, (11), 1875-1877.

6. Seebach, D.; Sting, A. R.; Hoffman, M., Self-Regeneration of Stereocenters (SRS)--Applications, Limitations, and Abandonment of a Synthetic Principle. *Angewandte Chemie-International Edition* **1996,** 35, 2708-2748.

7. Kawabata, T.; Fuji, K., Memory of Chirality: Asymmetric Induction Based on Dynamic Chirality of Enolates. In *Topics in Stereochemistry*, Denmark, S. E., Ed. John Wiley & Sons, Inc.: New York, 2003; Vol. 23, pp 175-205.

8. Eyring, H., The Activated Complex and the Absolute Rate of Chemical Reactions. *Chemistry Review* **1935,** 17, (1), 65-77.

9. Eliel, E. L.; Wilen, S. H.; Mander, L. N., Conformations of Acyclic Molecules. In *Stereochemistry of Organic Compounds*, John Wiley & Sons: New York, 1994; pp 597-606.

10. Eliel, E. L.; Wilen, S. H.; Mander, L. N., Biphenyls. Atropisomerism. In *Stereochemistry of Organic Compounds*, John Wiley & Sons: New York, 1994; pp 1142-1148.

11. Wirth, T., New Strategies to α-alkylated α-Amino Acids. *Angewandte Chemie-International Edition* **1997,** 36, 225-227.

12. Cativiela, C.; Díaz-de-Vellagas, M. D., Stereoselective synthesis of quaternary α-amino acids. Part 1: Acyclic Compounds. *Tetrahedron: Asymmetry* **1998,** 40, (9), 3517-3599.

13. Kawabata, T.; Wirth, T.; Yahiro, K.; Suzuki, H.; Fuji, K., Direct Asymmetric α-Alkylation of Phenylalanine Derivatives Using No External Chiral Sources. *Journal of the American Chemical Society* **1994,** 116, (23), 10809-10810.

14. Kawabata, T.; Suzuki, H.; Nagae, Y.; Fuji, K., A Chiral Nonracemic Enolate with Dynamic Axial Chirality: Direct Asymmetric α-Methylation of α-Amino Acid Derivatives. *Angewandte Chemie-International Edition* **2000,** 39, (12), 2155-2157.

15. Kawabata, T.; Chen, J.; Suzuki, H.; Fuji, K., Stereochemical Study on α-Alkylation of β-Branched α-Amino Acid Derivatives via Memory of Chirality. *Synthesis* **2005**, 1368-1377.

16. Cativiela, C.; Diaz-de-Villegas, M. D., Stereoselective Synthesis of quaternary α-amino acids. Part 2: Cyclic compounds. *Tetrahedron: Asymmetry* **2000,** 11, 645-732.

17. Kawabata, T.; Kawakami, S.; Majumdar, S., Asymmetric Cyclization via Memory of Chirality: A Concise Access to Cyclic Amino Acids with a Quaternary Stereocenter. *Journal of the American Chemical Society* **2003,** 125, 13012-13013.

18. Kawabata, T.; Majumdar, S.; Tsubaki, K.; Monguchi, D., Memory of chirality in intramolecular conjugate addition of enolates: a novel access to nitrogen heterocycles with contiguous quaternary and tertiary stereocenters. *Organic & Biomolecular Chemistry* **2005,** 3, (9), 1609-1611.

19. Kawabata, T.; Matsuda, S.; Kawakami, S.; Monguchi, D.; Moriyama, K., Stereochemical diversity in asymmetric cyclization via memory of chirality. *Journal of the American Chemical Society* **2006,** 128, (48), 15394-15395.

20. Kawabata, T.; Öztürk, O.; Chen, J.; Fuji, K., Chirality transfer during alkylation of chiral amides. *Chemical Communications* **2003**, 162-163.

21. Kawabata, T.; Kawakami, S.-p.; Fuji, K., Enantioselective a-allylation of a phenylalanine derivative under the control of aggregation of a chiral nonracemic enolate. *Tetrahedron Letters* **2002,** 43, 1465-1467.

22. Kawabata, T.; Kawakami, S.-p.; Shimada, S.; Fuji, K., Control of the enantioselectivity of alkylation of phenylalanine derivatives by regulation of the aggregate structure of chiral enolate intermediates. *Tetrahedron* **2003,** 59, 965-974.

23. Beagley, B.; Betts, M. J.; Pritchard, R. G.; Schofield, A.; Stoodley, R. J.; Vohra, S., A Cyclisation Reaction of Methyl (4R)-3-(2-Diazo-3-oxobutanoyl)thiazolidine-4-carboxylate which proceeds with Retention of Configuration, probably via a Planar Ester Enolate Intermediate possessing Axial Chirality. *Chemical Communications* **1991**, 924-925.

24. Beagley, B.; Betts, M. J.; Pritchard, R. G.; Schofield, A.; Stoodley, R. J.; Vohra, S., 'Hidden' Axial Chirality as a Stereodirecting Element in Reactions Involving Enol(ate) Intermediates. Part 1. Cyclisation Reactions of Methyl (4R)-3-(2-Diazo-3-oxobutanoyl)thiazolidine-4-carboxylate and Related Compounds. *Journal of the Chemical Society, Perkin Transactions I* **1993**, 1761-1770.

25. Betts, M. J.; Pritchard, R. G.; Schofield, A.; Stoodley, R. J.; Vohra, S., 'Hidden' axial chirality as a stereodirecting element in reactions involving enol(ate) intermediates. Part 2. Cyclisation reaction of methyl (4*R*)-3-(2-diazo-3-oxobutanoyl)-1,1-dioxo-1λ^6,3- (and 1-oxo-1λ^4,3-) thiazolidine-4-carboxylates. *Journal of the Chemical Society, Perkin Transactions I* **1999**, 1067-1072.

26. Brewster, A. G.; Frampton, C. S.; Jayatissa, J.; Mitchell, M. B.; Stoodley, R. J.; Vohra, S., Stereoselective intramolecular aldol reactions of (4*R*)-3-(3-oxobutanoyl)-1,3-thiazolidine-4-carboxylates believed to be directed by 'self-induced' axial chirality. *Chemical Communications* **1998**, 299-300.

27. Brewster, A. G.; Jayatissa, J.; Mitchell, M. B.; Schofield, A.; Stoodley, R. J., Memory of chirality effects in aldol cyclisations of 1-(3-oxobutyryl) derivatives of L-4-oxaproline and L-proline isopropyl esters. *Tetrahedron Letters* **2002,** 43, 3919-3922.

28. Gerona-Navarro, G.; Bonache, M. A.; Herranz, R.; García-López, M. T.; González-Muñiz, R., Entry to New Conformationally Constrained Amino Acids. First Synthesis of 3-Unsubstituted 4-Alkyl-4-carboxy-2-azetidinone Derivatives via an Intramolecular N^{α}-C^{α}-Cyclization Strategy. *Journal of Organic Chemistry* **2001,** 66, 3538-3547.

29. Bonache, M. A.; Gerona-Navarro, G.; Garcia-Aparicio, C.; Alias, M.; Martin-Martinez, M.; García-López, M. T.; Lopez, P.; Cativiela, C.; Gonzalez-Muniz, R., Memory of chirality in the stereoselective synthesis of b-lactams: importance of the starting amino acid derivative. *Tetrahedron: Asymmetry* **2003,** 14, 2161-2169.

30. Bonache, M. A.; Cativiela, C.; Garcia-Lopez, M. T.; Gonzalez-Muniz, R., beta-lactams derived from phenylalanine and homologues: effects of the distance between the aromatic rings and the alpha-stereogenic reactive center on the memory of chirality. *Tetrahedron Letters* **2006,** 47, (33), 5883-5887.

31. Gees, T.; Schweizer, W. B.; Seebach, D., An Unusual Rearrangement of a Lithiated N-Acyl-tetrahydroisoquinoline to an Amino-indan Skeleton and Structural Comparison of 3-Amino-2-methylindane- and -tetrahydronapthalene-2-carboxylic Acids as Possible Building Block for Peptide-Turn Mimics. *Helvetica Chimica Acta* **1993,** 76, 2640-2653.

32. Evans, B. E.; Rittle, K. E.; Bock, M. G.; DiPardo, R. M.; Freidinger, R. M.; Whitter, W. L.; Lundell, G. F.; Veber, D. F.; Anderson, P. S.; Chang, R. S. L.; Lotti, V. J.; Cerino, D. J.; Chen, T. B.; Kling, P. J.; Kunkel, K. A.; Springer, J. P.; Hirschfield, J., Methods for Drug Discovery: Development of Potent, Selective, Orally Effective Cholestocytokinin Antagonists. *Journal of Medicinal Chemistry* **1988,** 31, 2235-2246.

33. Ellman, J. A., Design, Synthesis, and Evaluation of Small-Molecule Libraries. *Accounts of Chemical Research* **1996,** 29, 132-143.

34. Carlier, P. R.; Zhao, H.; DeGuzman, J.; Lam, P. C.-H., Enantioselective Synthesis of "Quaternary" 1,4-Benzodiazepin-2-one Scaffolds via Memory of Chirality. *Journal of the American Chemical Society* **2003,** 125, 11482-11483.

35. Linscheid, P.; Lehn, J.-M., Étude cinétiques et conformationnelles par résonance magnétique nucléaire. VII.Inversion de cycle dans des benzo-diazépinones. *Bulletin de la Societe Chimique de France* **1967**, (3), 992-997.

36. Konowal, A.; Snatzke, G.; Alebic-Kolbah, T.; Kajfez, F.; Rendic, S.; Sunjic, V., General Approach to Chiroptical Characterization of Binding to Prochiral and Chiral 1,4-Benzodiazepin-2-ones to Human Serum Albumin. *Biochemical Pharmacology* **1979,** 28, 3109-3113.

37. Gilman, N. W.; Rosen, P.; Earley, J. V.; Cook, C.; Todaro, L. J., Atropisomers of 1,4-Benzodiazepines. Synthesis and Resolution of a Diazepam-Related 1,4-Benzodiazepine. *Journal of the American Chemical Society* **1990,** 112, 3969-3978.

38. Lam, P. C.-H.; Carlier, P. R., Experimental and Computational Studies of Ring Inversion of 1,4-Benzodiazepin-2-ones: Implications for Memory of Chirality Transformations. *Journal of Organic Chemistry* **2005,** 70, 1530-1538.

39. Sunjic, V.; Lisini, A.; Sega, A.; Kovac, T.; Kajfez, F.; Ruscic, B., Conformation of 7-Chloro-5-phenyl-d_5-3(*S*)-methyl-dihydro-1,4-benzodiazepin-2-one in Solution. *Journal of Heterocyclic Chemistry* **1979,** 16, 757-761.

40. MacQuarrie-Hunter, S.; Carlier, P. R., Highly enantioselective synthesis of rigid, quaternary 1,4-benzodiazepin-2,5-diones derived from proline *Organic Letters* **2005,** 7, 5305-5308.

41. Seebach, D.; Maetzke, T.; Petter, W.; Klötzer, B.; Plattner, D. A., Pyramidalization and reactivity of trigonal centers. X-ray Crystal Structure Analysis of Two Silyl Enol Ethers from 1-Benzoyl and 1-(Methoxycarbonyl)-2-*tert*-butyl-3,5-dimethyl-4-imidazolidinone (Reagents for Amino Acid Synthesis) *Journal of the American Chemical Society* **1991,** 113, (5), 1781-1786.

42. Carlier, P. R.; Lam, P. C.-H.; DeGuzman, J.; Zhao, H., Memory of Chirality Trapping of Low Inversion Barrier 1,4-Benzodiazepin-2-one Enolates. *Tetrahedron: Asymmetry* **2005,** 16, 2998-3002.

43. Carlier, P. R.; Zhao, H.; MacQuarrie-Hunter, S. L.; DeGuzman, J. C.; Hsu, D. C., Enantioselective synthesis of diversely substituted quaternary 1,4-benzodiazepin-2-ones and 1,4-benzodiazepine-2,5-diones. *Journal of the American Chemical Society* **2006,** 128, (47), 15215-15220.

44. Schmalz, H.-G.; Koning, C. B. d.; Bernicke, D.; Siegel, S.; Pfletschinger, A., Memory of Chirality in Electron Transfer Mediated Benzylic Umpolung Reactions of Arene-$Cr(CO)_3$ complexes. *Angewandte Chemie-International Edition* **1999,** 38, 1620-1623.

45. Griller, D.; Ingold, K. U.; Krusic, P. J.; Fischer, H., (radical inversion barrier). *Journal of the American Chemical Society* **1978,** 100, 6750-6752.

46. Buckmelter, A. J.; Kim, A. I.; Rychnovsky, S. D., Conformational Memory in Enantioselective Radical Reduction and a New Radical Clock Reaction. *Journal of the American Chemical Society* **2000,** 122, 9386-9390.

47. Dalgard, J. E.; Rychnovsky, S. D., Memory of Chirality in the Transannular Cyclization of Cyclodecenyl Radicals. *Organic Letters* **2004,** 6, 2713-2716.

48. Curran, D. P.; Liu, W.; Chen, C. H.-T., Transfer of Chirality in Radical Cyclizations. Cyclization of *o*-Haloacrylanilides to Oxindoles with Transfer of Axial Chirality to a Newly Formed Stereocenter. *Journal of the American Chemical Society* **1999,** 121, 11012-11013.

49. Curran, D. P.; Chen, C. H.-T.; Geib, S. J.; Lapierre, A. J. B., Asymmetric radical cyclization reactions of axially chiral *N*-allyl-*o*-iodoanilides to form enantioenriched *N*-acyl dihydroindoles. *Tetrahedron* **2004,** 60, 4413-4424.

50. Petit, M.; Geib, S. J.; Curran, D. P., Asymmetric reactions of axially chiral amides: use of removable *ortho*-substituents in radical cyclizations of *o*-iodoacrylanilides and *N*-allyl-*N*-*o*-iodoacrylamides. *Tetrahedron* **2004,** 60, 7543-7552.

51. Giese, B.; Wettstein, P.; Stähelin, C.; Barbosa, F.; Neuberger, M.; Zehnder, M.; Wessig, P., Memory of Chirality in Photochemistry. *Angewandte Chemie-International Edition* **1999,** 38, (17), 2586-2587.

52. Griesbeck, A. G.; Kramer, W.; Lex, J., Diastereo- and Enantioselective Synthesis of Pyrrolo[1,4]benzodiazepines through Decarboxylative Photocyclization. *Angewandte Chemie-International Edition* **2001,** 40, (3), 577-579.

53. Sakamoto, M.; Unosawa, A.; Kobaru, S.; Hasegawa, Y.; Mino, T.; Kasashima, Y.; Fujita, T., Diastereoselective photocycloaddition using memory effect of molecular chirality controlled by crystallization. *Chemical Communications* **2007**, (16), 1632-1634.

54. Matsumura, Y.; Shirakawa, Y.; Satoh, Y.; Umino, M.; Tanaka, T.; Maki, T.; Onomura, O., First Example of Memory of Chirality in Carbenium Ion Chemistry. *Organic Letters* **2000,** 2, (12), 1689-1691.

55. Shi, X.; Gorin, D. J.; Toste, F. D., Synthesis of 2-Cyclopentenones by Gold(I)-Catalyzed Rautenstrauch Rearrangement. *Journal of the American Chemical Society* **2005,** 127, (16), 5802-5803.

56. Faza, O. N.; López, C. S.; Álvarez, R.; de Lera, A. R., Mechanism of the gold(L)-catalyzed Rautenstrauch rearrangement: A center-to-helix-to-center chirality transfer. *Journal of the American Chemical Society* **2006,** 128, (7), 2434-2437.

57. Gorin, D. J.; Toste, F. D., Relativistic effects in homogeneous gold catalysis. *Nature* **2007,** 446, (7134), 395-403.

58. Dubé, P.; Toste, F. D., Synthesis of indenyl ethers by gold(I)-catalyzed intramolecular carboalkoxylation of alkynes. *Journal of the American Chemical Society* **2006,** 128, (37), 12062-12063.

Chapter 2. Mechanistic Studies on Memory of Chirality Alkylation of 1,4-Benzodiazepin-2-ones

2.1 Medicinal Importance of 1,4-Benzodiazepin-2-ones

1,4-Benzodiazepin-2-ones (BZDs) have received enormous attention due to the medicinal importance of these compounds.[1-3] The first potent BZD drug, diazepam **147** (Valium®) was developed in 1963, which showed high anxiolytic behavior (Figure 2.1). Clorazepate (Tranxene®) **148**, lorazepam (Ativan®) **149**, oxazepam (Sereax®) **150** and prazepam (Verstran®) **151** are other BZD derivatives used in anti-anxiety treatments. Moreover, clonazepam (Clonopin®) **152** and flurazepam (Dalmane®) **153** are marketed as hypnotic and antiepileptic drug respectively.[3]

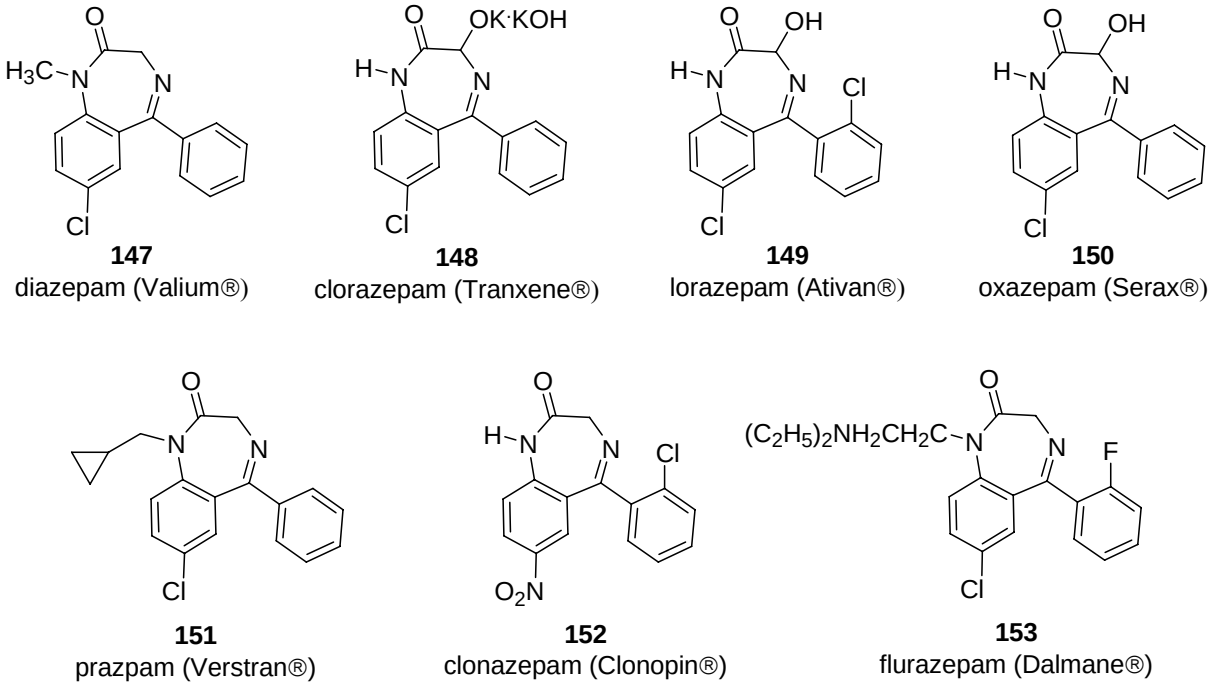

Figure 2.1 Medicinal use of 1,4-Benzodiazepin-2-ones

In addition, 1,4-Benzodiazepin-2-ones have proven useful as antagonists of the CCK-A (**154**)[4,5] and CCK-B (**155**),[6,7] the human Bradykinin B2 receptor (**156**),[8] and the HIV-1 Tat receptor (**157**) (Figure 2.2).[9] Derivatives of these structures have also shown activity as

inhibitors of Ras farnesylation (**158**)[10] and Src Protein Tyrosine Kinase (**159**),[11] and as antiarrhythmic agent (**160**).[12,13]

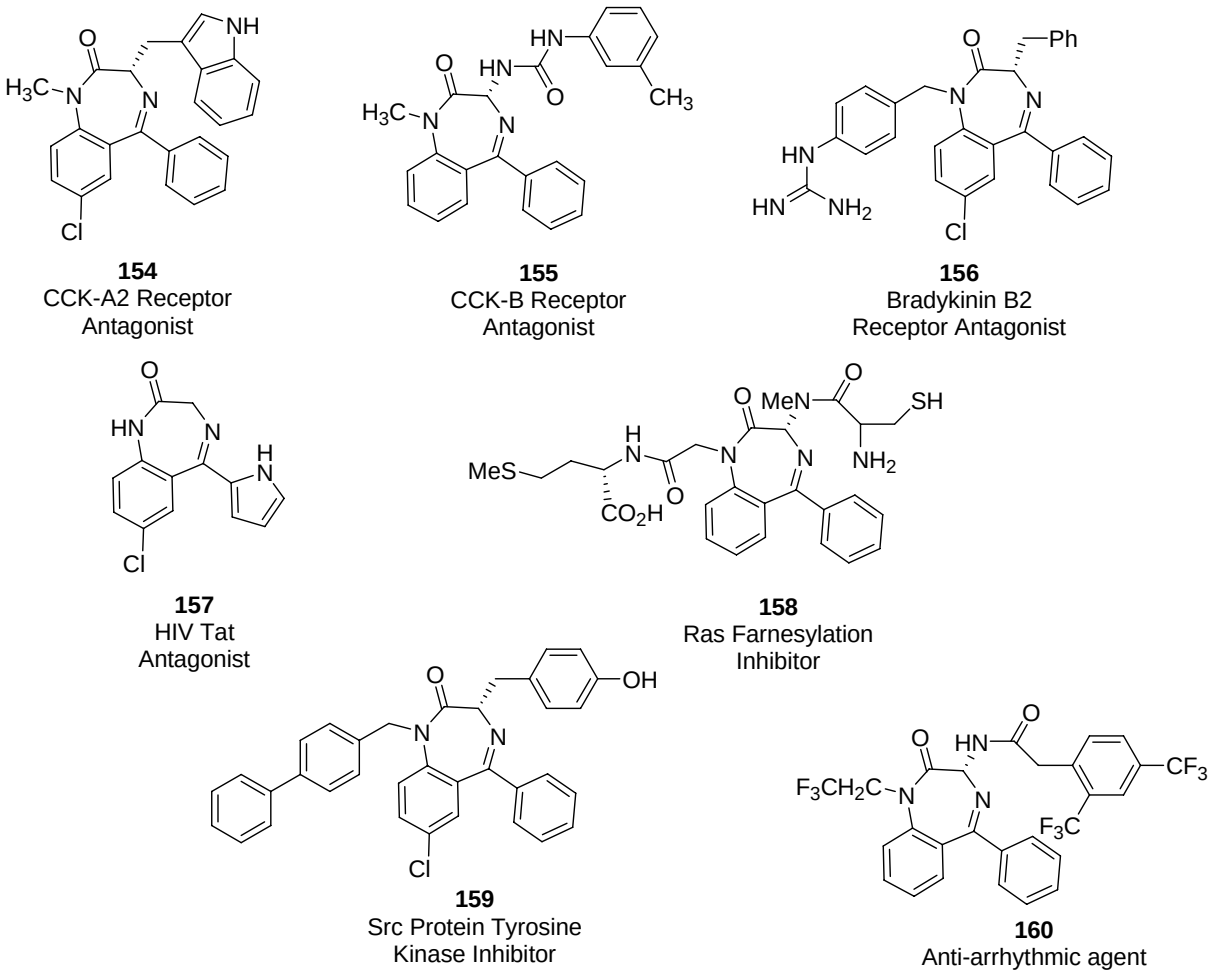

Figure 2.2 More medinical examples of 1,4-Benzodiazepin-2-ones

Historically, 1,4-Benzodiazepin-2-ones have most commonly been prepared from commercially available proteinogenic amino acid derivatives or their enantiomers.[14] Thus, before the work of the Carlier group,[15-18] enantiopure 3,3-disubstituted BZDs possessing "quaternary" chiral center were quite rare due to the scarcity of enantiopure quaternary amino acids.[19-22]

2.2 High Enantioselectivity and Retention of Configuration Resulted in Previous MOC Alkylations of 1,4-Benzodiazepin-2-ones

Due to the potential medicinal usefulness of 3,3-disubstituted 1,4-Benzodiazepin-2-ones, the Carlier group has invested great effort in the synthesis of the enantiopure quaternary scaffolds via memory of chirality.[15-18] As we dicussed in Chapter 1, our earliest example was enantioselective deprotonation/alkylation of Ala- and Phe-derived *N*-*i*-Pr BZDs at -78 °C (Table 1.7).[16] The bulkiness of the N(1) substituent was the key determinant to attain high enantioselectivity (Scheme 1.18).[23-25] Formation of a conformationally chiral nonracemic enolate was proposed to preserve the sense of the central chirality in the starting material; treatment with an electrophile then regenerated the stereochemical information as a new stereogenic center in the product with high fidelity. A similar protocol was applied to proline-derived 1,4-benzodiazepine-2,5-diones (Table 1.9).[18] Furthermore, in order to diversify the functionality at N(1), PMB and DAM groups had been used in the enantioselective synthesis of BZDs derived from a variety of commercially available α-amino acids (Table 1.10, 1.11 and 1.12).[15,17] The DAM group was preferred because of its bulkier size and the ease of its deprotection.

Retention of configuration in these reactions was established by hydrolysing quaternary BZDs into the known quaternary amino acids. Chiral stationary phase HPLC of H-D exchange products also established retentive substitution.[15,16]

2.3 Investigation of Ring Inversion Barrier of Glycine-derived 1,4-Benzodiazepin-2-ones

In order to understand how the aforementioned MOC reactions were carried out with high enantioselectivities and retention of configuration, a substituent was installed at C(9), so as to slow down the BZD ring inversion (Figure 2.3). Previous studies had shown that steric interaction of the C(9)-H and the N(1)-substituent provided the greatest impediment to ring inversion.[16,17,24]

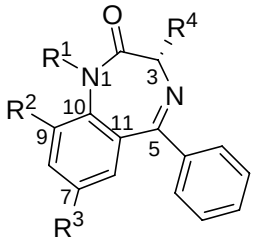

Figure 2.3 General structure of BZD

2.3.1 Synthesis of Glycine-derived BZDs

As a prelude to determining the inversion barrier of BZD enolates, we chose to investigate the ring inversion barrier of glycine-derived BZDs (R^4 = H). Due to the boat conformation it adopts, this type of BZD without a stereogenic center exists as a racemic mixture of (*M*)- and (*P*)-conformers (Table 1.8), where the helical descriptors (*M*)- and (*P*)- were applied to assign the sense of chirality of the ring in accordance with the sign of the C2-N1-C10-C11 dihedral angle (M = minus, P = positive).[25,26] Since the (M)- and (P)-conformers of Gly-derived BZDs are equally populated, these compounds are amenable to dynamic NMR studies of the inversion barrier. In contrast, BZDs derived from chiral "tertiary" amino acids exist in only 1 conformation (Scheme 1.18).[16,24] Thus, glycine-derived **161a** (R = Cl) and **162a** (R = Me) were synthesized as described below (Scheme 2.1-2.3). The first step of this synthesis based on Sternbach's protocol is shown in Scheme 2.1,[27] in

which 2,4-disubstituted aniline reacted with benzoyl chloride using $ZnCl_2$ as catalyst to afford the corresponding 2-aminobenzophenones **163** and **164** in 31% and 57% respectively.

Scheme 2.1 Synthesis of 2-aminobenzophenones **163** and **164**

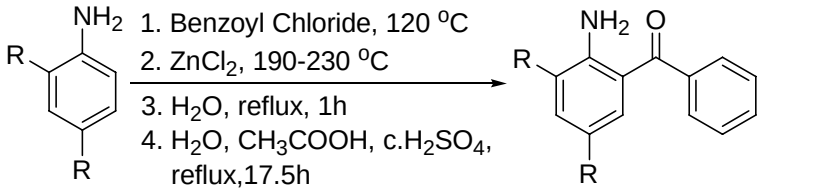

163 (R = Cl): 31% (lit.: 40%)
164 (R = Me): 57% (lit.: 40%)

Syntheses of **165** and **167** were also reported by Sternbach.[28] The 2-aminobenzophenones **163-164** were treated with bromoacetyl bromide to give **165** and **166** which were then cyclized with ammonia to form *N*-H BZDs **167** (R = Cl) and **168** (R = Me) (Scheme 2.2). It should be noted that **168** was previously prepared by a different synthetic route, but only in 10 % yield.[28]

Scheme 2.2 Synthesis of N-H BZDs **167** and **168**

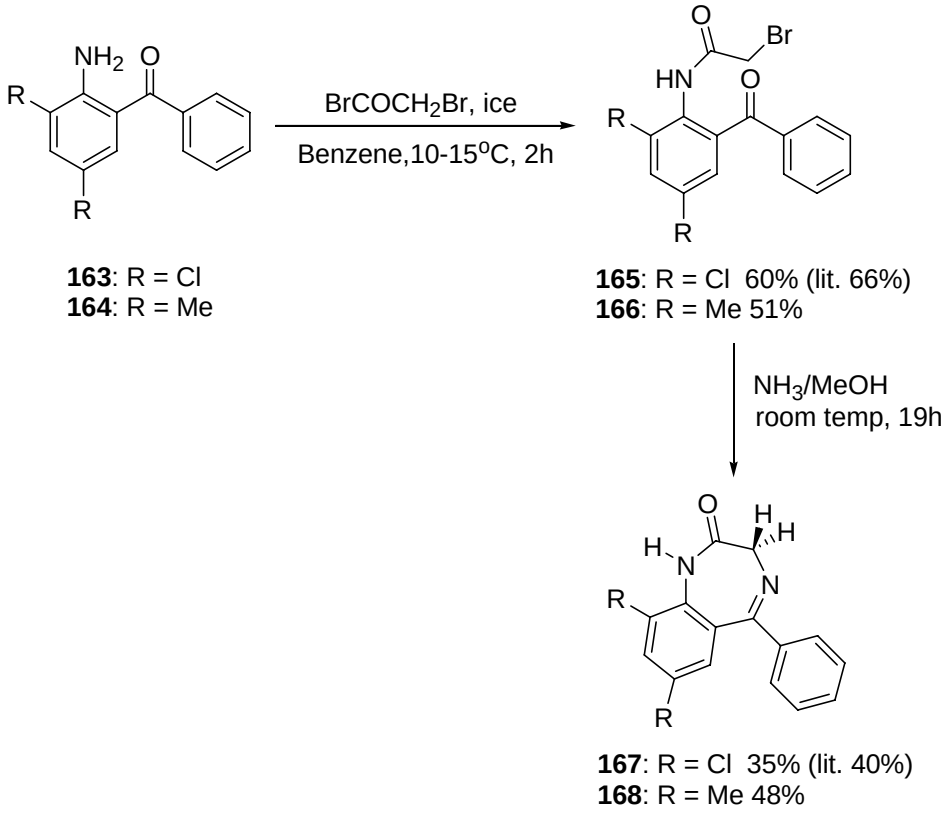

163: R = Cl
164: R = Me

165: R = Cl 60% (lit. 66%)
166: R = Me 51%

167: R = Cl 35% (lit. 40%)
168: R = Me 48%

Finally, *N*-methylation was performed to obtain **161a** and **162a** in 30% and 74% respectively (Scheme 2.3). The higher yield of **162a** relative to **161a** could be attributed to the stronger nucleophile generated by potassium hydride in the deprotonation of **168** compared to sodium hydride with **167**.

Scheme 2.3 Synthesis of *N*-Me **161a** and **162a**

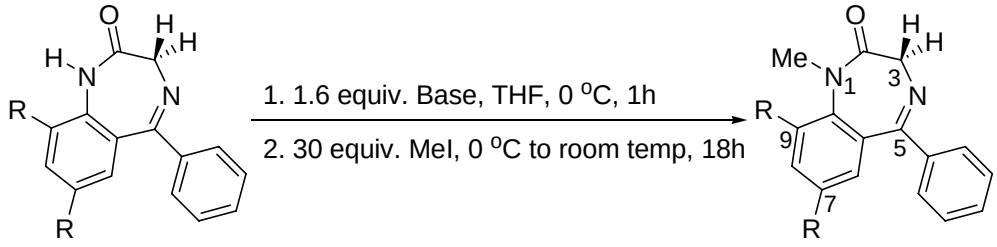

167: R = Cl; Base = NaH
168: R = Me; Base = KH

161a: 30%
162a: 74%

2.3.2 Coalescence Temperature Measurements of Glycine-derived BZDs

At room temperature, the axial and equatorial methylene protons of **169a-b** can be resolved into two discrete doublets in the ^{1}H NMR spectra, indicating slow ring inversion on the NMR timescale (Figure 2.4).[16,24] The inversion barriers $\Delta G^{\ddagger}$ for **169a-b** (18.0 ± 0.2 and 21.3 ± 0.2 kcal/mol respectively in d_6-DMSO) have already been determined by Lam[16,24] using coalescence temperature measurement with 400 MHz NMR and the standard equations.[29,30] The inversion barrier increases with increasing steric hindrance between N(1) and C(9).

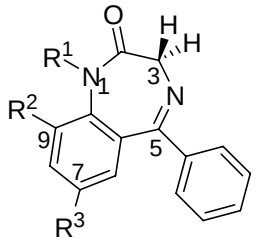

	R^1	R^2	R^3
169a	Me	H	Cl
169b	*i*-Pr	H	Cl
170b	*i*-Pr	H	H

Figure 2.4 Glycine-derived *N*-Me and *N*-*i*-Pr BZDs **169a-b** and **170b**

However, for both **161a** and **162a**, coalescence temperature could not be obtained under the same conditions. Even when the NMR temperature was raised up to the probe upper limit of 180 °C, the two doublets of both compounds were still far apart (Figure 2.5). We can only

present their inversion barriers as > 21.2 ± 0.2 kcal/mol. These much higher barriers may also be supported by the observation of the sharper doublet peaks in the ^{1}H NMR spectra at room temperature, representing slower ring inversion relative to the NMR timescale. It is noted that the two new peaks observed at temperature higher than 100 °C may be resulted from BZD decomposition. Table 2.1 summarizes the four inversion barriers that we have mentioned.

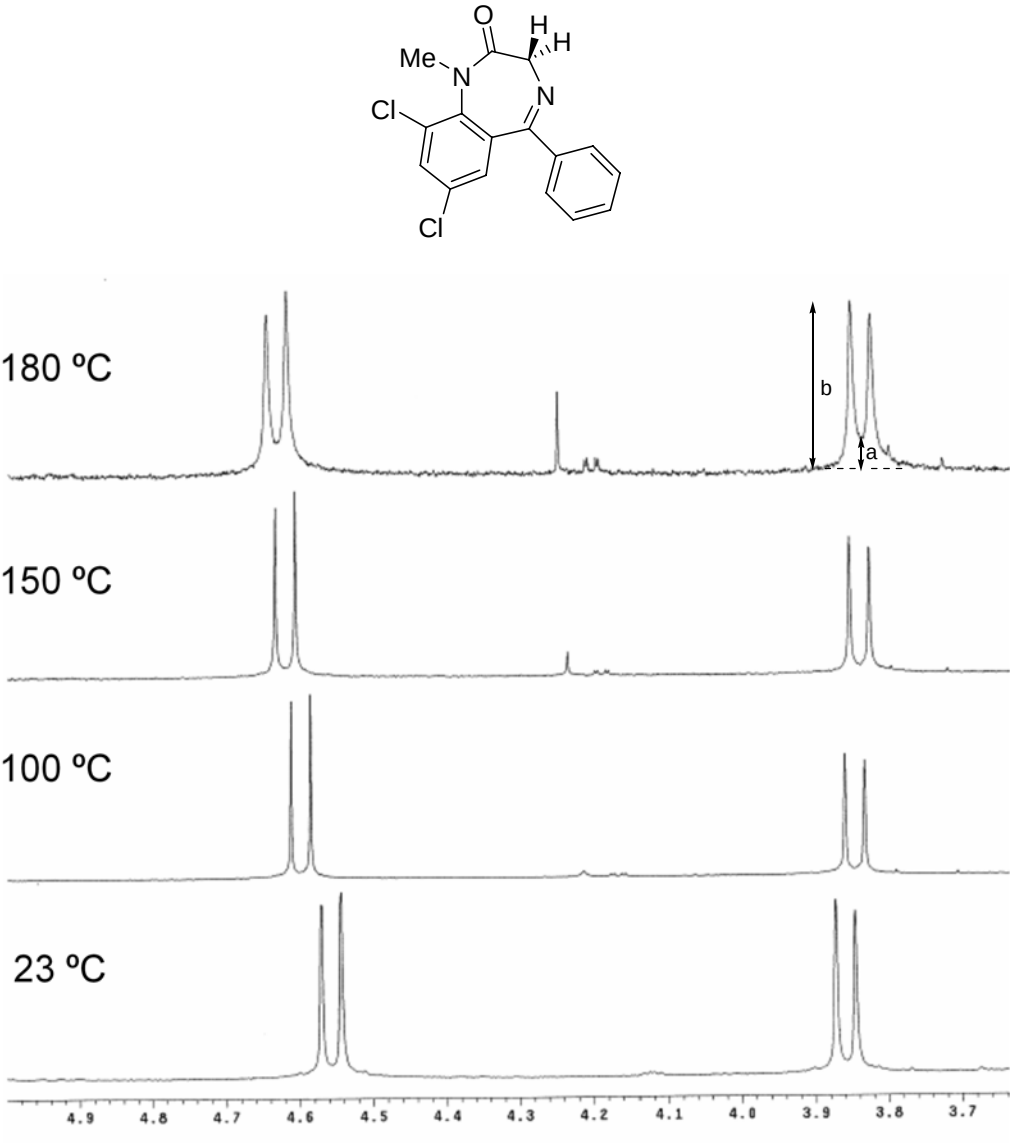

Figure 2.5 Variable temperature ^{1}H NMR of **161a**

Table 2.1 Comparison of inversion barrier

Compound	Substituents			$\Delta G^{\ddagger}$ (kcal/mol)
	N(1)	C(9)	C(7)	
169a	Me	H	Cl	18.0 ± 0.2[a]
169b	*i*-Pr	H	Cl	21.3 ± 0.2[a]
161a	Me	Cl	Cl	$> 21.2 \pm 0.2$
162a	Me	Me	Me	$> 21.2 \pm 0.2$

[a]Ref. 16 and 24

Subsequently, the gNMR application was used to simulate the line shape of the ^{1}H NMR spectra at various temperatures. This analysis incorporates both exchange broadening and exchange decoupling. The two doublets shown in the ^{1}H NMR spectrum at 100 ºC (Figure 2.5) were assigned to be at slow exchange, in which the natural line width was estimated to be 0.8 Hz. The exchange rate was increased in the software until the line shapes of the calculated doublet matched the experimental 180 ºC spectrum, based on the relative height of the peak valley of the doublet (a/b of the doublet in Figure 2.5). At 180 ºC, the rate of exchange of **161a** was estimated to be 9 Hz, corresponding to an inversion barrier of approximately 24.9 kcal/mol. Note that since a full line shape analysis could not be completed, this estimation is strictly approximate.

2.3.3 DFT Calculations of Ring Inversion Barrier of Glycine-derived BZDs

We then turned to conduct ab initio calculations at the density functional theory (DFT) level to estimate inversion barriers of **161a** and **162a**.[31-33] An excellent DFT computational study of BZDs was also reported by Lam in 2005.[24] By using B3LYP/6-31G(d) geometries and thermodynamic corrections, Lam calculated B3LYP/6-31+G(d) single point energies incorporating implicit salvation (DMSO, PCM),[34] and reproduced experimental inversion barriers to within 1.2 kcal/mol.

Equilibrium and ring inversion transition geometries were also optimized at B3LYP/6-31G(d) in our work. Vibrational frequencies were calculated at the same level to determine the zero-point vibrational energies (ZPVE) and the thermal corrections to the Gibbs free

energies. The calculated ring inversion transition structures were verified by their single imaginary frequency, the displacement vectors of which corresponded to the distortion from the "flat" transition structure towards the equilibrium geometry. The free energy difference between the transition structure and the equilibrium geometry resulted in the ring inversion barrier. Table 2.2 shows the comparison between computational and experimental results.

We note that application of the higher level (B3LYP/6-31+G(d)) single point energy does not appreciably alter the calculated inversion barriers. Moreover, the calculated inversion barrier of **161a** is close to the approximate result obtained from the gNMR line-shape analysis (0.3 kcal/mol difference). However, application of solvent correction (DMSO) using Tomasi's PCM model decreases the barriers by 2.9 and 3.9 kcal/mol respectively. In addition, application of MP2 single point energy corrections raise the inversion barriers by 2.7-3.4 kcal/mol, as Lam had seen previously for **169a** and **170b**. Thus, incorporating the results from single point calculations at B3LYP/6-31+G(d) with solvent correction and gNMR analysis, we estimate that the inversion barrier for **161a** is 21.6-24.9 kcal/mol, and for **162a** is 22.4-25.8 kcal/mol.

According to our group experience, the inversion barriers of Ala-derived BZD enolates are usually 4-8 kcal/mol lower than those of their corresponding Gly-derived BZDs.[15,24,35] Therefore, we estimate that the inversion barriers of the enolates from the Ala-derived analogues of **161a** and **162a** would be 17-21 kcal/mol and 18-22 kcal/mol respectively, corresponding to racemization half-lives larger than 268 hours and 148 days respectively at 195 K. These rough calculations encouraged us to attempt enantioselective alkylations of the Ala-derived BZDs **171a** and **172a** (Scheme 2.6).

Table 2.2 Comparison between computational and experimental inversion barriers for BZDs **161a**, **162a**, **169a** and **170b**

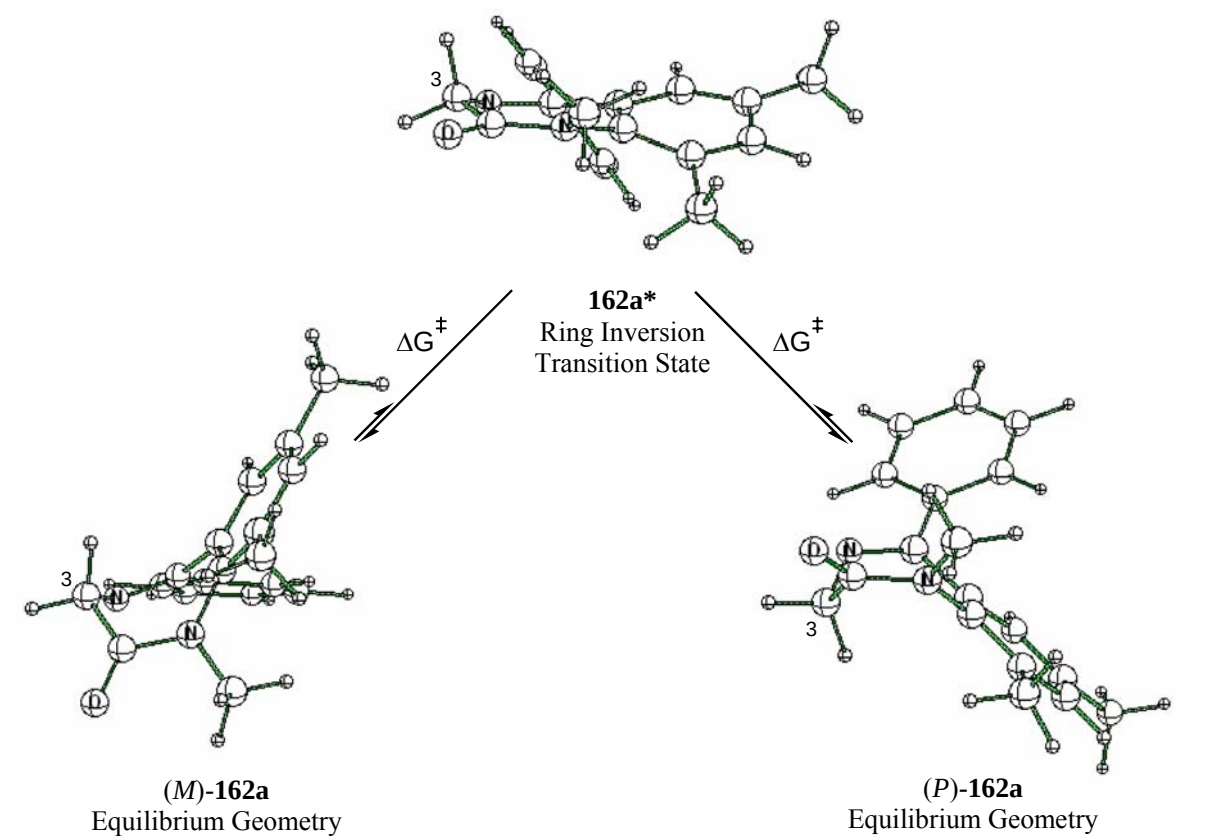

Cpd	Substituents		B3LYP/6-31G(d)[a]	B3LYP/6-31+G(d) //B3LYP/6-31G(d)		MP2/6-31G(d) //B3LYP/6-31G(d)	Experimental Inversion Barrier (kcal/mol)[e]
	N(1)	C(9)	ΔG‡ (kcal/mol)	ΔG‡ (kcal/mol)[b]	ΔG‡ (DMSO) (kcal/mol)[c]	ΔG‡ (kcal/mol)[d]	
169a	Me	H	NA	17.0	16.8	20.7	18.0 ± 0.2 (391K)
170b	*i*-Pr	H	NA	21.2	21.6	24.7	21.3 ± 0.2 (437K)
161a	Me	Cl	24.5	24.6	21.6	27.2	> 21.2 ± 0.2[f] ~ 24.9 kcal/mol[g]
162a	Me	Me	26.3	25.8	22.4	28.1	> 21.2 ± 0.2[f]

[a] Corrected by the Gibbs free energy correction factor calculated at B3LYP/6-31G(d) level at 298 K.

[b]Calculated from B3LYP/6-31+G(d) single point energy, including the Gibbs free energy correction factor calculated at B3LYP/6-31G(d) level; for Lam's data, it was calculated at the corresponding coalescence temperature.

[c]Calculated from B3LYP/6-31+G(d) single point energy in DMSO using Tomasi's polarized continuum model (PCM), including the Gibbs free energy correction factor.

[d]Calculated from MP2/6-31G(d) single point energy, including the Gibbs free energy correction factor.

[e]Experimental inversion Barrier for **169b** was used in comparison with the computational results for **170b**

[f]Based on failure at achieve coalescence at 453 K

[g]Estimate based on gNMR analysis

2.4 Enantioselective Alkylations of Alanine-derived BZD

2.4.1 Synthesis of Alanine-derived BZDs

After confirming the high inversion barrier in **161a** and **162a**, Ala-derived 1,4-benzodiazepin-2-ones **171a** and **172a** (Scheme 2.6) were synthesized for memory of chirality applications as follows. One problem encountered was that our published protocol for preparing Ala- and Phe-derived BZDs (R^2 = H) did not work with **163** and **164** (Figure 2.3),[16,36] probably due to the steric hindrance from the C(9) substituent during DCC coupling. Therefore, instead of a Boc-protected amino acid, a Fmoc-protected amino acid chloride[37] was used to react with 2-aminobenzophenone **163** or **164** (Scheme 2.4). The Fmoc group was employed due to its stability in the acidic environment of the coupling reaction.

Scheme 2.4 Synthesis of amides **173** and **174**

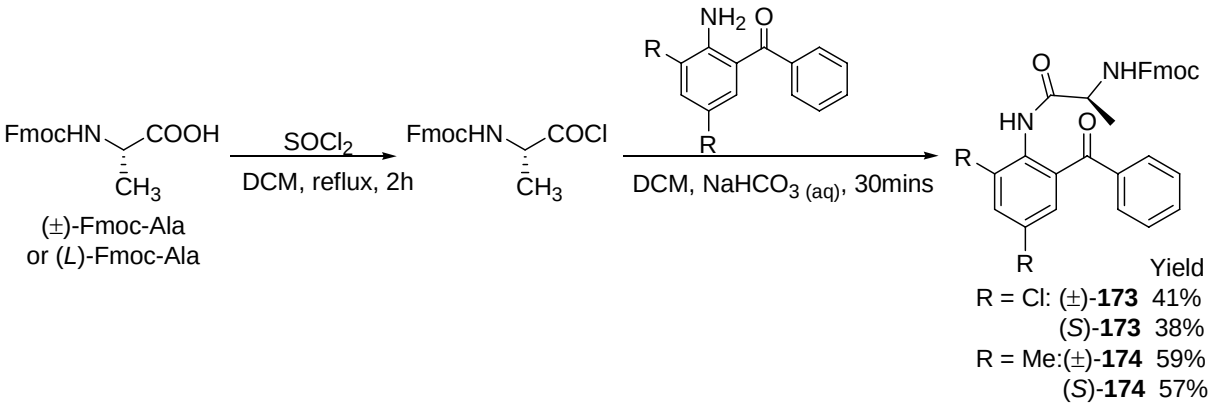

The Fmoc group in **173** and **174** was then deprotected by DBU and 1-octanethiol, followed by cyclization under basic conditions to give *N*-H BZDs **175** and **176** (Scheme 2.5). Early attempts at synthesizing (*S*)-**175** from enantiomerically pure (*L*)-Fmoc-alanine led to a disappointing 24% ee. It was suspected that the low enantiopurity obtained could be caused by the presence of excess strong base, sodium hydroxide, during cyclization, in which deprotonation/reprotonation occurred at the stereogenic center in aqueous solution. Thus, sodium bicarbonate was used to achieve excellent enantioselectivity (> 99.5% ee) in (*S*)-**175**

and (*S*)-**176**. The enantiomeric excess values for these compounds were determined by chiral stationary phase HPLC.

Scheme 2.5 Syntheis of N-H BZDs **175** and **176**

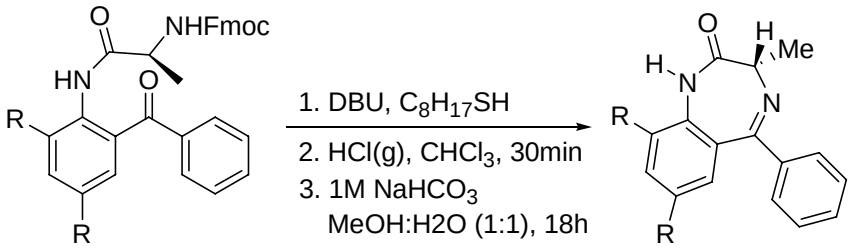

R = Cl: (±)-**173**
(*S*)-**173**
R = Me:(±)-**174**
(*S*)-**174**

R = Cl: (±)-**175** 78%
(*S*)-**175** 60% (> 99.5% ee)
R = Me:(±)-**176** 73%
(*S*)-**176** 63% (> 99.5% ee)

In the final step, **175** and **176** were deprotonated by potassium hydride and then treated with methyl iodide to provide enantiopure *N*-Me BZDs **171a** and **172a** (Scheme 2.6). The lower yield of (*S*)-**171a** relative to (±)-**171a** is curious and suggests that this reaction could be optimized.

Scheme 2.6 *N*-Methylation of **175** and **176**

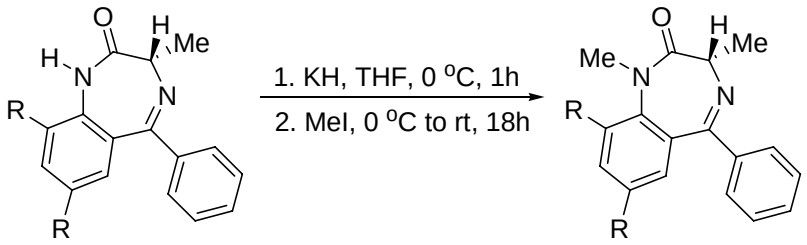

R = Cl: (±)-**175**
(*S*)-**175**
R = Me:(±)-**176**
(*S*)-**176**

Yield
R = Cl: (±)-**171a** 92%
(*S*)-**171a** 57% (> 99.5% ee)
R = Me:(±)-**172a** 82%
(*S*)-**172a** 86% (> 99.5% ee)

2.4.2 Memory of Chirality Alkylations of Alanine-derived BZDs

With the N(1), C(9)-dimethylsubstituted Ala-derived BZDs in hand, enantioselective deprotonation/alkylation was attempted according to the published protocol.[15,17] Deprotonation of (*S*)-**172a** by KHMDS in the presence of HMPA at -78 °C followed by treatment with electrophile gave the corresponding alkylated products **177a-180a** (Table 2.3). As hoped, excellent enantioselectivities (≥ 99% ee) were realized in these reactions, despite

the small N(1)-substituent. These results clearly point to the beneficial effect of C(9) substitution in raising enolate inversion barriers.

Compared to our previously developed procedure in which deprotonation was carried out by 2.5 equivalents of KHMDS for 30 minutes,[15,17] 5 equivalents of base were needed to achieve similar high product yield (Table 2.3, cf. entries 1 and 3, and 2 and 4). However, when the deprotonation time was extended to 2 hours, a high product yield was reproduced using only 2.5 equivalents of KHMDS (Table 2.3, cf. entries 3 and 7, 4 and 8, and 5 and 9). We conclude that deprotonation of **172a** is slower than other BZDs previously examined.[15,17] In addition, no decrease in enantioselectivity resulted from the lengthened deprotonation time, which implied that the corresponding BZD enolate racemized very slowly at -78 °C. Moreover, it was significant to note that HMPA was not required to attain acceptable yields and high enantioselectivities of the alkylated products from **172a**; in contrast, addition of HMPA was necessary for acceptable yields in our previous deprotonation/alkylation of 1,4-benzodiazepin-2-ones (**67b,e,f**, **69b,f**, **84f** and **85f**).[15-17] The role of HMPA in these reactions remains unclear.

Interestingly, early attempts on the reaction of dichloro-analogue **171a** with 2.5 equivalents of KHMDS and 6 equivalents of HMPA did not afford any apparent alkylated products (by TLC). Usually there is a distinct color change from colorless to blood red, which we believe signifies successful formation of BZD enolates. However, during the 30 minutes deprotonation step of **171a**, an orange color was observed. It was therefore suspected that only a small amount of enolate was formed under this condition. Due to the subsequent focus on the mechanistic studies with **172a** and its alkylated products, reaction of **171a** using optimized condition as carried out for **172a** was not pursued. We consider that such optimization should be possible.

Table 2.3 MOC alkylations of (*S*)-**172a**

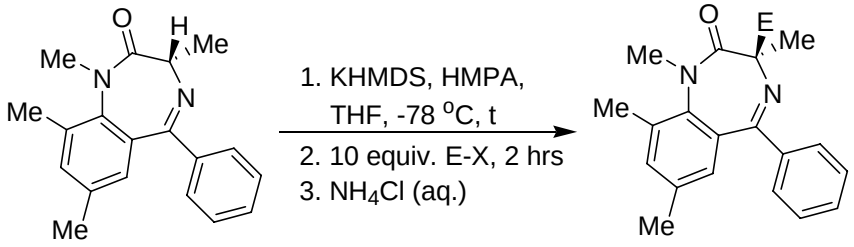

(*S*)-**172a** (*R*)-**177a-180a**

Entry	KHMDS (equiv.)	HMPA (equiv.)	t (hours)	E-X	Product	% Yield	% ee
1	2.5	6	0.5	BnBr	(+)-**177a**	54	> 99.5
2	2.5	6	0.5	CN-Tos	(+)-**178a**	52	> 99.5
3	5	6	0.5	BnBr	(+)-**177a**	80	99
4	5	6	0.5	CN-Tos	(+)-**178a**	70	> 99.5
5	5	6	0.5	Allyl Br	(+)-**179a**	87	> 99.5
6	5	6	0.5	2-C_6H_5BnBr	(+)-**180a**	80	NA[a]
7	2.5	6	2	BnBr	(+)-**177a**	85	99
8	2.5	6	2	CN-Tos	(+)-**178a**	81	> 99.5
9	2.5	6	2	Allyl Br	(+)-**179a**	90	> 99.5
10	2.5	0	2	BnBr	(+)-**177a**	75	99
11	2.5	0	2	CN-Tos	(+)-**178a**	63	99
12	2.5	0	2	Allyl Br	(+)-**179a**	77	99

[a]Enantiomeric excess could not be obtained by chiral stationary phase HPLC due to poor separation of conformational diastereomers

As mentioned in section 1.4.7, tertiary BZDs exist in a single conformation that presents the lone C(3)-substituent in a pseudoequatorial orientation. However, 3,3-disubstituted BZDs such as (*R*)-**177a** and (*R*)-**179a** adopt both Me-pseudoaxial and pseudoequatorial conformations, because of similar steric demands of the C(3) substituents. Characterization of BZD conformers will be discussed in detail in section 2.4.3. Interestingly, in the case of C(3)-cyanation product, only the Me-pseudoequatorial/CN-pseudoaxial conformer of (*R*)-**178a** is present in the ^{1}H NMR spectrum.[17] The anomeric effect may play some role in this conformational preference, but we believe that the strong preference for the CN-pseudoaxial conformer principally derives from the small size of the cyano group relative to that of methyl. For reference, the equatorial preferences for cyano and methyl groups in a cyclohexane ring are 0.20 and 1.74 kcal/mol respectively.[38]

Retentive benzylation and allylation of **172a** are assumed based on precedent;[15-17] retentive cyanation was confirmed by X-ray crystallography of (+)-**178a**, which also confirmed a CN-pseudoaxial conformation in the solid state (Figure 2.6). The X-ray structure also showed that the BZD molecule is not planar. The non-planar geometry adopted by BZD can be explained in terms of internal angles and bond angles. The internal angle of a regular heptagon is 129º. However, the bond angle of sp^3 and sp^2 atoms are usually 109º and 120º respectively. Since the seven-membered diazepine ring is composed of a mixture of sp^3 and sp^2 atoms, in order to relieve the angle strain, BZD adopts a non-planar conformation.

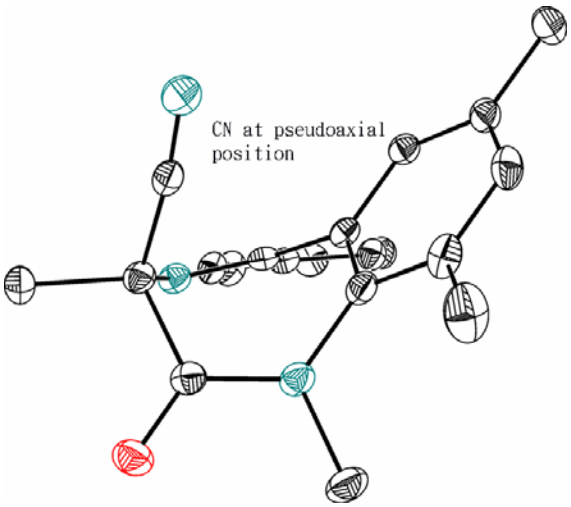

Figure 2.6 Retentive cyanation confirmed by X-ray structure of **178a** (thermal ellipsoid at 50% probability, hydrogens not shown)

2.4.3 Characterization of BZD conformers

The two different BZD conformers can be distinguished on the basis of ^{1}H NMR chemical shift as described previously.[17,24] Taking (*R*)-**179a** as an example, the signal of the pseudoequatorial methyl group appears at 1.72 ppm in the (*M*)-conformer while the pseudoaxial methyl is shifted to 0.68 ppm in the (*P*)-conformer due to the shielding cone of the annulated benzo ring (Figure 2.7).

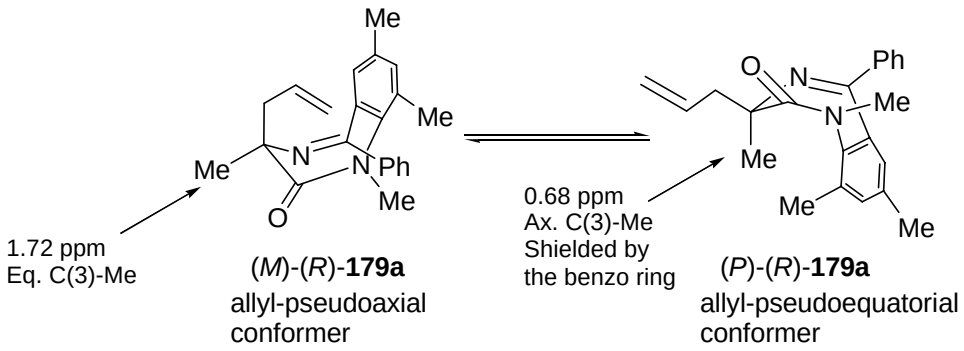

Figure 2.7 ^{1}H NMR studies in $CDCl_3$ for distinguishing between allyl-pseudoaxial and allyl-pseudoequatorial conformers of (*R*)-**179a**

Moreover, according to the computed structure of (*M*)-(*R*)-**179a** (Figure 2.8), the terminal protons of the axial allyl group are in the proximity of the C(9)-Me (2.9-3.5 Å). It is possible that other conformers are present around C(3)-X and X-Y bonds, but only the one drawn has allyl hydrogens within 4 Å of the C(9)-Me. Therefore, to support the calculated structure, ^{1}H-^{1}H NOE difference experiments were carried out. First, in order to distinguish the singlets for C(9)- and C(7)-Me, N(1)-Me was irradiated. This led to a 4% enhancement for the C(9)-Me signal at 2.23 ppm (Figure 2.9a). Consequently, irradiation of Hb and Hc resulted in 3% and 1% enhancement respectively for C(9)-Me (Figure 2.9b), consistent with the calculated distances and thus confirming the ^{1}H NMR assignment of the allyl-pseudoaxial of (*M*)-(*R*)-**179a**.

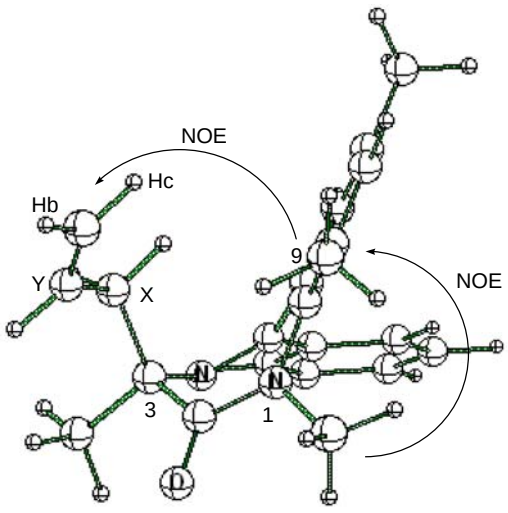

Figure 2.8 Calculated structure of (*M*)-(*R*)-**179a**

(a) Irradiation of N(1)-Me resulted in enhancement of C(9)-Me

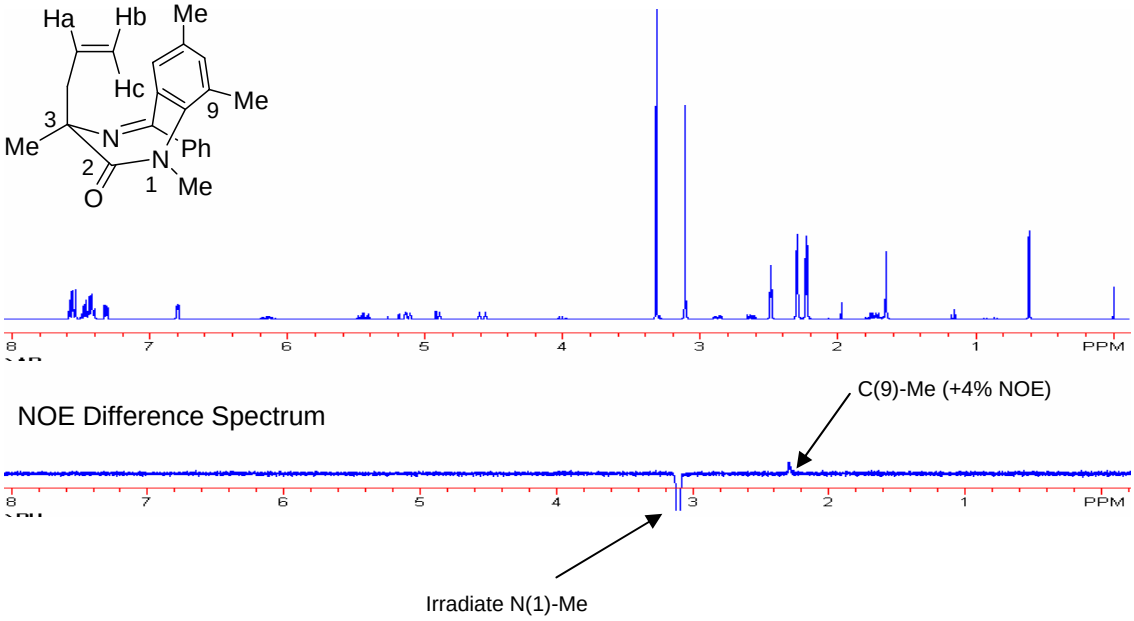

(b) Irradiation of the terminal protons of C(3)-allyl resulted in enhancement of C(9)-Me

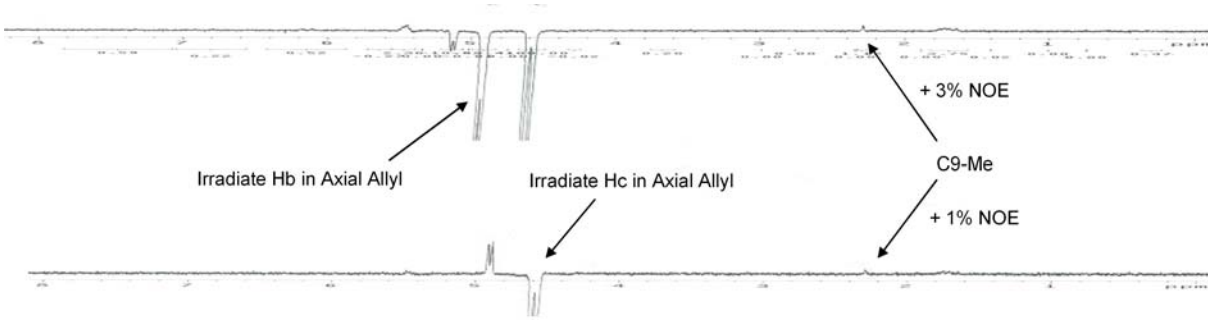

Figure 2.9 NOE difference experiments of (*M*)-(*R*)-**179a**

2.5 Proposal of Two Stereochemical Controlled Mechanisms

Retentive transformation of BZD (*S*)-**172a** to its benzylated derivative (*R*)-**177a** could proceed via deprotonation to enolate (*M*)-**181a**, and concave face alkylation to yield (*R*)-**177a** in an initial conformation featuring axial placement of the electrophile (Path **A**, Scheme 2.7). This pathway is attractive based on stereoelectronic considerations and on the known (*M*)-conformation of (*S*)-**172a**.[16,24] However, another scenario would involve invertive deprotonation to the (*P*)-enolate, and convex face alkylation to again yield (*R*)-**177a**, this time featuring initial equatorial placement of the electrophile (Path **B**, Scheme 2.7). Although the invertive deprotonation of Path **B** appears unlikely, the *concave* face alkylation of Path **A** also

appears unfavorable. In principle these pathways could be distinguished by determining the initial conformation of the product **177a**; however up to now, fast conformational equilibration of products (Figure 2.3, R^2 = H; R^1 = Me, PMB, 2°-alkyl) on the laboratory time scale has precluded this approach.[15-17,24] This equilibration rate is slow enough to allow both conformers to be resolved on the ^{1}H NMR time scale at room temperature.[17,24]

Scheme 2.7 Possible mechanism for retentive deprotonation/alkylation of **172a**

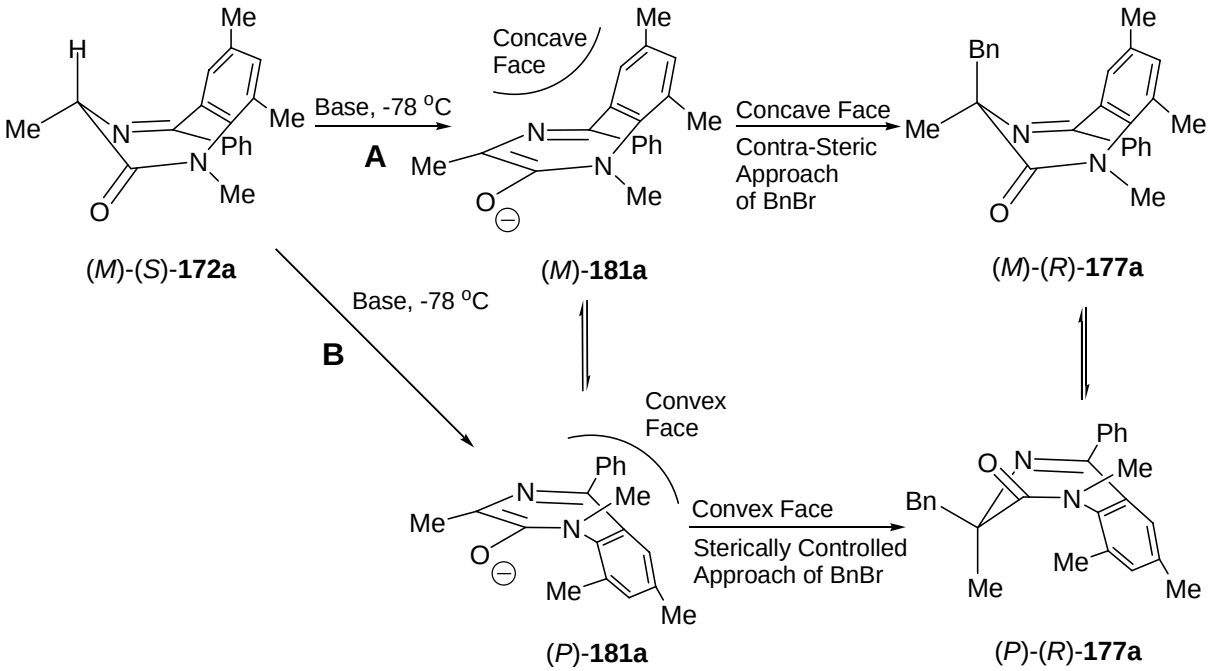

2.6 Possible Means to Discriminate between the Two Mechanisms

2.6.1 Inspiration from HPLC and 2D-TLC

The slow ring inversion of the alkylated products from (*S*)-**172a** led to an unexpected and intriguing phenomenon demonstrated by HPLC chromatograms and 2D-TLC. Instead of the usual two peaks expected from a racemic mixture in the HPLC chromatogram, surprisingly, (±)-**179a** was resolved into four peaks by the chiral stationary phase (Figure 2.10a). The four peaks correspond to all four conformational diastereomers, (*M*)-(*S*)-, (*M*)-(*R*)-, (*P*)-(*S*)- and (*P*)-(*R*)-**179a**, in the racemic mixture. In confirmation of this proposal, the chromatogram of (*R*)-**179a** shows two peaks, which represent the two conformational

diastereomers, (*M*)-(*R*) and (*P*)-(*R*) (Figure 2.10b). These chromatograms prove that conformational inversion is slow on the HPLC time scale.

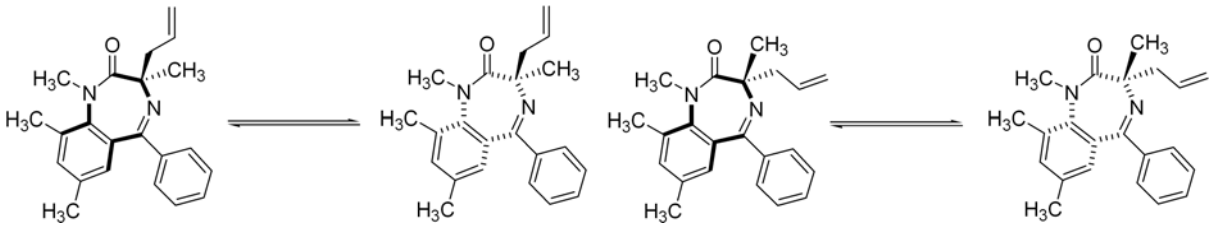

(*M*)-(*R*)-**179a**
allyl-pseudoaxial conformer

(*P*)-(*R*)-**179a**
allyl-pseudoequatorial conformer

(*M*)-(*S*)-**179a**
allyl-pseudoequatorial conformer

(*P*)-(*S*)-**179a**
allyl-pseudoaxial conformer

(a) Chromatogram: (±)-**179a** resolved into four peaks

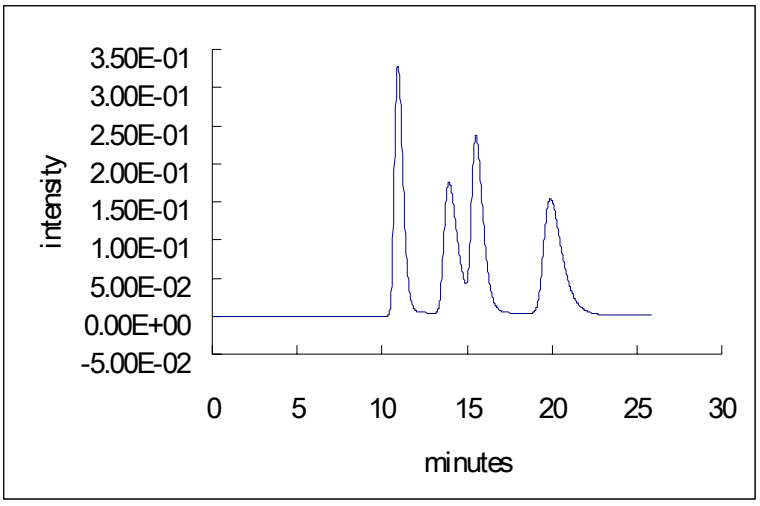

(b) Chromatogram: (*R*)-**179a** resolved into two peaks

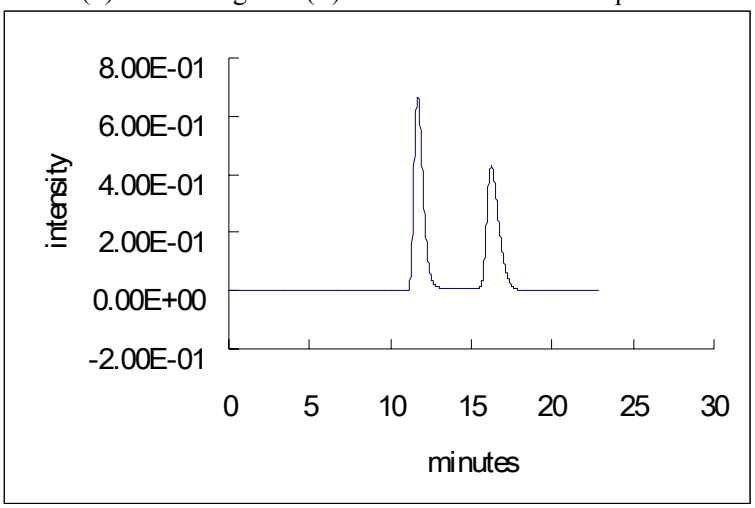

Figure 2.10 HPLC chromatograms of a) (±)-**179a** and b) (*R*)-**179a**. HPLC: [Chiralpak AD (0.46 cm x 25 cm) (from Daicel Chemical Ind., Ltd.)] Hexane/*i*-PrOH, 99/1, 1 mL/min.

After seeing the resolution of the conformational diastereomers by chiral stationary phase, analysis upon achiral stationary phase, 2D-TLC, was attempted to see if separation of conformational diastereomers might be possible on silica gel (Figure 2.11). Spotting (±)-**177a** in the lower left corner of a square TLC plate, followed by elution with 1:5 EtOAc/Hexanes, gave 2 spots (R_f: 0.29, 0.41). Rotating the plate 90º counter clockwise, followed by a second elution, gave only two diagonal spots. However, a repeat experiment in which the TLC plate was heated to 80º for 25 minutes before a second elution gave four spots. These 2D-TLC results clearly confirm our HPLC results to establish that (±)-**178a** consists of conformational diastereomers that do not interconvert within minutes at 25 ºC, but that interconvert within minutes at 80 ºC.

The above observations from HPLC and 2D-TLC inspired us to attempt two experiments that could distinguish the proposed mechanisms for retentive substitution. Thanks to the extremely slow ring inversion, the initial conformation of the alkylated product from (*S*)-**172a** may be determined by working up the MOC reaction at low temperature. We term this technique "freeze-frame observation", since it resembles "step-action" photography of an otherwise rapid phenomenon.

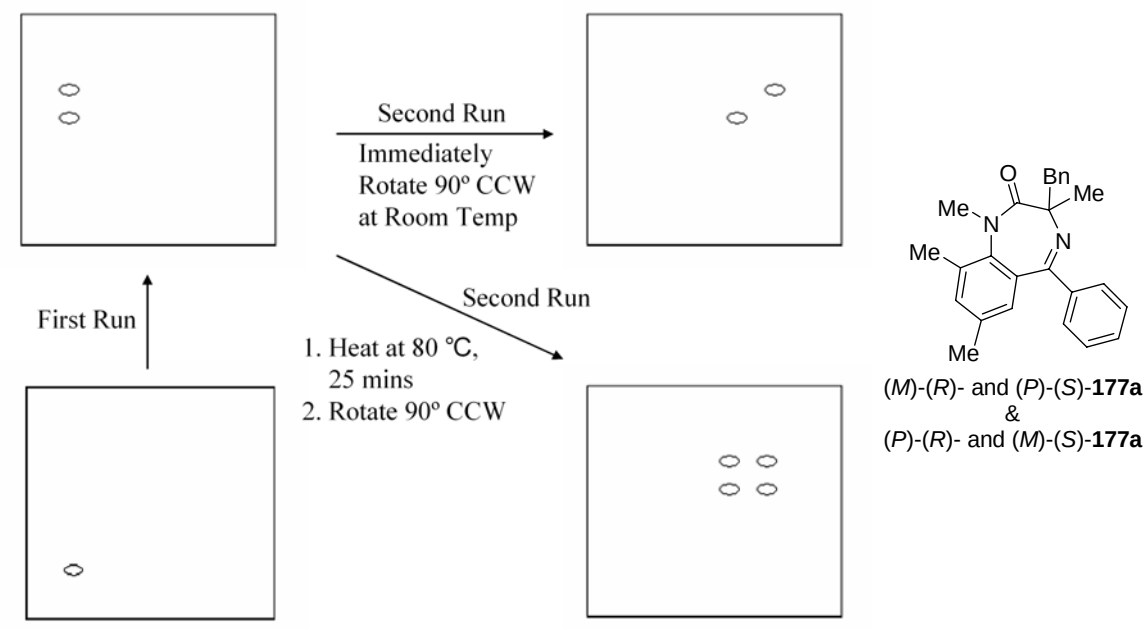

Figure 2.11 Resolution of conformational diastereomers by achiral stationary phase, 2D-TLC

2.6.2 Freeze Frame Observations after Cold Work-up

Deprotonation/alkylation experiments were then carried out on **172a** with benzyl bromide as before, but with a cold workup and isolation. ^{1}H NMR spectroscopy of the product before purification indicated exclusive formation of the Bn-pseudoaxial (**177a**) conformer (Figure 2.12), as predicted by the Path **A** mechanism in Scheme 2.7. After flash chromatography, ^{1}H NMR spectroscopy showed the expected mixture of conformers due to equilibration.

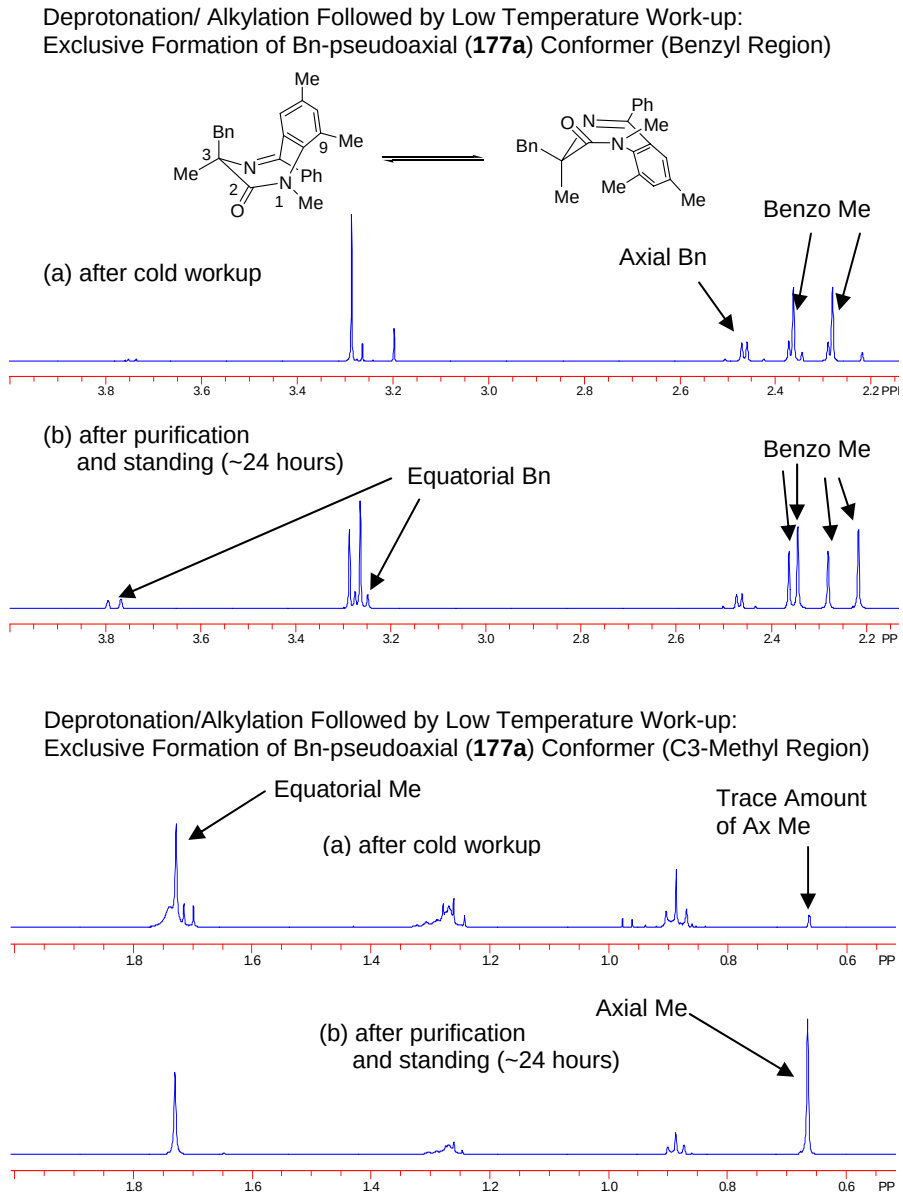

Figure 2.12 Freeze frame observations of (*M*)-(*R*)-**177a** after cold work-up by ^{1}H NMR: specific benzyl and methyl regions; mixture of (*R*)-**177a** conformers found after purification

Cold work-up experiments were also performed on **172a** with allyl bromide. Again, ^{1}H NMR spectroscopy of the product before purification indicated exclusive formation of the allyl-pseudoaxial (**179a**) conformer, confirming the Path A mechanism in Scheme 2.7. A mixture of conformers was also revealed in the ^{1}H NMR spectrum after flash chromatography. Thus, we have provided the first direct evidence of concave face alkylation of the BZD enolate.

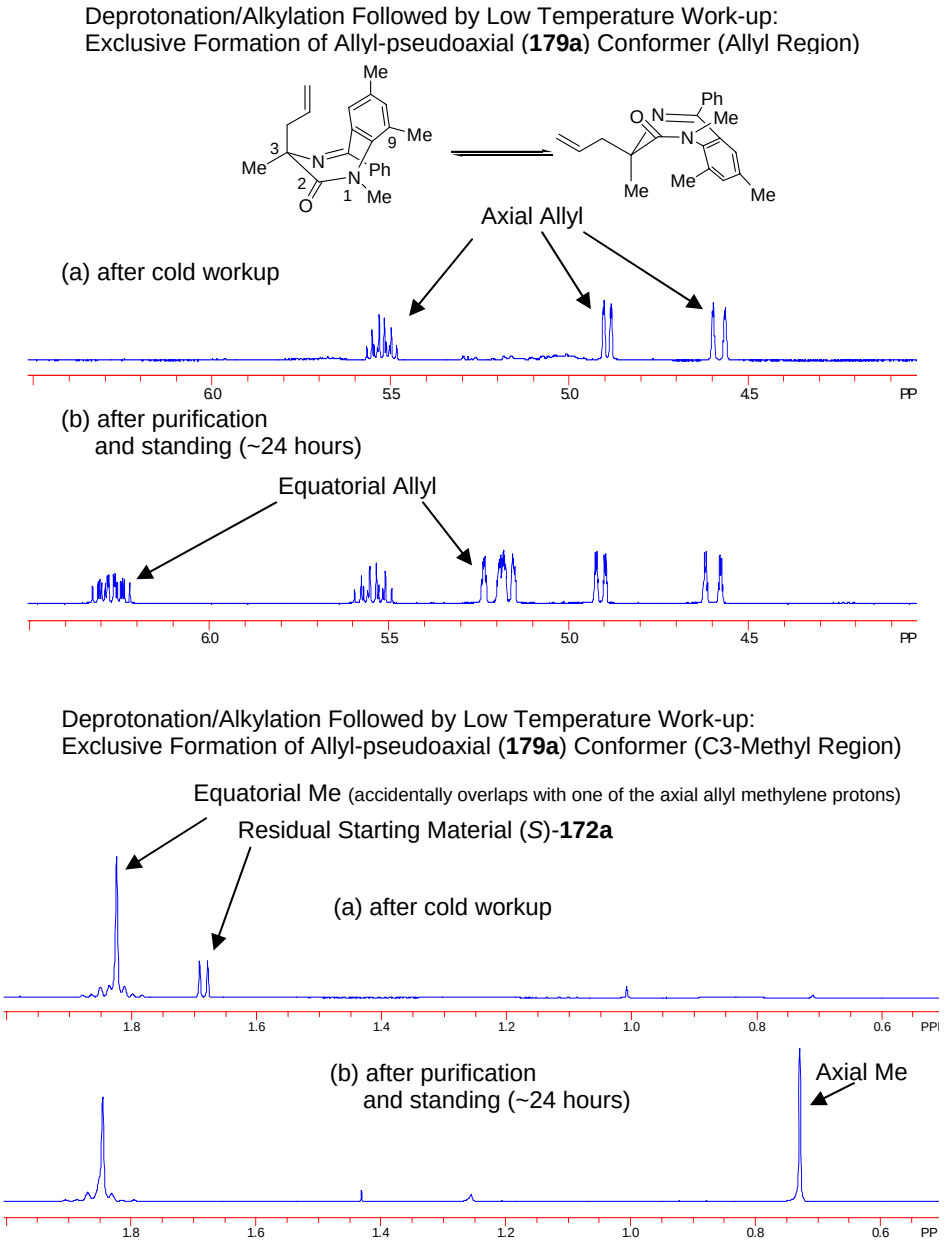

Figure 2.13 Freeze frame observations of (*M*)-(*R*)-**179a** after cold work-up by ^{1}H NMR: specific allyl and methyl regions; mixture of (*R*)-**179a** conformers found after purification

In order to gain a greater understanding of the enolate intermediate involved in these reactions, we explored isolation of the corresponding silyl enol. As will be seen below, these experiments unexpectedly provided even more direct evidence of the proposed retentive deprotonation/concave face alkylation mechanism. Several other workers in our lab had previously attempted isolation of BZD enolate as silyl enol ethers, but had been unsuccessful. We successfully prepared the TBS enol ether derivative **182a** in 69% yield by trapping **181a** with TBS-Cl at -78 °C (Scheme 2.8). My early attempts were unsuccessful; however, use of TBS-Cl instead of TMS-Cl, and trituration with cold anhydrous CH_3CN after flash chromatography proved critical to success. Diastereotopic methyls on silicon in ^1H NMR spectroscopy indicated that **182a** was chiral, and X-ray crystallography revealed the expected sofa conformation of the BZD ring (Figure 2.14).

Scheme 2.8 Preparation of TBS enol ether **182a**

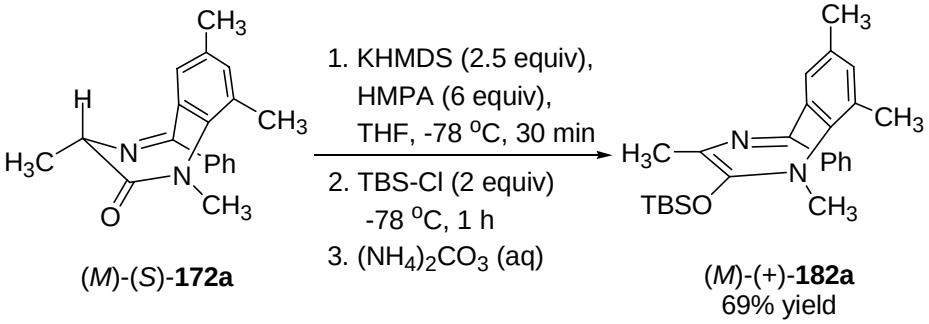

(*M*)-(*S*)-**172a**

(*M*)-(+)-**182a**
69% yield

Unexpectedly, crystallography revealed that **182a** had been isolated in *enantiopure* form in the (*M*)-conformation, which was indicated by the Flack parameter of -0.02 (± 0.03) determining from anomalous dispersion. Thus, the (M)-conformation unequivocally demonstrates *retentive* deprotonation (Path **A**, Scheme 2.7). Although we have not yet determined HPLC conditions that can separate the enantiomers of (±)-**182a**, trapping experiments of (*M*)-(+)-**182a** described below indicate that it was isolated in enantiopure form. Note as well that a significant optical rotation ($[\alpha]_D^{25} = +959°$, c = 1.85, $CHCl_3$) of (*M*)-(+)-**182a** was observed.

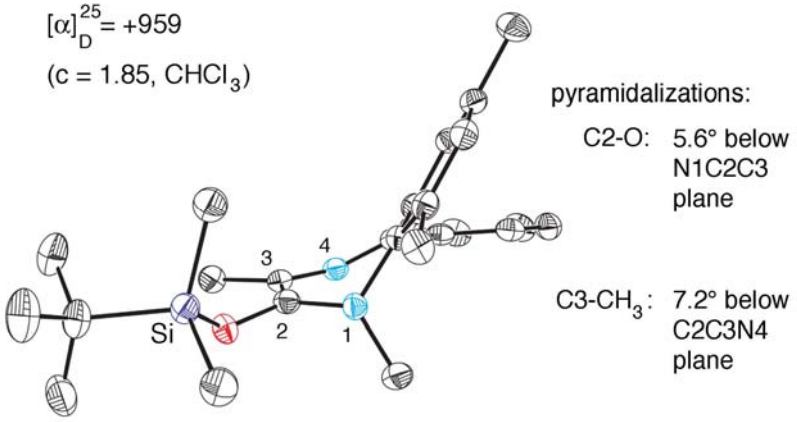

Figure 2.14 X-ray structure of the enantiopure TBS enol ether (*M*)-(+)-**182a** (thermal ellipsoid at 50% probability, hydrogens not shown).

As we will demonstrate below in section 2.8.1, the potassium enolate of **172a** has a racemization $t_{1/2}$ of 95 min at -16 ºC. We had thus expected to isolate the silyl enol ether in racemic form. Therefore, apparently the ligation of the TBS group significantly increased the inversion barrier in **182a**. B3LYP/6-31G* calculations[16,24,31] estimated the activation free energy for conformational inversion of **182a** to be 30.8 kcal/mol (298K), corresponding to $t_{1/2}$(rac) of 69 years; thus isolation of **182a** in enantiopure form appears feasible (Figure 2.15). Enol ethers of transiently non-racemic enolates have previously been isolated and their chirality demonstrated by HPLC[39] and ^{1}H NMR.[40] However, this is the first time that such a derivative has been isolated in enantiopure form and so characterized by X-ray crystallography for the determination of its sense of chirality.

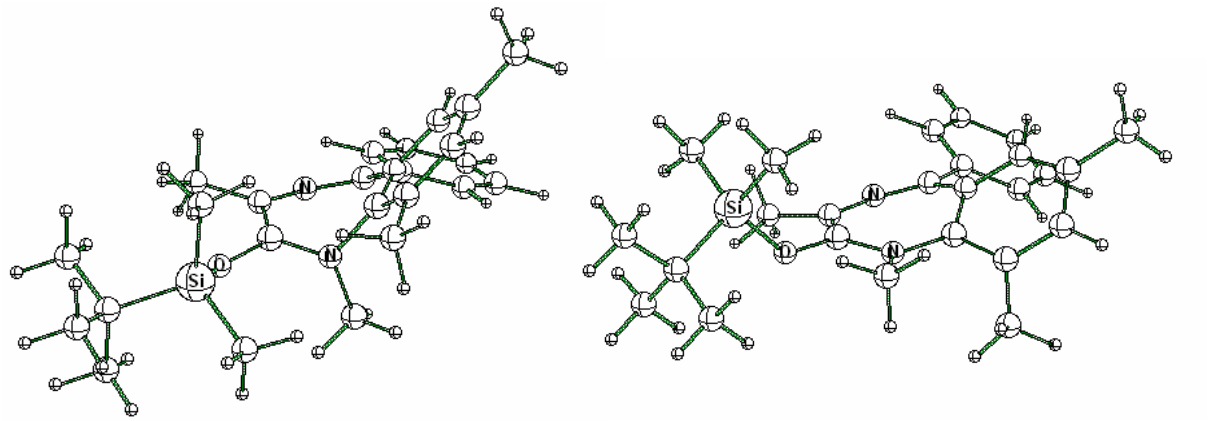

(*M*)-**182a**
Relative *G* (298K)
B3LYP/6-31G* = 0.0 kcal/mol

182a*
Relative *G* (298K)
30.8 kcal/mol

Figure 2.15 TBS enol ether equilibrium geometry **182a** and ring inversion transition structure **182a***

TBS enol (*M*)-(+)-**182a** provides us with a number of intriguing possibilities, since it represents another room temperature-stable source of a transiently non-racemic enolate. Desilylation was attempted with MeLi (-78 C → 25 ºC, 1 day) without success. The reaction with TBAF also did not proceed as expected, because this reagent is not an anhydrous fluoride source. Consequently, the resultant enolate was protonated to regenerate **172a**. Eventually, we successfully carried out an in situ desilylation/benzylation at -78 °C in DMF/THF, using tris(dimethylamino)sulfonium difluorotrimethylsilicate (TASF) to generate the metal-free enolate (Scheme 2.9). Note that TASF gave acceptable yields of alkylation products under in situ condition, presumably due to deprotonation of the solvent by the extremely basic metal-free enolate.[41] Upon cold extractive workup and isolation, the product **177a** was analyzed by ^{1}H NMR spectroscopy and was found to be exclusively in the Bn-pseudoaxial conformation (Figure 2.16), as predicted by the Path **A** mechanism in Scheme 2.7. Subsequent chromatographic purification and HPLC analysis of **177a** indicated 99% ee and 76% yield. In summary, stereochemical information transfer in the conversion of (*S*)-**172a** to (*R*)-**177a** and (*R*)-**179a** is shown conclusively to proceed via Path **A**.

Scheme 2.9 Freeze-frame isolation of quaternary BZD **177a** in the Bn-pseudoaxial conformation

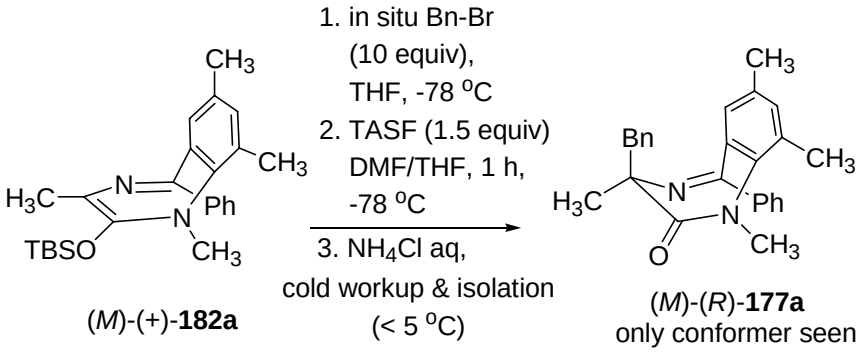

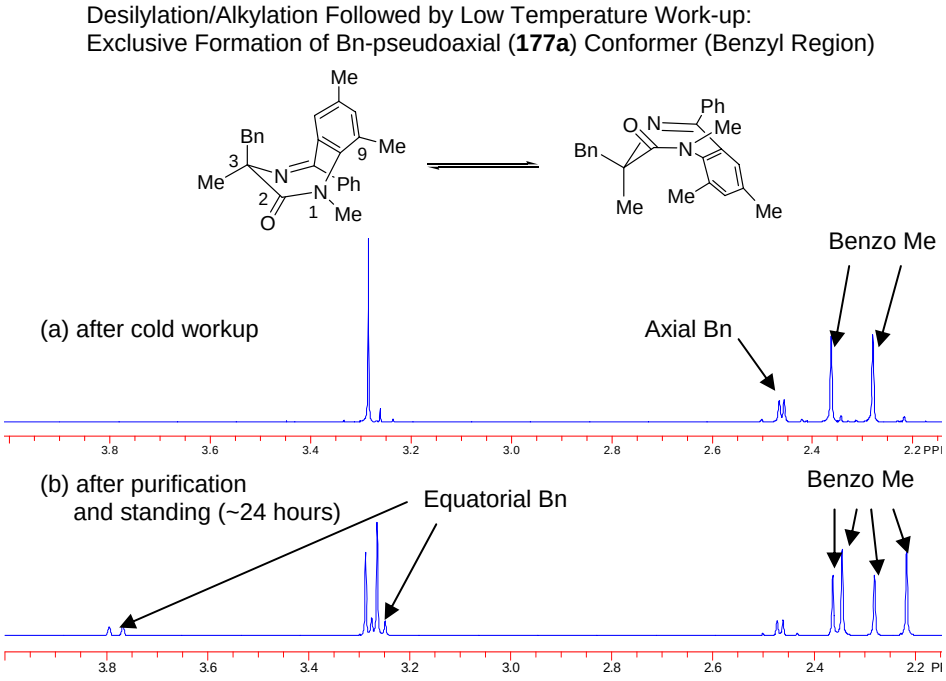

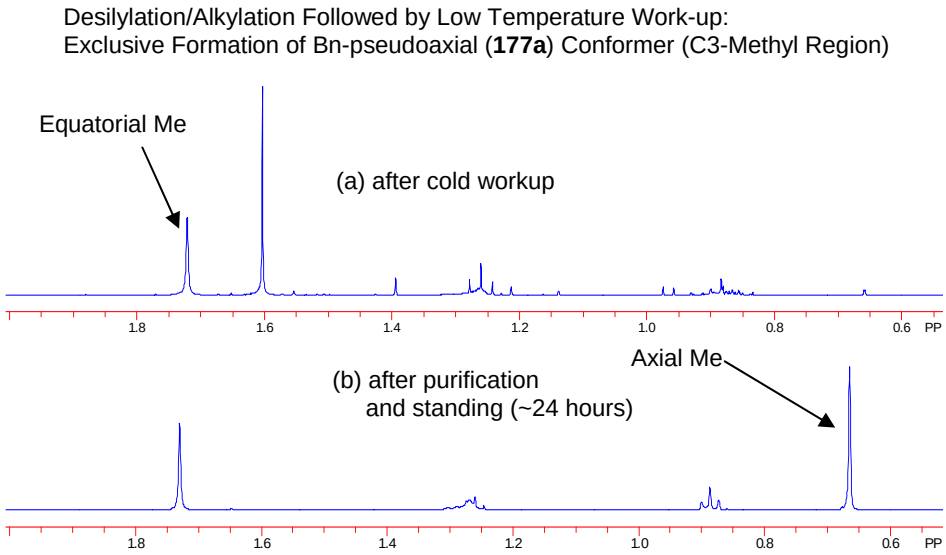

Figure 2.16 Freeze frame observations of (*M*)-(*R*)-**177a** after cold work-up by ^{1}H NMR: specific benzyl and methyl regions; mixture of (*R*)-**177a** conformers found after purification

2.7 DFT Calculations of the BZD Deprotonation Transition Structures

As mentioned in the last chapter, there are three essential requirements for a successful MOC reaction (Scheme 1.2).[42] In order to investigate the mechanism in detail, we complemented our experimental work with computational studies on the deprotonation step using both lithium and potassium amides, according to our published protocols.[15-17] Because it is known that LDA is a disolvated dimer in ethereal solvents (e.g. **183**, figure 2.17),[43-45] and because both monomer and open dimer transition states have been demonstrated kinetically by Collum for ketone/ester deprotonation (e.g. **184**),[46-51] transition structures corresponding to the deprotonation of (*S*)-**172a** by monomeric and dimeric lithium dimethylamides were both modeled.

To confirm that the retentive and invertive deprotonation transition structures located (e.g. (*M*)-(*S*)- and (*P*)-(*S*)-**185a** in Figure 2.18) do indeed result from the corresponding reactant complexes, the C(3)-bonds were shortened slightly (0.3 Å) and the structures reoptimized to afford the corresponding equilibrium geometries (e.g. (*M*)-(*S*)- and (*P*)-(*S*)-**186a** in Figure 2.19). Similarly, the C(3)-bonds in both TS were lengthened slightly (0.3 Å) and the structures reoptimized to give the corresponding enolate complexes (e.g. (*M*)- and (*P*)-**187a** in Figure 2.20). IRC calculations could also have been undertaken but our "shorten/lengthen" approach requires less computational time. All the equilibrium and deprotonation transition geometries in this section were optimized at B3LYP/6-31G(d). Single point energies were calculated at B3LYP/6-31+G(d), MP2/6-31G(d) and MP2/6-31+G(d).

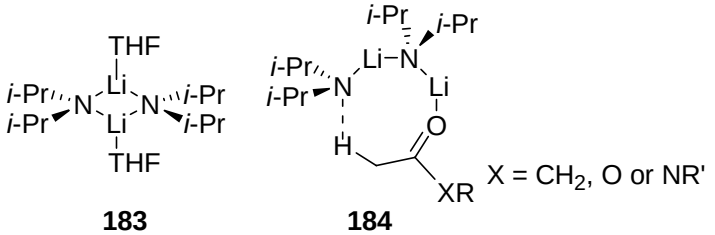

183 **184**

Figure 2.17 LDA disolvated dimer **183** and open dimer deprotonation transition state **184**

First, transition structures for deprotonation by solvent-free monomeric lithium base are shown in Figure 2.18. Lithium dimethylamide was used instead of the isopropyl analogue for computational economy. However, calculated $\Delta\Delta G^{\ddagger}$ values based on (*M*)-(*S*)- and (*P*)-(*S*)-**185a** are either ~0 or in wrong direction, which do not predict retentive deprotonation.

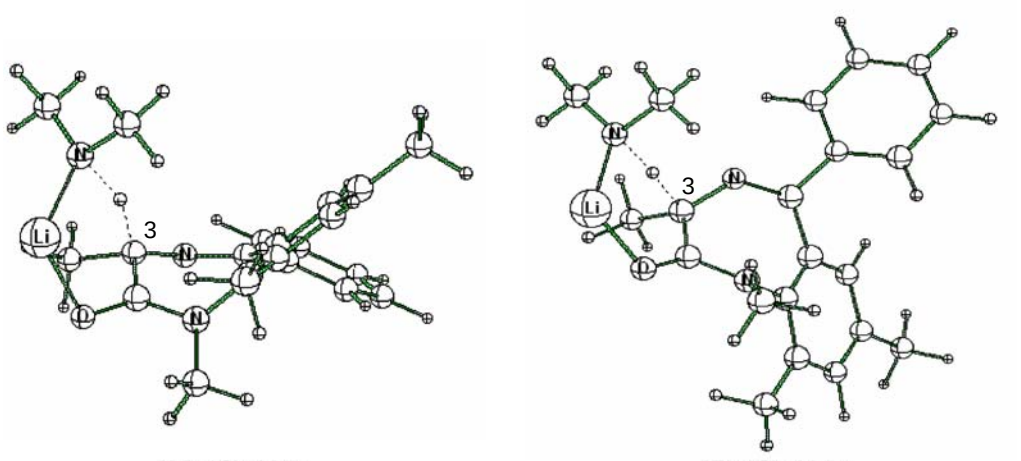

(*M*)-(*S*)-**185a** Retentive Deprotonation	(*P*)-(*S*)-**185a** Invertive Deprotonation
Relative *G* (195K) in kcal/mol	Relative *G* (195K) in kcal/mol
B3LYP/6-31G* = 1.7	0.0
B3LYP/6-31+G*// B3LYP/6-31G* = 1.9	0.0
MP2/6-31G*//B3LYP/6-31G* = 0.06	0.0
MP2/6-31+G*//B3LYP/6-31G* = 0.0	0.2

Figure 2.18 Unsolvated transition structures for deprotonation of (*S*)-**172a** by monomeric $LiNMe_2$

The energy differences between equilibrium geometries of reactant complexes (*M*)-(*S*)- and (*P*)-(*S*)-**186a** (Figure 2.19) make sense as they match the structural preference that the (3*S*)-stereochemistry induces the BZD to adopt the (*M*)-conformation (Scheme 1.18). Moving to the enolate complexes, we attribute the energy difference between *syn*-(*M*)- and *anti*-(*P*)-**187a** (Figure 2.20) to the diastereomeric placement of the $Li(HNMe_2)$ unit (syn vs anti to the benzo ring). The instability of the (*M*)-enolate may be attributed to the steric interaction of the coordinated amine with the benzo group.

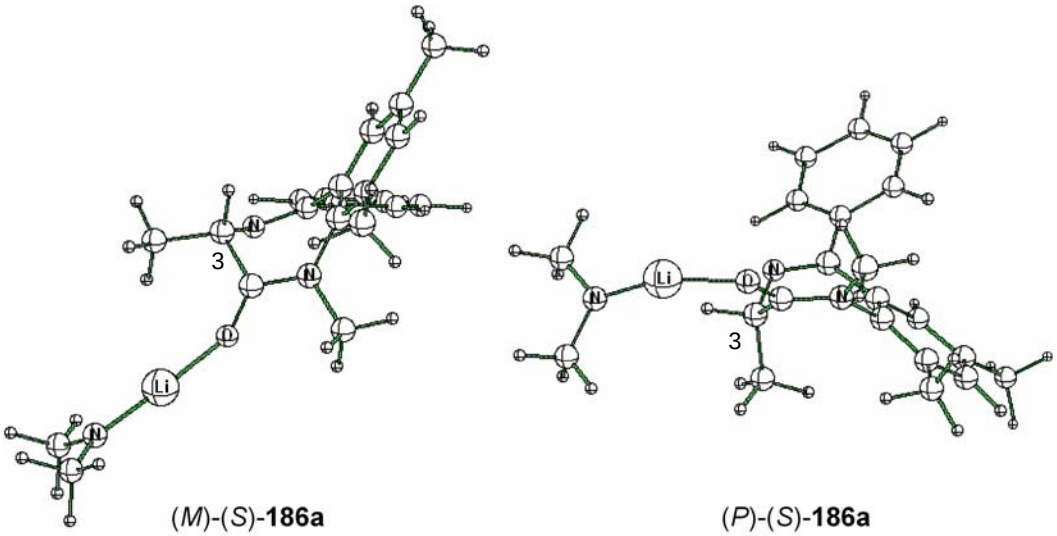

(*M*)-(*S*)-**186a**

Relative *G* (195K) in kcal/mol
B3LYP/6-31G* = 0.0
B3LYP/6-31+G*// B3LYP/6-31G* = 0.0
MP2/6-31G*//B3LYP/6-31G* = 0.0
MP2/6-31+G*//B3LYP/6-31G* = 0.0

(*P*)-(*S*)-**186a**

Relative *G* (195K) in kcal/mol
6.0
6.1
4.9
4.1

Figure 2.19 Reactant complexes of (*S*)-**172a** and unsolvated $LiNMe_2$

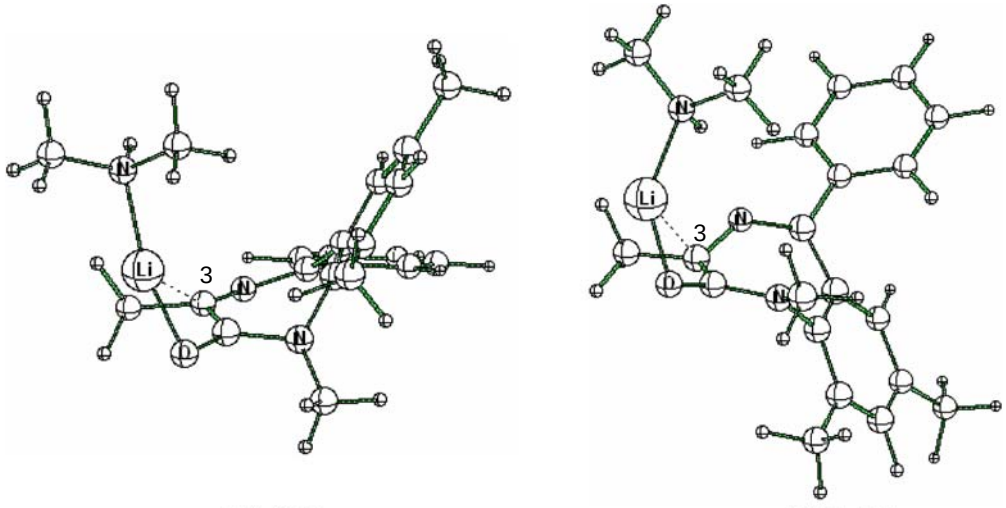

syn-(*M*)-**187a**

Relative *G* (195K) in kcal/mol
B3LYP/6-31G* = 3.0
B3LYP/6-31+G*// B3LYP/6-31G* = 2.8
MP2/6-31G*//B3LYP/6-31G* = 3.4
MP2/6-31+G*//B3LYP/6-31G* = 3.9

anti-(*P*)-**187a**

Relative *G* (195K) in kcal/mol
0.0
0.0
0.0
0.0

Figure 2.20 Enolate complexes resulting from deprotonation of (*S*)-**172a** by monomeric $LiNMe_2$ (unsolvated).

Similarly, transition structures for deprotonation by solvated monomeric lithium dimethylamides (Figure 2.21), and the equilibrium geometries of the reactant and enolate complexes were computed (Figure 2.22 and 2.23). Dimethylether was used in calculations

instead of THF for computational economy. These structures are more realistic as the lithium amide is solvated under the condition of deprotonation. Interestingly, the single point calculations at MP2 suggested a preference for retentive deprotonation while calculations at B3LYP indicated preferred inversion (Figure 2.21). Despite lack of consensus of the deprotonation step, reactant complex (*M*)-(*S*)-**189a** is stable than (*P*)-(*S*)-**189a**, as expected. Note that the lithium amide nitrogen formed hydrogen bonding with C(3)-H in (*P*)-(*S*)-**189a** (Figure 2.22). Again, an energetic preference is seen for the anti-enolate complex, *anti*-(*P*)-**190a**.

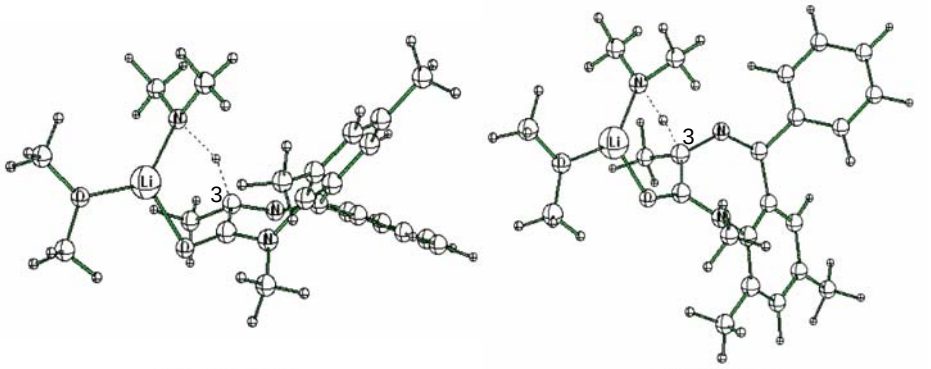

(*M*)-(*S*)-**188a** Retentive Deprotonation	(*P*)-(*S*)-**188a** Invertive Deprotonation
Relative *G* (195K) in kcal/mol	Relative *G* (195K) in kcal/mol
B3LYP/6-31G* = 1.2	0.0
B3LYP/6-31+G*// B3LYP/6-31G* = 1.4	0.0
MP2/6-31G*//B3LYP/6-31G* = 0.0	1.0
MP2/6-31+G*//B3LYP/6-31G* = 0.0	1.5

Figure 2.21 Monosolvated (Me_2O) transition structures for deprotonation of (*S*)-**172a** by $LiNMe_2$

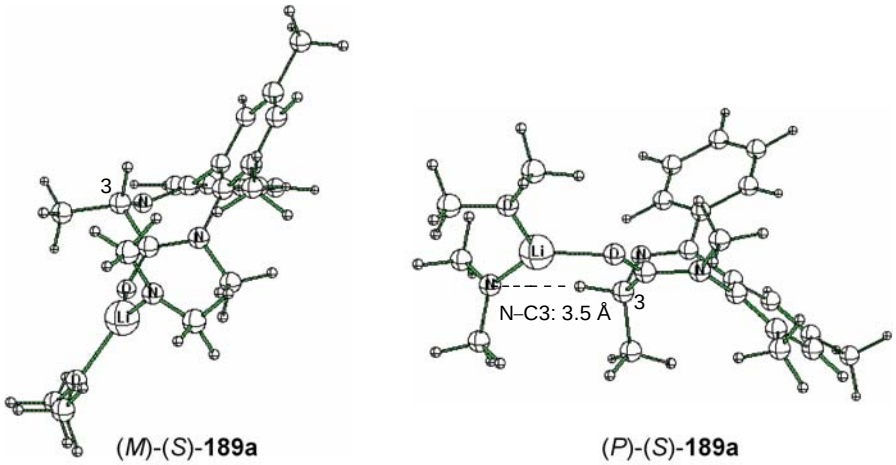

(*M*)-(*S*)-**189a**	(*P*)-(*S*)-**189a**
Relative *G* (195K) in kcal/mol	Relative *G* (195K) in kcal/mol
B3LYP/6-31G* = 0.0	5.6
B3LYP/6-31+G*// B3LYP/6-31G* = 0.0	5.3
MP2/6-31G*//B3LYP/6-31G* = 0.0	6.7
MP2/6-31+G*//B3LYP/6-31G* = 0.0	6.5

Figure 2.22 Monosolvated (Me_2O) reactant complexes of (*S*)-**172a** with $LiNMe_2$

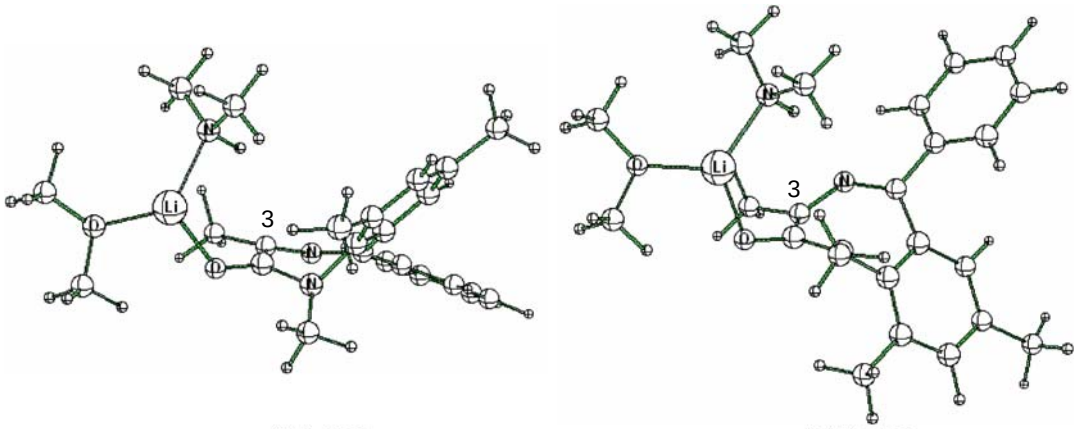

syn-(*M*)-**190a**	*anti*-(*P*)-**190a**
Relative *G* (195K) in kcal/mol	Relative *G* (195K) in kcal/mol
B3LYP/6-31G* = 1.3	0.0
B3LYP/6-31+G*// B3LYP/6-31G* = 0.4	0.0
MP2/6-31G*//B3LYP/6-31G* = 3.5	0.0
MP2/6-31+G*//B3LYP/6-31G* = 3.5	0.0

Figure 2.23 Monosolvated (Me_2O) lithium enolate dimethylamine complexes

Since the energies of the unsolvated and monosolvated deprotonation transition structures with monomeric lithium dimethylamide do not predict retentive deprotonation (our experimental result), open-dimer based transition structures were located by using the same calculation methods.

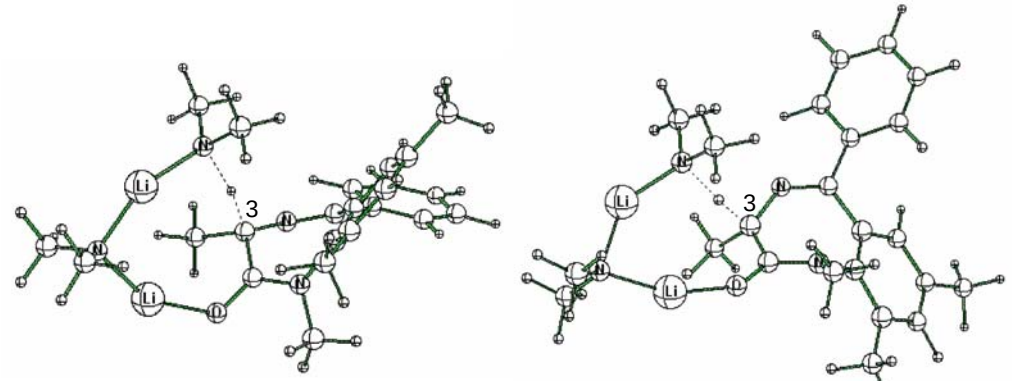

(*M*)-(*S*)-**191a** Retentive Deprotonation	(*P*)-(*S*)-**191a** Invertive Deprotonation
Relative *G* (195K) in kcal/mol	Relative *G* (195K) in kcal/mol
B3LYP/6-31G* = 0.0	5.5
B3LYP/6-31+G*// B3LYP/6-31G* = 0.0	5.4
MP2/6-31G*//B3LYP/6-31G* = 0.0	8.2
MP2/6-31+G*//B3LYP/6-31G* = 0.0	8.4

Figure 2.24 Unsolvated open dimer deprotonation transition structures from (*S*)-**172a** and $(LiNMe_2)_2$

Interestingly, as shown in Figure 2.24, energies at both B3LYP and MP2 (6-31G(d) and 6-31+G(d)) on the B3LYP/6-31G* geometries consistently show that retentive deprotonation is

more favorable at 195 K. The energetic preferences are quite significant, being by 5 and 8 kcal/mol respectively.

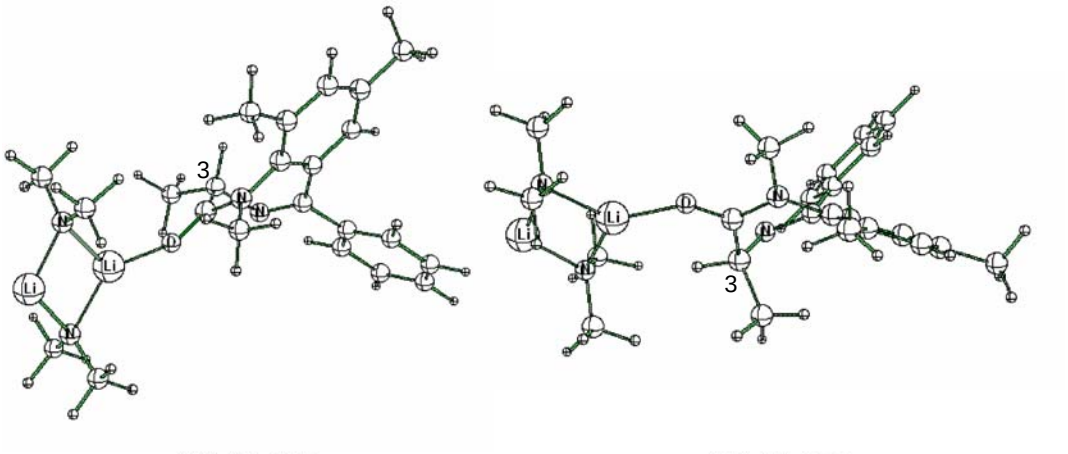

(*M*)-(*S*)-**192a**	(*P*)-(*S*)-**192a**
Relative *G* (195K) in kcal/mol	Relative *G* (195K) in kcal/mol
B3LYP/6-31G* = 0.0	6.7
B3LYP/6-31+G*// B3LYP/6-31G* = 0.0	6.8
MP2/6-31G*//B3LYP/6-31G* = 0.0	5.8
MP2/6-31+G*//B3LYP/6-31G* = 0.0	5.5

Figure 2.25 Unsolvated reactant complexes of (*S*)-**172a** and $(LiNMe_2)_2$

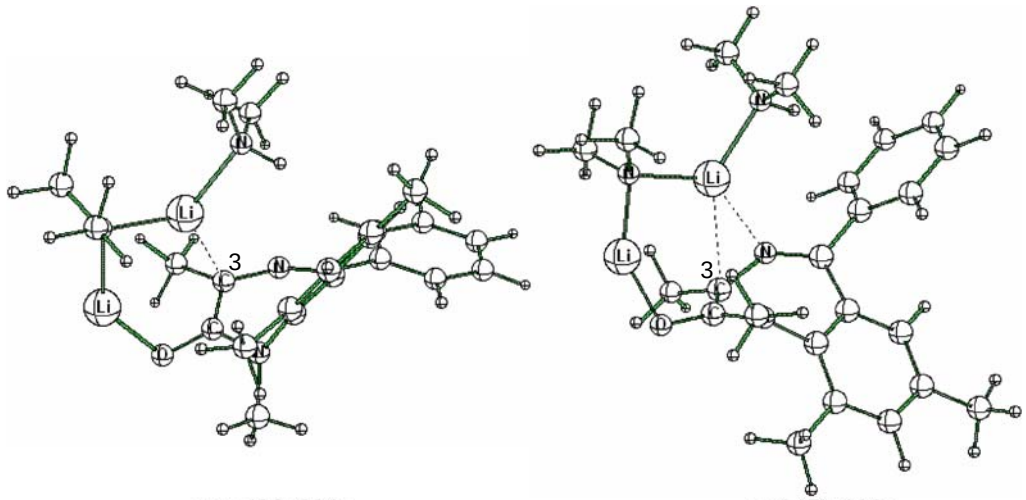

syn-(*M*)-**193a**	*anti*-(*P*)-**193a**
Relative *G* (195K) in kcal/mol	Relative *G* (195K) in kcal/mol
B3LYP/6-31G* = 4.5	0.0
B3LYP/6-31+G*// B3LYP/6-31G* = 3.8	0.0
MP2/6-31G*//B3LYP/6-31G* = 5.2	0.0
MP2/6-31+G*//B3LYP/6-31G* = 3.6	0.0

Figure 2.26 Unsolvated lithium enolate · $LiNMe_2$ complexes: *syn*-(*M*)-**193a** and *anti*-(*P*)-**193a**

As shown in Figure 2.25, shortening the C(3)-H in both transition structures of (*M*)-(*S*)- and (*P*)-(*S*)-**191a** resulted in the equilibrium geometries of lithium amide dimer−BZD

reactant complex. This precomplex is believed to be the species leading to the open-dimer deprotonation transition state.[46,48-51] As expected, (*M*)-(*S*)-**192a** bearing a pseudoequatorial C(3)-Me is lower in energy than the pseudoaxial C(3)-Me conformer (*P*)-(*S*)-**192a**.

As was seen for enolate complexes derived from monomeric $LiNMe_2$, the *anti*-enolate complex is lower in energy (Figure 2.26).

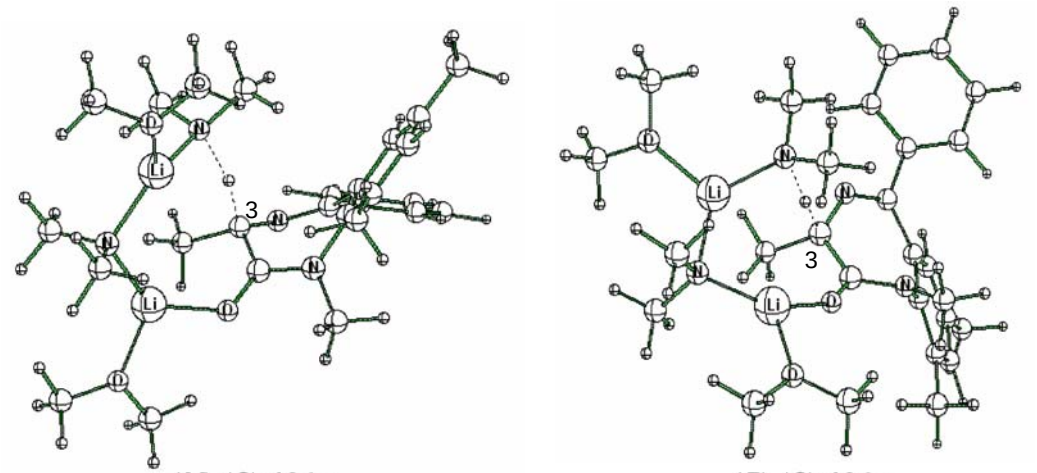

(*M*)-(*S*)-**194a** Retentive Deprotonation	(*P*)-(*S*)-**194a** Invertive Deprotonation
Relative *G* (195K) in kcal/mol	Relative *G* (195K) in kcal/mol
B3LYP/6-31G* = 0.0	7.0
B3LYP/6-31+G*// B3LYP/6-31G* = 0.0	7.1
MP2/6-31G*//B3LYP/6-31G* = 0.0	9.6
MP2/6-31+G*//B3LYP/6-31G* = 0.0	11.0

Figure 2.27 Disolvated open dimer deprotonation transition structures from (*S*)-**172a** and $(LiNMe_2)_2$

Disolvated open dimer deprotonation transition structures from (*S*)-**172a** and $(LiNMe_2)_2$ were then calculated as well (Figure 2.27). Compared to the solvent-free transition structures shown in Figure 2.24, the energetic preferences for (*M*)-(*S*)-**194a** at both B3LYP and MP2 (6-31G(d) and 6-31+G(d)) are even higher (7 – 11 kcal/mol). Similarly, the calculated energies of the solvated reactant complex (*M*)-(*S*)-**195a** are 5.5 – 6.2 kcal/mol lower than that of (*P*)-(*S*)-**195a** (Figure 2.28), indicating once again there is a distinct preference for (*M*)-conformation in the starting material. In Figure 2.29, we can see that the dimeric base no longer forms a six-membered ring with the enolate due to the displacement of the C(3) coordination by the solvent molecule (cf. Figure 2.26); but still, the metal chelated *syn*-(*M*)-enolate is less stable than the *anti*-(*P*)-conformer because of the steric effect. It should be also

stressed that a hydrogen bonding was formed between C(3) and N(base)-H in enolate complex *syn*-(*M*)-**196a**, forming an eight-membered ring.

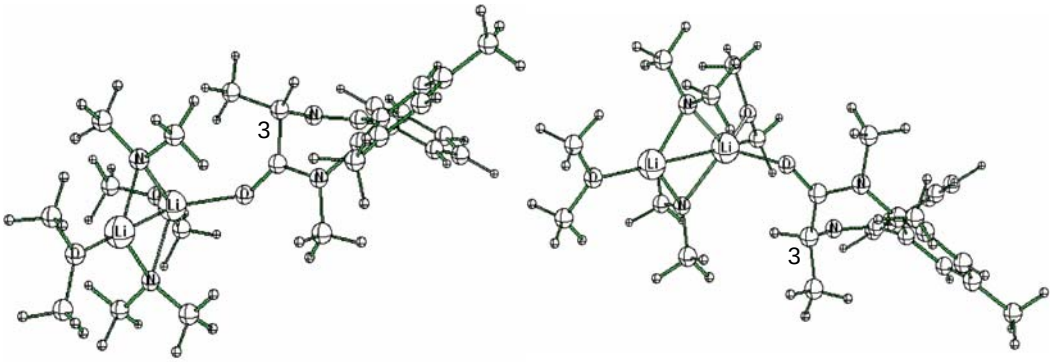

(*M*)-(*S*)-**195a**	(*P*)-(*S*)-**195a**
Relative *G* (195K) in kcal/mol	Relative *G* (195K) in kcal/mol
B3LYP/6-31G* = 0.0	6.0
B3LYP/6-31+G*// B3LYP/6-31G* = 0.0	6.1
MP2/6-31G*//B3LYP/6-31G* = 0.0	5.5
MP2/6-31+G*//B3LYP/6-31G* = 0.0	6.2

Figure 2.28 Disolvated reactant complexes of $(LiNMe_2)_2$ and (*S*)-**172a**

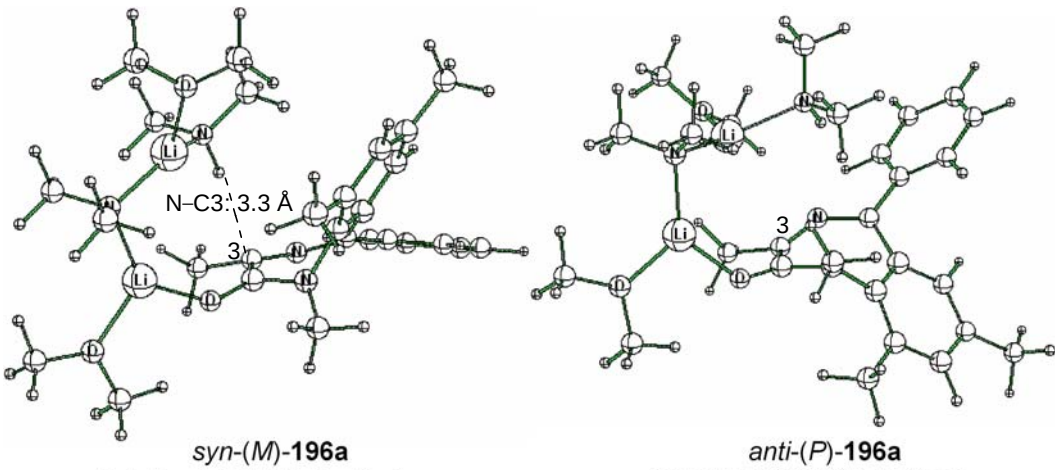

syn-(*M*)-**196a**	*anti*-(*P*)-**196a**
Relative *G* (195K) in kcal/mol	Relative *G* (195K) in kcal/mol
B3LYP/6-31G* = 3.1	0.0
B3LYP/6-31+G*// B3LYP/6-31G* = 2.6	0.0
MP2/6-31G*//B3LYP/6-31G* = 5.9	0.0
MP2/6-31+G*//B3LYP/6-31G* = 6.5	0.0

Figure 2.29 Disolvated lithium enolate · $LiNMe_2$ complexes: *syn*-(*M*)-**196a** and *anti*-(*P*)-**196a**

Although we used LDA in our earliest MOC alkylation protocol,[16] subsequent procedures used KHMDS, and in my experimental work it was used exclusively.[15,17] Therefore, similar calculations with monomeric potassium dimethylamide were carried out. Contrary to the deprotonation with monomeric lithium amide, transition structures with

monomeric potassium dimethylamide predict retentive deprotonation. Transition structure (*M*)-(*S*)-**197a** is favored by 3.7-6.9 kcal/mol at 195 K relative to (*P*)-(*S*)-**197a** (Figure 2.30).

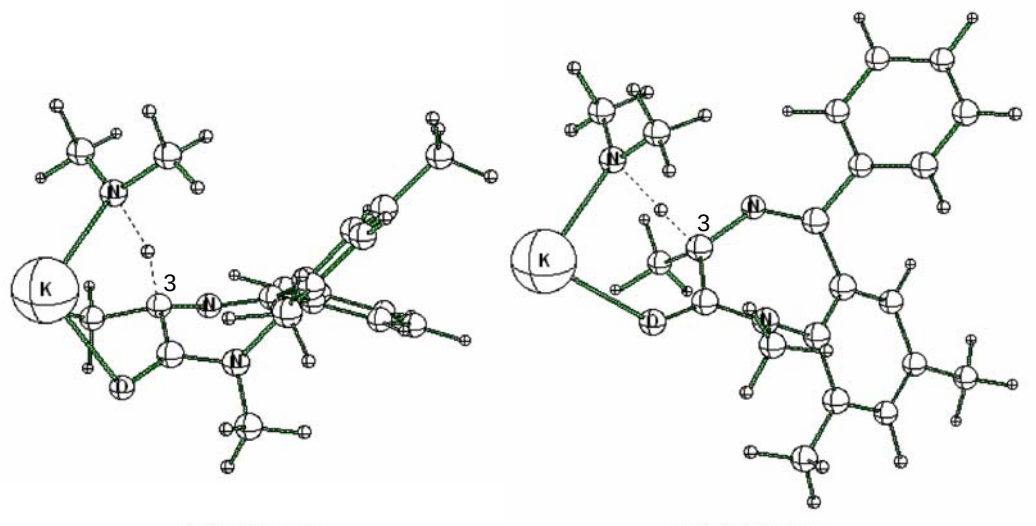

(*M*)-(*S*)-**197a** Retentive Deprotonation	(*P*)-(*S*)-**197a** Invertive Deprotonation
Relative *G* (195K) in kcal/mol	Relative *G* (195K) in kcal/mol
B3LYP/6-31G* = 0.0	3.7
B3LYP/6-31+G*// B3LYP/6-31G* = 0.0	3.6
MP2/6-31G*//B3LYP/6-31G* = 0.0	5.7
MP2/6-31+G*//B3LYP/6-31G* = 0.0	6.9

Figure 2.30 Unsolvated deprotonation transition structures of (*S*)-**172a** by $KNMe_2$

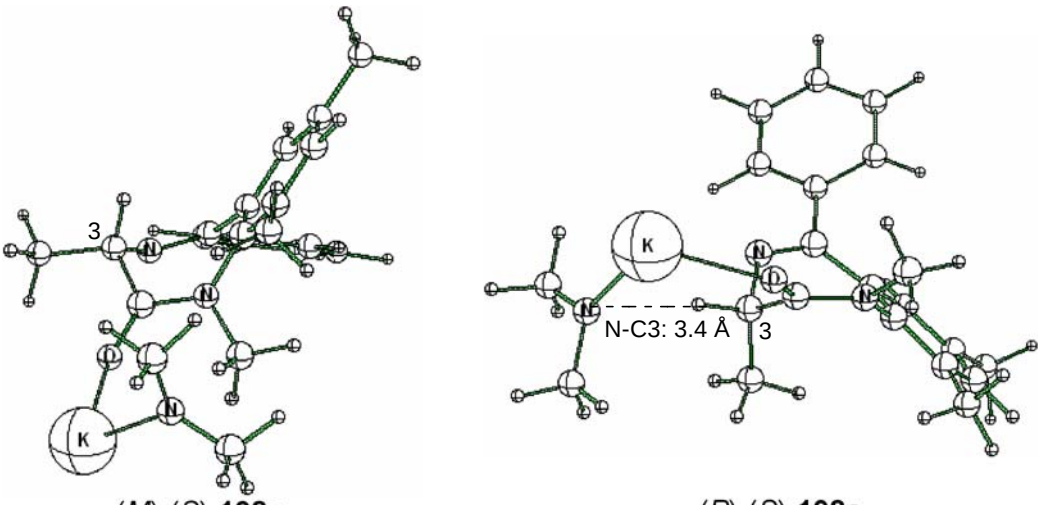

(*M*)-(*S*)-**198a**	(*P*)-(*S*)-**198a**
Relative *G* (195K) in kcal/mol	Relative *G* (195K) in kcal/mol
B3LYP/6-31G* = 0.0	7.6
B3LYP/6-31+G*// B3LYP/6-31G* = 0.0	6.4
MP2/6-31G*//B3LYP/6-31G* = 0.0	7.0
MP2/6-31+G*//B3LYP/6-31G* = 0.0	6.3

Figure 2.31 Unsolvated reactant complexes of (*S*)-**172a** and $KNMe_2$

In concord with the above examples of reactant complexes, (*M*)-(*S*)-**198a** is preferred (Figure 2.31). Potassium enolate amine complex *syn*-(*M*)-**199a** is higher in energy than the *anti*-(*P*)-conformer, also due to the steric bulk between the amine and benzo ring at the concave face (Figure 2.32).

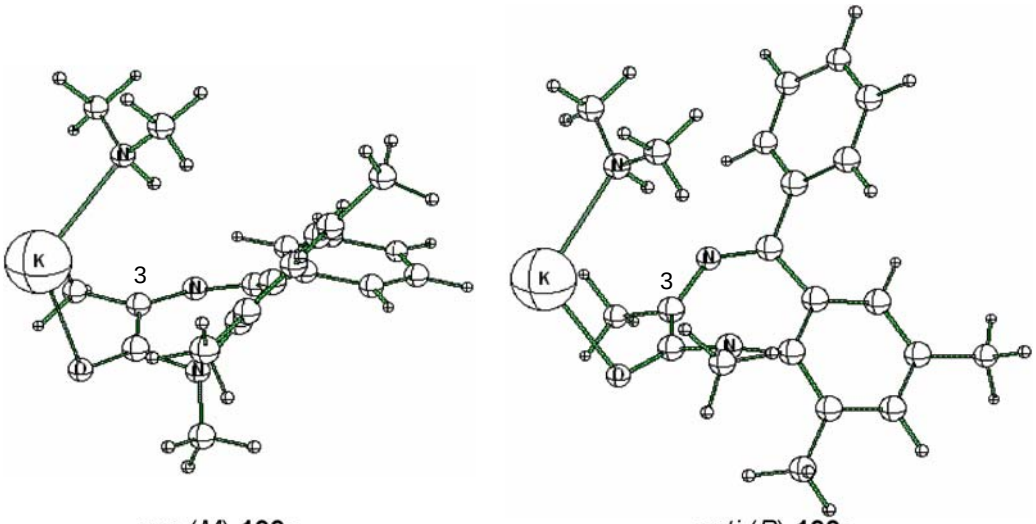

syn-(*M*)-**199a**	*anti*-(*P*)-**199a**
Relative *G* (195K) in kcal/mol	Relative *G* (195K) in kcal/mol
B3LYP/6-31G* = 3.6	0.0
B3LYP/6-31+G*// B3LYP/6-31G* = 3.4	0.0
MP2/6-31G*//B3LYP/6-31G* = 3.7	0.0
MP2/6-31+G*//B3LYP/6-31G* = 3.6	0.0

Figure 2.32 Potassium enolate amine complexes

Furthermore, transition structures for deprotonation of (*S*)-**172a** by tris (OMe_2) solvated $KNMe_2$ were also calculated (Figure 2.33). As can be seen in Figure 2.33, the energetic preferences for retentive deprotonation increases upon solvation at both B3LYP and MP2 (6-31G(d) and 6-31+G(d)). The calculated reactant complexes (Figure 2.34) and enolate complexes (Figure 2.35) also follow the established trends.

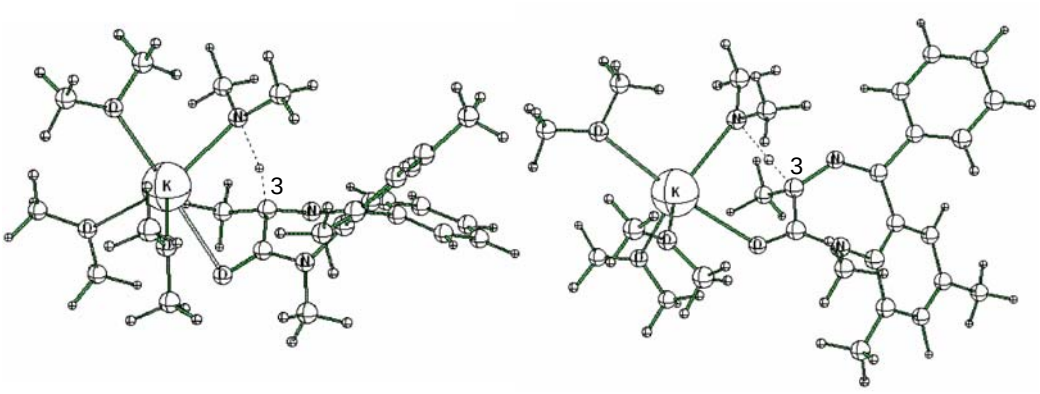

(*M*)-(*S*)-**200a** Retentive Deprotonation	(*P*)-(*S*)-**200a** Invertive Deprotonation
Relative *G* (195K) in kcal/mol	Relative *G* (195K) in kcal/mol
B3LYP/6-31G* = 0.0	3.7
B3LYP/6-31+G*// B3LYP/6-31G* = 0.0	3.6
MP2/6-31G*//B3LYP/6-31G* = 0.0	5.7
MP2/6-31+G*//B3LYP/6-31G* = 0.0	6.9

Figure 2.33 Transition structures for deprotonation of (*S*)-**172a** by tris(OMe_2) solvated $KNMe_2$

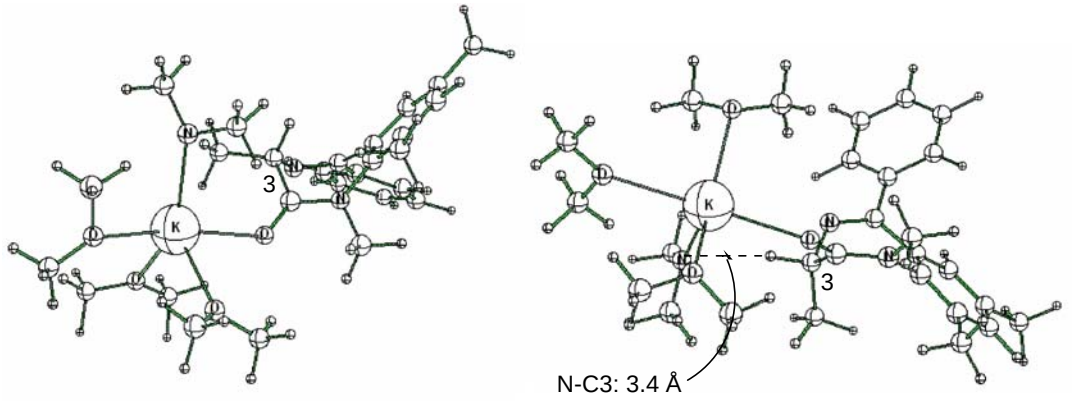

(*M*)-(*S*)-**201a**	(*P*)-(*S*)-**201a**
Relative *G* (195K) in kcal/mol	Relative *G* (195K) in kcal/mol
B3LYP/6-31G* = 0.0	7.6
B3LYP/6-31+G*// B3LYP/6-31G* = 0.0	6.4
MP2/6-31G*//B3LYP/6-31G* = 0.0	7.0
MP2/6-31+G*//B3LYP/6-31G* = 0.0	6.3

Figure 2.34 Tris(OMe_2) solvated reactant complexes of $KNMe_2$ and (*S*)-**172a**

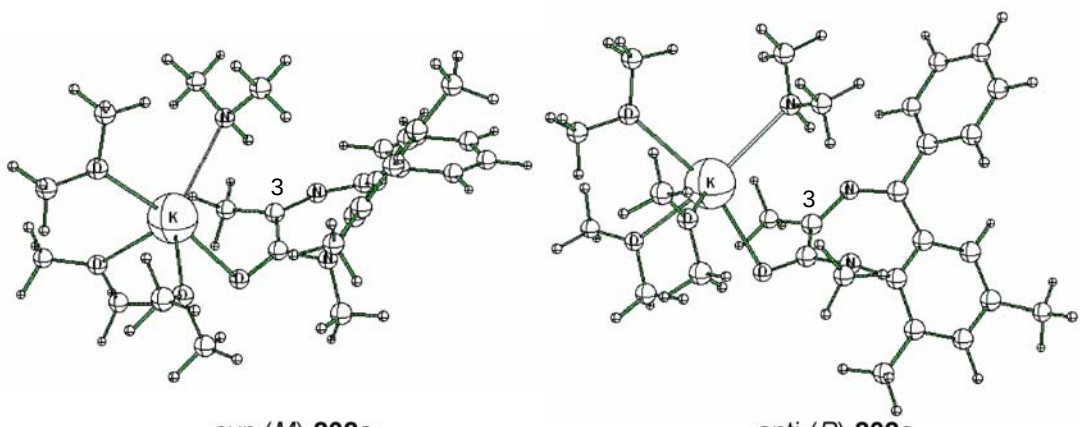

syn-(*M*)-**202a**	anti-(*P*)-**202a**
Relative *G* (195K) in kcal/mol	Relative *G* (195K) in kcal/mol
B3LYP/6-31G* = 3.6	0.0
B3LYP/6-31+G*// B3LYP/6-31G* = 3.4	0.0
MP2/6-31G*//B3LYP/6-31G* = 3.7	0.0
MP2/6-31+G*//B3LYP/6-31G* = 3.6	0.0

Figure 2.35 Tris(OMe_2) solvated potassium enolate amine complexes

To account for the difference in calculated stereochemical outcome between monomeric $LiNMe_2$ and dimeric $LiNMe_2$, as well as between $LiNMe_2$ and $KNMe_2$, structural parameters of the corresponding deprotonation transition structures are summarized in Table 2.4. We will focus on the dihedral angle O-C(2)-C(3)-H, Φ, and angle N(base)-H-C(3), θ. The optimum Φ for deprotonation of acetaldehyde was reported to be 103º,[52] while θ values near 180º are expected to be favored for H^+ transfer. The angle Φ in (*M*)-(*S*)-**185a** and **188a** with monomeric lithium amide are 75° and 78° respectively, while that in (*M*)-(*S*)-**197a** and **200a** with monomeric potassium base are 92° and 98° (cf. Table 2.4, entries 3 and 11, and 5 and 13). Consequently, it is noted that the π orbital overlapping is less effective in the former two during deprotonation. This difference may be attributed to the size of metal counterion, which results in longer O-K and K-N bond lengths relative to the Li analogue. Due to the smaller 6-membered ring in the lithium amide deprotonation transition state, the C(3)-H has to be bent away from the right angle to the carbonyl group (cf. Figure 2.17 and 2.29, and 2.20 and 2.32). Furthermore, θ in monomeric lithium transition structures (*M*)-(*S*)-**185a** and **188a** is smaller than that in potassium transition structures (*M*)-(*S*)-**197a** and **200a** for the same

reason (cf. Table 2.4, entries 3 and 11, and 5 and 13). As a result, the lone pair to σ* interaction is weaker in the former two transition states.

However, when dimeric lithium base is used, the deficiencies in the aforementioned orbital overlapping can be relieved by the expanded 8-membered ring in the corresponding deprotonation transition states. By means of the open dimers, Φ becomes 100° and 102° in (*M*)-(*S*)-**191a** and **194a** respectively (cf. Table 2.4, entries 7 and 11, and 9 and 13). Also, the θ in these two transition structures are even larger than that in potassium amide deprotonation structures (*M*)-(*S*)-**197a** and **200a**. We suggest that the reason for the solvated and unsolvated monomeric $LiNMe_2$ deprotonation being calculated to give (*P*)-enolate is due to the unfavorable θ value of 154º in the (*M*)-(*S*)-transition structures. All of the other transition structures feature more linear proton transfer. Overall, the deprotonation transition structures with dimeric lithium amide and monomeric potassium amide work well to offer explanation for the preferred retentive deprotonation of (*S*)-**172a**.

Table 2.4 Selected structural parameters of BZD amides and transition structures in deprotonation

Entry	Structure	Base	Counterion	∠O-C2-C3-H	∠N(base)-H-C(3)
1	(*M*)-(*S*)-**172a**	na	na	135°	na
2	(*P*)-(*S*)-**172a**	na	na	3°	na
3	(*M*)-(*S*)-**185a**	unsolvated monomer	Li	75°	154°
4	(*P*)-(*S*)-**185a**	unsolvated monomer	Li	41°	174°
5	(*M*)-(*S*)-**188a**	solvated monomer	Li	78°	154°
6	(*P*)-(*S*)-**188a**	solvated monomer	Li	41°	175°
7	(*M*)-(*S*)-**191a**	unsolvated dimer	Li	100°	173°
8	(*P*)-(*S*)-**191a**	unsolvated dimer	Li	49°	167°
9	(*M*)-(*S*)-**194a**	solvated dimer	Li	102°	167°
10	(*P*)-(*S*)-**194a**	solvated dimer	Li	48°	175°
11	(*M*)-(*S*)-**197a**	unsolvated monomer	K	92°	162°
12	(*P*)-(*S*)-**197a**	unsolvated monomer	K	44°	177°
13	(*M*)-(*S*)-**200a**	solvated monomer	K	98°	166°
14	(*P*)-(*S*)-**200a**	solvated monomer	K	45°	175°

2.8 Kinetic and Computational Studies of the 1,4-Benzodiazepin-2-one Enolate Racemization Barrier

2.8.1 Kinetic Studies on BZD Enolate Racemization Barrier

As discussed in section 2.7, computational studies supported retentive deprotonation of (*S*)-**172a** by dimeric $LiNMe_2$ and monomeric $KNMe_2$. The enantioselectivity of the BZD deprotonation/alkylation is time and temperature dependent due to the dynamic conformational chirality in the BZD enolate.[16,24,42] Therefore, to confirm that this reactive intermediate in the MOC reactions is transiently non-racemic, experiments were performed on **172a** at 257K, wherein the time between additions of KHMDS and BnBr was varied from 5 to 15 min (Scheme 2.10).

Scheme 2.10 Kinetic studies of racemization barrier of **181a**

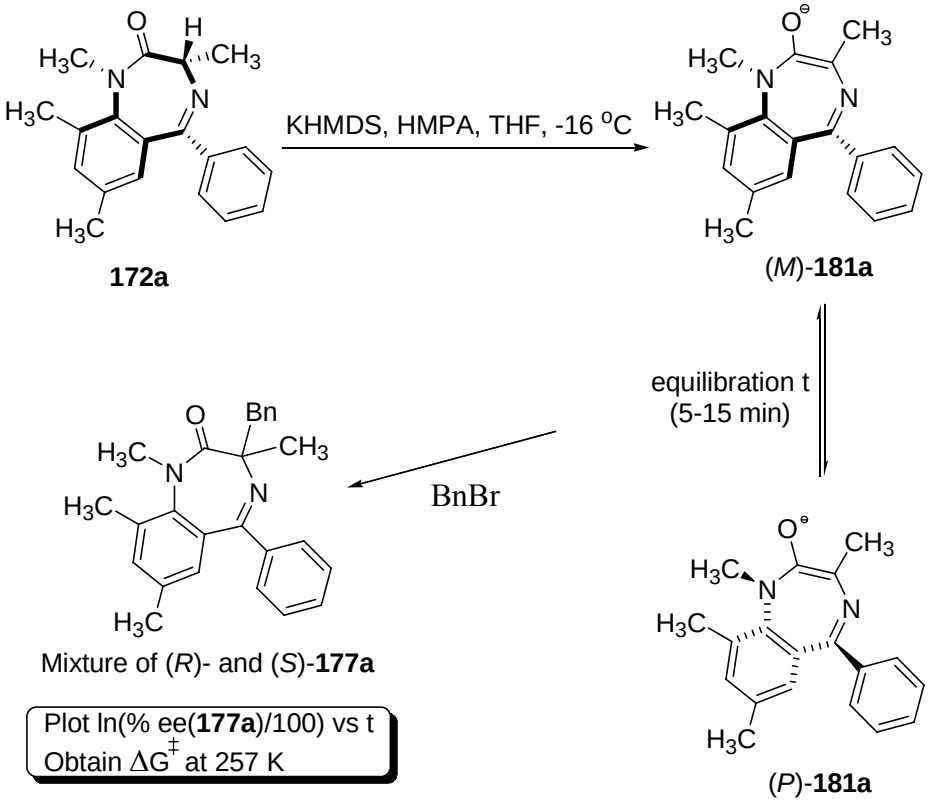

By plotting ln (% ee(**177a**)/100) vs time we determined a racemization $t_{1/2}$ for the enolate of 95 ± 6 min, corresponding to an activation free energy for racemization of 19.9 ±

0.1 kcal/mol (Figure 2.36).[53] If the same racemization barrier is applied at 195K, the corresponding $t_{1/2}$ will be over 54 years, which accounts for the perfect enantioselectivities observed in the alkylations of **172a**.

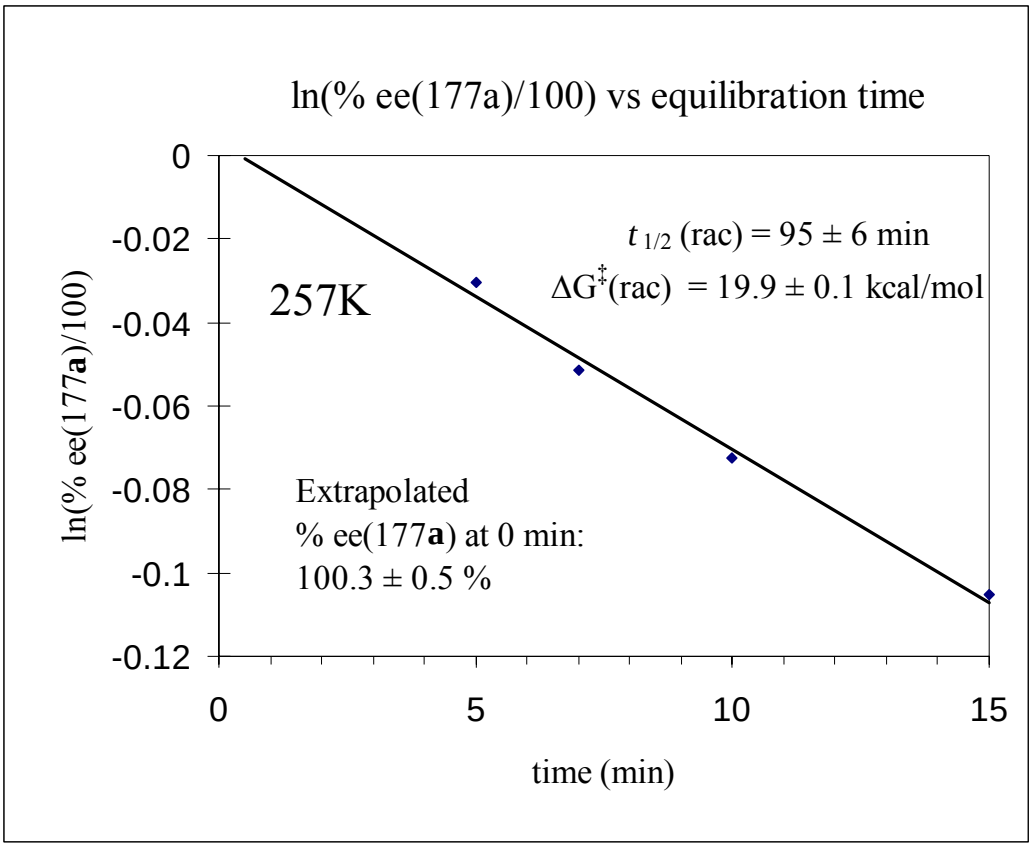

Figure 2.36 Plot of ln (% ee (**177a**)/100) vs deprotonation time at 257K, demonstrating racemization of the potassium enolate derived from (*S*)-**172a** .

2.8.2 DFT Calculations of BZD Enolate Racemization Barrier

The structure of the conformationally chiral enolate derived from (*S*)-**172a** in solution is not known, particularly its aggregation, solvation, and the ionization states. In order to gain further insight into the racemization of **181a**, the equilibrium geometries and ring inversion transition structures for the enolate free anion (**203a**, **203a***) and the corresponding $Li(OMe_2)_3$ (**204a**, **204a***) and $K(OMe_2)_4$ (**205a**, **205a***) salts were located at B3LYP/6-31+G(d) (Figure 2.37).[31] The choice of the 6-31+G(d) basis set for these geometries was made in view of the importance of diffuse functions for proper electronic description of

anionic species. The B3LYP/6-31+G* activation free energy for ring inversion of free anion **203a** at 257 K is 14.3 kcal/mol, corresponding to a racmization $t_{1/2}$ of 15 minutes at 195 K. This value is far below the experimental result. However, the activation free energy of solvated potassium enolate **205a** for racemization is 21.2 kcal/mol at 257 K, within 2 kcal/mol of the experimentally determined barrier for the potassium enolate in THF. As for solvated lithium enolate **204a**, a higher calculated racemization barrier of 23.8 kcal/mol was obtained. The 2 kcal/mol higher barrier calculated for the lithium salt may be a reflection of the shorter Li-O bond lengths (1.8-2.1 Å) relative to K-O (2.5-2.9 Å). These shorter bond lengths would likely cause greater steric hindrance between the solvated metal and the N(1)-Me in the ring inversion transition structures. We attribute the high experimental inversion barrier of TBS enol **182a** relative to that of the potassium enolate to the same effect.

To summarize, DFT calculations agree with the experimental studies that the enolate derived from (*S*)-**172a** has enough conformational stability at -78 °C to carry out enantioselective deprotonation/alkylation without racemization.

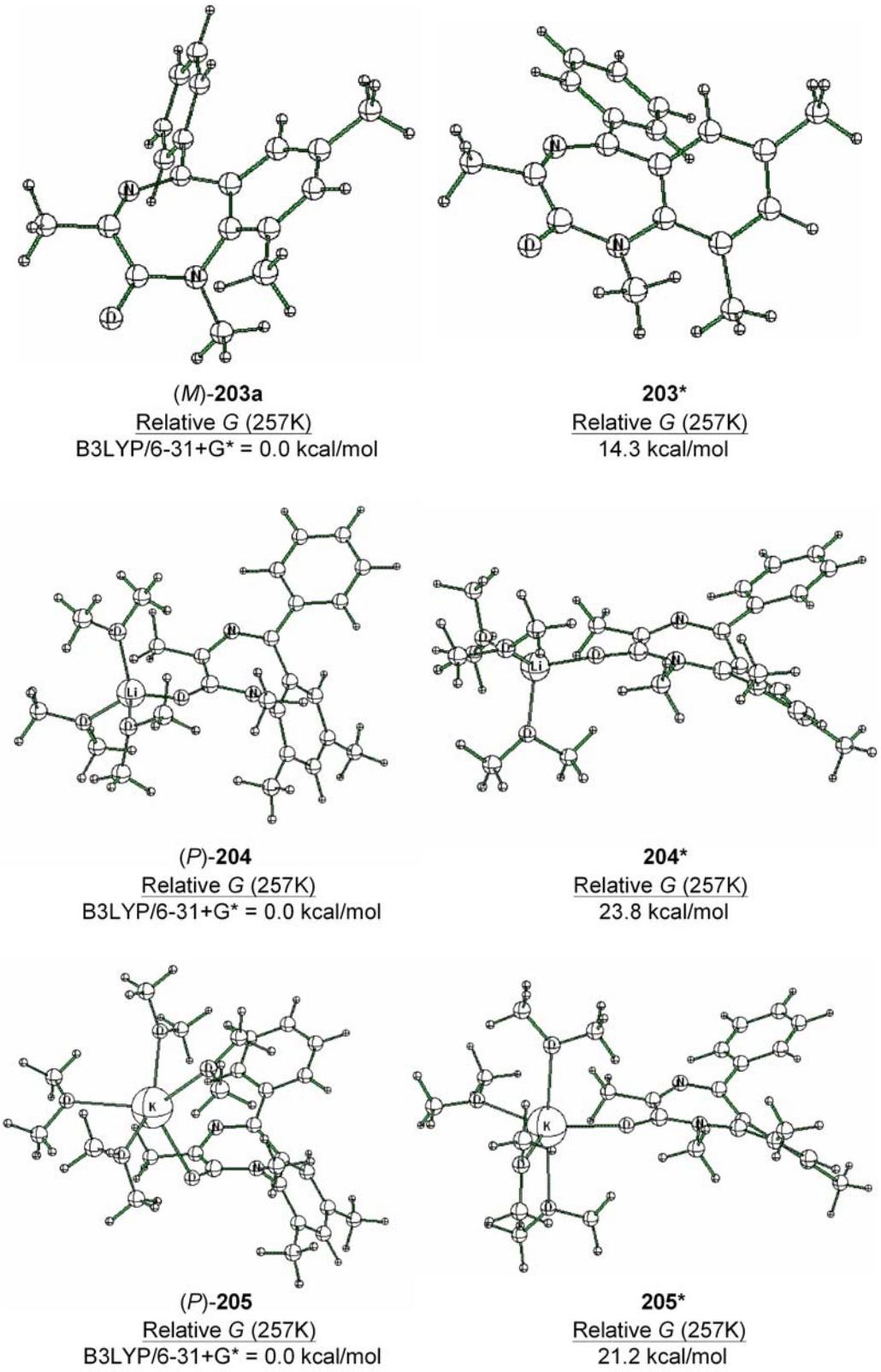

Figure 2.37 Equilibrium geometries and ring inversion transition structures for the enolate free anion (**203a**, **203a***) and the corresponding $Li(OMe_2)_3$ (**204a**, **204a***) and $K(OMe_2)_4$ (**205a**, **205a***) salts derived from **172a**

2.9 Computational Studies of Enantioselective Alkylation of BZD Enolate

2.9.1 DFT Studies of BZD Enolate

Enolate alkylation is a popular strategy for achieving enantioselective C-C bond formation, and the basis for the diastereofacial selectivity in these reactions has been vigorously argued. Seebach and co-workers attributed stereoselectivity to structural preferences that also caused slight pyramidalization of the enolate.[54,55] As shown in Scheme 2.11, Seebach presented an X-ray structure of a silyl enol ether **206** wherein pyramidalization of trigonal C(5) pointed in the same direction as where protonation occurred. It should be noted that alternation of pyramidalization of trigonal centers in **206** are caused by torsional effects.

Scheme 2.11 Protonation stereoselectivity attributed to pyramidalization of enolate β-carbon in **206**

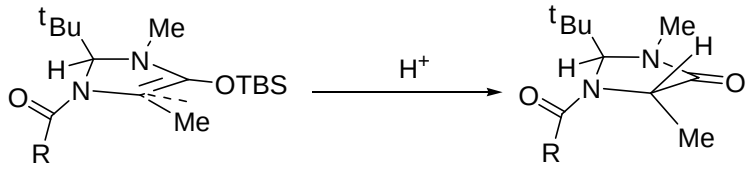

206 **207**

In addition, Meyers et al. suggested an electronic effect favoring electronic approach anti to the nitrogen lone pair which can override steric factors in amide enolate alkylation (Scheme 2.12).[56,57]

Scheme 2.12 Stereoselectivity due to electronic effect anti to nitrogen lone pair

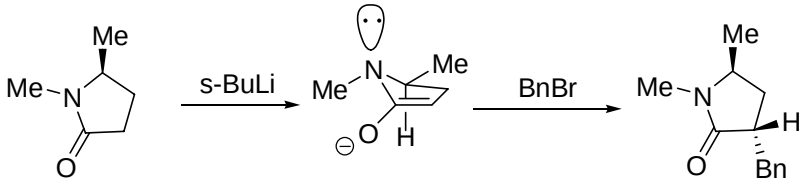

208 **209** **210** (99% de)

However, Houk counter-proposed that this facial diastereoselectivity found its origin in the torsional strain from allylic CH bonds in the transition states (Figure 2.38).[58] Moreover, Tomoda proposed that the π-facial stereoselectivity in pyrrolidinone enolates may be

attributed to the metal cation coordination (Scheme 2.13),[59] but recently Ando[60] and Luque[61] independently argued by computational studies that this complexation does not play an important role in determining the stereochemical outcome.

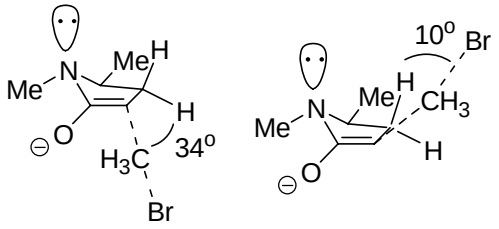

Relative E (RHF/6-31+G(d)): 0 1.7 kcal/mol

Figure 2.38 Stereoselectivity of reaction in Scheme 2.10 attributed to torsional strain from allylic CH bond in transition state

Scheme 2.13 Stereoselectivity due to Li coordination

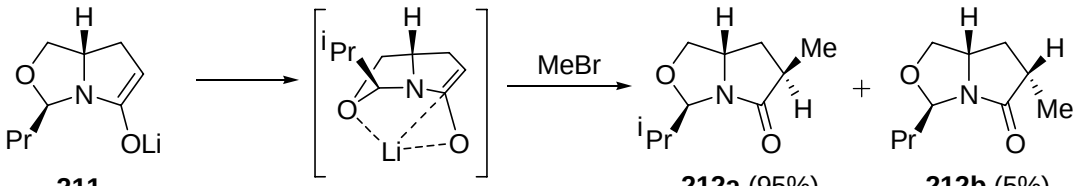

From our freeze frame observations mentioned in section 2.6.2, contra-steric concave face alkylation of the (*M*)-enolate derived from (*S*)-**172a** is preferred, which resulted in retention of configuration with excellent enantioselectivity (> 99% ee). To better understand why the alkylation pathway A in Scheme 2.7 is more favorable, computational studies were carried out. We hypothesize that the alkylation transition state is "reactant-like", which is reasonable for an exothermic reaction, so that the stereochemical outcome can be determined primarily by the geometry of the starting enolate. Examination of the calculated enolate (**203a**, **204a** and **205a**) and TBS enol ether **182a** equilibrium geometries, and the X-ray structure of TBS enol **182a** reveal that their C(2) and C(3) are slightly concurrent pyramidalized toward the concave face, the favored trajectory of the electrophile,[54,55] as summarized in Table 2.5. We assign the sense of pyramidalization as "α" when the deformation angle at C(3) is below the plane of C(2)-C(3)-N(4), and vice versa for "β". The deformation angles at C(2) and C(3)

in the X-ray structure of **182a** are 5.6° (α) and 7.2° (α) respectively. For comparison, the corresponding calculated equilibrium geometry was calculated to have 7.3° (α) at C(2) and 9.1° (α) at C(3), within 2° of the experimentally determined deformation angles. Furthermore, the pyramidalization at C(2) is similar among the species; however, the one at C(3) becomes smaller with stronger covalency in the C(2)-O bonding: it ranges from 16.6º (α) in the free anion to 9.1º (α) for the TBS enol. Also, this deformation causes the weakening of C(2)-C(3) double bond as a result of partial transformation of the p orbitals into hybrids toward sp^3 (Table 2.5).[62,63] Therefore, in a sense, a lone pair electrons at C(3) is pointing toward the concave face for electrophilic attack. This proposal is supported by inspecting the HOMO that the larger coefficient was found at C(3) in the concave face of the (*M*)-enolate (Figure 2.39).[56,57]

Table 2.5 Pyramidalization angles and C2=C3 bond length in **182a**, **203a**, **204a** and **205a**

Species	Enol/enolate derivative	Deformation Angle at C2[a]	Deformation Angle at C3[b]	C2=C3 Bond Length (Å)
182a (X-ray)	TBS enol	5.6° (α)	7.2° (α)	1.35
182a (computed)	TBS enol	7.3° (α)	9.1° (α)	1.36
203a (computed)	Li $(OMe_2)_3$	5.9° (α)	11.5° (α)	1.41
204a (computed)	K $(OMe_2)_4$	7.9° (α)	14.0° (α)	1.43
205a (computed)	Free anion	7.3° (α)	16.6° (α)	1.45

[a] deformation of C2-O below the plane N1C2C3
[b] deformation of C3-Me below the plane C2C3N4

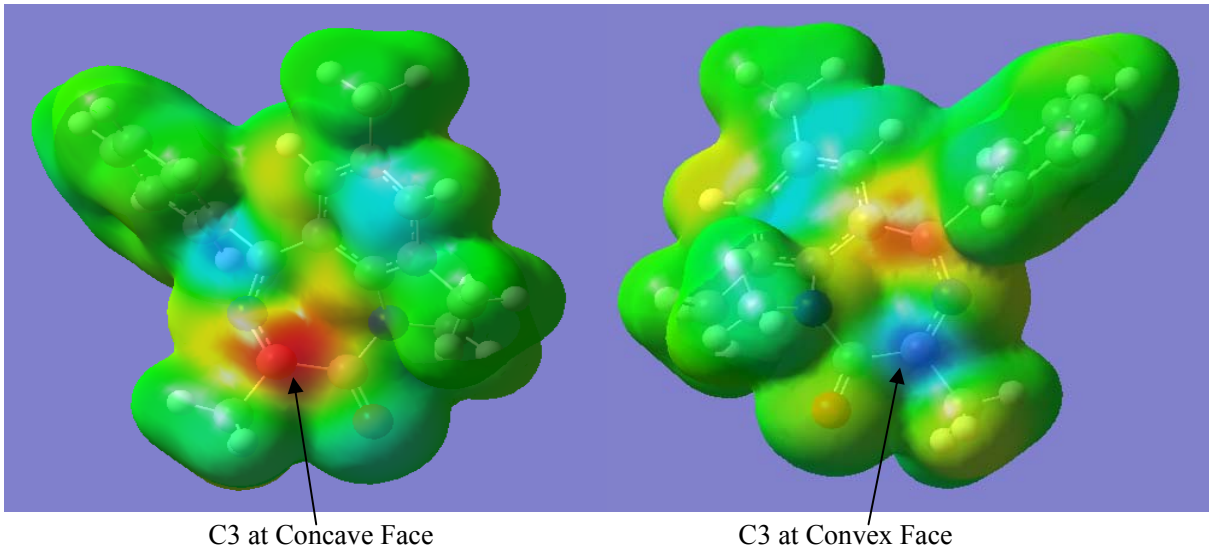

Figure 2.39 Electron density isosurface of the HOMO of BZD free enolate **202a** by mapping the value of the HOMO onto total density (red: higher electron density)

Wipff,[64] Houk[65-67] and Seebach[54] indicated that trigonal centers pyramidalize in an unsymmetrical environment. To rationalize the origin of the concurrent pyramidalization at C(2) and C(3), first, we inspected the electronic effect of the two nitrogen lone pairs next to the enol group in the X-ray structure of **182a**. Different from the electronic effect described by Meyers (Scheme 2.10),[56,57] the nitrogen lone pairs are not anti, but almost perpendicular, to the favored trajectory of the electrophile (Figure 2.40); meanwhile, the two alkene carbons are still pyramidalized. We conclude that Meyers' hypothesis cannot be applied to our BZD system.

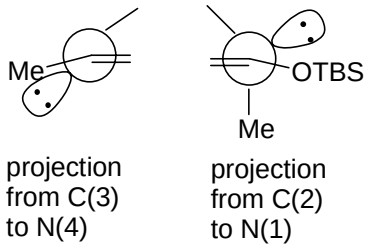

Figure 2.40 Newman projection looking along from C(2) to N(1) and from C(3) to N(4) in X-ray structure of **182a**

Both Houk[65-67] and Burkert[68] proposed that "ground state" pyramidalization of alkenes is a consequence of relief of torsional repulsion. We found that this theory could be applied to the C(2) only if the torsion between C(2)-O and N(1) lone pair is considered in the X-ray structure of TBS enol **182a** (Figure 2.41a). However, in the calculated equilibrium geometries of the free and solvated lithium and potassium BZD enolates, this pyramidalization at C(2) appears to increase the torsional interaction between C(2)-O and N(1)-Me (Figure 2.41b). Also, pyramidalization at C(3) increases the torsional repulsion between C(3)-Me and N(4) lone pair, in both X-ray and calculated structures (Figure 2.41c). Furthermore, a major torsional interaction should be between C(2)-O and C(3)-Me, but the observed concurrent pyramidalization does not relieve this torsion (Figure 2.41d and Table 2.5). Therefore, torsional effects do not appear to be responsible for the observed pyramidalizations at C(2) and C(3).

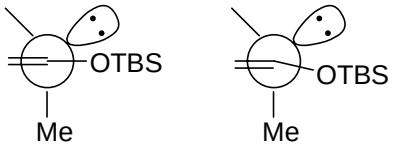

planar C(2) pyramidalized C(2)

a) Newman projection looking along from C(2) to N(1) in X-ray structure of **182a**

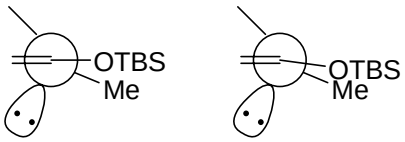

planar C(2) pyramidalized C(2)

b) Newman projection looking along from C(2) to N(1) in equilibrium geometry of **203a**

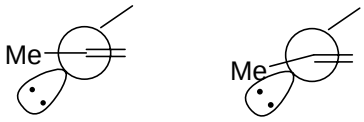

planar C(3) pyramidalized C(3)

c) Newman projection looking along from C(3) to N(4) in both X-ray and equilibrium geometry

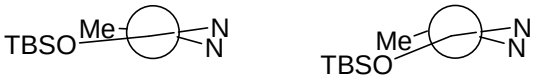

planar C(2) and C(3) concurrently pyramidalized C(2) and C(3)

d) Newman projection looking along from C(2) to C(3) in X-ray structure of **182a**

Figure 2.41 Newman projections to show the torsional repulsion at C(2) and C(3) in **182a** and **203a**

In contrast, Vogel suggested the deformation of alkene in syn-oxasesquinorbornene derivative **213** might be due to the repulsion between endo allylic σ bond and the alkene π orbital (Figure 2.41).[69] Bartlett proposed a similar explanation that the ground-state alkene carbons in syn-sesquinorbornene derivative **214** concurrently pyramidalize so as to relieve the repulsion between endo β hydrogen and the π orbital (Figure 2.42).[70]

repulsion between allylic σ bond and π orbital

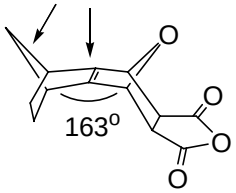

213

repulsion between endo β hydrogens and π orbital

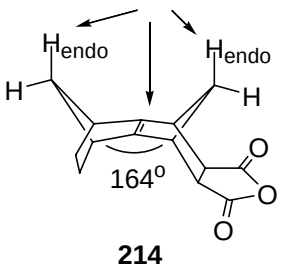

214

Figure 2.42 Deformation of alkenes in syn-sesquinorbornene derivative **213** and **214**

To investigate if the pyramidalization at C(2) and C(3) could be attributed to electrostatic repulsion, we undertook calculations on diverse simplified BZD systems (Figure 2.43). Our intent was to vary the electron density in the structure opposite C(3) to see if the predicted change in pyramidalization would result. To avoid convoluting this electronic effect with local steric effects, we performed constrained optimizations. Based on the calculated structure of the free enolate **203a**, angles C2-N1-C10 and N4-C5-C11, and dihedral angles C3-C2-N1-C10 and C3-N4-C5-C11 are fixed at the same values as in **203a** in all constrained calculations.

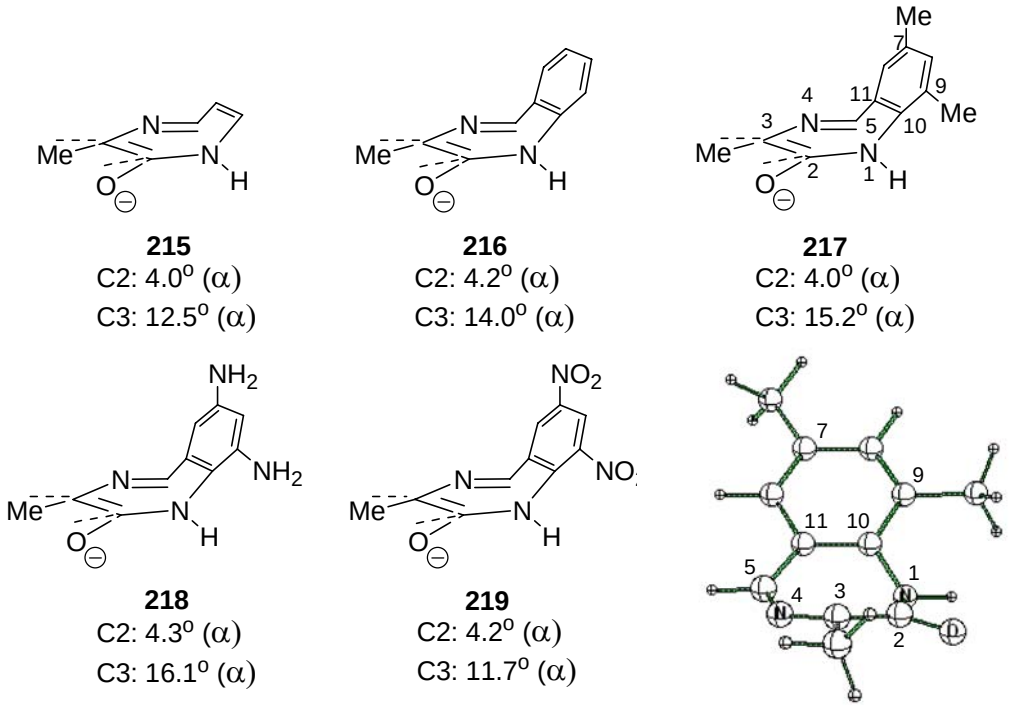

Figure 2.43 Deformation angles at C2 and C3 in different enolates located at B3LYP/6-31+G(d). Constraints at angles C2-N1-C10 and N4-C5-C11 and at dihedral angles C3-C2-N1-C10 and C3-N4-C5-C11. The picture at right bottom corner is front view of the calculated structure **217**.

The simplest diazepine ring **215** shows that C(2) and C(3) are still pyramidalized when the benzo ring is replaced with a double bond. Addition of a benzo ring in **216** indicates that the enhanced π electron density increases the deformation angle at C(3) by 1.5°, suggesting larger electrostatic repulsion between the π system in the benzo ring and the alkene π orbital at C(3). C(7),C(9)-dimethyl substitution in **217** mimics our BZD free enolate **203a**, in which

the deformation angle at C(3) is raised to 15.2°. In **218**, the C(7)- and C(9)- substituents are replaced by stronger electron-donating amino groups. The increased pyramidalization is consistent with increased electrostatic repulsion. Finally, placement of strong electron-withdrawing nitro groups at C(7) and C(9) in **219** induces the C(3) deformation angle to decrease by 4.4°, even smaller than the one in the simplified system **215**. Thus we believe that as in Vogel's and Bartlett's explanations of **213** and **214**, electrostatic repulsion plays a role in pyramidalizing the sp^2-C(3). Since ^{1}H NMR showed that the pseudoaxial substituent at C(3) is shielded by the benzo ring in tertiary and quaternary BZDs (Figure 2.7),[17,24] it should be little surprise that electrostatic repulsion exists between the benzo π system and the C(3) π orbital.

However, note that the C(2) deformation angle is almost unchanged with the variation of the benzo ring π electron density, suggesting that the pyramidalization at C(2) is caused by another controlling factor. Inspection of the calculated structure of **217** suggests that the π electron cloud of the benzo ring impinges upon C(3) only (see the front view of **217** in Figure 2.42). C(2) in the simplified BZDs may be pyramidalized by relieving the electrostatic repulsion from the endo allylic σ bond N(1)-C(10),[69] or the torsional strain from the N(1)-proton (C(2)-O bent away from N(1)-H in these structures).[65-68]

2.9.2 DFT Calculations of Alkylation Transition Structures of BZD enolate

Up to now, our explanations of concave face alkylation here relied upon a reactant-like transition state and pyramidalization in the enolate. Such analyses constitute "ground state" arguments. Will the energies of calculated concave-face and convex-face alkylation transition structures also predict concave-face alkylation? Polo Lam has previously calculated alkylation transition structures for enolate free anions of **76a** and **76b**.[35] At B3LYP/6-31G(d) his calculations showed a consistent 2.5 – 6.9 kcal/mol preference for concave face alkylations. We thus performed similar calculations to determine alkylation transition

structures for the free enolate of **203a**. As can be seen in Figure 2.44, concave face benzylation of the enolate free anion derived from **203a** is predicted to be favored by 7.1kcal/mol. Similarly, concave face allylation is favored by 8.6 kcal/mol (Figure 2.45). An interesting common feature of the concave face alkylation transition structures is the longer C(3)-C(12) contacts relative to those of the convex face. These bond lengths are consistent with the idea of greater steric hindrance to concave face alkylation.

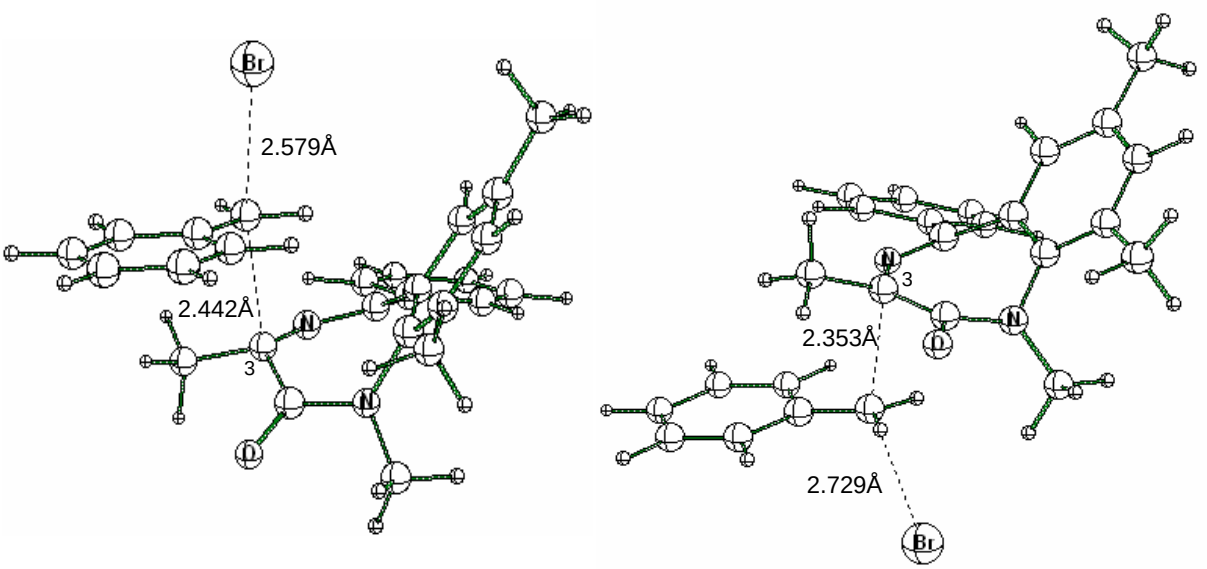

220
Concave face benzylation
Relative *G*: 0.0 kcal/mol
Deformation angle at C(3): 38.3º (α)

221
Convex face benzylation
Relative *G*: 7.1 kcal/mol
Deformation angle at C(3): 13.7º (β)

Figure 2.44 Transition structures for concave face and convex face benzylation at B3LYP/6-31+g(d)//B3LYP/6-31g(d). Sense of deformation angle at C(3): (α) stands for pyramidalization below the plane of C(2)-C(3)-N(4); (β) stands for pyramidalization above the plane of C(2)-C(3)-N(4).

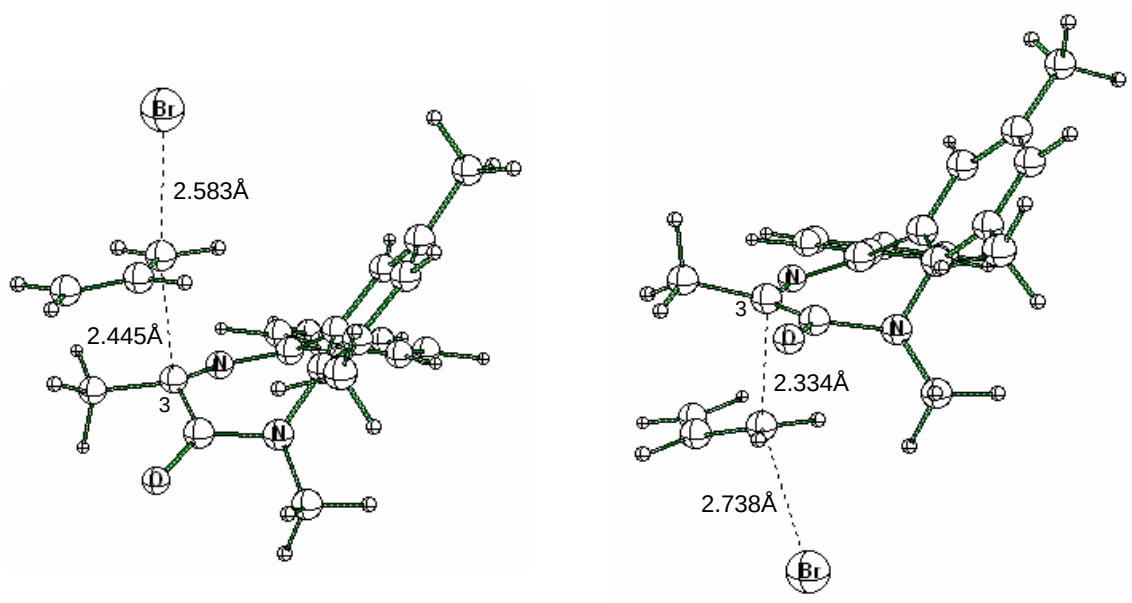

222
Concave face allylation
Relative *G*: 0.0 kcal/mol
Deformation angle at C(3): 37.3º (α)

223
Convex face allylation
Relative *G*: 8.6 kcal/mol
Deformation angle at C(3): 14.3º (β)

Figure 2.45 Transition structures for concave face and convex face allylation at B3LYP/6-31+g(d)//B3LYP/6-31g(d). Sense of deformation angle at C(3): (α) stands for pyramidalization below the plane of C(2)-C(3)-N(4); (β) stands for pyramidalization above the plane of C(2)-C(3)-N(4).

Concave and convex face allylation transition structures also vary in the sense of pyramidalization at C(3). In concave face alkylation transition structures the pyramidalization at C(3) is enhanced relative to the enolate equilibrium geometries, yet not as pyramidalized as the products. In the convex face alkylations the sense of pyramidalization is reversed, and reduced in magnitude.

How much does it cost to invert the sense of pyramidalization at C(3) caused by convex face attack? Our constrained optimization of the enolate free anion (Table 2.6) suggests that perhaps 3 kcal/mol of destabilization might be contributed by the inverted pyramidalization seen in convex face alkylation transition structures **221** and **223**.

Table 2.6 Relative electronic energy changing with deformation angle at C(3) in constrained optimization[a] of **203a**

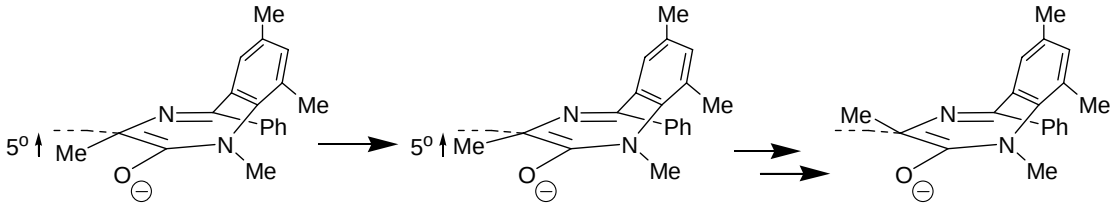

C(3) deformation angle: 16.6° (α) 11.6° (α) 14.6° (β)

Deformation angle[b,c]	Relative Electronic Energy (kcal/mol)
16.6° (α)	0
11.6° (α)	0.1
6.6° (α)	0.4
1.6° (α)	0.8
4.6° (β)	1.4
14.6° (β)	3.1

[a]Moving the C(3)-Me in 2D fashion to change the deformation angle with reference to the plane of C(2)-C(3)-N(4).
[b] Sense of deformation angle at C(3): (α) stands for pyramidalization below the plane of C(2)-C(3)-N(4); (β) stands for pyramidalization above the plane of C(2)-C(3)-N(4)
[c]For the first constrained calculation of **203a**, the deformation angle is increased 4 times by 5° from 16.6° to -4.6°.
[d]For the second constrained calculation of **203a**, the deformation angle is increased 1 time by 30° from 16.6° to -14.6°.

2.10 Kinetic and Computational Studies on Ring Equilibration of Quaternary BZD

2.10.1 Kinetic Studies on Ring Equilibration of Quaternary BZD

Section 2.6 showed that ring equilibration of the quaternary BZDs derived from deprotonation/alkylation of (*S*)-**172a** is very slow such that the "freeze-frame" of the exclusive Bn- and Allyl-pesudoaxial conformers can be observed after cold extractive workup. In order to obtain the corresponding activation parameters and equilibration half-life for conformational inversion in the products, kinetic studies were performed. MOC alkylation was carried out on (*S*)-**172a** with benzyl bromide as before, but with a separation of the Bn-pseudoaxial and Bn-pseudoequatorial conformers of **177a** by flash column. By monitoring the change of either equatorial or axial C(3)-Me peak in NMR spectrum (Figure 2.46), the equilibration of the two conformers was followed at 40 °C, 50 °C, 60 °C and 70 °C. The

forward inversion rate constant, namely k_1, is defined by the inversion from the Bn-pseudoequatorial conformer to the Bn-pseudoaxial conformer; and vice versa for the definition of the backward inversion rate constant, k_{-1}.

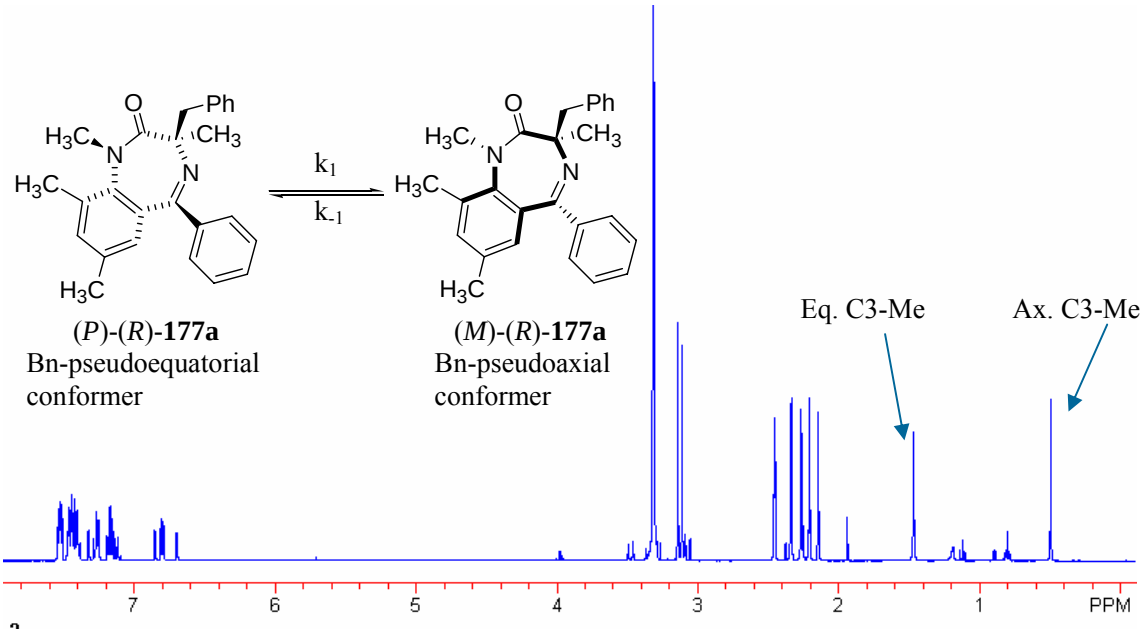

Figure 2.46 NMR spectrum of (*R*)-**177a** in equilibrium

An example of the determination of k_1 and k_{-1} at 40 °C is shown in Figure 2.47. By plotting ln (($[P]_t$-$[P]_e$)/($[P]_o$-$[P]_e$)) vs time, where [P] is the concentration of the (*P*)-conformer (Bn-pseudoequatorial), the slope of line is the sum of k_1 and k_{-1}. By using the equilibrium constant obtained at this temperature, we determined k_1 and k_{-1} as 0.000231 ± 0.00008 s^{-1} and 0.000197 ± 0.00008 s^{-1} respectively. Similar kinetic studies were also performed at 50 °C, 60 °C and 70 °C.

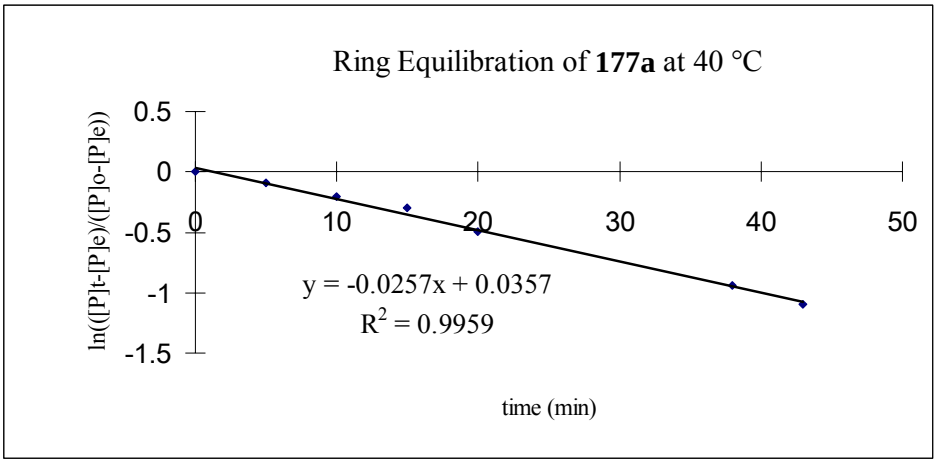

Figure 2.47 Ring equilibration of **177a** at 40 °C, where $[P]_t$ is the concentration of the (*P*)-conformer (Bn-pseudoequatorial) at time t, $[P]_o$ is the one at time 0 and $[P]_e$ is the one at equilibrium.

Due to the fast equilibration rate at temperatures higher than 70 °C, we turned to study the kinetics by 2D-EXSY ^{1}H NMR.[71] Rate constants k_1 and k_{-1} at 120 °C and 130 °C were obtained from the measurement of the exchange rates and mole fractions at the corresponding temperatures. By obtaining rate constants k_1 and k_{-1} at temperatures ranging over 90 °C (Table 2.7), activation parameters $\Delta H^{\ddagger}$ and $\Delta S^{\ddagger}$ for both the forward and backward processes can be determined by plotting ln (k_1h/Tk_B) and ln ($k_{-1}h/Tk_B$) vs $1/T$, where h is Plank constant and k_B is Boltzmann constant. Error analysis is described in experimental section.

Table 2.7 Summary of k_1 and k_{-1} over a range 90 K

Source	Temperature (K)	k_1 (s^{-1})	k_{-1} (s^{-1})
1H-NMR	313	0.000231	0.000197
1H-NMR	323	0.000343	0.000249
1H-NMR	333	0.00199	0.00143
1H-NMR	343	0.00327	0.00239
2D-EXSY	393	0.365	0.294
2D-EXSY	403	0.937	0.868

As shown in Figure 2.48, the enthalpies of activation for the ring inversion of **177a** from the Bn-pesudoequatorial and Bn-pesudoaxial conformers are 21.6 ± 0.9 and 21.9 ± 1 kcal/mol respectively; also, as expected for a unimolecular process, their entropies of activation are -6.5 ± 1 and -6.0 ± 1 cal/mol/K respectively. As a result, the free energies of activation at 298 K for the forward and backward are 23.5 ± 0.9 and 23.7 ± 1 kcal/mol

respectively, corresponding to equilibration $t_{1/2}$ of 189 minutes. At 273 K, the $t_{1/2}$ will be 121 hours which accounts for our ability to make "freeze frame" observations after cold workup.

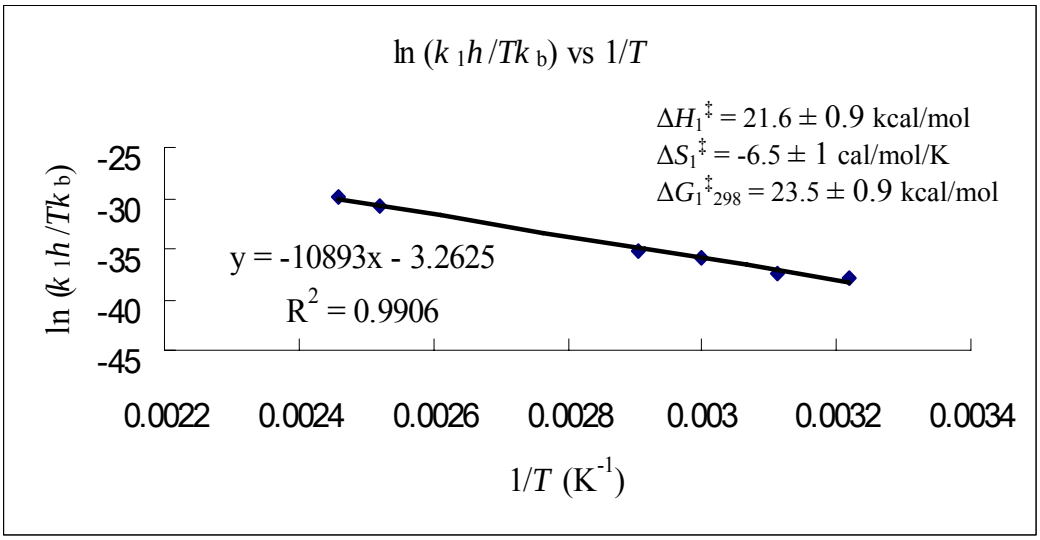

a) Plot of ln (k_1h/Tk_B) vs 1/T for the forward inversion of **177a**

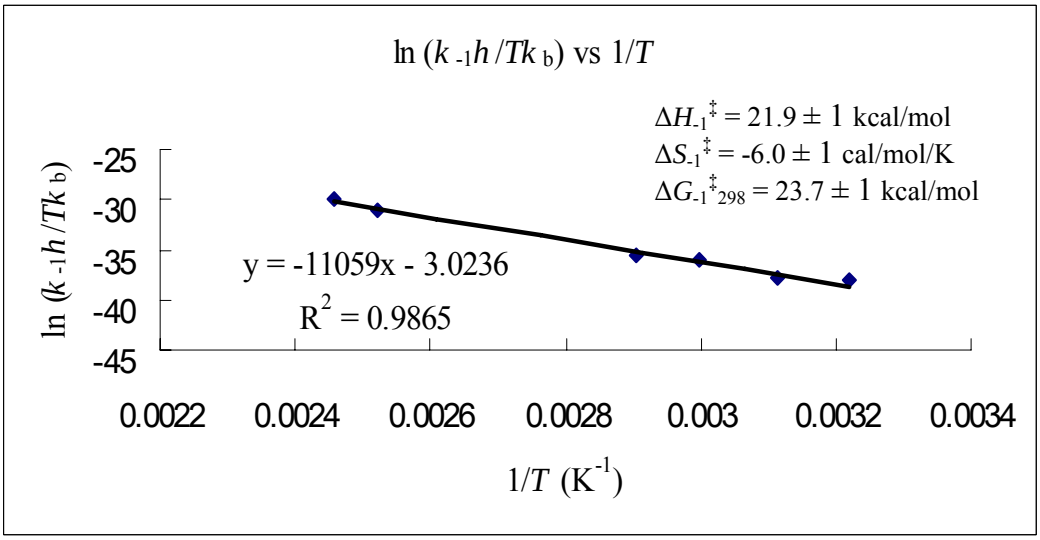

b) Plot of ln ($k_{-1}h/Tk_B$) vs 1/T for the backward inversion of **177a**

Figure 2.48 Eyring plots for determination of activation parameters from the ring inversion of **177a**

2.10.2 DFT Calculations of Ring Inversion Barrier of Quaternary BZD

Similar to the aforementioned computational studies of the ring inversion barriers of the Gly-derived BZDs, the structures of **177a** and **177a*** were optimized at B3LYP/6-31G(d). Single point energies using Tomasi's PCM model[34] with DMSO, same as the solvent used in the kinetics, were calculated at B3LYP/6-31+G(d) and MP2/6-31+G(d). The thermal

correction to the Gibbs free energies using vibrational data from 6-31G(d) were applied to calculate the activation free energies. The results are summarized in Table 2.8.

Table 2.8 Comparison between computational and experimental ring inversion barriers of **177a**

Equilibrium Geometry[a]	Transition Structure	B3LYP/6-31+G(d)// B3LYP/6-31G(d)	MP2/6-31+G(d)// B3LYP/6-31G(d)	Experimental[b]
		$\Delta G^{\ddagger}_{298}$ (DMSO)	$\Delta G^{\ddagger}_{298}$ (DMSO)	$\Delta G^{\ddagger}_{298}$ (DMSO)
(*M*)-(*R*)-**177a** (ψax-Bn)	(*M*)-(*R*)-**177a***	23.7 kcal/mol	26.6 kcal/mol	23.7 kcal/mol
	(*P*)-(*R*)-**177a***	24.2 kcal/mol	26.7 kcal/mol	
(*P*)-(*R*)-**177a** (ψeq-Bn)	(*M*)-(*R*)-**177a***	21.8 kcal/mol	24.5 kcal/mol	23.5 kcal/mol
	(*P*)-(*R*)-**177a***	22.3 kcal/mol	24.5 kcal/mol	

[a]Two equilibrium geometries exist, representing (*M*)-(*R*) and (*P*)-(*R*)conformers. The (*M*)-(*R*)conformer is lower in energy, consistent with NMR studies.
[b]Calculated at 298 K by using the activation parameters obtained from kinetic studies.

In our NMR and calculations studies, the Bn-pseudoaxial conformer (*M*)-(*R*)-**177a** is lower in energy than the Bn-pseudoequatorial counterpart (*P*)-(*R*)-**177a**. An example of energy diagram calculated at B3LYP/6-31+G(d)//B3LYP/6-31G(d) is shown in Figure 2.49. However, the calculated free energy difference at B3LYP/6-31+G(d)//B3LYP/6-31G(d) between the two conformers is 1.9 kcal/mol, while the one at MP2/6-31+G(d)//B3LYP/6-31G(d) is 2.1 kcal/mol; both are higher than the experimental value of 0.2 kcal/mol.

Two conformationally diastereomeric ring-inversion transition structures were found, in which one consists of a pseudoaxial Bn and the other contains a pseudoequatorial Bn. The single point energies are close in these two ring-inversion transition structures, differing only by 0.5 kcal/mol at B3LYP/6-31+G(d) and 0.03 kcal/mol at MP2/6-31+G(d). It should be noted that the barrier to inversion from (*M*)-(*R*)-**177a** to (*M*)-(*R*)-**177a*** calculated at B3LYP/6-31+G(d)//B3LYP/6-31G(d) is exactly the same as the one obtained from the kinetic studies. However, the corresponding inversion barrier for the (*P*)-(*R*) conformer is lower than the experimental value. This discrepancy is due to an overestimate of the energy difference of the (*M*)-(*R*) and (*P*)-(*R*) conformers. Again, single point calculations at MP2/6-31+G(d) overestimate the inversion barriers. In general, the calculated inversion barriers of (*M*)-(*R*)-**177a** are higher than those of (*P*)-(*R*)-**177a**, in agreement with the trend of the experimental results.

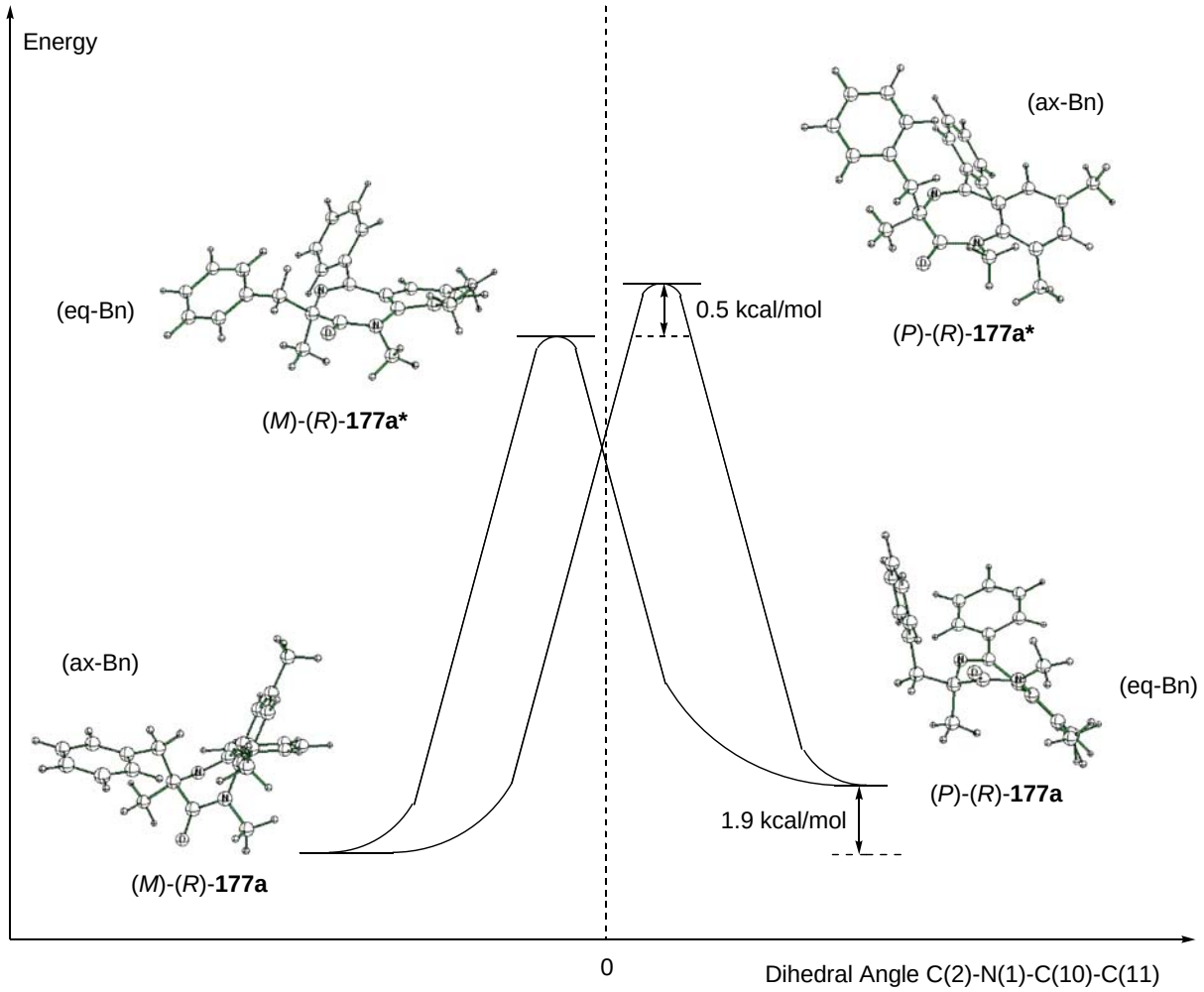

Figure 2.49 Ring inversion process for (*R*)-**177a**. For equilibrium geometries, the Bn-pseudoaxial conformer (*M*)-(*R*)-**177a** is 1.9 kcal/mol lower in energy than the Bn-pseudoequatorial counterpart, (*P*)-(*R*)-**177a**. Two nearly equienergetic ring inversion transition structures (*M*)-(*R*)-**177a*** and (*P*)-(*R*)-**177a*** were located.

2.11 Conclusions

We have proposed two possible stereochemical-controlled mechanisms for the memory of chirality alkylation of BZD, and discriminated the mechanisms by experimental and computational studies. By successfully trapping the BZD enolate as silyl enol ether and utilizing cold work-up, the step-wise mechanism was deduced. DFT calculations and kinetic studies further support our results.

The inversion barriers of Gly-derived BZDs **161a** and **162a** could not be determined experimentally by variable temperature 1H NMR, as a result of the steric hindrance between N(1) and C(9) substituents. Using DFT calculations and gNMR line shape simulation, their inversion barriers were calculated to be 24 – 26 kcal/mol, indicating that the corresponding BZD enolates have a high barrier to racemize.

We found that alkylations of **172a** proceeded in the absence of HMPA, suggesting that an HMPA-free procedure might be developed for the synthesis of other quaternary BZDs. Moreover, retentive alkylation was established from the X-ray crystal structure of 3-cyanated BZD **178a**.

The X-ray crystal structure of chiral non-racemic silyl enol **182a** indicated enantiopure formation of BZD enolate by retentive deprotonation (Path A). Freeze frame observations of exclusive formation of Bn- and allyl-pseudoaxial conformers provided the first direct evidence of concave face alkylation of the BZD enolate. Therefore, we ruled out the Path B mechanism of invertive deprotonation and convex face alkylation.

Kinetic and computational studies allowed further insight into the proposed mechanisms. Using DFT calculations, we were able to model transition structures for deprotonation of (*S*)-**172a** by different lithiated and potassiated dimethylamides in both solvent-free and solvated forms. All these calculation supported the generation of enantiomerically pure BZD (*M*)-enolate by retentive deprotonation. Moreover, both kinetic

and computational results indicated that the enolate has high racemization barrier, accounting for the excellent enantioselectivity observed in our MOC alkylations of BZD. Consistent with the X-ray structure of silyl enol ether **182a**, DFT calculations also showed that C(3) in the enolate equilibrium geometry is pyramidalized towards the concave face, suggesting that contra-steric concave face alkylation is more favorable. By studying simplified BZD systems, we postulated that the pyramization of C(3) might be due to π-π repulsion between the benzo ring and the π orbital of alkene C(2)-C(3). Furthermore, alkylation transition structures at B3LYP/6-31+G(d)//B3LYP/6-31G(d) predicted the retentive trajectory of the electrophilic attack. Convex face alkylation transition structures are unfavorable possibly because of the pyramidal inversion at C(3). Constrained optimization predicted a cost of 3 kcal/mol for this inversion process. Finally, kinetic and computational studies provided activation parameters for the ring equilibration of quaternary BZD. The corresponding ring inversion half-life accounts for the feasibility of freeze frame observations.

The present studies provide a greater understanding of the MOC mechanism, which is helpful for the design and synthesis of enantiopure BZD derivatives in the absence of external chiral catalyst. Furthermore, it is our hope that this increased understanding might guide the development of entirely new MOC reactions.

References for Chapter 2

1. Ellman, J. A., Design, Synthesis, and Evaluation of Small-Molecule Libraries. *Accounts of Chemical Research* **1996,** 29, 132-143.

2. Evans, B. E.; Rittle, K. E.; Bock, M. G.; DiPardo, R. M.; Freidinger, R. M.; Whitter, W. L.; Lundell, G. F.; Veber, D. F.; Anderson, P. S.; Chang, R. S. L.; Lotti, V. J.; Cerino, D. J.; Chen, T. B.; Kling, P. J.; Kunkel, K. A.; Springer, J. P.; Hirschfield, J., Methods for Drug Discovery: Development of Potent, Selective, Orally Effective Cholestocytokinin Antagonists. *Journal of Medicinal Chemistry* **1988,** 31, 2235-2246.

3. Sternbach, L. H., The Benzodiazepine Story. *Journal of Medicinal Chemistry* **1979,** 22, 1-7.

4. Evans, B. E.; E., R. K.; Bock, M. G.; DiPardo, R. M.; Freidinger, R. M.; Whitter, W. L.; Gould, N. P.; Lundell, G. F.; Homnick, C. F.; Veber, D. F.; Anderson, P. S.; Chang, R. S. L.; Lotti, V. J.; Cerino, D. J.; Chen, T. B.; King, P. J.; A., K. K.; Springer, J. P.; Hirschfield, J., Design of Nonpeptidal Ligands for a Peptide Receptor: Cholecystokinin Antagonists. *Journal of Medicinal Chemistry* **1987,** 30, 1229-1239.

5. Willson, T. M.; Henke, B. R.; Momtahen, T. M.; Meyers, P. L.; Sugg, E. E.; Unwalla, R. J.; Croom, D. K.; Dougherty, R. W.; Grizzle, M. K.; Johnson, M. F.; Queen, K. L.; Rimele, T. J.; Yingling, J. D.; James, M. K., 3-[2-(*N*-Phenylacetamide)]-1,5-benzodiazepines: Orally Active, Binding Selective CCK-A Agonists. *Journal of Medicinal Chemistry* **1996,** 39, 3030-3034.

6. Sadée, W., NMR-Spektroskopische Untersuchungen über die Ringinversion von 1,3-Dihydro-5-phenyl-1,4-benzodiazepin-2on-derivaten. *Archiv der Pharmazie* **1969,** 302, (10), 769-774.

7. Sherrill, R. G.; Sugg, E. E., An Improved Synthesis and Resolution of 3-Amino-1,3-dihydro-5-phenyl-2H- 1,4-benzodiazepin-2-ones. *Journal of Organic Chemistry* **1995,** 60, (3), 730-4.

8. Dziadulewicz, E. K.; Brown, M. C.; Dunstan, A. R.; Lee, W.; Said, N. B.; Garratt, P. J., The Design of Non-Peptide Human Bradykinin B_2 Receptor Antagonists Employing the Benzodiazepine Peptidomimetic Scaffold. *Bioorganic & Medicinal Chemistry Letters* **1999,** 9, 463-468.

9. Hsu, M.-C.; Schutt, A. D.; Holly, M.; Slice, L. W.; Sherman, M. I.; Richman, D. D.; Potash, M. J.; Volsky, D. J., Inhibition of HIV Replication in Acute and Chronic Invections in Vitro by a Tat Antagonist. *Science* **1991,** 254, 1799-1802.

10. James, G. L.; Goldstein, J. L.; Brown, M. S.; Rawson, T. E.; Somers, T. C.; McDowell, R. S.; Crowley, C. W.; Lucas, B. K.; Levinson, A. D.; Masters, J. C., Benzodiazepine Peptidomimetics: Potent Inhibitors of Ras Farnesylation in Animal Cells. *Science* **1993,** 260, 1937-1942.

11. Ramdas, L.; Bunnin, B. A.; Plunkett, M. J.; Sun, G.; Ellman, J.; Gallick, G.; Budde, R. J. A., Benzodiazepine Compounds as Inhibitors of the Src Protein Tyrosine Kinase: Screening of a Combinatorial Library of 1,4-Benzodiazepines. *Archives of Biochemistry and Biophysics* **1999,** 368, (2), 394-400.

12. Baboul, A. G.; Curtis, L. A.; Redfern, P. C.; Raghavachari, K., Gaussian-3 theory using density functional geometries and zero-point energies. *Journal of Chemical Physics* **1999,** 110, 7650-7657.

13. Butcher, J. W.; Liverton, N. J.; Claremon, D. A.; Freidinger, R. M.; Jurkiewicz, N. K.; Lynch, J. J.; Salata, J. J.; Wang, J.; Dieckhaus, C. M.; Slaughter, D. E.; Vyas, K., Novel 5-cyclopropyl-1,4-benzodiazepin-2-ones as potent and selective I(Ks)-blocking class III antiarrhythmic agents. *Bioorganic & Medicinal Chemistry Letters* **2003,** 13, (6), 1165-8.

14. Cativiela, C.; Díaz-de-Vellagas, M. D., Stereoselective synthesis of quaternary α-amino acids. Part 1: Acyclic Compounds. *Tetrahedron: Asymmetry* **1998,** 40, (9), 3517-3599.

15. Carlier, P. R.; Lam, P. C.-H.; DeGuzman, J.; Zhao, H., Memory of Chirality Trapping of Low Inversion Barrier 1,4-Benzodiazepin-2-one Enolates. *Tetrahedron: Asymmetry* **2005,** 16, 2998-3002.

16. Carlier, P. R.; Zhao, H.; DeGuzman, J.; Lam, P. C.-H., Enantioselective Synthesis of "Quaternary" 1,4-Benzodiazepin-2-one Scaffolds via Memory of Chirality. *Journal of the American Chemical Society* **2003,** 125, 11482-11483.

17. Carlier, P. R.; Zhao, H.; MacQuarrie-Hunter, S. L.; DeGuzman, J. C.; Hsu, D. C., Enantioselective synthesis of diversely substituted quaternary 1,4-benzodiazepin-2-ones and 1,4-benzodiazepine-2,5-diones. *Journal of the American Chemical Society* **2006,** 128, (47), 15215-15220.

18. MacQuarrie-Hunter, S.; Carlier, P. R., Highly enantioselective synthesis of rigid, quaternary 1,4-benzodiazepin-2,5-diones derived from proline *Organic Letters* **2005,** 7, 5305-5308.

19. Avdagic, A.; Lesac, A.; Majer, Z.; Hollosi, M.; Sunjic, V., Lipase-Catalyzed Acetylation of 3-Substituted 2,3-Dihydro-1*H*-1,4-benzodiazepin-2-ones: Effect of Temperature and Conformation on Enantioselectivity and Configuration. *Helvetica Chimica Acta* **1998,** 81, 1567-1582.

20. Avdagic, A.; Sunjic, V., On the Way to a-Methyl-a-amino Acids; Unusual Elimination-addition in 3,3-Disubstituted 1,4,-Benzodiazepin-2-ones and Inversion of Enantioselectivity in the Lipase Catalyzed Acetylation. *Croatica Chemica Acta* **2000,** 73, (3), 743-753.

21. Reitter, B. E.; Sachdeva, Y. P.; Wolfe, J. F., Metalation of Diazepam and Use of the Resulting Carbanion Intermediate in a New Synthesis of 3-Substituted Diazepam Derivatives. *Journal of Organic Chemistry* **1981,** 46, 3945-3949.

22. Simonyi, M.; Kaksay, G.; Kovacs, I.; Tegyey, Z.; Parkanyi, L.; Kalman, A.; Otvos, L., Conformational Recognition by Central Benzodiazepine Receptors. *Bioorganic Chemistry* **1990,** 18, 1-12.

23. Gilman, N. W.; Rosen, P.; Earley, J. V.; Cook, C.; Todaro, L. J., Atropisomers of 1,4-Benzodiazepines. Synthesis and Resolution of a Diazepam-Related 1,4-Benzodiazepine. *Journal of the American Chemical Society* **1990,** 112, 3969-3978.

24. Lam, P. C.-H.; Carlier, P. R., Experimental and Computational Studies of Ring Inversion of 1,4-Benzodiazepin-2-ones: Implications for Memory of Chirality Transformations. *Journal of Organic Chemistry* **2005,** 70, 1530-1538.

25. Linscheid, P.; Lehn, J.-M., Étude cinétiques et conformationnelles par résonance magnétique nucléaire. VII.Inversion de cycle dans des benzo-diazépinones. *Bulletin de la Societe Chimique de France* **1967**, (3), 992-997.

26. Konowal, A.; Snatzke, G.; Alebic-Kolbah, T.; Kajfez, F.; Rendic, S.; Sunjic, V., General Approach to Chiroptical Characterization of Binding to Prochiral and Chiral 1,4-Benzodiazepin-2-ones to Human Serum Albumin. *Biochemical Pharmacology* **1979,** 28, 3109-3113.

27. Sternbach, L. H.; Reeder, E.; Keller, O.; Metlesics, W., Quinazolines and 1,4-Benzodiazepines. III. Substituted 2-Amino-5-phenyl-3H-1,4-benzodiazepine-4-Oxides. *Journal of Organic Chemistry* **1961,** 26, 4488-4497.

28. Sternbach, L. H.; Fryer, R. I.; Metlesics, W.; Reeder, E.; Sach, G.; Saucy, G.; Stempel, A., Quinazolines and 1,4-Benzodiazepines. VI. Halo-, Methyl-, and Methoxy-substituted 1,3-Dihydro-5-phenyl-2*H*-1,4-benzodiazepin-2-ones. *Journal of Organic Chemistry* **1962,** 27, 3788-3796.

29. Bain, A. D., Chemical exchange in NMR. *Progress in Nuclear Magnetic Resonance Spectroscopy* **2003,** 43, (3-4), 63-103.

30. Friebolin, H., *Basic one- and two- dimensional NMR spectroscopy*. 3rd rev. ed.; Wiley-Vch: Weinheim: New York, 1998; p xxiv, 386.

31. Gaussian 03, Revision B.05, M. J. Frisch, G. W. Trucks, H. B. Schlegel, G. E. Scuseria, M. A. Robb, J. R. Cheeseman, J. A. Montgomery, Jr., T. Vreven, K. N. Kudin, J. C. Burant, J. M. Millam, S. S. Iyengar, J. Tomasi, V. Barone, B. Mennucci, M. Cossi, G. Scalmani, N. Rega, G. A. Petersson, H. Nakatsuji, M. Hada, M. Ehara, K. Toyota, R. Fukuda, J. Hasegawa, M. Ishida, T. Nakajima, Y. Honda, O. Kitao, H. Nakai, M. Klene, X. Li, J. E. Knox, H. P. Hratchian, J. B. Cross, C. Adamo, J. Jaramillo, R. Gomperts, R. E. Stratmann, O. Yazyev, A. J. Austin, R. Cammi, C. Pomelli, J. W. Ochterski, P. Y. Ayala, K. Morokuma, G. A. Voth, P. Salvador, J. J. Dannenberg, V. G. Zakrzewski, S. Dapprich, A. D. Daniels, M. C. Strain, O. Farkas, D. K. Malick, A. D. Rabuck, K. Raghavachari, J. B. Foresman, J. V. Ortiz, Q. Cui, A. G. Baboul, S. Clifford, J. Cioslowski, B. B. Stefanov, G. Liu, A. Liashenko, P. Piskorz, I. Komaromi, R. L. Martin, D. J. Fox, T. Keith, M. A. Al-Laham, C. Y. Peng, A. Nanayakkara, M. Challacombe, P. M. W. Gill, B. Johnson, W. Chen, M. W. Wong, C. Gonzalez, and J. A. Pople, Gaussian, Inc., Pittsburgh PA, 2003.

32. Geerlings, P.; De Proft, F.; Langenaeker, W., Conceptual density functional theory. *Chemical Reviews* **2003,** 103, (5), 1793-1873.

33. Jalbout, A. F.; Nazari, F.; Turker, L., Gaussian-based computations in molecular science. *Journal of Molecular Structure-Theochem* **2004,** 671, (1-3), 1-21.

34. Tomasi, J.; Cammi, R.; Mennucci, B.; Cappelli, C.; Corni, S., Molecular properties in solution described with a continuum solvation model. *Physical Chemistry Chemical Physics* **2002,** 4, (23), 5697-5712.

35. Lam, P. C.-H., *PhD Thesis, Virginia Tech (US)* **2005**.

36. Hart, B. R.; Rush, D. J.; Shea, K. J., Discrimination between Enantiomers of Structurally Related Molecules: Separation of Benzodiazepines by Molecularly Imprinted Polymers. *Journal of the American Chemical Society* **2000,** 122, 460-465.

37. Beyermann, M.; Bienert, M.; Niedrich, H.; Carpino, L. A.; Sadat-Aalee, D., Rapid Continuous Peptide Syntheses via FMOC Amino Acid Chloride Coupling and 4-(Aminomethyl)piperidine Deblocking. *Journal of Organic Chemistry* **1990,** 55, 721-728.

38. Eliel, E. L.; Wilen, S. H., cyclohexane A-value. In *Stereochemistry of Organic Molecules*, John Wiley & Sons: New York, 1994; pp 696-697.

39. Kawabata, T.; Yahiro, K.; Fuji, K., Memory of Chirality: Enantioselective Alkylation Reactions at an Asymmetric Carbon Adjacent to a Carbonyl Group. *Journal of the American Chemical Society* **1991,** 113, (25), 9694-9696.

40. Kawabata, T.; Suzuki, H.; Nagae, Y.; Fuji, K., A Chiral Nonracemic Enolate with Dynamic Axial Chirality: Direct Asymmetric α-Methylation of α-Amino Acid Derivatives. *Angewandte Chemie-International Edition* **2000,** 39, (12), 2155-2157.

41. Banerjee, K. G.; Hogenesch, T. E., Stereochemical Kinetics of Polymerization of Methyl-Methacrylate under Group-Transfer Polymerization Conditions - C-13 Nmr Analysis of Poly(Methyl Methacrylate) Terminated with Labeled End-Groups. *Macromolecules* **1994,** 27, (8), 2187-2193.

42. Zhao, H.; Hsu, D. C.; Carlier, P. R., Memory of Chirality: an Emerging Strategy for Asymmetric Synthesis. *Synthesis* **2005**, 1-16.

43. Collum, D. B., Solution Structures of Lithium Dialkylamides and Related N-Lithiated Species: Results from ^{6}Li-^{15}N Double Labeling Experiments. *Accounts of Chemical Research* **1993,** 26, (5), 227-234.

44. Gregory, K.; Schleyer, P. V.; Snaith, R., Structures of Organonitrogen Lithium Compounds - Recent Patterns and Perspectives in Organolithium Chemistry. *Advances in Inorganic Chemistry* **1991,** 37, 47-142.

45. Mulvey, R. E., Meldola Medal Lecture - Ring-Stacking and Ring-Laddering in Organonitrogenlithium Compounds - the Development of Concepts with Wide Applicability Throughout Lithium Structural Chemistry. *Chemical Society Reviews* **1991,** 20, (2), 167-209.

46. Bernstein, M. P.; Collum, D. B., Metalation of Imines by Lithium Diisopropylamide Solvated by N,N,N',N'-Tetramethylethylenediamine - Evidence for Solvent-Free Open Dimer Reactive Intermediates. *Journal of the American Chemical Society* **1993,** 115, (2), 789-790.

47. Matsuda, H.; Hamatani, T.; Matsubara, S.; Schlosser, M., Hydrogen-Fluoride Abstraction from Vicinal Difluoroalkanes - Reaction Conditions and Syn/Anti-Stereoselectivity. *Tetrahedron* **1988,** 44, (10), 2865-2874.

48. Remenar, J. F.; Collum, D. B., Structure and Reactivity of Lithium Diisopropylamide Solvated by Polyamines: Evidence of Monomer- and Dimer-based Dehydrohalogenations. *Journal of the American Chemical Society* **1998,** 120, 4081-4086.

49. Remenar, J. F.; Lucht, B. L.; Kruglyak, D.; Romesberg, F. E.; Gilchirst, J. H.; Collum, D. B., Lithium 2,2,6,6-tetramethylpiperidide and lithium 2,2,4,6,6-pentamethylpiperidide: Influence of TMEDA and related chelating ligands on the solution structures. Characterization of higher cyclic oligomers, cyclic dimers, open dimers, and monomers. *Journal of Organic Chemistry* **1997,** 62, (17), 5748-5754.

50. Sun, X.; Collum, D. B., Lithium Diisopropylamide-Mediated Enolizations: Solvent-Independent Rates, Solvent-Dependent Mechanisms. *Journal of the American Chemical Society* **2000,** 122, 2452-2458.

51. Zhao, P. J.; Collum, D. B., Ketone enolization by lithium hexamethyidisilazide: structural and rate studies of the accelerating effects of trialkylamines. *Journal of the American Chemical Society* **2003,** 125, (47), 14411-14424.

52. Behnam, S. M.; Behnam, S. E.; Ando, K.; Green, N. S.; Houk, K. N., Stereoelectronic, Torsional, and Steric Effects on Rates of Enolization of Ketones. *Journal of Organic Chemistry* **2000,** 65, 8970-8978.

53. Kinetic studies on BZD enolate racemization barrier. ln (% ee(**177a**)/100) = $(k_1 + k_{-1})t$, where $k_1 + k_{-1}$ is racemization constant

54. Seebach, D.; Maetzke, T.; Petter, W.; Klötzer, B.; Plattner, D. A., Pyramidalization and reactivity of trigonal centers. X-ray Crystal Structure Analysis of Two Silyl Enol Ethers from 1-Benzoyl and 1-(Methoxycarbonyl)-2-*tert*-butyl-3,5-dimethyl-4-imidazolidinone (Reagents for Amino Acid Synthesis) *Journal of the American Chemical Society* **1991,** 113, (5), 1781-1786.

55. Seebach, D.; Zimmerman, J.; Gysel, U.; Ziegler, R.; Ha, T.-K., Totally Stereoselective Additions to 2,6-disubstituted 1,3-Dioxin-4-ones (Chiral Acetoacetic Acid Derivatives). Synthetic and Mechanistic Aspects of Remote Stereoselectivity. *Journal of the American Chemical Society* **1988,** 110, 4763-4772.

56. Meyers, A. I.; Seefeld, M. A.; Lefker, B. A.; Blake, J. F., Origin of stereochemistry in simple pyrrolidinone enolate alkylations. *Journal of the American Chemical Society* **1997,** 119, (19), 4565-4566.

57. Meyers, A. I.; Seefeld, M. A.; Lefker, B. A.; Blake, J. F.; Williard, P. G., Stereoselective alkylations in rigid systems. Effect of remote substituents on pi-facial additions to lactam enolates. Stereoelectronic and steric effects. *Journal of the American Chemical Society* **1998,** 120, (30), 7429-7438.

58. Ando, K.; Green, N. S.; Li, Y.; Houk, K. N., Torsional and Steric Effects Control the Stereoselectivities of Alkylations of Pyrrolidine Enolates. *Journal of the American Chemical Society* **1999,** 121, 5334-5335.

59. Ikuta, Y.; Tomoda, S., Origin of stereochemical reversal in Meyers-type enolate alkylations. Importance of intramolecular Li coordination and solvent effects. *Organic Letters* **2004,** 6, (2), 189-192.

60. Ando, K., A theoretical study on the origin of pi-facial stereoselectivity in the alkylation of enolates derived from 4-substituted gamma-butyrolactones. *Journal of the American Chemical Society* **2005,** 127, (11), 3964-3972.

61. Soteras, I.; Lozano, O.; Gomez-Esque, A.; Escolano, C.; Orozco, M.; Amat, M.; Bosch, J.; Luque, F. J., On the origin of the stereoselectivity in the alkylation of oxazolopiperidone enolates. *Journal of the American Chemical Society* **2006,** 128, (20), 6581-6588.

62. Borden, W. T., Pyramidalized Alkenes. *Chemical Reviews* **1989,** 89, (5), 1095-1109.

63. House, H. O.; Umen, M. J., The Chemistry of Carbanions. XXIV. Comparison of Stereochemistry in Alkylation and the Michael Reaction. *Journal of Organic Chemistry* **1973,** 38, (5), 1000-1003.

64. Wipff, G.; Morokuma, K., Non-Planarity of Pi Systems - an Abinitio Study of Norbornene and Norbornadiene. *Tetrahedron Letters* **1980,** 21, (46), 4445-4448.

65. Houk, K. N.; Rondan, N. G.; Brown, F. K., Electronic-Structures and Reactivities of Pyramidal Alkenes and Carbonyls. *Israel Journal of Chemistry* **1983,** 23, (1), 3-9.

66. Houk, K. N.; Rondan, N. G.; Brown, F. K.; Jorgensen, W. L.; Madura, J. D.; Spellmeyer, D. C., Electronic Origins and Consequences of Pyramidalization of Asymmetric Alkenes in Ground and Triplet Excited-States. *Journal of the American Chemical Society* **1983,** 105, (19), 5980-5988.

67. Rondan, N. G.; Paddonrow, M. N.; Caramella, P.; Houk, K. N., Nonplanar Alkenes and Carbonyls - a Molecular Distortion Which Parallels Addition Stereoselectivity. *Journal of the American Chemical Society* **1981,** 103, (9), 2436-2438.

68. Burkert, U., Non-Planar Double-Bonds and Increased Reactivity in Olefins with Low Strain. *Angewandte Chemie-International Edition in English* **1981,** 20, (6-7), 572-573.

69. Hagenbuch, J. P.; Vogel, P.; Pinkerton, A. A.; Schwarzenbach, D., The Pi-Anisotropy of the Double-Bond of a Syn-11-Oxasesquinorbornene Derivative-1) - Stereoselectivity of the Diels-Alder Additions of (2-Norborneno)[C]Furan2) - Crystal-Structure of 11-Oxa-Endo-Tetracyclo[6.2.1.13,6.02,7]-Dodec-2(7)-Ene-9,10-Exo-Dicarboxylic Anhydride. *Helvetica Chimica Acta* **1981,** 64, (6), 1818-1832.

70. Bartlett, P. D.; Roof, A. A. M.; Winter, W. J., Hydrogenation on the Hindered Face of Syn-Sesquinorbornene Photosensitized by Acetone. *Journal of the American Chemical Society* **1981,** 103, (21), 6520-6522.

71. Perrin, C. L.; Dwyer, T. J., Application of 2-Dimensional NMR to Kinetics of Chemical Exchange. *Chemical Reviews* **1990,** 90, 935-967.

Chapter 3. Inhibition of Acetylcholinesterase: Free Cysteine Targeting

3.1 Family of Cholinesterase

Cholinesterases are vital for the hydrolysis of the neurotransmitter acetylcholine (ACh) in both central and peripheral nervous systems. The family of cholinesterases is composed of two distinct enzymes which are similar in both structure and function, namely acetylcholinesterase (AChE) and butyrylcholinesterase (BuChE). AChE plays an important role in the cholinergic brain synapses, neuromuscular junctions, and the hematopoietic system of vertebrates.[1,2] BuChE is mainly found in liver, kidney and blood serum; nevertheless, the primary physiological role of BuChE is still unclear, but it may be involved in the metabolism of dietary esters.[1,3]

When a nerve impulse moves down to the cholinergic terminal, the ACh molecules are released from the presynaptic neuron into the synaptic cleft. The neurotransmitter migrates across the cleft to the postsynaptic area and binds to its various receptors.[4] After initiating a response, the ACh molecules are liberated from the receptors back into the synaptic cleft. The free ACh molecules are then hydrolyzed into acetate and choline by means of the AChE catalysis. The hydrolysis of ACh prevents receptor over-stimulation from the build up of the neurotransmitter which would in turn lead to cholinergic toxicity.[4] Tremors, convulsions, paralysis and death are the possible consequences of the toxicity.[5]

Acetylcholine hydrolysis can be catalyzed by both enzymes with similarly high efficiency, but larger substrates such as butyrylcholine and benzoylcholine are hydrolyzed much faster by BuChE.[1,3] This difference is mainly due to the small but important steric restriction in the proximity of the active site of the enzymes (vide infra).[6] Furthermore, recent

studies suggested that when AChE activity is diminished, BuChE may act as substitute to a certain extent.[7-9]

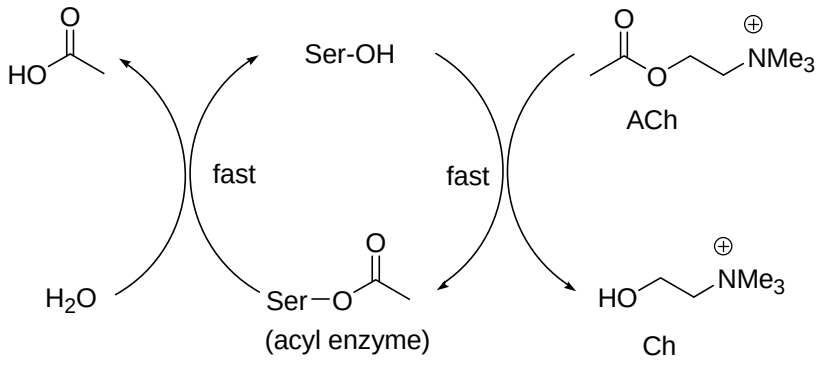

Figure 3.1 Catalytic cycle: hydrolysis of ACh to acetic acid and choline by AChE

3.2 Structure and Function of Acetylcholinesterase

The first successful X-ray structure of AChE was obtained by Sussman et al. for a saltwater electric fish, *Torpedo californica* (*Tc*AChE), with inhibitor decamethonium at 2.8 Å resolution in 1991 (original PDB code, 1ace).[10] Earlier attempts for the AChE structure of the freshwater eel, *Electrophorus electricus*, failed due to insufficient quantity of homogeneous pure enzyme.[11,12] Later on, Sussman and co-workers attained the first ligand-free *Tc*AChE crystal structure by using different inhibitor for enzyme purification in 1997 (Figure 3.2, original PDB code, 2ace).[13]

The first mammalian crystal structure of AChE was determined from mouse in 1995,[14] while the one from human was obtained in 2000.[15] Similar to the first example of *Tc*AChE, the two mammalian crystal structures were analyzed in complex with potent inhibitors; the first ligand-free AChE structure of mouse was elucidated in 2003.[16] To date, the only insect AChE with a known 3-D structure is from *Drosophila melanogaster*, which was solved in 2000 by Harel et al.[17] Crystallization of BuAChE has proved more difficult, perhaps due to the high extent of glycosylation.[18,19]

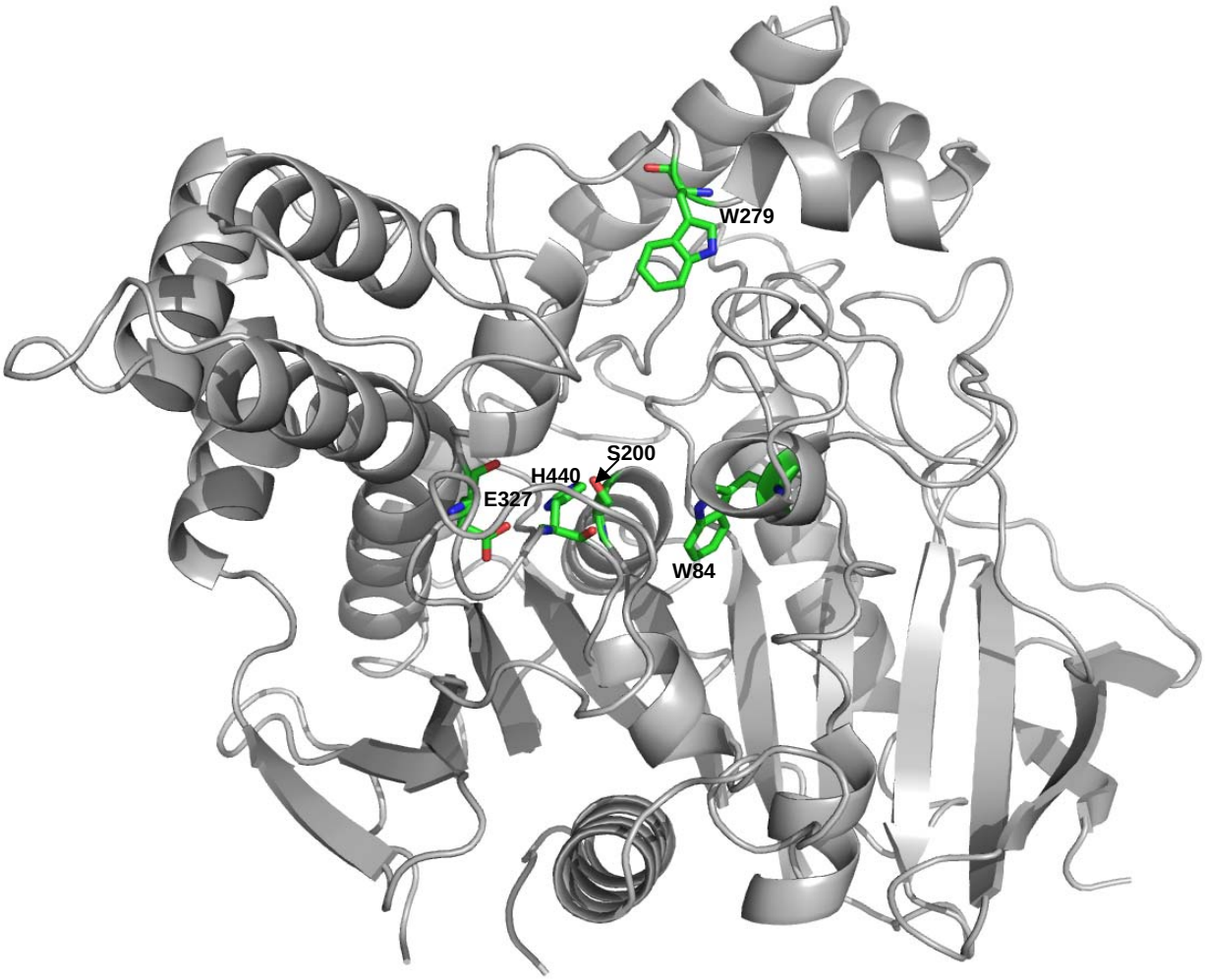

Figure 3.2 Crystal structure of ligand-free *Torpedo californica* AChE (pdb code: 2ACE).[13] Catalytic triad residues: S200, H440 and E327. Picture created by PyMOL[20]

Sussman's X-ray crystal structure confirmed many conclusions previously made by biochemical and site-directed mutagenesis studies. The catalytic triad found in most cholinesterases consists of Ser200, His440 and Glu327, as shown in Figure 1.[10,21] Surprisingly, this catalytic anionic site (CAS) is located at 20 Å deep from the mouth of the gorge. During catalysis of ACh hydrolysis, His400 and Glu327 play a key role in increasing the nucleophilicity at the serine side chain (Figure 3.3).[22]

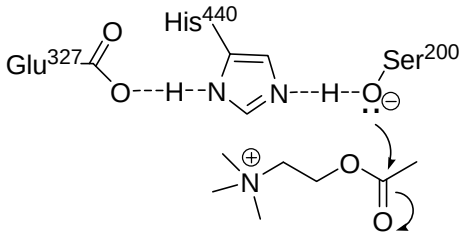

Figure 3.3 Ser200, His440 and Glu327 function in catalytic triad

Apart from the catalytic triad, a number of other residues play significant role in the catalytic activity of cholinesterases. In AChE, the aromatic Trp233, Phe288, Phe290 and Phe331 create an acyl pocket to provide hydrophobic binding area for the alkyl or aryl groups of the substrate (Figure 3.4).[23-25] It was found that Phe288 and Phe290 are replaced by smaller aliphatic residues in BuAChE, offering a larger space in BuChE for better binding with bulky substrates and inhibitors.[6,26,27]

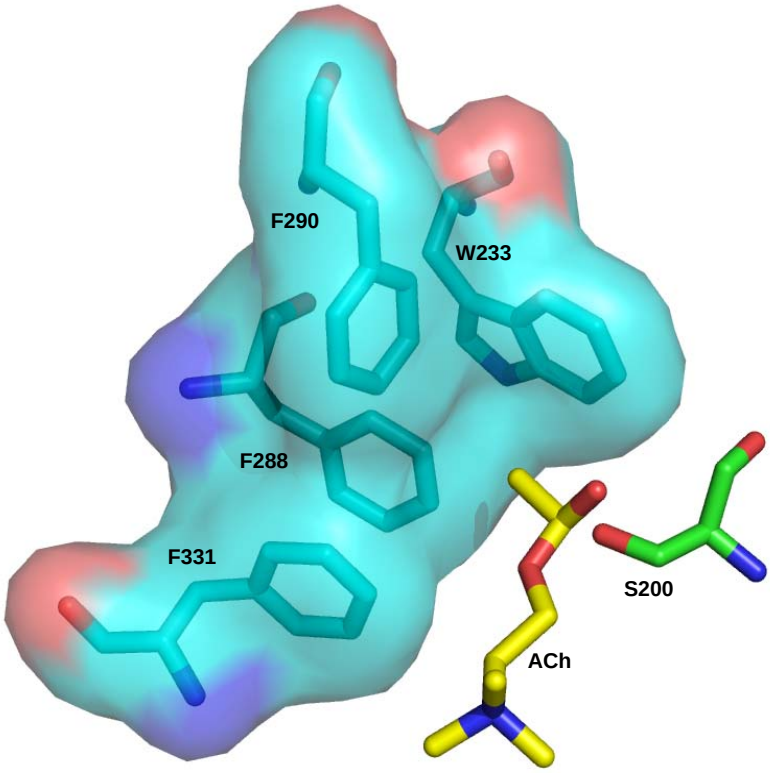

Figure 3.4 Acyl pocket in the crystal structure of ligand-free *Torpedo californica* AChE (pdb code: 2ACE).[13] Acyl pocket residues: W233, F288, F290, F331; ACh: docked in the active site. Picture created by PyMOL[20]

In addition, the so-called oxyanion hole is generated by Gly118, Gly119 and Ala201 (Figure 3.5).[25,28,29] The corresponding amide protons form hydrogen bonds with the carbonyl oxygen of ACh during hydrolysis, stabilizing the tetrahedral transition state formed from the nucleophilic attack of the active serine (Figure 3.3). In addition, the phosphoryl oxygen of organophosphate inhibitors can also be attracted by the electrophilic oxyanion hole.[1]

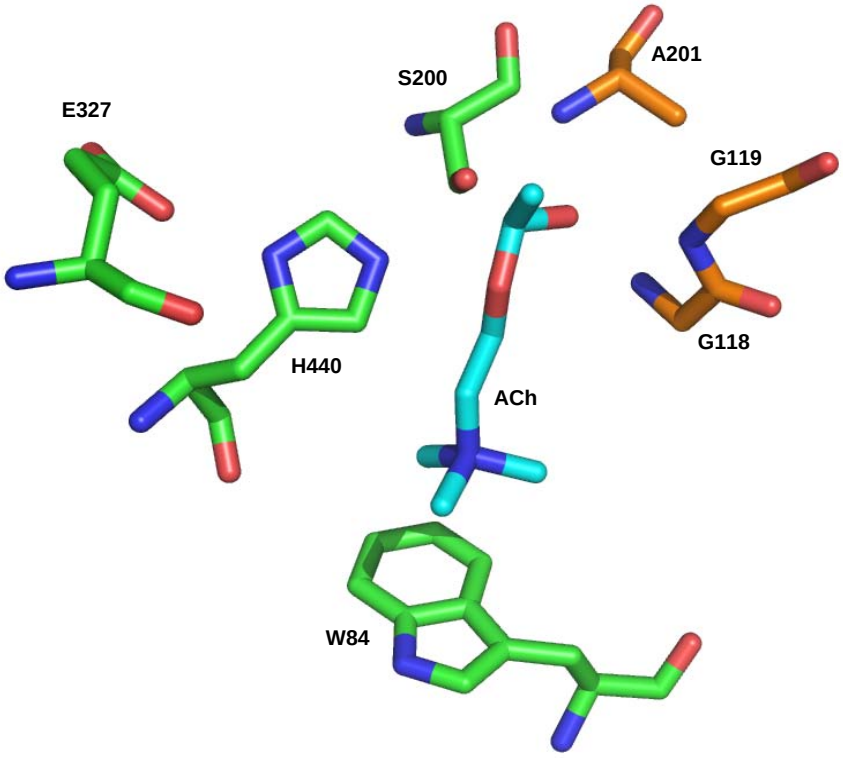

Figure 3.5 Oxyanion hole and Trp84 in the crystal structure of ligand-free *Torpedo californica* AChE (pdb code: 2ACE).[13] Oxyanion hole residues: G118, G119, A201; ACh: docked in the active site. Picture created by PyMOL[20]

At the base of the active site gorge, Trp84 is referred as the choline binding site, since it helps to bind the ammonium ion of ACh (Figure 3.5).[10,23] The aromatic ring of Trp84 provides stabilization for positively charge substrate by cation-π interaction.[10,23,30]

Approximately 14 Å from the catalytic triad, the peripheral anionic site (PAS), formed by Tyr70, Tyr121 and Trp279, is located at the entrance of the gorge.[31] These aromatic residues, which are not found in BuAChE,[26] specifically bind to hydrophobic inhibitors that are too large[14,32] to enter the active site gorge, or the head group of appropriately spaced

bivalent inhibitors[31-33] by cation-π and π-π stacking interaction. Figure 3.6 shows an example of Carlier's bivalent inhibitor (*S*,*S*)-(-)-bis(12)-hupyridone (E12E) interacting with Trp84 at the active site and Trp279 at the peripheral site.[31]

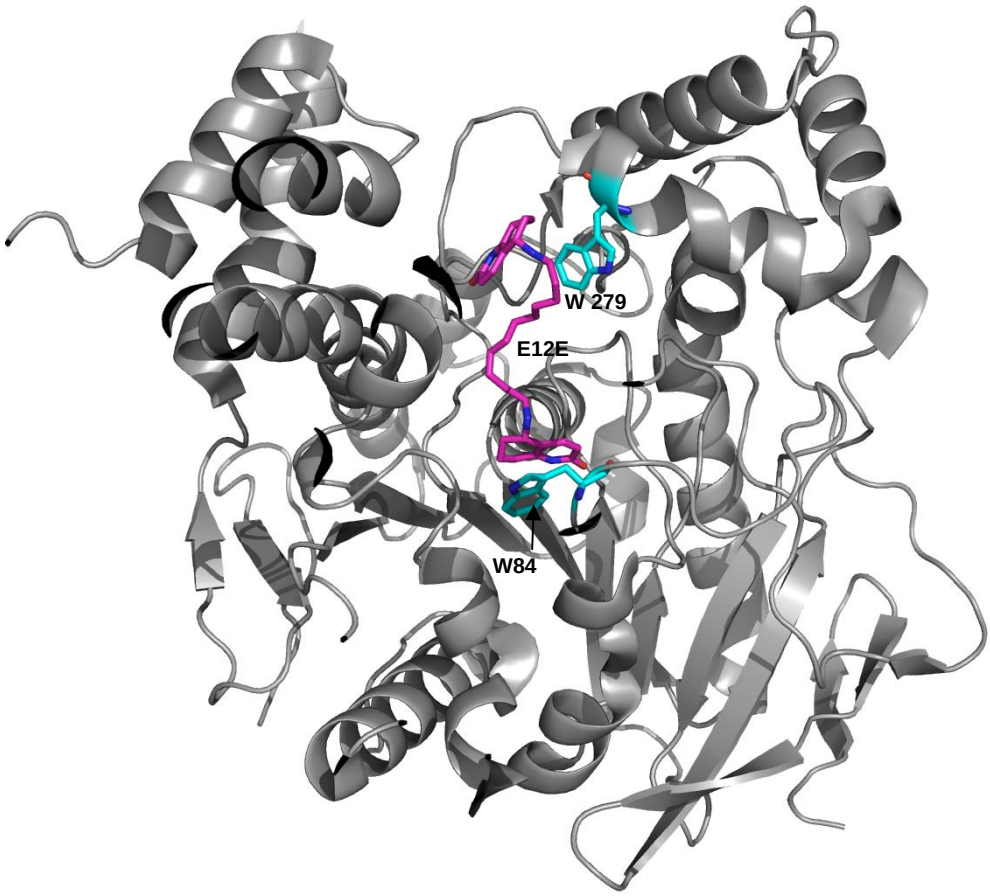

Figure 3.6 π-π interaction between bivalent inhibitor, (*S*,*S*)-(-)-Bis(12)-Hupyridone (E12E), and Trp84 and Trp279 in the crystal structure of *Torpedo californica* AChE (pdb code: 1H23).[31] Picture created by PyMOL[20]

The catalytic power of AChE can be revealed by the following comparison: at pH 7.0 the rate constant of the water hydrolysis of ACh is 8 x 10^{-10} s^{-1},[34] while one of the highest known k_{cat} of the enzymatic reaction is 1.6 x 10^{4} s^{-1}.[35,36] Thus, the rate of hydrolysis is enhanced by 2 x 10^{13} by AChE. Interestingly, in spite of the larger opening and volume of the active site gorge, BuChE has a slower catalytic turnover. Taylor attributed the slower rate to the less hydrophobic, and therefore more water-accessible, active center gorge of BuChE.[1]

3.3 AChE Inhibition

Due to the biological importance of the cholinergic neurotransmission, tremendous attention has been paid to the development of AChE inhibitors. Reversible inhibitors have been developed for human therapeutic use, e.g. in Alzheimer's disease;[37] while irreversible inhibitors are designed for insecticides[38] and warfare agents[39] due to the lethal consequences of systemic AChE inhibition.

3.3.1 Reversible Inhibitors

Reversible inhibitors can interact with AChE in a competitive or non-competitive manner. Competitive inhibitors mimic substrate and thus occupy the active site. Non-competitive inhibitors either bind the acyl enzyme, or inhibit cholinesterase by steric blockade[40-42] or allosteric alteration.[16,43,44] Steric blockade consists of obstructing the traffic of substrate to the entrance of the active site, while allosteric inhibitors bind to the peripheral site, and induce a conformational change of the enzyme. The mode of inhibition adapted depends on the structure of the inhibitor. The reversible AChE inhibitors propidium, fasciculin, tacrine, and carbamates will be discussed in this section.

Propidium, as shown in Figure 3.7, was identified as a PAS inhibitor in 1975.[45] The dissociation constant for the *Tc*AChE-propidium complex obtained from fluorimetric titration was 0.26 μM.[45] Moreover, for mouse AChE complexed with propidium, the X-ray structure showed that the phenylphenanthridinium bound with Trp286, corresponding to Trp287 in *Tc*AChE, at the peripheral site via π-π stacking.[16] As per the discussion previously, the mode of binding by reversible PAS inhibitors is controversial. Schafferman carried out site-directed mutagenesis experiments to support the allosteric modification model;[46] however, Gentry provided evidence for the steric blockade.[47]

Fasciculin is a 61-amino acid polypeptide toxin from snake venom with a characteristic of three-finger shape tertiary structure (Figure 3.8),[14] exhibiting sub-nanomolar AChE inhibition.[48] Some researchers believe that the inhibition by fasciculin is due to steric blockade.[14,49] The polypeptide blocks the access to the active site attributed to the halfway entry of the central finger into the gorge, meanwhile the rest of the molecule binds to the peripheral site. Alternatively, allosteric modification was also supported by experimental results.[50,51]

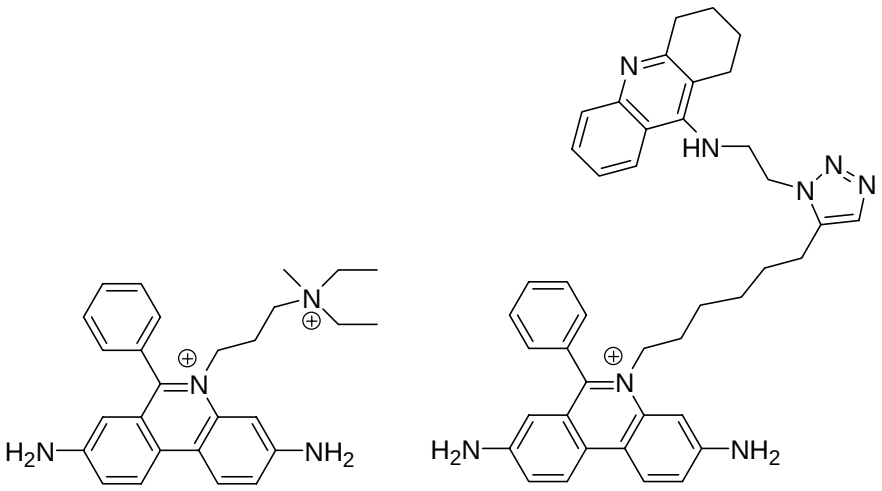

224 **225**

Figure 3.7 Propidium **224** and triazole-linked tacrine-propidium conjugate **225**

Sharpless, Finn, Carlier, Taylor, and co-workers designed a type of bivalent inhibitor, triazole-linked tacrine-propidium conjugate **225** (Figure 3.7), formed by *in situ* cycloaddition between two libraries of acetylene and azide substituent-bearing compounds, interacting with both the active site and peripheral site.[32,52] It should be noted that out of 49 possible compounds generated by the "click" chemistry, only one was detected in the enzyme. This strategy provided exceptionally high binding affinity to AChE, exhibiting dissociation constant in femtomolar range, due to dual site interaction.

Figure 3.8 X-ray crystal structure of mouse AChE-fasciculin II complex (pdb code: 1MAH).[14] Three-finger like fasciculin resides at the peripheral site. Picture created by PyMOL[20]

Carbamates covalently modify Ser200 but are generally reversible inhibitors, because the carbamoylated enzyme is slowly hydrolysed (Figure 3.9). This type of AChE inhibitor is sometimes termed "pseudo-irreversible" and mainly used as insecticide because of its biodegradable property.[53] Carbofuran and propoxur are common examples applied in agriculture (Figure 3.10).

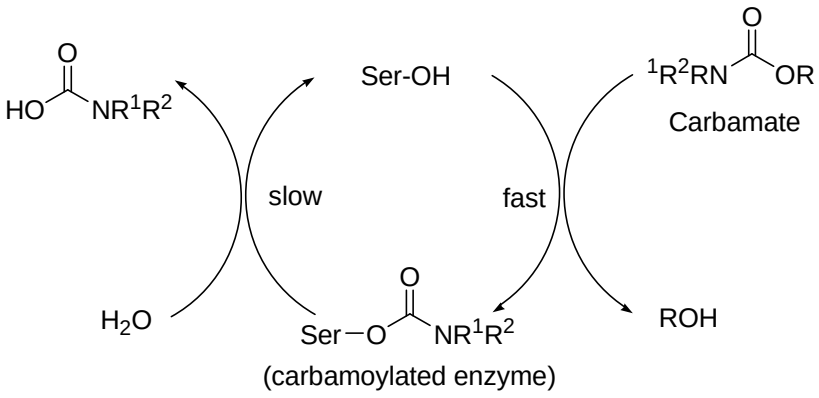

Figure 3.9 Catalytic cycle for carbamate inhibition of AChE

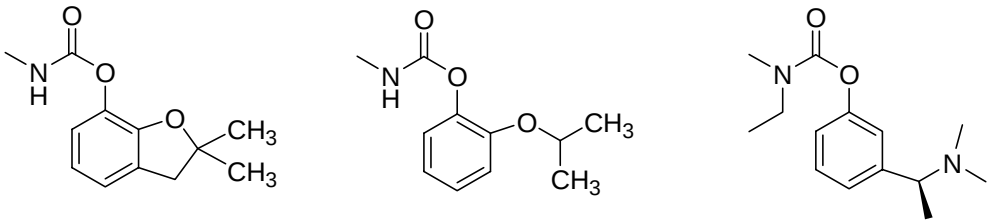

226 Carbofuran **227** Propoxur **228** Rivastigmine

Figure 3.10 Insecticide carbamate, carbofuran and propoxur, and FDA approved drug for AD, rivastigmine

Furthermore, rivastigmine (Exelon®) has been developed as a human AChE inhibitor for the treatment of AD memory loss (Figure 3.10). The X-ray crystal structure of rivastigmine-*Tc*AChE complex was determined by Sussman and coworkers in 2002 (Figure 3.11).[54] The enzyme was found to be carbamoylated as expected, and the phenol leaving group had left the gorge. The carbamate substituents resided at the acyl pocket, having hydrophobic interaction with aromatic residues Phe288 and Phe290. The carbonyl oxygen formed hydrogen bonding with the amide protons of Gly119 and Ala201 in the oxyanion hole. In addition, the crystal structure showed that the steric bulk from N-ethyl disrupted the hydrogen bonding between His440 and Glu327 in the active center, preventing reactivation of the enzyme from nucleophilic attack by water molecule.

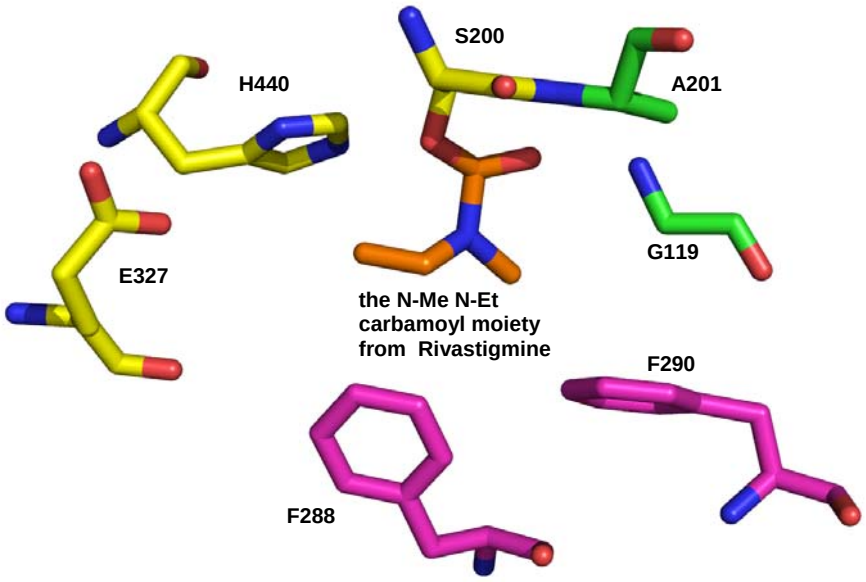

Figure 3.11 Catalytic triad, acyl pocket and oxyanion hole in the crystal structure of *Tc*AChE-Rivastigmine complex (pdb code: 1GQR).[54] Catalytic triad residues: S200, H440, E327; acyl pocket residues: F288, F290; oxyanion hole residues: G119, A201. Picture created by PyMOL[20]

3.3.2 Irreversible Inhibitors

Irreversible inhibitors bind covalently with the active serine, thereby inactivating the nucleophile in the enzyme active site and preventing the hydrolysis of ACh. Organophosphates (OPs) are the most examples of common irreversible inhibitors of AChE. OPs are usually used as insecticides because they can cause cholinergic toxicity which leads to the death of insects.[53,55] Unfortunately, some volatile OP are also used as chemical warfare agents.

OPs usually have a good leaving group to facilitate nucleophilic attack by the active serine. Representative inhibitors in this class of anticholinesterase insecticides[56] include malaoxon and paraoxon (Figure 3.12). After intensive and continuous use of insecticides, some insects such as mosquitoes and flies have developed insecticide resistance.[57,58] It is believed that under selection pressure the insect AChE structures mutate to be less reactive towards OPs and still retain sufficient ACh hydrolysis activity,[57,58] because the sizes of organophosphate and acetylcholine molecules are significantly different.

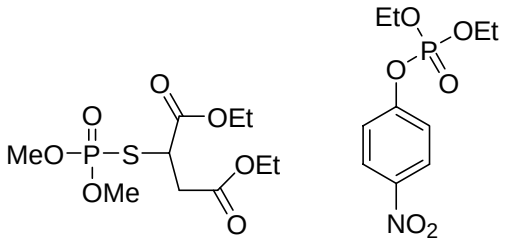

229 Malaoxon **230** Paraoxon

Figure 3.12 Insecticides: malaoxon and paraoxon

Normally, nerve warfare agents such as sarin and soman undergo "aging" very quickly (Figure 3.13). Aging is referred to the loss of an alkyl group from a phosphorylated or phosphonylated enzyme which generates a negative charge at the OP moiety, as shown in Figure 3.14.[18,59] Due to the negative charge the aged enzyme is quite resistant to the reactivation of the active serine by water hydrolysis or any nucleophilic attack, and thus leads to irreversible inhibition. Usually aging of chemical warfare agents takes place in minutes,

while that of OP insecticides needs days to complete.[18,59] Moreover, Shafferman et al. proposed that Trp84 is involved in the aging process as the evolved carbocation can be stabilized by cation-π interaction.[60]

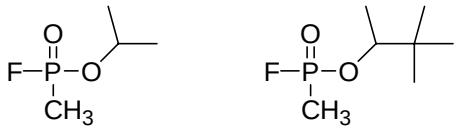

231 Sarin **232** Soman

Figure 3.13 Nerve warfare agents: sorin and soman

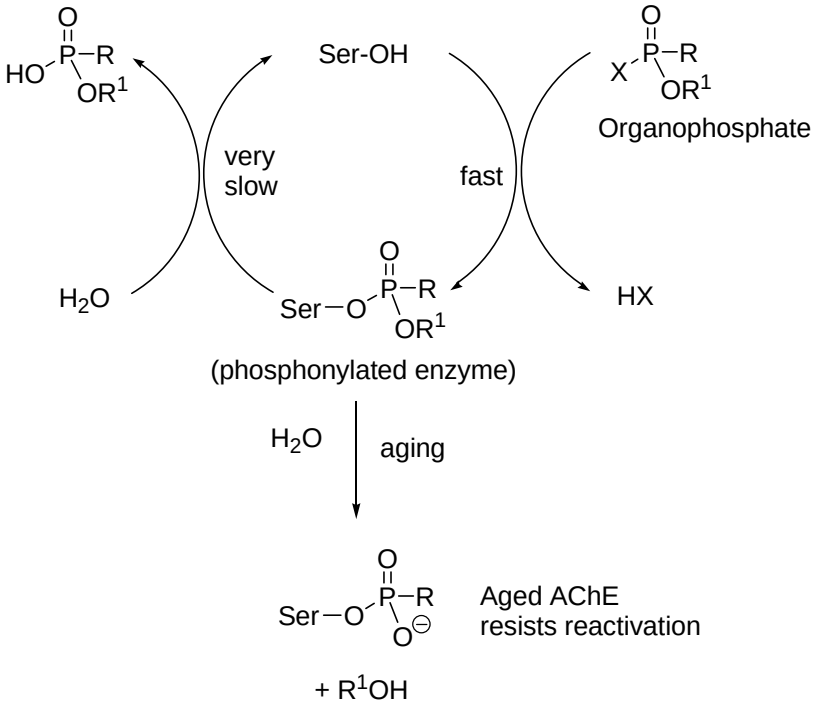

Figure 3.14 Organophosphates as inhibitors (reversible and irreversible) and substrates of acetylcholinesterase

3.4 Free Cysteine Targeting: Reaction with Sulfhydryl Reagents

3.4.1 Free Cysteine in AChE

It is known that at least seven cysteines are present in most of the acetylcholinesterase sequences.[61] Six of them usually form intramolecular disulfide bonds, while the seventh one is responsible for the formation of AChE homodimers via intermolecular disulfide bond in the proximity of the C-terminus. Furthermore, it is interesting to note that an extra unpaired one or two cysteines are found in most insects, usually located in between the disulfide loops.[1]

Before gene sequencing techniques and modern alignment tools were readily available, the presence of a free cysteine was often deduced on the basis of sensitivity to sulfhydryl reagents (Table 3.1). For example, since there is no free cysteine in AChE from electric eel *Electrophorus*, this enzyme is insensitive towards sulfhydryl agents: Karlin reported that p-chloromercuribenzoate (PCMB) and dithiothreitol (DTT) did not inactivate *Ee*AChE.[62] In addition, Cohen and coworkers gave further support that *Ee*AChE was not sensitive to dithiopyridine (DTP).[63]

Table 3.1 General structures of sulfhydryl reagents

Sulfhydryl Reagents	General Structures
Dithiothreitol (DTT)	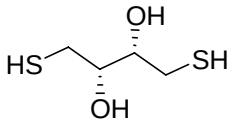
Dithiopyridine (DTP)	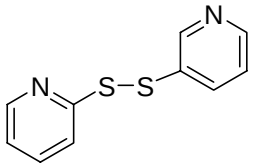
5,5'-dithiobis-(2-nitrobenzoic acid) (DTNB)	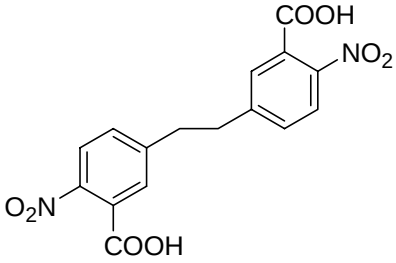
p-Chloromercuribenzoate (PCMB)	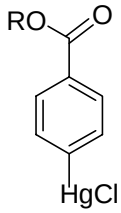
Methanethiosulfinates (MTS)	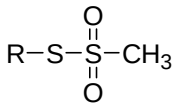
Disulfides	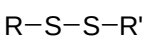
Maleimides	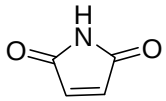
Haloacetamides	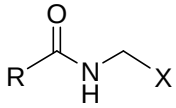 X = halogen atom
α–ketoamides	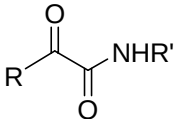

Moreover, at that time similar experiments gave also no evidence of non-C-terminal free cysteines in mammalian AChE. The Silman group demonstrated that acetylthiocholine (ATCh) hydrolysis of typical Ellman assay[64] by rat AChE was insensitive to DTP;[65] however,

DTP was able to deactivate the G234C mutant (corresponding to C231 in *Tc*AChE). In addition, Rosenberry et al. studied the H287C mutant of human with methanethiosulfinates (MTS). They suggested that the degree of the ATCh hydrolysis activity loss was dependent on the effectiveness of steric blockade, i.e. the size of the covalently attached ligand and its ability to occupy the active site. For example, MTS **235** induced the slowest rate of ATCh hydrolysis among the three compounds shown in Figure 3.15. Taylor et al. also carried out similar studies on Y124C, A262C, and H287C mutants of mouse with MTS, demonstrating that the extent of ATCh hydrolysis reduction varied with the size of the modifier.[66,67] Furthermore, Rosenberry showed by radiolabeling that AChE from human red blood cell, bovine brain and bovine blood have no free sulfhydryl groups before treatment of disulfide reduction.[68-70]

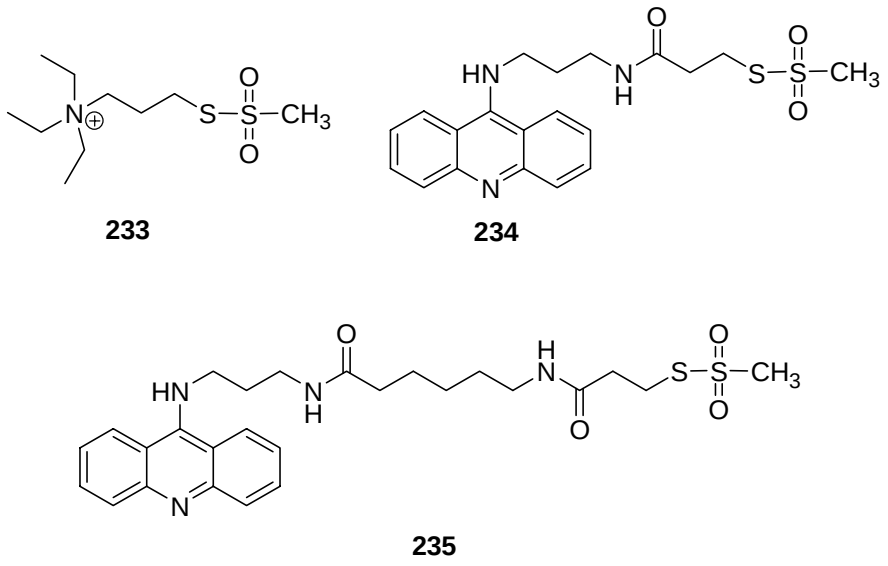

Figure 3.15 MTS reagents used for inhibition of H287C mutated human AChE. Degree of ATCh hydrolysis loss depends on the size of the modifier.

It was found that Cys231 was buried in proximity of the *Tc*AChE active site, approximately 8Å from Ser200.[10,71] As for the reactivity of *Tc*AChE towards sulfhydryl reagents, Silman and coworkers reported that 10 nM of 5,5'-dithiobis-(2-nitrobenzoic acid) (DTNB) and 5 mM of *N*-ethylmaleimide (NEM) deactivated the enzyme with half-lives of

578 min and 51 min respectively.[71] Also, their titration studies showed that the sulfhydryl reagent reacted with 1.0 free cysteine per subunit, where the one cysteine is Cys231.[71] The deduction of free cysteine by Ellman assay using DTNB will be discussed in chapter 4.

Subsequently, Silman et al. proposed that chemical modification of *Tc*AChE with thiol-disulfide exchange reaction at Cys231 caused the formation of a "molten globule" state of the enzyme.[72] The resulting enzyme cannot be de-modified and thus reactivated.

Massoulie and Rosenberry showed that *Torpedo* AChE can be thermally inactivated by DTNB, in which the inactivation rate increased about 5 fold at 30 and 37 °C.[73] However, they observed that even the C231S mutant gave about 3-fold increase in inactivation rate than the wild type. Thus, they concluded that part of the destabilization induced by DTNB did not involve the reaction with Cys231. The mechanistic origin of DTNB inactivation of *Tc*AChE remains unresolved to this date. In related structures Silman found that the L282A and L282S mutants of *Torpedo marmorata* AChE (*Tm*AChE) are much more rapidly inhibited by DTNB than *Tc*AChE, suggesting increased access to Cys231. They also indicated that DTP can deactivate wild type and L282S mutant of *Tm*AChE similarly. Finally, Cohen reported that a 14C-labeled alpha-bromoketone covalently labeled C231 of the *Torpedo nobliana* AChE (*TnAChE*).[63]

DTNB inactivation has also been studied in insect AChEs. Zahavi and coworkers pointed out that *Myzus persicae*, green peach aphid, AChE was extremely sensitive to DTNB.[74] Unless DTNB was added at the end, the Ellman assay could not be performed because of the fast reaction of DTNB with the free cysteine. Manulis also reported that DTNB had to be added at the end of the assay on AChE of the spirea aphid, *Aphis citricola* van der Groot.[75] For comparison, AChE of bovine red blood cell (RBC), medfly head and spider mite were not susceptible to DTNB. It is interesting to note that aphid AChE was only slightly sensitive to iodoacetate and oxidized glutathione, indicating that either the rate of

modification or the activity of the modified enzyme can be affected by the structure of the sulfhydryl reagents.

It was stated that the aphid disulfide bonds were especially accessible, or rupture of the bond caused more rapid protein unfolding than those of other species.[76] Smissart et al. indicated that 2-mercaptoethanol or DTT can reduce the disulfide bonds in AChE of electric eel, ox brain, bovine RBC and mite without inactivation; while 2-pyridyldisulfide (2-PDS) decreased the enzyme activity to less than 50% and then remained stable.[76] After purification of the latter modified enzyme, same activity was still shown. Hence, they suggested the possibility of the development of selective sulfhydryl-based aphidicide.

Brestkin et al. found both AChE and BuChE in homogenates of whole aphids *Schizaphis gramina* (*R*).[77] Apart from lower thermostability, the difference between purified SgAChE and human RBC AChE was that inhibition on the former by DTNB was irreversible. Also, Novoshilov et al. compared several species of insects including aphids.[78] They found that only aphid AChE was inhibited by DTNB, while those of suborders psylla (Pysllinea), coccids (Coccinea), whitefly (Aleyrodinea), and leafhopper (Cicadinea) were not sensitive to DTNB.

Pezzementi and coworkers reported that AChE from the amphioxus (a fish-like invertebrate), *Branchistoma floridae*, was inhibited by DTNB slowly due to free Cys310 in proximity to the acyl pocket (Figure 3.16).[79,80] The F312I mutant was inactivated by DTNB much more rapidly than wild type, which the author attributed to greater accessibility of the Cys310. It was noted that there was another free cysteine in this enzyme, Cys466, located near the choline-binding site. Moreover, the authors undertook site-specific mutagenesis and found that both cysteines were inactivated by DTNB and NEM, but that Cys310 was more accessible.

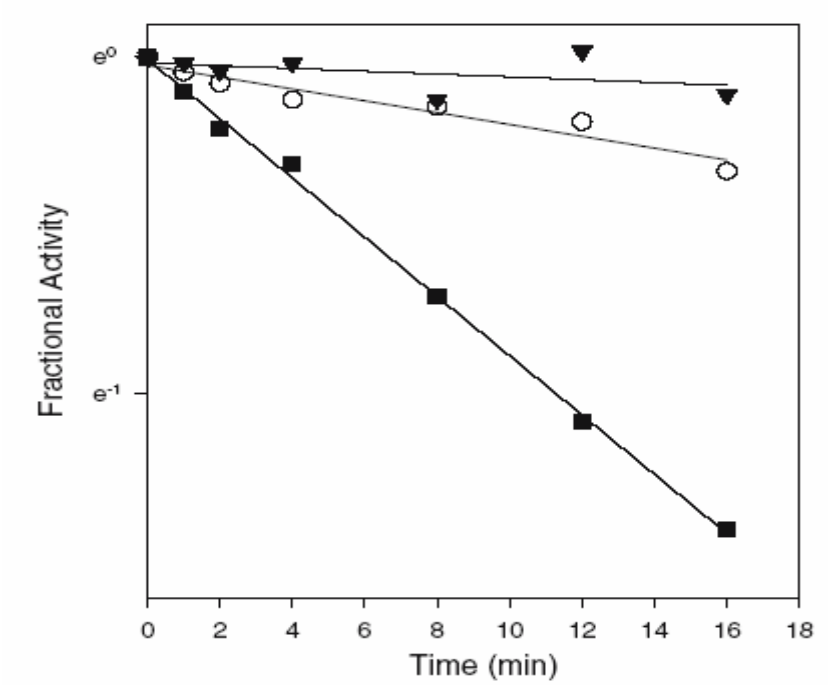

Figure 3.16 Representative data for the inactivation of wild type and mutant ChE2 by DTNB. ChE2 was incubated with DTNB and inactivation rates were determined. (open circle) Wild type ChE2, $1x10^{-3}$ M DTNB; (filled square) ChE2 F312I, $4.76x10^{-5}$ M DTNB; (filled inverted triangle) ChE2 C310A/C466A, $1x10^{-3}$ M DTNB. Reproduced with permission from ref. 80. Copyright 2006 Springer.

As shown in Figure 3.17, Pezzementi was the first in print to do a sequence alignment of AChE from amphioxus (*B. floridiae*), mosquitoes (*A. gambiae* and *C. pipiens*), aphids (*A. gossypii, S. gramium* and *M. persicae*), honeybee (*A. mellifera*), human (*H. sapiens*) and fish (*T. californica*). Except H. sapiens and T. californica, the rest of species possess the corresponding Cys310. Therefore, bivalent inhibitor interacting with free cysteine at the acyl pocket and certain residues at the active site could be good candidates for selective insecticide targeting *Anopheles gambiae*, the species in which we are most interested in. Note however that the other insects possessing a free cysteine at this position would also be affected by such inhibitors.

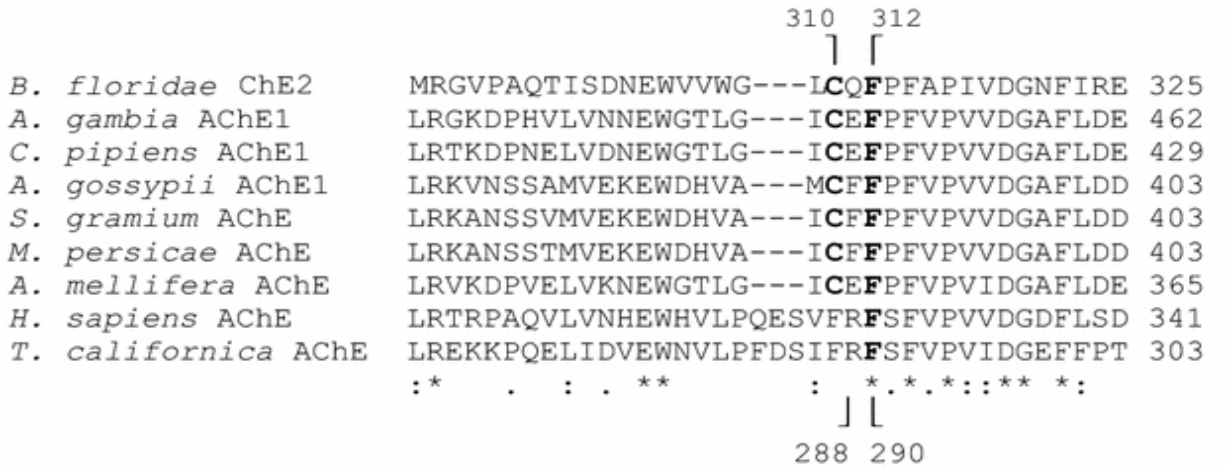

Figure 3.17 Alignment of AChEs containing a cysteine in the region of the acyl pocket. All AChEs known to have a cysteine in the vicinity of the acyl pocket are aligned. The Cys310 and Phe312 (of the acyl pocket) of Branchiostoma floridae, B. floridae (Genbank Accession No. U74381) are numbered and the conservation of these residues in other sequences is indicated by bold type. The Phe288 and Phe290 of the acyl pocket of Torpedo AChE are also numbered. Phe312 of the acyl pocket of ChE2 is homologous to Phe290 of Torpedo AChE and Cys310 is in the position homologous to Phe288. In invertebrates, the second aromatic amino acid of the acyl pocket is at the position homologous to Val400 in Torpedo AChE and is not shown; in ChE2 it is Phe422. Sequence alignment was performed with Clustal W. Reproduced with permission from ref. 80. Copyright 2006 Springer.

3.4.2 Sulfhydryl Reagents

Some of the sulfhydryl reagents have been mentioned previously, e.g. methanethiosulfinates (MTS), disulfides (DTNB, DTP, DTT and 2-PDS), maleimides (NEM), and α-haloketones. It is commonly observed that greater reactivity is accompanied by less selectivity. Hence, more reactive functionality may be less selective and may cause unwanted non-target toxicity. It should be noted that, compared to disulfides and maleimides, haloacetamides are a class of sulfhydryl reagent which have moderate reactivity towards the thiol group, and thus appear to be suitable candidate with which to begin our investigation.

Presumably, the order of haloacetamide reactivity depends on the halide leaving group (Table 3.1), i.e. in descending order $I^- > Br^- > Cl^-$. However, the fluoro derivative is seldom used as a sulfhydryl reagent due to its low reactivity. Borgna et al. evaluated the binding affinity to estrogen receptor by the haloacetamido derivatives of estradiol.[81] Interestingly, they found that chloroacetamide showed a higher binding affinity than the bromo- analogue. The former was reported to irreversibly bind a cysteine at the binding pocket, suggesting that

the haloacetamide reactivity may be affected by other features particular to the protein structures. Meares demonstrated ligation of a chloroacetamide and a bromoacetamide to a cysteine side chain of an antibody CHA255 in an 2-hour incubation at 37 °C.[82] Schröder showed that the chloroacetamide herbicide metazachlor (Figure 3.18) covalently bound to the active site cysteine of plant type III polyketide synthase.[83] Furthermore, a bromoacetamide was used to ligate luminescent thiol-reactive chelates to myosin or DNA.[84] In addition, it was found that bromo- and iodoacetamides were irreversible inhibitors of aldose reductase, but the chloro derivative was reversible.[85] Portoghese reported that bromoacetamide and iodoacetamide derivatives of naltrexone (Figure 3.16) bound irreversibly to μ opioid receptors.[86] Wong demonstrated that *N*-(*β*-saccharide) iodoacetamides can be applied for linking sugars to peptides and proteins with cysteine side chain, particularly useful in site-specific glycosylation and solid-phase enzymic oligosaccharide synthesis.[87]

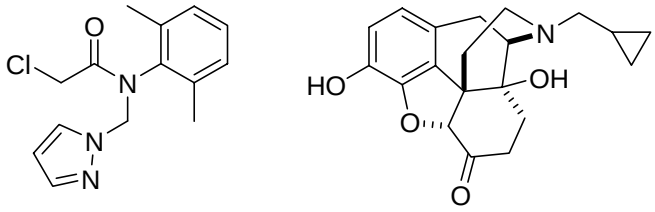

236 metazachlor **237** naltrexone

Figure 3.18 Metazachlor and naltrexone

3.5 Summary

Acetylcholinesterase (AChE) and butyrylcholinesterase (BuChE) belong to the cholinesterase family, which is responsible for catalyzing the hydrolysis of the neurotransmitter acetylcholine (ACh) in both central and peripheral nervous systems. The first successful X-ray structure of AChE was obtained for *Torpedo californica* (*Tc*AChE) with inhibitor decamethonium in 1991. Accompanied with site-directed mutagenesis, the

catalytic triad was found as Ser200, His440 and Glu327 located at 20 Å deep from the mouth of the gorge. The acyl pocket, oxyanion hole, choline-binding site and peripheral anionic site are also important domains in AChE.

Basically, there are two types of AChE inhibitors. Reversible inhibitors can be applied for human therapeutic use; while irreversible and pseudo-irreversible inhibitors are useful as insecticides and nerve warfare agents.

Usually at least seven cysteines are present in cholinesterases: 6 are involved in intra-chain disulfide bonds, and one at the C-terminal is used to form enzyme homodimers. No free cysteines are present in electric eel or mammalian AChE. An extra one or two cysteines are found unpaired in Torpedo californica (marmorata, and nobliana) and several insect species. The accessibility of this free cysteine varies greatly, depending on its location (e.g. acyl pocket) and the steric shielding that nearby residues can provide. Sulfhydyl regents such as methanethiosulfinate, disulfide, maleimide, haloacetamide and α-haloketone can be used for targeting solvent accessible free cysteine. Among these reagents, haloacetamide could be good candidate for selective insecticide because of its moderate reactivity to thiol group.

References for Chapter 3

1. Radić, Z.; Taylor, P., Structure and Function of Cholinesterases. In *Toxicology of Organophosphate and Carbamate Compounds*, Gupta, R. C., Ed. Elsevier: Amsterdam, 2006; pp 161-186.

2. Tougu, V., Acetylcholinesterase: Mechanism of Catalysis and Inhibition *Curr. Med. Chem. - Central Nervous System Agents* **2001,** 1, 155-170.

3. Lassiter, T. L.; Barone, S., Jr.; Padilla, S., Ontogenetic differences in the regional and cellular acetylcholinesterase and butyrylcholinesterase activity in the rat brain. *Brain Res Dev Brain Res* **1998,** 105, (1), 109-23.

4. Cannon, J. G., The Cholinergic System. In *Pharmacology for Chemists*, Oxford University Press: New York, NY, 1999; pp 116-133.

5. Metcalf, R. L., Structure-Activity Relationships for Carbamates. *Bull. W.H.O.* **1971,** 44, 43-78.

6. Jarv, J., Stereochemical Aspects of Cholinesterase Catalysis. *Bioorganic Chemistry* **1984,** 12, (4), 259-278.

7. Adler, M.; Manley, H. A.; Purcell, A. L.; Deshpande, S. S.; Hamilton, T. A.; Kan, R. K.; Oyler, G.; Lockridge, O.; Duysen, E. G.; Sheridan, R. E., Reduced acetylcholine receptor density, morphological remodeling, and butyrylcholinesterase activity can sustain muscle function in acetylcholinesterase knockout mice. *Muscle Nerve* **2004,** 30, (3), 317-27.

8. Bolognesi, M. L.; Bartolini, M.; Cavalli, A.; Andrisano, V.; Rosini, M.; Minarini, A.; Melchiorre, C., Design, synthesis, and biological evaluation of conformationally restricted rivastigmine analogues. *Journal of Medicinal Chemistry* **2004,** 47, (24), 5945-5952.

9. Yu, Q. S.; Zhu, X. X.; Holloway, H. W.; Whittaker, N. F.; Brossi, A.; Greig, N. H., Anticholinesterase activity of compounds related to geneserine tautomers. N-oxides and 1,2-oxazines. *Journal of Medicinal Chemistry* **2002,** 45, (17), 3684-3691.

10. Sussman, J. L.; Harel, M.; Frolow, F.; Oefner, C.; Goldman, A.; Toker, L.; Silman, I., Atomic Structure of Acetylcholinesterase from *Torpedo californica*: A Prototype Acetylcholine-Binding Protein. *Science* **1991,** 253, 872-879.

11. Chothia, C.; Leuzinger, W., Acetylcholinesterase: the structure of crystals of a globular form from electric eel. *J Mol Biol* **1975,** 97, (1), 55-60.

12. Schrag, J. D.; Schmid, M. F.; Morgan, D. G.; Phillips, G. N., Jr.; Chiu, W.; Tang, L., Crystallization and preliminary X-ray diffraction analysis of 11 S acetylcholinesterase. *J Biol Chem* **1988,** 263, (20), 9795-800.

13. Raves, M. L.; Harel, M.; Pang, Y.-P.; Silman, I.; Kozikowski, A. P.; Sussman, J. L., Structure of acetylcholinesterase complexed with the nootropic alkaloid (-)-huperzine A. *Nature Structural Biology* **1997,** 4, 57-63.

14. Bourne, Y.; Taylor, P.; Marchot, P., Acetylcholinesterase Inhibition by Fasciculin: Crystal Structure of the Complex. *Cell* **1995,** 83, 503-512.

15. Kryger, G.; Harel, M.; Giles, K.; Toker, L.; Velan, B.; Lazar, A.; Kronman, C.; Barak, D.; Ariel, N.; Shafferman, A.; Silman, I.; Sussman, J. L., Structures of recombinant native and E202Q mutant human acetylcholinesterase complexed with the snake-venom toxin fasciculin-II. *Acta Crystallogr D Biol Crystallogr* **2000,** 56, (Pt 11), 1385-94.

16. Bourne, Y.; Taylor, P.; Radic, Z.; Marchot, P., Structural insights into ligand interactions at the acetylcholinesterase peripheral anionic site. *EMBO Journal* **2003,** 22, (1), 1-12.

17. Harel, M.; Kryger, G.; Rosenberry, T. L.; Mallender, W. D.; Lewis, T.; Fletcher, R. J.; Guss, J. M.; Silman, I.; Sussman, J. L., Three-dimensional structures of *Drosophila melanogaster* acetylcholinesterase and of its complexes with two potent inhibitors. *Protein Science* **2000,** 9, 1063-1072.

18. Nachon, F.; Asojo, O. A.; Borgstahl, G. E.; Masson, P.; Lockridge, O., Role of water in aging of human butyrylcholinesterase inhibited by echothiophate: the crystal structure suggests two alternative mechanisms of aging. *Biochemistry* **2005,** 44, (4), 1154-62.

19. Nachon, F.; Nicolet, Y.; Viguie, N.; Masson, P.; Fontecilla-Camps, J. C.; Lockridge, O., Engineering of a monomeric and low-glycosylated form of human butyrylcholinesterase: expression, purification, characterization and crystallization. *Eur J Biochem* **2002,** 269, (2), 630-7.

20. DeLano, W. L. *The PyMOL Molecular Graphics System*, 0.99; DeLano Scientific: San Carlos, CA, USA, 2006.

21. Gibney, G.; Taylor, P., Biosynthesis of Torpedo acetylcholinesterase in mammalian cells. Functional expression and mutagenesis of the glycophospholipid-anchored form. *J Biol Chem* **1990,** 265, (21), 12576-83.

22. Sultatos, L. G., Interactions of Organophophorous and Carbamate Compounds with Cholinesterases. In *In Toxicology of Organophosphate and Carbamate Compounds*, Gupta, R. C., Ed. Elesevier Academic Press: Burlington, MA, 2006; pp 209-218.

23. Ariel, N.; Ordentlich, A.; Barak, D.; Bino, T.; Velan, B.; Shafferman, A., The 'aromatic patch' of three proximal residues in the human acetylcholinesterase active centre allows for versatile interaction modes with inhibitors. *Biochemical Journal* **1998,** 335, 95-102.

24. Hasinoff, B. B., Kinetics of Acetylthiocholine Binding to Electric-Eel Acetylcholinesterase in Glycerol Water Solvents of Increased Viscosity - Evidence for a Diffusion-Controlled Reaction. *Biochimica Et Biophysica Acta* **1982,** 704, (1), 52-58.

25. Ordentlich, A.; Barak, D.; Kronman, C.; Flashner, Y.; Leitner, M.; Segall, Y.; Ariel, N.; Cohen, S.; Velan, B.; Shafferman, A., Dissection of the Human Acetylcholinesterase Active-Center Determinants of Substrate-Specificity - Identification of Residues Constituting the Anionic Site, the Hydrophobic Site, and the Acyl Pocket. *Journal of Biological Chemistry* **1993,** 268, (23), 17083-17095.

26. Radic, Z.; Pickering, N. A.; Vellom, D. C.; Camp, S.; Taylor, P., Three Distinct Domains in the Cholinesterase Molecule Confer Selectivity for Acetyl- and Butyrylcholinesterase Inhibitors. *Biochemistry* **1993,** 32, 12074-12084.

27. Vellom, D. C.; Radic, Z.; Li, Y.; Pickering, N. A.; Camp, S.; Taylor, P., Amino acid residues controlling acetylcholinesterase and butyrylcholinesterase specificity. *Biochemistry* **1993,** 32, (1), 12-7.

28. Harel, M.; Quinn, D. M.; Nair, H. K.; Silman, I.; Sussman, J. L., The X-ray Structure of a Transition State Analog Complex Reveals the Molecular Origins of the Catalytic Power and Substrate Specificity of Acetylcholinesterase. *Journal of the American Chemical Society* **1996,** 118, 2340-2346.

29. Selwood, T.; Feaster, S. R.; States, M. J.; Pryor, A. N.; Quinn, D. M., Parallel Mechanisms in Acetylcholinesterase-Catalyzed Hydrolysis of Choline Esters. *Journal of the American Chemical Society* **1993,** 115, (23), 10477-10482.

30. Weise, C.; Kreienkamp, H. J.; Raba, R.; Pedak, A.; Aaviksaar, A.; Hucho, F., Anionic Subsites of the Acetylcholinesterase from Torpedo-Californica - Affinity Labeling with the Cationic Reagent N,N-Dimethyl-2-Phenyl-Aziridinium. *Embo Journal* **1990,** 9, (12), 3885-3888.

31. Wong, D. M.; Greenblatt, H. M.; Dvir, H.; Carlier, P. R.; Han, Y.-F.; Pang, Y.-P.; Silman, I.; Sussman, J. L., Acetylcholinesterase Complexed with Bivalent Ligands Related to Huperzine A: Experimental Evidence for Species-Dependent Protein-Ligand Complementarity. *Journal of the American Chemical Society* **2003,** 125, (2), 363-373.

32. Bourne, Y.; Kolb, H. C.; Radic, Z.; Sharpless, K. B.; Taylor, P.; Marchot, P., Freeze-frame inhibitor captures acetylcholinesterase in a unique conformation. *Proceedings of the National Academy of Sciences of the United States of America* **2004,** 101, 1449-1454.

33. Carlier, P. R.; Du, D.-M.; Han, Y.-F.; Liu, J.; Perola, E.; Williams, I. D.; Pang, Y.-P., Dimerization of an Inactive Fragment of Huperzine A Produces a Drug with Twice the Potency of the Natural Product. *Angewandte Chemie, International Edition* **2000,** 39, (10), 1775-1777.

34. Schowen, R. L., In *Transition States of Biochemical Processes*, Gandour, R. D. S., R. L., Ed. Plenum: New York, 1978; p 77.

35. Fuxreiter, M.; Warshel, A., Origin of the catalytic power of acetylcholinesterase: Computer simulation studies. *Journal of the American Chemical Society* **1998,** 120, (1), 183-194.

36. Rosenberry, T. L., Acetylcholinesterase. In *Advances in Enzymology*, Meister, A., Ed. John Wiley & Sons: New York, 1975; Vol. 43, pp 103-218.

37. Du, D.-M.; Carlier, P. R., Development of Bivalent Acetycholinesterase Inhibitors as Potential Therapeutic Drugs for Alzheimer's Disease. *Current Pharmaceutical Design* **2004,** 10, 3141-3156.

38. Silman, I.; Sussman, J. L., Acetylcholinesterase: 'classical' and 'non-classical' functions and pharmacology. *Current Opinion in Pharmacology* **2005,** 5, 293-302.

39. Quinn, D. M., Acetylcholinesterase - Enzyme Structure, Reaction Dynamics, and Virtual Transition-States. *Chemical Reviews* **1987,** 87, (5), 955-979.

40. Eastman, J.; Wilson, E. J.; Cervenansky, C.; Rosenberry, T. L., Fasciculin-2 Binds to the Peripheral Site on Acetylcholinesterase and Inhibits Substrate Hydrolysis by Slowing a Step Involving Proton-Transfer during Enzyme Acylation. *Journal of Biological Chemistry* **1995,** 270, (34), 19694-19701.

41. Mallender, W. D.; Szegletes, T.; Rosenberry, T. L., Organophosphorylation of acetylcholinesterase in the presence of peripheral site ligands - Distinct effects of propidium and fasciculin. *Journal of Biological Chemistry* **1999,** 274, (13), 8491-8499.

42. Rosenberry, T. L.; Mallender, W. D.; Thomas, P. J.; Szegletes, T., A steric blockade model for inhibition of acetylcholinesterase by peripheral site ligands and substrate. *Chemico-Biological Interactions* **1999,** 120, 85-97.

43. Dajas-Bailador, F. A.; Heimala, K.; Wonnacott, S., The allosteric potentiation of nicotinic acetylcholine receptors by galantamine is transduced into cellular responses in neurons: Ca2+ signals and neurotransmitter release. *Mol Pharmacol* **2003,** 64, (5), 1217-26.

44. Saxena, A.; Hur, R.; Doctor, B. P., Allosteric control of acetylcholinesterase activity by monoclonal antibodies. *Biochemistry* **1998,** 37, (1), 145-54.

45. Taylor, P.; Lappi, S., Interaction of Fluorescence Probes with Acetylcholinesterase. The Site and Specificity of Propidium Binding. *Biochemistry* **1975,** 14, 1989-1997.

46. Barak, D.; Ordentlich, A.; Bromberg, A.; Kronman, C.; Marcus, D.; Lazar, A.; Ariel, N.; Velan, B.; Shafferman, A., Allosteric modulation of acetylcholinesterase activity by peripheral ligands involves a conformational transition of the anionic subsite. *Biochemistry* **1995,** 34, (47), 15444-52.

47. Grubic, Z.; Stalc, A.; Sentjurc, M.; Pecar, S.; Gentry, M. K.; Doctor, B. P., Different effects of two peripheral anionic site-binding ligands on acetylcholinesterase active-site gorge topography revealed by electron paramagnetic resonance. *Biochim Biophys Acta* **1995,** 1249, (2), 155-60.

48. Durán, R.; Cerveñansky, C.; Dajas, F.; Tipton, K. F., Fasciculin inhibition of acetylcholinesterase is prevented by chemical modification of the enzyme at a peripheral site. *Biochimica et Biophysica Acta* **1994,** 1201, 381-388.

49. Harel, M.; Kleywegt, G. J.; Ravelli, R. B. G.; Silman, I.; Sussman, J. L., Crystal Structure of an acetylcholinesterase-fasciculin complex: interaction of a three-fingered toxin from snake venom with its target. *Structure* **1995,** 3, 1355-1366.

50. Radic, Z.; Taylor, P., Interaction kinetics of reversible inhibitors and substrates with acetylcholinesterase and its fasciculin 2 complex. *J Biol Chem* **2001,** 276, (7), 4622-33.

51. Rosenberry, T. L.; Rabl, C. R.; Neumann, E., Binding of the neurotoxin fasciculin 2 to the acetylcholinesterase peripheral site drastically reduces the association and dissociation rate constants for N-methylacridinium binding to the active site. *Biochemistry* **1996,** 35, (3), 685-90.

52. Lewis, W. G.; Green, L. G.; Grynszpan, F.; Radic, Z.; Carlier, P. R.; Taylor, P.; Finn, M. G.; Sharpless, K. B., Click Chemistry In Situ: Acetylcholinesterase as a Reaction Vessel

for the Selective Assembly of a Femtomolar Inhibitor from an array of Building Blocks. *Angewandte Chemie, International Edition* **2002,** 41, (6), 1053-1057.

53. Kuhr, R. J.; Dorough, H. W., In *Carbamate Insectisides: Chemistry, Biochemistry and Toxiology*, CRC Press: Cleveland, OH, 1976; pp 1-101.

54. Bar-On, P.; Millard, C. B.; Harel, M.; Dvir, H.; Enz, A.; Sussman, J. L.; Silman, I., Kinetic and structural studies on the interaction of cholinesterases with the anti-Alzheimer drug rivastigmine. *Biochemistry* **2002,** 41, (11), 3555-3564.

55. Taylor, P., Anticholinesterase Agents. In *The Pharmacological Basis of Therapeutics*, 10th ed.; Hardman, J. G.; Limbird, L. E., Eds. McGraw-Hill: New York, 2005; pp 161-176.

56. Gupta, R. C., Introduction. In *Toxicology of Organophosphate and Carbamate Compounds*, Elsevier Academic Press: Burlington, MA, 2006; pp 3-4.

57. Hemingway, J.; Hawkes, N. J.; McCarroll, L.; Ranson, H., The molecular basis of insecticide resistance in mosquitoes. *Insect Biochemistry and Molecular Biology* **2004,** 34, (7), 653-665.

58. Menozzi, P.; Shi, M. A.; Lougarre, A.; Tang, Z. H.; Fournier, D., Mutations of acetylcholinesterase which confer insecticide resistance in Drosophila melanogaster populations. *Bmc Evolutionary Biology* **2004,** 4, -.

59. Timchalk, C., Physiologically Based Pharmacokinetic Modeling of Organophosphorus and Carbamate pesticides. In *Toxicology of Organophosphate and Carbamate Compounds*, Gupta, R. C., Ed. Elsevier Academic Press: Burlington, MA, 2006; pp 103-125.

60. Shafferman, A.; Ordentlich, A.; Barak, D.; Stein, D.; Ariel, N.; Velan, B., Aging of phosphylated human acetylcholinesterase: catalytic processes mediated by aromatic and polar residues of the active centre. *Biochemical Journal* **1996,** 318 (Pt 3), 833-40.

61. MacPhee-Quigley, K.; Vedvick, T. S.; Taylor, P.; Taylor, S. S., Profile of the disulfide bonds in acetylcholinesterase. *Journal of Biological Chemistry* **1986,** 261, (29), 13565-70.

62. Karlin, A., Chemical distinctions between acetylcholinesterase and the acetylcholine receptor. *Biochimica et Biophysica Acta* **1967,** 139, 358-362.

63. Salih, E.; Howard, S.; Chishti, S. B.; Cohen, S. G.; Liu, W. S.; Cohen, J. B., Labeling of Cysteine 231 in Acetycholinesterase from Torpedo nobliana by the Active-site Directed Reagent, 1-Bromo-2-[^{14}C]pinacolone. *Journal of Biological Chemistry* **1993,** 268, 245-251.

64. Ellman, G. L.; Courtney, K. D.; Andres, V. J.; Featherstone, R. M., A new and rapid colorimetric determination of acetylcholinesterase activity. *Biochemical Pharmacology* **1961,** 7, 88-95.

65. Morel, N.; Bon, S.; Greenblatt, H. M.; Van Belle, D.; Wodak, S. J.; Sussman, J. L.; Massoulié, J.; Silman, I., Effect of Mutations within the Peripheral Anionic Site on the Stability of Acetylcholinesterase. *Molecular Pharmacology* **1999,** 55, 982-992.

66. Boyd, A. E.; Marnetti, A. B.; Wong, L.; Taylor, P., Probing the Active Center Gorge of Acetylcholinesterase by Fluorophores Linked to Substituted Cysteines. *Journal of Biological Chemistry* **2000,** 275, (29), 22401-22408.

67. Shi, J.; Boyd, A. E.; Radic, Z.; Taylor, P., Reversibly Bound and Covalently Attached Ligands Induce Conformational Changes in the Omega Loop, Cys69-Cys96, of Mouse Acetylcholinesterase. *Journal of Biological Chemistry* **2001,** 276, 42196-42204.

68. Haas, R.; Jackson, B. C.; Reinhold, B.; Foster, J. D.; Rosenberry, T. L., Glycoinositol phospholipid anchor and protein C-terminus of bovine erythrocyte acetylcholinesterase: analysis by mass spectroscopy and by protein and DNA sequencing. *Biochemical Journal* **1996,** 314, 817-825.

69. Roberts, W. L.; Doctor, B. P.; Foster, J. D.; Rosenberry, T. L., Bovine Brain Acetylcholinesterase Primary Sequence Involved in Intersubunit Disulfide Linkages. *Journal of Biological Chemistry* **1991,** 266, 7481-7487.

70. Rosenberry, T. L.; Scoggin, D. M., Structure of Human Erythrocyte Acetylcholinesterase. *Journal of Biological Chemistry* **1984,** 259, 5643-5652.

71. Steinberg, N.; Roth, E.; Silman, I., *Torpedo* Acetylcholinesterase is Inactivated by Thiol Reagents. *Biochemistry International* **1990,** 21, 1043-1050.

72. Dolginova, E. A.; Roth, E.; Silman, I.; Weiner, L. M., Chemical Modification of *Torpedo* Acetylcholinesterase by Disulfides: Appearance of a "Molten Globule" State. *Biochemistry* **1992,** 31, 12248-12254.

73. Wilson, E. J.; Massoulié, J.; Bon, S.; Rosenberry, T. L., The rate of thermal inactivation of *Torpedo* acetylcholinesterase is not reduced in the C231S mutant. *FEBS Letters* **1996,** 379, 161-164.

74. Zahavi, M.; Tahori, A. S.; Kilmer, F., An acetylcholinesterase sensitive to sulfhydryl inhibitors. *Biochimica et Biophysica Acta* **1972,** 276, 577-583.

75. Manulis, S.; Ishaaya, I.; Perry, A. S., Acetylcholinesterase of *Aphis citricola*: Properties and Significance in Determining Toxicity of Systemic Organophosphorus and Carbamate Compounds. *Pesticide Biochemistry and Physiology* **1981,** 15, 261-274.

76. Smissaert, H. R., Reactivity of a Critical Sulfhydryl Group of the Acetylcholinesterase from Aphids (*Myzus persicae*). *Pesticide Biochemistry and Physiology* **1976,** 6, 215-222.

77. Brestkin, A. P.; Maizel, E. B.; Moralev, S. N.; Novozhilov, K. V.; Sazonova, I. N., Isolation, Partial Purification and Some Properties of Cholinesterases from Spring Grain Aphid *Schizaphis Gramina (Rond). Insect Biochemistry* **1985,** 15, 309-314.

78. Novozhilov, K. V.; Brestkin, A. P.; Khovanskikh, A. E.; Maizel, E. B.; Moralev, S. N.; Nikanorova, E. V.; Sazonova, I. N., Cholinesterases of Aphids-III. Sensitivity of Acetylcholinesterases to Several Inhibitors as a Possible Phylogenetic Character. *Insect Biochemistry* **1989,** 19, 15-18.

79. Pezzementi, L.; Johnson, K.; Tsigelny, I.; Cotney, J.; Manning, E.; Barker, A.; Merritt, S., Amino acids defining the acyl pocket of an invertebrate cholinesterase. *Comparative Biochemistry & Physiology Part B* **2003,** 136, 813-832.

80. Pezzementi, L.; Rowland, M.; Wolfe, M.; Tsigelny, I., Inactivation of an invertebrate acetylcholinesterase by sulfhydryl reagents: the roles of two cysteines in the catalytic gorge of the enzyme. *Invertebrate Neuroscience* **2006,** 6, 47-55.

81. Aliau, S.; Delettre, G.; Mattras, H.; El Garrouj, D.; Nique, F.; Teutsch, G.; Borgna, J.-L., Steroidal Affinity Labels of the Estrogen Receptor α. 4. Electrophilic 11β-Aryl Derivatives of Estradiol. *Journal of Medicinal Chemistry* **2000,** 43, 613-628.

82. Chmura, A. J.; Orton, M. S.; Meares, C. F., Antibodies with infinite affinity. *Proceedings of the National Academy of Sciences of the United States of America* **2001,** 98, 8480-8484.

83. Eckermann, C.; Matthes, B.; NImtz, M.; Reiser, V.; Lederer, B.; Böger, P.; Schröder, J., Covalent binding of chloroacetamide herbicides to the active site cysteine of plant type III polyketide synthases. *Phytochemistry* **2003,** 64, 1045-1054.

84. Chen, J.; Selvin, P. R., Thiol-Reactive Luminescent Chelates of Terbium and Europium. *Bioconjugate Chemistry* **1999,** 10, 311-315.

85. Smar, M. W.; Ares, J. J.; Nakayama, T.; Itabe, H.; Kador, P. F.; Miller, D. D., Selective Irreversible Inhibitors of Aldose Reductase. *Journal of Medicinal Chemistry* **1992,** 35, 1117-1120.

86. Sayre, L. M.; Larson, D. L.; Takemori, A. E.; Portoghese, P. S., Design and Synthesis of Naltrexon-Derived Affinity Labels with Nonequlibrium Opiod Agonist and Antagonist Activities. Evidence for the Existence of Different μ Receptor Subtypes in Different Tissues. *Journal of Medicinal Chemistry* **1984,** 27, 1325-1335.

87. Wong, S. Y. C.; Guile, G. R.; Dwek, R. A.; Arsequell, G., Synthetic Glycosylation of Proteins Using N-(Beta-Saccharide) Iodoacetamides - Applications in Site-Specific Glycosylation and Solid-Phase Enzymatic Oligosaccharide Synthesis. *Biochemical Journal* **1994,** 300, 843-850.

Chapter 4. Structural-based Design of Insecticidal AChE Inhibitors for Malaria Mosquito, Anopheles gambiae

4.1 Malaria Vector Control

Approximately 2 million deaths, mostly children, are caused by malaria every year in the world.[1] In total, roughly 3.2 billion people are living under the risk of malaria transmission.[2] To reduce the toll of this disease, particular attention has been focused on the control of major African malaria insect vectors, e.g. Anopheles gambiae (*Ag*). Current use of anticholinesterase insecticides has been limited by their toxicity to human beings. The majority of AChE-targeting insecticides are carbamates (CM) and organophosphates (OP) (**226** and **227** in Figure 3.10, and **229** and **230** in Figure 3.12 respectively), which attack the common serine residue at the active site present in all species of AChE, thereby disabling the enzyme. A recent report from the U.S. Environmental Protection Agency indicated that CM and OP may be especially toxic to the developing nervous system in fetuses and young children.[3] Limitations in the use of anticholinesterase insecticides are also related to the emergence of resistance, which in turn is caused by the G119S mutation in *Ag*AChE.[4,5] It should be also noted that eight malaria cases were found locally in Florida in 2003, implying the potential threat for the reintroduction of the disease to America.[6] Therefore, new selective insecticides should be investigated for malaria vector control.

4.2 Molecular Modeling of Susceptible AChE of *Anopheles gambiae*

In order to search for any unique sites that are only present in *Ag*AChE for selective insecticidal design, homology modeling of *Ag*AChE was carried out by Dr. Yuan-Ping Pang, our initial collaborator from Mayo Clinic, refining with multiple sequence alignment based on the X-ray structures of two mouse (code: 1J07 and 1N5R) and one electric eel (code: 1C2O) AChEs.[7] The computational model was first generated by the SWISS-MODEL

program,[8] and then refined by the multiple molecular dynamics simulations (MMDSs). In the structure that emerged, Cys286 and Arg339 were found near the surface of the active site gorge of *Ag*AChE. Note that these residues are not present at *h*AChE. These two conserved residues were estimated to be partially solvent accessible (Figure 4.1). The thiol group of Cys286 was found to be near to Trp280 and Tyr333, while the guanidino group of Arg339 was surrounded by Phe75, Phe 78, Tyr332 and Trp431. Thus, in addition to strategies targeting C286, one could envision targeting both C286 and R339.

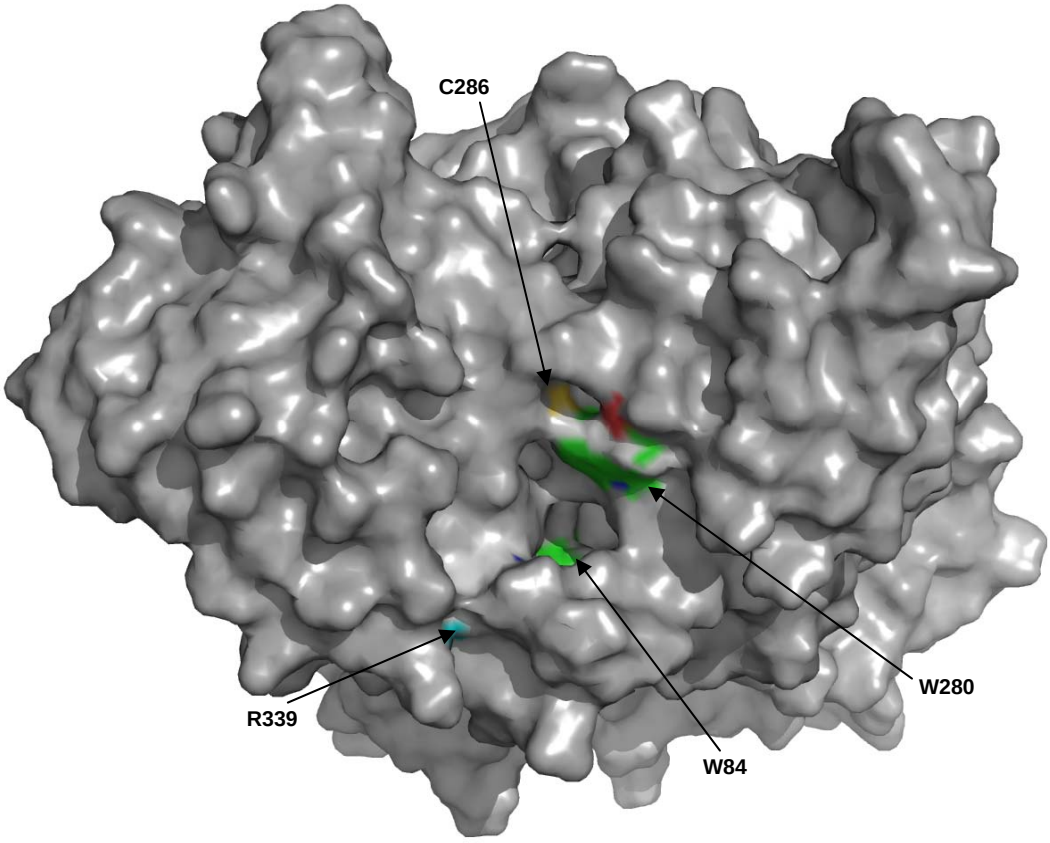

Figure 4.1 Top view of the homology model *Ag*AChE, showing the partially solvent accessible C286 and R339, and also W84 and W280 corresponding to the bivalent ligand design for hAChE. (PDB code: 2AZG).[7] Picture created by PyMOL.[9]

Since Dr. Pang has left our team, we obtained two new homology models of *Ag*AChE from Dr. Max Totrov, our second collaborator from Molsoft, LLC (La Jolla, CA). These two models were developed using ICM 3.5, a Molsoft proprietary application which relies upon Monte Carlo simulation to generate reasonable models. One homology model was based on

the X-ray structure of mouse (code: 1N5R)[10] and a second was based on electric fish (code: 1W4L).[11] An example of the model based on electric fish is shown in Figure 4.2. These two models differ from Pang's homology model with regard to several loop conformations. Most relevant to our present study is that the Molsoft models suggest access to Cys286 should be quite limited. It is important to keep in mind however that neither X-ray structures nor homology models adequately convey dynamic information on the protein structure. Thus, it is necessary to synthesize and assay inhibitors.

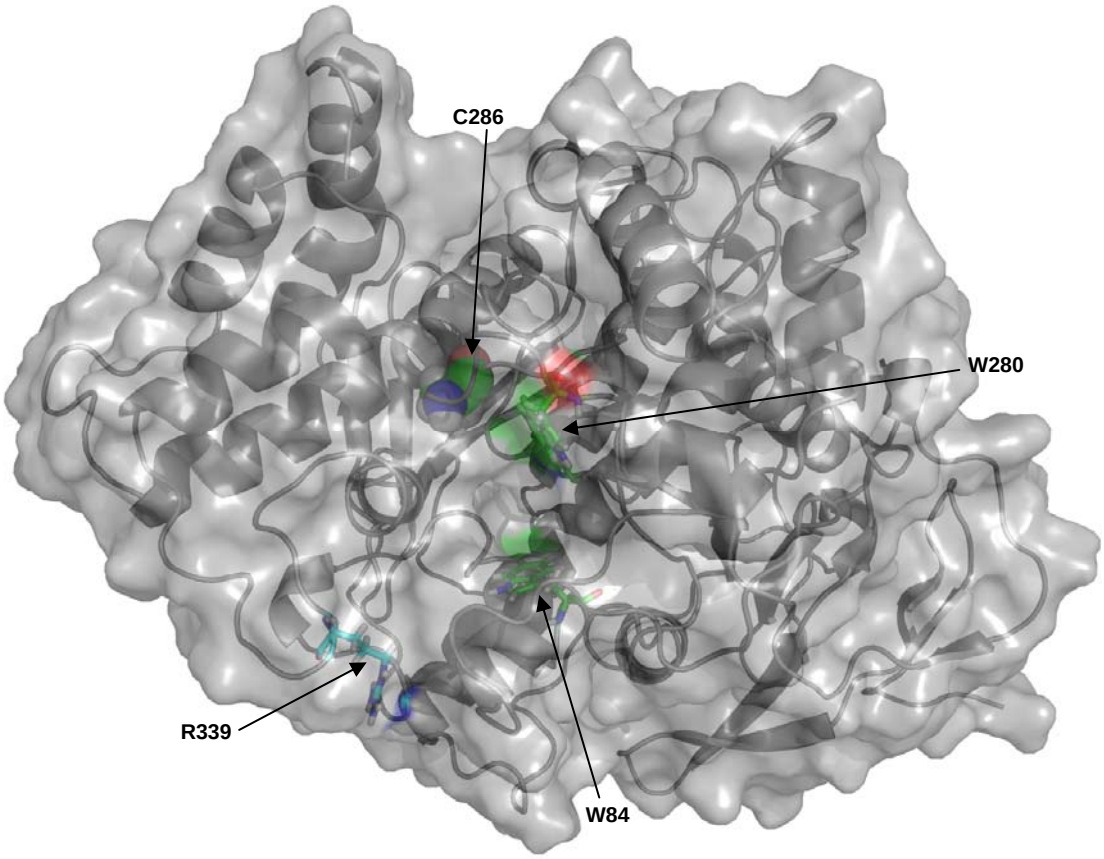

Figure 4.2 Top view of the homology model *Ag*AChE, showing that C286 is not solvent accessible C286. Structural coordinate: aces_w4l_10_2loop1.ent, created by Molsoft, LLC. Picture created by PyMOL.[9]

4.3 Design and Synthesis of Selective AChE Inhibitors for Anopheles gambiae

4.3.1 Design of Selective *Ag*AChE Inhibitors

Based on the Carlier group's successful experience in the preparation of potent mammalian AChE inhibitors for Alzheimer's disease,[12-16] the strategy of dual-site binding was applied to the design and synthesis of selective inhibitor for *Ag*AChE. Tacrine was chosen to be the core structure interacting with Trp84 in the active site, while sulfhydryl-reacting groups (haloacetamides) would be responsible for the covalent binding with the free cysteine at the peripheral site (Figure 4.3).

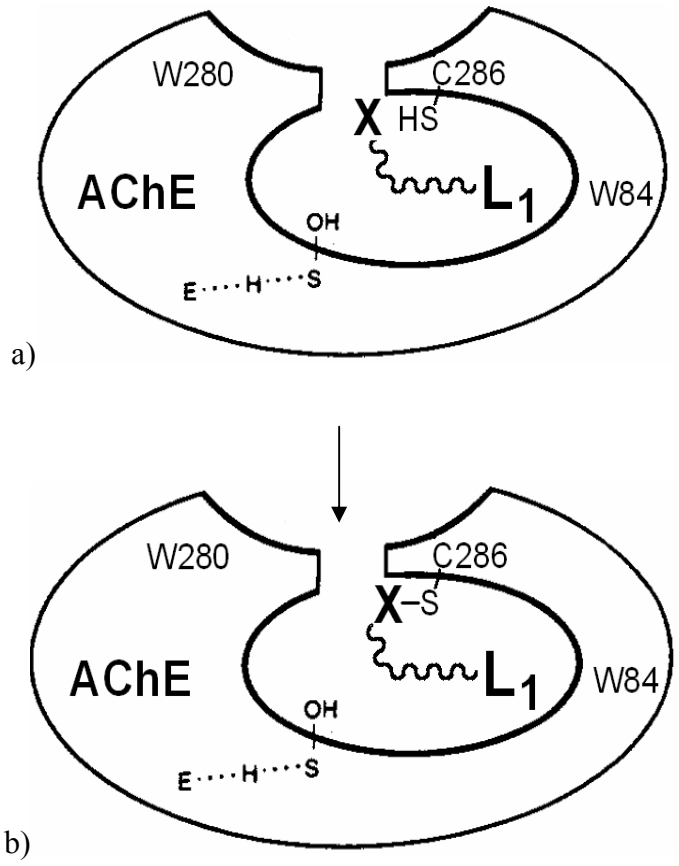

Figure 4.3 Cartoon of bivalent binding of design inhibitor of *Ag*AChE. a) initial non-covalent binding, b) inhibitor now covalently attached. L_1 = tacrine; X = haloacetamide

4.3.2 Synthesis of *Ag*AChE Inhibitors

Rosenberry presented an excellent example of potent inhibition of the H287C mutant of hAChE by covalent attachment of a tethered active site ligand (tacrine).[17] He treated the mutant enzyme with tacrine-tethered methanethiosulfinate reagent **235** (Figure 3.15). The purified, covalently labeled enzyme was then determined to possess only 1/400 th of the catalytic efficiency of the unlabeled mutant, thus providing 99.8% apparent inhibition. Since methanethiosulfinates are too reactive to ever be used on insecticide treated nets, we explored proven sulfhydryl-reactive functionality that would be expected to have greater stability under ambient conditions.

Carlier and co-workers previously prepared a series of tacrine heterodimers as bivalent inhibitors of AChE.[12] They found that the AChE inhibition potency is tether length-dependent, in which compounds **236** and **237** (Figure 4.4) showed the highest IC_{50} on rat AChE (12.8 and 8.8 nM respectively).

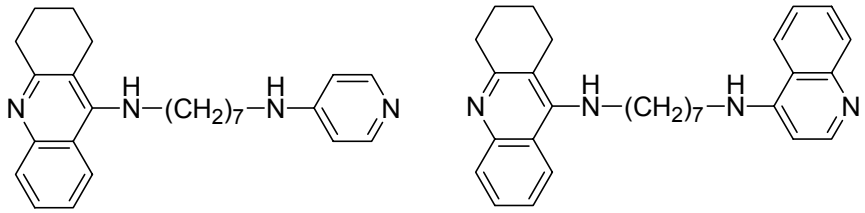

Figure 4.4 Tacrine heterodimers **236** and **237**

According to our successful experience, we carried out the synthesis of the designed bivalent compounds as *Ag*AChE inhibitors. 9-chloro-1,2,3,4-tetrahydroacridine **238** was first reacted with diaminoalkanes to give **239**-**247**, namely $A2NH_2$-$A12NH_2$, in 54-79 % yield. $A8NH_2$ (**215**) was synthesized by Dr. Dawn Wong in our group (Table 4.1). Compounds **239**-**247** were first prepared by Ella Chow Clement in our group.[12]

Table 4.1 Alkylation of 9-Chloro-1,2,3,4-tetrahydroacridine (**238**) by diaminoalkanes

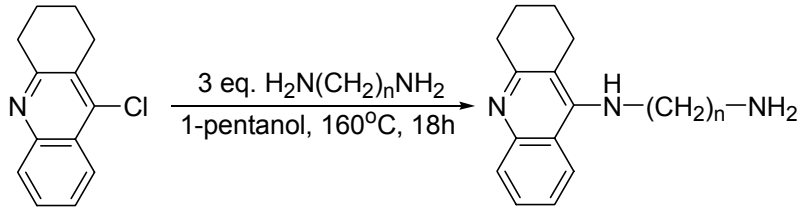

238 **239-247**

Compounds	**239**	**240**	**241**	**242**	**243**	**244**	**245**[a]	**246**	**247**
n	2	3	4	5	6	7	8	10	12
% yield	57	54	62	75	72	79	83	58	60

[a]$A8NH_2$ (**245**) was made by Dr. Dawn Wong in our group

With the exception of $A2NH_2$, bivalent tacrine-tethered (An) haloacetamides **248-255 (a-c)** were synthesized by treating **240-247** with different haloacetic halides and iodoacetic anhydride (Table 4.2). Compound **232d** serves as a control, since it lacks a sulfhydryl-reacting group; it was prepared by treating **244** with acetic anhydride. The products of the reaction with $A2NH_2$ (**239**) could not be purified, probably because of an intramolecular cyclization (Scheme 4.1). However, it is not clear why **255b** and **255c** were obtained in lower yields.

With **248a-c** to **255a-c** in hand, it should be possible to test whether C286 in *Ag*AChE is accessible to the solvent. By varying the tether length, we will allow the tacrine moiety to reversibly anchor itself in the active site, and present the reactive haloacetamide at different distances up the gorge. We hope to be able to place the haloacetamide in precisely the right place to enable facile nucleophilic attack by the C286 thiol. By varying the leaving group, we hope to assess what level of reactivity is needed to allow this covalent bond to form rapidly. Our assumption is that the iodoacetamides should give the most rapid rates for ligation of C286.

Table 4.2 Synthesis of bivalent compounds **248-255 (a-c)**

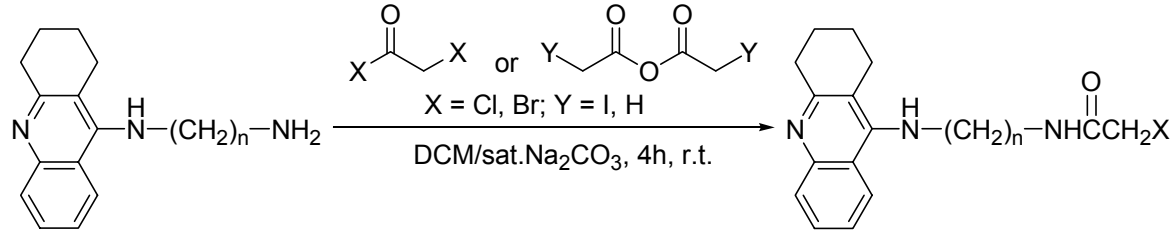

239-247

X = Cl: **250a** - **255a**
Br: **250b** - **255b**
Y = I: **248c** - **255c**
H: **252d** (n = 7)

Compounds	n	X	% Yield
248c	3	I	59
249c	4	I	62
250a	5	Cl	59
250b	5	Br	66
250c	5	I	74
251a	6	Cl	58
251b	6	Br	63
251c	6	I	64
252a	7	Cl	52
252b	7	Br	59
252c	7	I	77
252d	7	H	69
253a	8	Cl	69
253b	8	Br	72
253c	8	I	71
254a	10	Cl	87
254b	10	Br	76
254c	10	I	77
255a	12	Cl	78
255b	12	Br	33
255c	12	I	46

Scheme 4.1 Possible intramolecular side reaction leading to impure product derived from $A2NH_2$ (**239**)

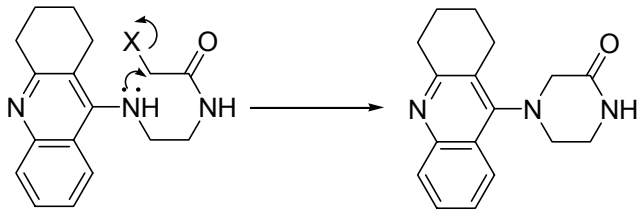

All tacrine-tethered chloro- and bromoacetamides were converted into their corresponding hydrochloric and hydrobromic salts before submission to Bloomquist lab (Entomology department, Virginia Tech) for bioassay, preventing any undesired oxidation or carboxylation of the amino groups in the compounds. However, treatment of the iodo-

analogues with hydroiodic acid resulted in hydrolysis of the compounds back to their starting materials $AnNH_2$. Therefore, the iodoacetamides were submitted in free base form.

4.3.3 Kinetic Models for Covalent Modification of AChE

Before describing the pharmacological results, it is appropriate to consider possible kinetic models for interaction of the tacrine haloacetamides with *Ag*AChE. We will consider three limiting scenarios.

$$E^H + I\text{-}X \underset{k_{-1}}{\overset{k_1}{\rightleftharpoons}} E^H{\bullet}\, I\text{-}X \xrightarrow{k_2} E\text{-}I + HX$$

1. If k_2 is very slow, inhibitors I-X will function as reversible inhibitors and will give normal dose response curves. Potent, tether length-dependent inhibition may be observed with these inhibitors due to hydrophobic interactions of the enzyme with the halide, or hydrogen bonding to the pendant amide moiety. To distinguish these possibilities we prepared a simple acetamide derivative **252d**.

2. If k_2 is very fast, inhibitors I-X may give very significant inhibition at concentrations approaching that of the enzyme; under typical assay conditions we roughly estimate the concentration of active sites to be 50 pM. Note that since covalent modification is not occurring at the active site, but at a remote location, enzyme activity may not be completely eradicated. This may be explained in terms of a two-site model, where the pendant active site ligand is in the active site, or outside the enzyme (Figure 4.5 a and b).

3. If k_2 is in some intermediate domain, potent inhibition may not be achieved below the nanomolar range, and dose-response curves may appear consistent with reversible inhibition. Due to the 10 minute incubation times of enzyme and inhibitor, the extent of conversion to E-I will depend upon the concentration of I-X. To discriminate this scenario from the completely reversible scenario 1, kinetic studies involving different pre-incubation times with the inhibitor could be undertaken. Since non-covalent equilibration of the inhibitor with the enzyme is not instantaneous, plots of ln (v/v_0) vs time should display an initial downward

slope consistent with formation of a steady-state concentration of E^{H}·I-X. Once this steady state is reached, the line of ln (v/v_0) vs time should flatten out. A second downward slope of the plot of ln(v/v_0) vs t will then emerge as E^{H}·I-X is converted to E-I. Depending on the value of k_2 relative to k_{-1}, a biphasic plot in ln(v/v_0) may be seen.

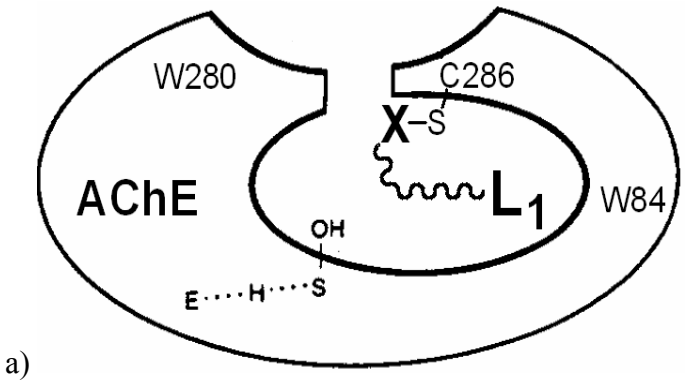

a)

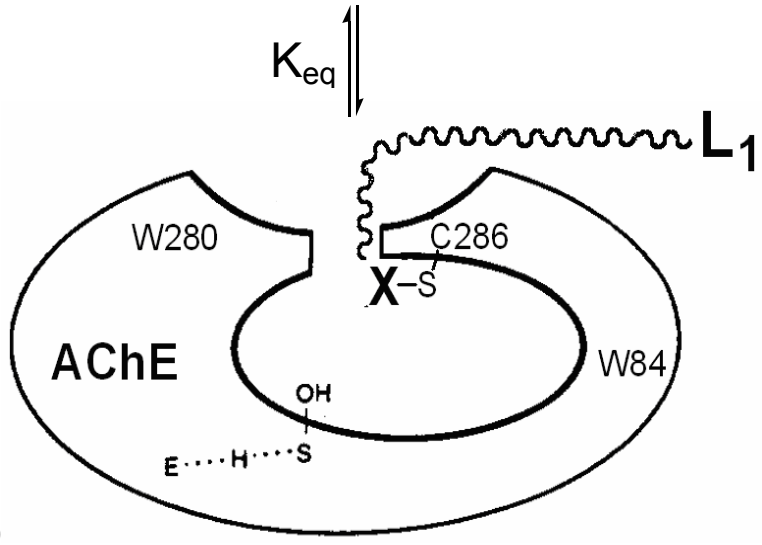

b)

Figure 4.5 Cartoon of bivalent binding of design inhibitor of *Ag*AChE. a) pendant active site ligand is in the active site, b) pendant ligand outside the enzyme. L_1 = tacrine; X = haloacetamide

4.4 Bioassay Results

4.4.1 Principle of Ellman Assay

For the sake of colorimetric measurement, Ellman employed acetylthiocholine (ATCh) in place of acetylcholine (ACh) to determine enzyme velocities.[18] This replacement is feasible because the rate of hydrolysis of ATCh is similar to that of ACh. 5,5'-dithiobis-(2-nitrobenzoic acid) (DTNB) reacts with thiocholine anion in a second fast step to generate a yellow dye (Scheme 4.2), whose concentration is measured using a colorimeter at 405 nm. AChE is incubated with inhibitor for 10 min, followed by addition of a mixture of DTNB-ATCh. The optical density of the resultant mixture is determined for up to 30 min by colorimetry.

Scheme 4.2 Formation of yellow dye in Ellman assay

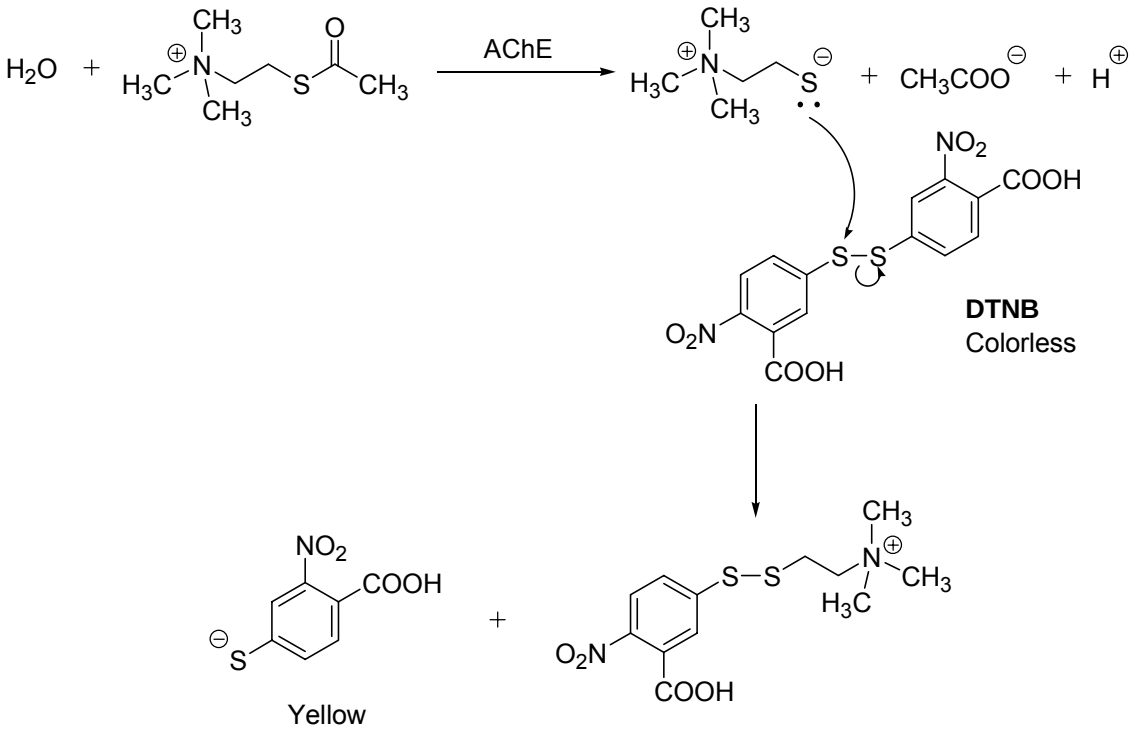

4.4.2 DTNB Incubation Studies

As discussed in section 3.4.1, the color former DTNB used in the standard Ellman assay has been implicated in reactions with free cysteine on the surface of several species of AChE. DTNB sensitivity has been noted for two insect species, Aphid AChE[3, 4] and *Culex*

spp. AChE.[19] As we have mentioned previously, similar to *Ag*, genomics studies showed that both Aphid and *Culex pipiens* have a free Cys in the acyl pocket.[1, 2] In the case of *Culex spp.*, an insecticide-resistant strain was 37-fold more quickly inactivated than the wild type (susceptible) strain.[19]

Incubation of various enzyme sources with 1000 μM DTNB were therefore carried out by Dr. Troy Anderson in the Bloomquist lab. By plotting ln (v/v_0) vs incubation time, a convincing first order loss of AChE activity for green peach Aphid (*Myzus persicae*), wild type homogenate (aphid WT hmg), and recombinant resistant strain *Ag*AChE (ace1-R) enzymes were demonstrated. However, almost no loss of activity was observed for *Ag* WT homogenate (hmg) and recombinant WT *Ag*AChE (ace1-S) (Figure 4.6).

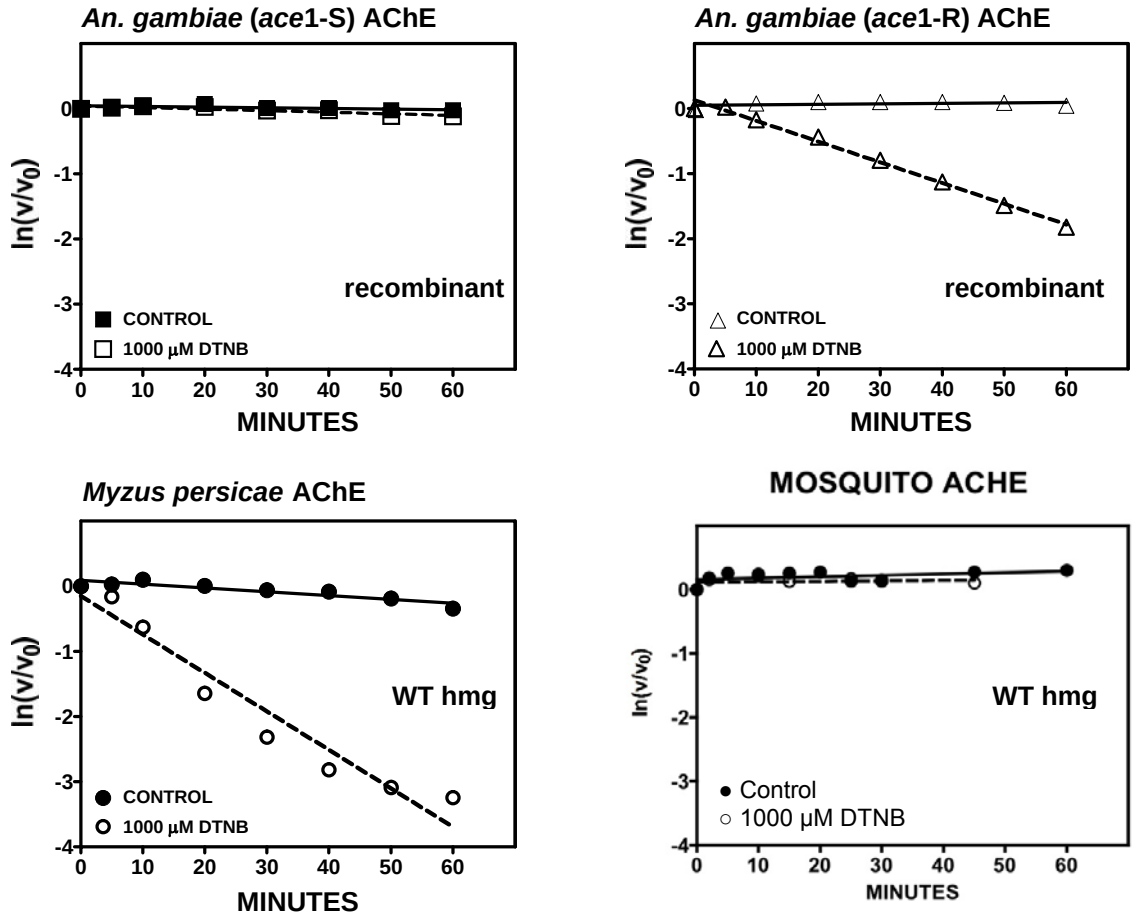

Figure 4.6 Kinetic studies test the DTNB sensitivity to recombinant Ag ace1-S and ace1-R AChE, Aphid, *Myzus persicae*, WT hmg AChE, and *Ag* WT hmg AChE.

As a result, not only was the literature report of DTNB sensitivity of Aphid WT homogenate AChE reproduced, but, more significantly, the DTNB **insensitivity** of WT *Ag*AChE (both recombinant and from homogenate) was first demonstrated. In addition, the resistant strain *Ag* ace1-R AChE was shown to be sensitive to DTNB. These results are comparable to Dary's findings on susceptible and resistant *Culex* spp. AChE,[19] and thus, give us important implications for the design of inhibitors for insectide-resistant *Anopheles gambiae*.

4.4.3 AChEs Screening for the Designed Inhibitors

In total, 21 tacrine-tethered haloacetamides **248-255 (a-d)** were screened for their activities as AChE inhibitors using the Ellman assay performed by Dr. Troy Anderson. These compounds were assessed using 5 different enzyme sources: *Ag* WT hmg, Aphid WT hmg, *Ag* ace1-S, *Ag* ace1-R and *h*AChE. We will make comparisons between a) different insect WT hmg AChEs, b) WT hmg and WT recombinant AChEs of the same species, and c) different recombinant AChEs (e.g. ace1-S vs ace1-R, and ace1-S vs *h*AChE). In order to gain further insight, the standard AChE insecticide propoxur, and the bivalent inhibitor BW284c51, were also assayed with the different enzyme sources.

As shown in Table 4.3, IC_{50} values towards Aphid WT hmg AChE are not generally lower than they are towards *Ag* WT hmg. This is unexpected based on the DTNB inactivation studies, which suggested the Aphid Cys286 thiol was more readily accessible than that in *Ag*. Furthermore, the most potent inhibitor at *Ag* WT hmg is A3I (**248c**), with an IC_{50} of 26 nM. Although the corresponding bromoacetamide has not been made, A6Br (**251b**) has an IC_{50} of 52 nM. Both of these compounds are much more potent than the non-reactive control **252d**, which might suggest slow covalent modification of *Ag* AChE by **248c** and **251b**. We will discuss such possibilities in greater detail below.

Table 4.4 shows the comparison of IC_{50} between WT hmg and WT recombinant AgAChE. A large portion of the inhibitors give similar values for these enzymes, with IC_{50}

ratios from 0.9 to 4.7. However, we found that six inhibitors present significant differences (bold in Table 4.4), with IC_{50} ratios from 7.4 to 26. These high ratios are unusual, and the reason for them is difficult to rationalize.

Table 4.3 BW284c51, propoxur and haloacetamides **248-255 (a-d)** inhibitory potency towards Ag WT hmg and Aphid WT hmg*

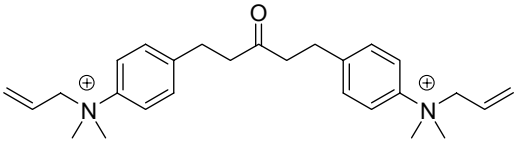

BW284c51

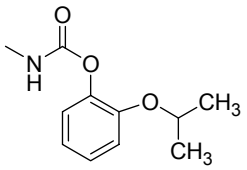

Propoxur

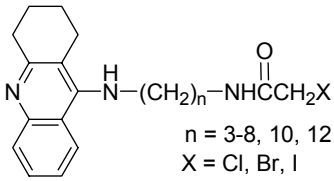

Haloacetamides

Compound	n	X	*Ag* WT hmg IC_{50} (nM)	Aphid (*Myzus persicae*) WT hmg IC_{50} (nM)
BW284c51	NA	NA	30	Not determined
Propoxur	NA	NA	371	Not determined
252d	7	H	23,540	1614
250a	5	Cl	5408	1152
251a	6	Cl	587	494
252a	7	Cl	>10000	>10000
253a	8	Cl	2132	948
254a	10	Cl	646	359
255a	12	Cl	330	533
250b	5	Br	1633	1077
251b	6	Br	52	427
252b	7	Br	746	413
253b	8	Br	605	709
254b	10	Br	6559	11310
255b	12	Br	1718	1458
248c	3	I	26	Not determined
249c	4	I	295	Not determined
250c	5	I	189	153
251c	6	I	293	255
252c	7	I	259	989
253c	8	I	270	199
254c	10	I	337	223
255c	12	I	2522	2771

*IC_{50} values determined by Dr. Troy Anderson, Bloomquist lab

Later, when recombinant susceptible (ace1-S) and recombinant resistant strain (ace1-R) *Ag*AChEs became available, BW284c51, propoxur, and **248-255 (a-d)** were assayed with these enzymes. In order to screen for species selectivity, recombinant human AChE (*h*AChE) was also tested (Table 4.5). Although it is still not clear why the IC_{50} values towards *Ag* WT hmg are 1.3-26 fold higher than those towards the recombinant ace1-S, it would be prudent to compare the IC_{50} values only from different recombinant enzymes.

Table 4.4 BW284c51, propoxur and haloacetamides **248-255 (a-d)** inhibitory potency towards WT hmg and WT recombinant ace1-S *Ag*AChEs[a]

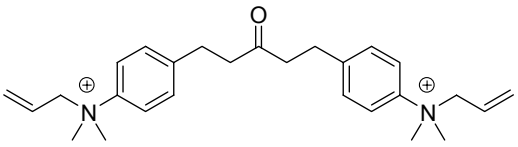

BW284c51

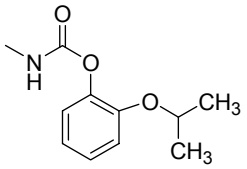

Propoxur

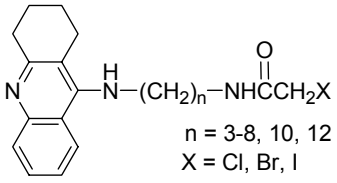

Haloacetamides

Compound	n	X	*Ag* WT hmg IC_{50} (nM)	*Ag* WT recombinant ace1-S IC_{50} (nM)[b]
BW284c51	NA	NA	30	33 (0.9x)
Propoxur	NA	NA	371	213 (2.7x)
252d	7	H	23,540	Not determined
250a	5	Cl	5408	>1000
251a	6	Cl	587	436 (1.3x)
252a	7	Cl	>10000	>1000
253a	8	Cl	2132	>1000
254a	10	Cl	646	687 (0.9x)
255a	12	Cl	330	132 (2.5x)
250b	**5**	**Br**	**1633**	**123 (13x)**
251b	**6**	**Br**	**52**	**4 (13x)**
252b	7	Br	746	550 (1.4x)
253b	8	Br	605	228 (2.7x)
254b	10	Br	6559	>1000
255b	12	Br	1718	639 (2.7x)
248c	3	I	26	12 (2.2x)
249c	4	I	295	97 (3.0x)
250c	5	I	189	57 (3.3x)
251c	**6**	**I**	**293**	**15 (20x)**
252c	7	I	259	55 (4.7x)
253c	**8**	**I**	**270**	**21 (13x)**
254c	**10**	**I**	**337**	**13 (26x)**
255c	**12**	**I**	**2522**	**343 (7.4x)**

[a] IC_{50} values determined by Dr. Troy Anderson, Bloomquist lab
[b] IC_{50} ratios in parentheses are with respect to Ag WT hmg

For *Ag* ace1-S, A6 bromoacetamide and A3-10 iodoacetamides show high inhibition potency, IC_{50} values of 4-97 nM (Table 4.5). In addition, almost all the haloacetamides are more potent at *Ag* ace1-R than they are at ace1-S; in particular iodoacetamides **248c-253c** are 1-14 fold higher. Disturbingly, it is found that our bivalent compounds give much stronger inhibition of *h*AChE than they do of *Ag* ace1-S and ace1-R. As a consequence, opposite to our original purpose, several tacrine-tethered haloacetamides are surprisingly potent selective inhibitors for *h*AChE. This outcome was completely unexpected and proves that the high potency of the haloacetamides at AgAChE need NOT be attributed to ligation of Cys286. We propose three possible explanations for the selectivity towards *h*AChE: 1) some form of

hydrophobic or hydrogen bonding interaction with the haloacetamide is much more effective for hAChE than for AgAChE, 2) the haloacetamides react with certain solvent accessible amino- or hydroxyl group bearing residues unique to the peripheral site of *h*AChE, or 3) the thiocholine anion resulting from ATCh hydrolysis reacts either with haloacetamide directly or with DTNB followed by haloacetamide (Scheme 4.3). Both reactions lead to compounds that can form either a cation-π or a π-π interaction with Trp286 (corresponding to Trp280 in the homology model) at the peripheral site in *h*AChE, similar to previous successful bivalent inhibitors for AD.[12-16] Such cation-π and π-π interactions may be more effective at *h*AChE than at *Ag*AChE.

Table 4.5 BW284c51, propoxur, and haloacetamides **248-255 (a-d)** inhibitory potency towards recombinant *Ag* ace1-S and ace1-R, and hAChE*

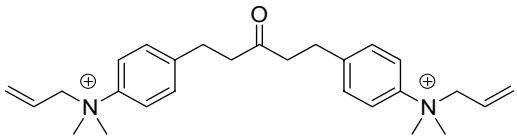

BW284c51

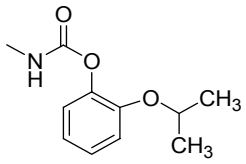

Propoxur

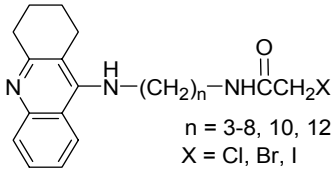

Haloacetamides

Compound	n	X	*Ag* ace1-S IC_{50} (nM)	*Ag* ace1-R IC_{50} (nM)	*h*AChE IC_{50} (nM)
BW284c51	NA	NA	33	406	22
Propoxur	NA	NA	213	>1,000	444
232	7	H	Not determined	1,150	Not determined
230a	5	Cl	>1,000	>1000	105
231a	6	Cl	436	225	18
232a	7	Cl	>1,000	>1000	780
233a	8	Cl	>1,000	354	4
234a	10	Cl	687	184	0.04
235a	12	Cl	132	44	0.2
230b	5	Br	123	234	22
231b	6	Br	4	24	6
232b	7	Br	550	229	16
233b	8	Br	228	65	4
234b	10	Br	>1,000	3040	7
235b	12	Br	639	787	0.2
228c	3	I	12	4	Not determined
229c	4	I	97	31	Not determined
230c	5	I	57	9	0.5
231c	6	I	15	14	0.03
232c	7	I	55	4	0.3
233c	8	I	21	2	0.1
234c	10	I	13	56	0.5
235c	12	I	343	368	0.7

*IC_{50} values determined by Dr. Troy Anderson, Bloomquist lab

Scheme 4.3 Proposed reactions for explaining the haloacetamide inhibition selectivity towards hAChE

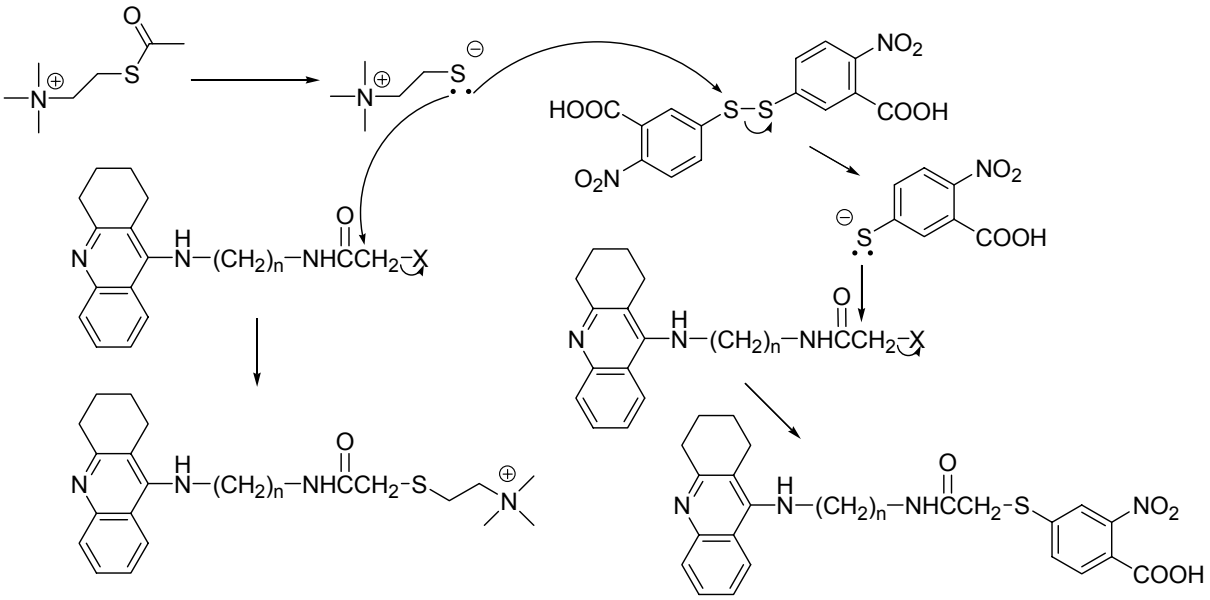

4.4.4 Incubation Studies for Tacrine-tethered Haloacetamides

Despite the confusingly high affinities seen for the tacrine-tethered haloacetamides at *h*AChE, incubation studies were carried out again by Dr. Anderson to see if the inhibition of *Ag* ace1-S AChE by tacrine-tethered haloacetamides is irreversible (Figure 4.7). Surprisingly, different from the straight lines seen for DTNB, plots of $\ln(v/v_0)$ vs time showed sigmoid curves in several cases. In particular, experiments with 30 and 100 nM **248c** (A3I) show initial steady-state reversible inhibition consistent with the IC_{50} value (12 nM) measured with a 10 minute incubation. However, the 30 nM incubation shows a second downward slope at 40 minutes, whereas this second downward slope emerges at 20 minutes in the 100 nM incubation. Similar behavior is seen for A5I, A7I and A8I. These curves may represent biphasic behavior of the designed bivalent compounds. For example, the first slope might show the π-π interaction at the active site by the tacrine core structure, followed by a short period of plateau, the second slope might correspond to the covalent binding with free cysteine at the peripheral site.

This biphasic behavior is tantalizing, yet many questions remain unanswered. More work must be done with potent AChE inhibitors that present no possibility of covalent modification, to ensure that biphasic plots are not observed with them. In addition, incubation experiments must be performed with ace1-R to confirm that it shows further onset of the second downward slope, consistent with the DTNB inactivation studies. Lastly, incubation experiments must be performed with hAChE, to ascertain whether there is any irreversible component to the observed high inhibition potencies of the haloacetamides.

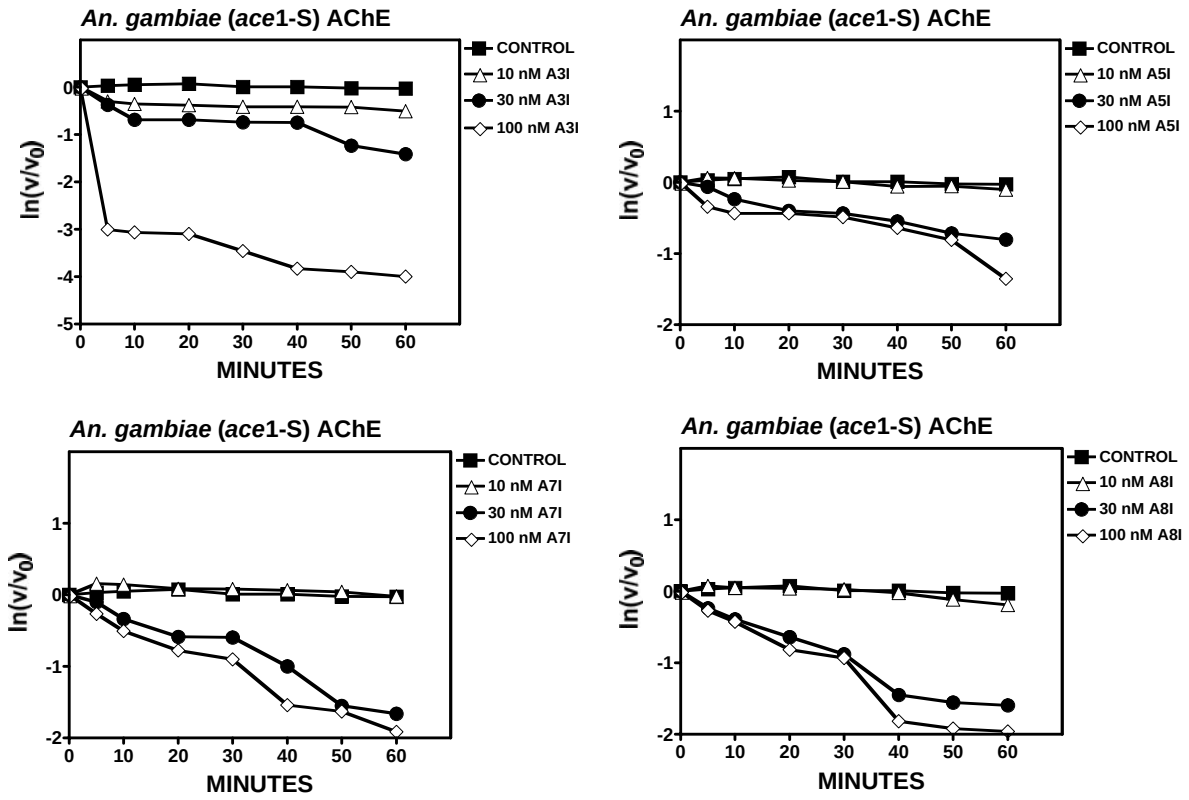

Figure 4.7 Kinetic studies for **248c** (A3I), **250c** (A5I), **252c** (A7I) and **253c** (A8I) towards recombinant *Ag* ace1-S AChE

4.5 Conclusions

To conclude, we tested the DTNB sensitivity of recombinant Ag ace1-S and ace1-R AChE, and Aphid WT hmg AChE. These experiments suggested that the free cysteine is solvent accessible at the peripheral site of resistant strain Ag AChE and aphid AChE. We synthesized and assayed (Dr. Troy Anderson, Bloomquist group) tacrine-tethered haloacetamides, which were designed to react with C286 in *Ag*AChE. In total 21 compounds were examined at AChEs from *Ag* WT hmg, aphid WT hmg, recombinant *Ag* ace1-S and ace1-R, and recombinant *Homo sapiens* (human). We found that A3I **248c** showed promising inhibition in both WT hmg and recombinant *Ag*AChE. Iodoacetamides showed the highest inhibition potency compared to the other analogues. In all, 4 compounds were single digit nanomolar inhibitors of *Ag* ace1-R recombinant enzyme.

The desired selectivity was not realized because all haloacetamides gave very high potency on *h*AChE; nine compounds showed IC_{50} values in the sub-nanomolar range. Indeed, these compounds may give new insight into the development of new therapeutic drugs for AD memory loss, provided that we can find out how they interact with the human enzyme.

Kinetic studies were also undertaken by Dr. Anderson (Bloomquist group) for 4 haloacetamides on *Ag* ace1-S AChE. Biphasic behavior was observed, consistent with the idea of initial fast reversible association, followed by slow covalent bond formation. Future studies are needed however before any firm conclusions can be drawn.

References for Chapter 4

1. Galvez, J.; de Julian-Ortiz, J. V.; Garcia-Domenech, R., Application of molecular topology to the prediction of potency and selection of novel insecticides active against malaria vectors. *Journal of Molecular Structure-Theochem* **2005,** 727, (1-3), 107-113.

2. World Malaria Report. In World Health Organization & UNICEF, United Nation: 2005.

3. Fialka, J. J., EPA Scientists Cite Pressure In Pesticide Study Union Files Letter Blasting Agency Managers, Industry Over Tests on Toxics Family *Wall Street Journal* 2006, p A4.

4. Hemingway, J.; Hawkes, N. J.; McCarroll, L.; Ranson, H., The molecular basis of insecticide resistance in mosquitoes. *Insect Biochemistry and Molecular Biology* **2004,** 34, (7), 653-665.

5. Menozzi, P.; Shi, M. A.; Lougarre, A.; Tang, Z. H.; Fournier, D., Mutations of acetylcholinesterase which confer insecticide resistance in Drosophila melanogaster populations. *Bmc Evolutionary Biology* **2004,** 4: 4.

6. Filler, S. J.; MacArthur, J. R.; Parise, M.; Wirtz, R.; Eliades, M. J.; Dasilva, A.; Steketee, R., Locally acquired mosquito-transmitted malaria: A guide for investigations in the United States. *MMWR Morb Mortal Wkly Rep* **2006**, (55), 1-9.

7. Pang, Y. P., Novel acetylcholinesterase target site for malaria mosquito control. *PLoS ONE* **2006,** 1, e58.

8. Schwede, T.; Kopp, J.; Guex, N.; Peitsch, M. C., SWISS-MODEL: An automated protein homology-modeling server. *Nucleic Acids Research* **2003,** 31, (13), 3381-5.

9. DeLano, W. L. *The PyMOL Molecular Graphics System*, 0.99; DeLano Scientific: San Carlos, CA, USA, 2006.

10. Bourne, Y.; Taylor, P.; Radic, Z.; Marchot, P., Structural insights into ligand interactions at the acetylcholinesterase peripheral anionic site. *EMBO Journal* **2003,** 22, (1), 1-12.

11. Greenblatt, H. M.; Guillou, C.; Guenard, D.; Argaman, A.; Botti, S.; Badet, B.; Thal, C.; Silman, I.; Sussman, J. L., The complex of a bivalent derivative of galanthamine with torpedo acetylcholinesterase displays drastic deformation of the active-site gorge: Implications for structure-based drug design. *Journal of the American Chemical Society* **2004,** 126, 15405-15411.

12. Carlier, P. R.; Chow, E. S.-H.; Han, Y.; Liu, J.; Yazal, J. E.; Pang, Y.-P., Heterodimeric Tacrine-Based Acetylcholinesterase Inhibitors: Investigating Ligand-Peripheral Site Interactions. *Journal of Medicinal Chemistry* **1999,** 42, 4225-4231.

13. Carlier, P. R.; Du, D.-M.; Han, Y.-F.; Liu, J.; Pang, Y.-P., Potent, Easily Synthesized Huperzine A-Tacrine Hybrid Acetylcholinesterase Inhibitors. *Bioorganic & Medicinal Chemistry Letters* **1999,** 9, 2335-2338.

14. Carlier, P. R.; Du, D.-M.; Han, Y.-F.; Liu, J.; Perola, E.; Williams, I. D.; Pang, Y.-P., Dimerization of an Inactive Fragment of Huperzine A Produces a Drug with Twice the Potency of the Natural Product. *Angewandte Chemie, International Edition* **2000,** 39, (10), 1775-1777.

15. Carlier, P. R.; Han, Y. F.; Chow, E. S.-H.; Li, C. P.-L.; Wang, H.; Lieu, T. X.; Wong, H. S.; Pang, Y.-P., Evaluation of Short-Tether Bis-THA AChE Inhibitors. A Further Test of the Dual Binding Site Hypothesis. *Bioorganic & Medicinal Chemistry* **1999,** 7, 351-357.

16. Han, Y. F.; Li, C. P.-L.; Chow, E. S.-H.; Wang, H.; Pang, Y.-P.; Carlier, P. R., Dual-Site Binding of Bivalent 4-Aminopyridine and 4-Aminoquinoline-based AChE Inhibitors: Contribution of the Hydrophobic Alkylene Tether to Monomer and Dimer Affinities. *Bioorganic & Medicinal Chemistry* **1999,** 7, 2569-2575.

17. Johnson, J. L.; Cusack, B.; Hughes, T. F.; McCullough, E. H.; Fauq, A.; Rmanovskis, P.; Spatola, A.; Rosenberry, T. L., Inhibitors Tethered Near the Acetylcholinesterase Active Site Serve as Molecular Rulers of the Peripheral and Acylation Sites. *Journal of Biological Chemistry* **2003,** 278, 38948-38955.

18. Ellman, G. L.; Courtney, K. D.; Andres, V. J.; Featherstone, R. M., A new and rapid colorimetric determination of acetylcholinesterase activity. *Biochemical Pharmacology* **1961,** 7, 88-95.

19. Dary, O. Purification, Characterization, and Kinetic Studies of a Wild- and Insecticide-Insensitive Acetylcholinesterase from Mosquito (Culex spp.). PhD, University of California, Riverside, Riverside, California, 1989.

Chapter 5. Experimental Procedures

5.1 Experimental Procedures for Chapter 2

General

THF was distilled from Na/benzophenone immediately before use. (*S*)-Fmoc- Ala was purchased from Advanced ChemTech and was used as received. 2-amino-3,5-dimethylbenzophenone,[1] 2-amino-3,5-dichlorobenzophenone[1] and *N*1-H Gly-derived 1,4-benzodiazepin-2-one[2] were prepared according to the literature method. ^{1}H NMR Spectra were recorded at 500 and 400 MHz; the corresponding ^{13}C NMR resonant frequencies were 125 and 100 MHz respectively. High resolution mass spectra were recorded under FAB conditions (NBA. PEG) and EI using a VG 70SE instrument (70 eV, perfluorokerosine); in each case the expected molecular formula (M+1, ^{35}Cl or M^{+}) gave the closest match among all possible formulas. In conjunction with the ^{1}H and ^{13}C NMR spectra, the HRMS data confirm the proposed identity of each compound. Enantiomeric excess of all compounds were assessed by HPLC (Chiralcel AD and OD).

General procedure for *N*1-Me Gly-derived 1,4-benzodiazepin-2-ones

The Gly-derived 1,4-benzodiazepin-2-one (0.60 g, 2.2 mmol, 1 equiv.) dissolved in anhydrous THF (15 mL) was added to potassium hydride (0.47 g, 3.5 mmol, 1.6 equiv., 30 % suspension in mineral oil) or sodium hydride (0.14 g, 3.5 mmol, 1.6 equiv, 60 % suspension in mineral oil) at 0 ºC under nitrogen. The resulting solution was stirred at 0 ºC for 30 min. Methyl iodide (4.1 mL, 66 mmol, 30 equiv.) was added dropwise to the solution. The reaction mixture was stirred overnight at room temperature. It was quenched by sat. NH_4Cl (aq) and extracted with CH_2Cl_2 (3 x 30 mL). The combined

organic extracts were dried over Na_2SO_4, filtered and concentrated. The crude product was purified by flash column chromatography on silica gel (2:1 EtOAc/Hexanes).

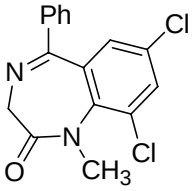

7,9-dichloro-1,3-dihydro-1-methyl-5-phenyl-2*H*-1,4-benzodiazepin-2-one [161a]

The general procedure was followed: **165** (0.60 g, 2.2 mmol, 1 equiv), NaH (0.14 g, 3.5 mmol, 1.6 equiv, 60 % suspension in mineral oil), Methyl iodide (4.1 mL, 66 mmol, 30 equiv.). Purification with flash column chromatography on silica gel (1:1 EtOAc/Hexanes) provided **161a** (6.0 mg, 30.0 %) as colorless oil. ^{1}H NMR ($CDCl_3$): δ 7.66-7.62 (m, 3H), δ 7.53-7.42 (m, 3H), δ 7.22 (apparent d, *J* = 2.4 Hz, 1H), δ 4.84 (d, *J* = 10.8, 1H), δ 3.77 (d, *J* = 10.8, 1H), δ 3.30 (s, 3H). ^{13}C NMR ($CHCl_3$): δ 169.65, 168.06, 140.15, 137.85, 133.26, 132.90, 131.66, 131.19, 130.90, 129.54, 128.78, 128.28, 57.02, 36.84. HRMS (EI) calcd. for $C_{16}H_{12}Cl_2N_2O$ (M^+) 318.032669, found 318.032300 (1.2 ppm, 0.4 mDa).

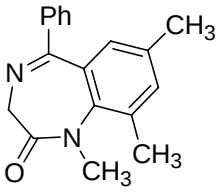

1,3-dihydro-1,7,9-trimethyl-5-phenyl-2*H*-1,4-benzodiazepin-2-one [162a]

The general procedure was followed: **165** (0.60 g, 2.2 mmol, 1 equiv), KH (0.47 g, 3.5 mmol, 1.6 equiv., 30 % suspension in mineral oil), Methyl iodide (4.1 mL, 66 mmol, 30 equiv.). Purification with flash column chromatography on silica gel (2:1

EtOAc/Hexanes) provided **162a** (17.4 mg, 74 %) as colorless oil. ^{1}H NMR ($CDCl_3$): δ 7.55-7.53 (m, 2H), δ 7.48-7.40 (m, 3H), δ 7.29 (s, 1H), δ 6.77 (s, 1H), δ 4.43 (d, *J* = 10.8, 1H), δ 3.62 (d, *J* = 10.8, 1H), δ 3.03 (s, 3H), δ 2.29 (s, 3H), δ 2.20 (s, 3H). ^{13}C NMR (DMSO): δ 170.48, 170.32, 140.81, 139.00, 135.78, 135.54, 133.58, 131.18, 130.12, 129.68, 129.08, 127.42, 56.81, 36.77, 20.88, 19.79. HRMS (EI) calcd. for $C_{18}H_{18}N_2O$ (M^+) 278.141913, found 278.143077 (-4.2 ppm, -1.2 mDa).

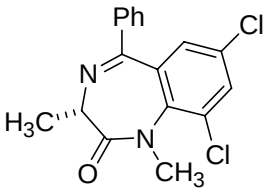

(3*S*)-(+)-7,9-dichloro-1,3-dihydro-1,3-dimethyl-5-phenyl-2*H*-1,4-benzodiazepin-2-one [(*S*)-(+)-171a]

To a stirred solution of (*L*)-Fmoc-Ala-OH·H_2O (2.1 g, 6.7 mmol, 1 equiv.) in anhydrous DCM (20 mL) was injected $SOCl_2$ (4.9 mL, 67 mmol, 10 equiv.) at room temperature under nitrogen. The reaction mixture was heated to reflux for 2 hours. Solvent and excess $SOCl_2$ were removed in vacuo. The resultant residue was dissolved in anhydrous benzene and followed by evaporation to make sure that $SOCl_2$ was removed completely, which afforded white solid. The acid chloride was then dissolved in DCM (22 mL) and added dropwise to a vigorously stirred two-phase system consisting of 2-amino-3,5-disubstituted benzophenone[1] (0.88 g, 3.3 mmol, 0.5 equiv.) in CH_2Cl_2 (15 mL) and 10% $NaHCO_3$ (aq) (15 mL) at room temperature. The resulting mixture was stirred for 30 min. The organic layer was separated and the aqueous layer was extracted with CH_2Cl_2 (3 x 20 mL). The combined organic solution was dried over Na_2SO_4, and concentrated in vacuo.

Purification with flash column chromatography on silica gel (1:4 EtOAc/Hexanes) provided Fmoc-protected amide (1.4 g) as white solid.

To a stirred solution of amide in anhydrous THF (30 mL) was added 1-octanethiol (4.4 mL, 25 mmol, 10 equiv.) followed by dropwise addition of catalytic 1,8-diazabicyclo[5.4.0]undec-7-ene (170 μL, 1.2 mmol, 0.46 equiv.). The reaction mixture was stirred at room temperature for 30 min. After removal of solvent in vacuo, the resulting residue was dissolved in $CHCl_3$ (15 mL) and bubbled with HCl (g). Solvent was removed to afford white solid which was then washed with Et_2O (3 x 20 mL). The white solid was then dissolved in CH_3OH/H_2O (10 mL/10 mL). NaOH (aq) was added until pH=8.5. The reaction mixture was stirred for 17 hours. Solvent was evaporated and the resulting residue was purified by flash column chromatography on silica gel (1:3 EtOAc/Hexanes) to afford a white solid (0.46 g).

The white solid (0.46 g, 1.5 mmol, 1 equiv.) dissolved in anhydrous THF (15 mL) and was added to potassium hydride (0.32 g, 2.4 mmol, 1.6 equiv., 30 % suspension in mineral oil) at 0 °C under nitrogen. The resulting solution was stirred at 0 °C for 30 min.

Methyl iodide (2.8 mL, 45 mmol, 30 equiv.) was added dropwise to the solution. The reaction mixture was stirred overnight at room temperature. It was quenched by sat. NH_4Cl (aq) and extracted with CH_2Cl_2 (3 x 30 mL). The combined organic extracts were dried over Na_2SO_4, filtered and concentrated. The crude product was purified by flash column chromatography on silica gel (2:1 EtOAc/Hexanes) provided (*S*)-(+)-**171a** (0.21 g, 57 %) as off-white solid. ^{1}H NMR ($CDCl_3$): δ 7.64-7.60 (m, 3H), δ 7.48-7.40 (m, 3H), δ 7.21 (s, 1H), δ 3.73 (q, *J* = 6.4 Hz, 1H), δ 3.29 (s, 3H), δ 1.73 (d, *J* = 6.4 Hz, 3H). ^{13}C NMR ($CDCl_3$): δ171.12, 166.05, 139.85, 137.83, 133.71, 132.81, 131.47, 131.03, 130.83,

129.58, 128.75, 128.08, 59.13, 36.94, 17.23. HPLC t_r 24.6 (S), 32.5 (R) [Chiralcel OD (0.46 cm x 25 cm) (from Daicel Chemical Ind., Ltd.)] Hexane/i-PrOH, 99/1, 1 mL/min, >99.5% ee. HRMS (EI) calcd. for $C_{17}H_{14}Cl_2N_2O$ (M^+) 332.048319, found 332.048300 (0.1 ppm, 0.0 mDa). Mp: 122.5–123.7 °C.

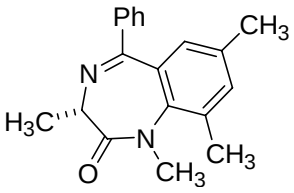

(3*S*)-(+)-1,3-dihydro-1,3,7,9-tetramethyl-5-phenyl-2*H*-1,4-benzodiazepin-2-one [(*S*)-(+)-172a]

To a stirred solution of (*L*)-Fmoc-Ala-OH·H_2O (2.1 g, 6.7 mmol, 1 equiv.) in anhydrous DCM (20 mL) was injected $SOCl_2$ (4.9 mL, 67 mmol, 10 equiv.) at room temperature under nitrogen. The reaction mixture was heated to reflux for 2 hours. Solvent and excess $SOCl_2$ were removed in vacuo. The resultant residue was dissolved in anhydrous benzene and followed by evaporation to make sure that $SOCl_2$ was removed completely, which afforded white solid. The acid chloride was then dissolved in DCM (22 mL) and added dropwise to a vigorously stirred two-phase system consisting of 2-amino-3,5-disubstituted benzophenone[1] (0.75 g, 3.3 mmol, 0.5 equiv.) in CH_2Cl_2 (15 mL) and 10% $NaHCO_3$ (aq) (15 mL) at room temperature. The resulting mixture was stirred for 30 min. The organic layer was separated and the aqueous layer was extracted with CH_2Cl_2 (3 x 20 mL). The combined organic solution was dried over Na_2SO_4, and concentrated in vacuo. Purification with flash column chromatography on silica gel (1:4 EtOAc/Hexanes) provided Fmoc-protected amide (1.6 g) as white solid.

To a stirred solution of amide in anhydrous THF (30 mL) was added 1-octanethiol (5.4 mL, 31 mmol, 10 equiv.) followed by dropwise addition of catalytic 1,8-diazabicyclo[5.4.0]undec-7-ene (220 μL, 1.4 mmol, 0.46 equiv.). The reaction mixture was stirred at room temperature for 30 min. After removal of solvent in vacuo, the resulting residue was dissolved in $CHCl_3$ (15 mL) and bubbled with HCl (g). Solvent was removed to afford white solid which was then washed with Et_2O (3 x 20 mL). The white solid was then dissolved in CH_3OH/H_2O (10 mL/10 mL). NaOH (aq) was added until pH=8.5. The reaction mixture was stirred for 17 hours. Solvent was evaporated and the resulting residue was purified by flash column chromatography on silica gel (1:3 EtOAc/Hexanes) to afford a white solid (0.60 g).

The white solid (0.60 g, 2.2 mmol, 1 equiv.) dissolved in anhydrous THF (15 mL) and was added to potassium hydride (0.47 g, 3.5 mmol, 1.6 equiv., 30 % suspension in mineral oil) at 0 ºC under nitrogen. The resulting solution was stirred at 0 ºC for 30 min. Methyl iodide (4.1 mL, 66 mmol, 30 equiv.) was added dropwise to the solution. The reaction mixture was stirred overnight at room temperature. It was quenched by sat. NH_4Cl (aq) and extracted with CH_2Cl_2 (3 x 30 mL). The combined organic extracts were dried over Na_2SO_4, filtered and concentrated. The crude product was purified by flash column chromatography on silica gel (2:1 EtOAc/Hexanes) provided (*S*)-(+)-**172a** (0.59 g, 32 %) as white solid. $[\alpha]_D^{25}$ = +119 (c = 1.65, $CHCl_3$). ^{1}H NMR ($CDCl_3$): δ 7.66 (apparent d, *J* = 4 Hz, 2H), 7.45-7.37 (m, 3H), 7.19 (s, 1H), 6.91 (s, 1H), 3.73 (q, *J* = 6.6 Hz, 1H), 3.19 (s, 3H), 2.36 (s, 3H), 2.28 (s, 3H), 1.70 (d, *J* = 4 Hz, 3H). ^{13}C NMR ($CDCl_3$): δ 171.97, 168.36, 140.54, 139.23, 135.29, 134.93, 132.83, 130.98, 130.31, 129.72, 128.40, 127.67, 58.70, 36.84, 21.01, 19.88, 17.36. HRMS (EI) calcd. for

$C_{19}H_{20}N_2O$ (M^+) 292.157700, found 292.157563 (-0.5 ppm, -0.1 mDa). HPLC t_r 28.7 min (*S*); t_r 34.5 min (*R*) [Chiralcel OD (0.46 cm x 25 cm) (from Daicel Chemical Ind., Ltd.)] Hexane/i-PrOH, 99/1, 1 mL/min, >99.5% ee. Mp: 153.7–155.4 °C.

General Procedure for C3-Alkylation of 172a with HMPA

At -78 ºC under nitrogen, to a stirred solution of (*S*)-**172a** (30.0 mg, 0.10 mmol, 1 equiv) and HMPA (110 μL, 0.62 mmol, 6 equiv) in anhydrous THF (1 mL) was added KHMDS (0.5 mL, 0.25 mmol, 2.5 equiv, 0.5 M in toluene). The resulting solution was stirred for a further 2 h. Electrophile (10.0 equiv) was added dropwise and then stirred for 2 h at -78 ºC. The reaction was quenched at -78 ºC with sat. NH_4Cl (aq) (1 mL), and extracted with CH_2Cl_2 (3 x 10 mL). The combined organic extracts were dried over anhydrous Na_2SO_4, filtered and concentrated under reduced pressure. The crude product was purified by flash column chromatography on silica gel.

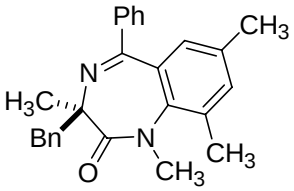

(3*R*)-(+)-3-benzyl-1,3-dihydro-1,3,7,9-tetramethyl-5-phenyl-2*H*-1,4-benzodiazepin-2-one [(*R*)-(+)-176a]

The general procedure was followed: (*S*)-(+)-**172a** (30.0 mg, 0.10 mmol, 1 equiv), HMPA (110 μL, 0.62 mmol, 6 equiv), KHMDS (0.5 mL, 0.25 mmol, 2.5 equiv, 0.5 M in toluene) and benzyl bromide (120 μL, 1.0 mmol, 10 equiv). Purification with flash column chromatography on silica gel (1:5 EtOAc/Hexanes) provided (*R*)-(+)-**177a** (33.4 mg, 85%) as colorless oil. $[\alpha]_D^{25}$ = + 23.0 (c = 0.3, $CHCl_3$). ^1H NMR ($CDCl_3$) indicated a

43:57 ratio of Bn-pseudoequatorial and Bn-pseudoaxial conformers. Assignments are based on comparison with the pure conformers (see below): δ 7.67-7.64 (m, 2H x 0.43 Bn-ψeq, 2H x 0.57 Bn-ψax), δ 7.57 (d, *J* = 7.5 Hz, 2H x 0.43 Bn-ψeq), δ 7.47-7.39 (m, 3H x 0.43 Bn-ψeq, 3H x 0.57 Bn-ψax), δ 7.35-7.32 (m, 2H x 0.43 Bn-ψeq), δ 7.28-7.25 (m, 1H x 0.43 Bn-ψeq), δ 7.20-7.15 (m, 2H x 0.43 Bn-ψeq, 3H x 0.57 Bn-ψax), δ 6.95 (s, 1H x 0.57 Bn-ψax), δ 6.86 (d, *J* = 8 Hz, 2H x 0.57 Bn-ψax), δ 6.78 (s, 1H x 0.43 Bn-ψeq), δ 3.78 (apparent d, actually collapsed AB pattern of benzylic protons of Bn-ψeq conformer, *J* = 11.6 Hz, 1H x 0.43), δ 3.29 (s, 3H x 0.57 Bn-ψax), δ 3.28 + 3.25 (apparent d, actually collapsed AB pattern of benzylic protons of Bn-ψeq conformer, *J* = 10.8 Hz, 1H x 0.43), δ 3.26 (s, 3H x 0.43 Bn-ψeq), δ 2.47 (dd, *J* = 20 Hz, 14 Hz, 2H x 0.57 Bn-ψax), δ 2.36 (s, 3H x 0.57 Bn-ψax), δ 2.34 (s, 2H x 0.43 Bn-ψeq), δ 2.28 (s, 3H x 0.57 Bn-ψax), δ 2.22 (s, 2H x 0.43 Bn-ψeq), δ 1.73 (s, 3H x 0.57 Bn-ψax), δ 0.66 (s, 2H x 0.43 Bn-ψeq). ^{13}C NMR ($CDCl_3$) was consistent with an approximate 1:1 of Bn-pseudoequorial and Bn-pseudoaxial conformers (42 resonances found for a possible 2 x 22 unique carbons): δ 174.0, 173.4, 167.0, 166.4, 141.0, 140.8 (2 partially resolved peaks), 140.7, 139.0, 137.6, 135.5, 135.2, 135.1, 134.8, 132.7, 132.4 (2 partially resolved peaks), 132.3, 132.2, 130.1, 129.9 (2 partially resolved peaks), 129.8, 128.4, 128.3, 127.9, 127.8, 127.6, 126.5, 126.2, 67.8, 65.9, 47.6, 39.6, 39.3, 37.8, 28.5, 21.0, 20.9, 20.2, 19.9, 17.0. HRMS (FAB) calcd. for $C_{26}H_{27}N_2O$ (M+1) 383.2123, found 383.2101 (-5.8 ppm, -2.2 mmu). HPLC (27 °C) t_r 28.8 min (*S*); t_r 42.7 min (*R*); t_r 44.9 min (*R*); t_r 47.5 min (*S*) [Chiralcel OD (0.46 cm x 25 cm) (from Daicel Chemical Ind., Ltd.)] Hexane/*i*-PrOH, 99/1, 0.5 mL/min, 99% ee.

Separation of Bn-ψeq and Bn-ψax conformers: The two conformers were isolated with flash column chromatography on silica gel (1:5 EtOAc/Hexanes). The collection of eluents and solvent removal were performed at <5 °C, and the ^{1}H NMR tubes were kept at <5 °C. NMR data was collected immediately after chromatography at room temperature. Rf values: 0.26 (Bn-ψeq), 0.15 (Bn-ψax).

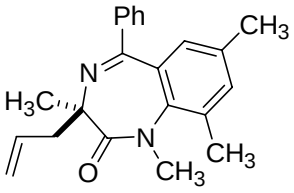

(3*R*)-(+)-3-allyl-1,3-dihydro-1,3,7,9-tetramethyl-5-phenyl-2*H*-1,4-benzodiazepin-2-one [(*R*)-(+)-179a]

The general procedure was followed: (*S*)-(+)-**172a** (32.5 mg, 0.11 mmol, 1 equiv), HMPA (120 μL, 0.67 mmol, 6 equiv), KHMDS (0.56 mL, 0.28 mmol, 2.5 equiv, 0.5 M in toluene) and allyl bromide (100 μL, 1.1 mmol, 10 equiv). Purification with flash column chromatography on silica gel (1:5 EtOAc/Hexanes) provided (*R*)-(+)-**179a** (30.8 mg, 90%) as colorless oil. $[\alpha]_D^{25}$ = + 33.0 (c = 0.8, $CHCl_3$). ^{1}H NMR (DMSO) indicated a 47:53 ratio of allyl-pseudoequatorial and allyl-pseudoaxial conformers. Assignments are based on comparison wit the pure conformers (see below): δ 7.58-7.53 (m, 2H x 0.47 allyl-ψeq, 2H x 0.53 allyl-ψax), δ 7.50-7.45 (m, 1H x 0.47 allyl-ψeq, 1H x 0.53 allyl-ψax), δ 7.44-7.39 (m, 2H x 0.47 allyl-ψeq, 2H x 0.53 allyl-ψax), δ7.33 (s, 1H), δ 7.31 (s, 1H), δ 6.80 (broad s, 1H x 0.47 allyl-ψeq, 1H x 0.53 allyl-ψax), δ 6.15-6.13 (m, 1H x 0.47 allyl-ψeq), δ 5.48-5.41 (m, 1H x 0.53 allyl-ψax), δ 5.19-5.10 (m, 2H x 0.47 allyl-ψeq), δ 4.91 (apparent d, *J* = 10 Hz, 1H x 0.53 allyl-ψax), δ 4.58 (apparent d, *J* = 16 Hz, 1H x 0.53 allyl-ψax), δ 3.11 (s, 6H), δ 2.87 (dd, *J* = 13.6 Hz, 6.4 Hz, 1H x 0.47 allyl-

ψeq), δ 2.63 (dd, *J* = 14 Hz, 8 Hz, 1H x 0.47 allyl-ψeq), δ 2.29 (two overlapping singlet, 6H), δ 2.23 (two overlapping singlet, 6H), δ 1.76-1.67 (m, 2H x 0.53 allyl-ψax), δ 1.65 (s, 3H x 0.53 allyl-ψax), δ 0.61 (s, 3H x 0.47 allyl-ψeq). ^{13}C NMR (DMSO) was consistent with an approximate 1:1 of allyl-pseudoequatorial and allyl-pseudoaxial conformers (38 resonances found for a possible 2 x 20 unique carbons): δ 172.8, 172.4, 166.7, 166.4, 140.9, 140.5, 140.2 (2 partially resolved peaks), 136.4, 135.8, 135.7, 135.3, 135.2, 133.6, 133.4, 133.3, 131.8, 130.8, 129.8, 129.7, 128.9, 128.8, 127.5, 127.4, 118.9, 118.7, 79.8, 67.1, 65.2, 47.4, 39.3, 39.1, 37.1, 28.8, 20.9, 20.0, 19.9, 17.3. HRMS (FAB) calcd. for $C_{22}H_{25}N_2O$ (M+1) 333.1967, found 333.1960 (-2.0 ppm, -0.7 mmu). HPLC t_r 10.9 min (*R*); t_r 13.9 min (*S*); t_r 15.5 min (*R*); t_r 19.9 min (*S*) [Chiralpak AD (0.46 cm x 25 cm) (from Daicel Chemical Ind., Ltd.)] Hexane/*i*-PrOH, 99/1, 1 mL/min, >99.5% ee.

Separation of allyl-pseudoequatorial and allyl-pseudoaxial conformers: The two conformers were isolated with flash column chromatography on silica gel (1:5 EtOAc/Hexanes). The collection of eluents and solvent removal were performed at <5 °C, and the ^{1}H NMR tubes were kept at <5 °C. NMR data was collected immediately after chromatography at room temperature. Rf values: 0.31 (allyl-ψeq), 0.21 (allyl-ψax).

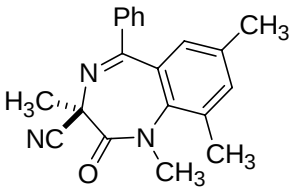

(3*R*)-(+)-3-cyano-1,3-dihydro-1,3,7,9-tetramethyl-5-phenyl-2*H*-1,4-benzodiazepin-2-one [(*R*)-(+)-178a]

The general procedure was followed: (*S*)-(+)-**172a** (30.0 mg, 0.10 mmol, 1 equiv), HMPA (110 μL, 0.62 mmol, 6 equiv), KHMDS (0.5 mL, 0.25 mmol, 2.5 equiv, 0.5 M in toluene) and *p*-toluenesulfonyl cyanide (196 mg, 1.0 mmol, 10 equiv). Purification with flash column chromatography on silica gel (1:5 EtOAc/Hexanes) provided (*R*)-(+)-**178a** (26.5 mg, 81%) as white solid. The cyanated product exists as a single CN-pseudoaxial conformer.[3] $[\alpha]_D^{25}$ = +122 (c = 0.1, $CHCl_3$) ^{1}H NMR ($CDCl_3$): δ 7.69 (apparent d, *J* = 8 Hz, 2H), 7.53-7.50 (m, 1H), 7.44-7.41 (m, 2H), 7.31 (s, 1H), 6.95 (s, 1H), 3.27 (s, 3H), 2.41 (s, 3H), 2.32 (s, 3H), 2.16 (s, 3H). ^{13}C NMR ($CDCl_3$): δ 171.69, 165.23, 139.87, 138.40, 136.93, 136.72, 133.55, 131.47, 130.53, 130.12, 128.61, 128.17, 116.41, 57.76, 38.56, 26.44, 21.21, 19.84. HRMS (FAB) calcd. for $C_{20}H_{20}N_3O$ (M+1) 318.1606, found 318.1621 (+4.6 ppm, +1.5 mmu). HPLC (27 °C) t_r 16.2 min (*S*); t_r 18.1 min (*R*) [Chiralcel OD (0.46 cm x 25 cm) (from Daicel Chemical Ind., Ltd.)] Hexane/i-PrOH, 99/1, 1 mL/min, >99.5% ee. Mp: 218.3– 219.8 ºC. X-ray crystallography indicates (*R*)-stereochemistry and CN-pseudoaxial conformation.

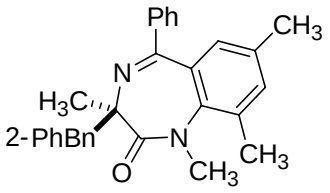

(3*R*)-(+)-1,3-dihydro-1,3,7,9-tetramethyl-5-phenyl-3-(2-phenylbenzyl)-2*H*-1,4-benzodiazepin-2-one [(*R*)-(+)-180a]

The general procedure was followed: (*S*)-(+)-**172a** (30.0 mg, 0.10 mmol, 1 equiv), HMPA (110 μL, 0.62 mmol, 6 equiv), KHMDS (0.5 mL, 0.25 mmol, 2.5 equiv, 0.5 M in toluene) and benzyl bromide (120 μL, 1.0 mmol, 10 equiv). Purification with flash column chromatography on silica gel (1:5 EtOAc/Hexanes) provided (*R*)-(+)-**180a** (25.2 mg, 80%) as colorless oil. $[\alpha]_D^{25}$ = + 74.0 (c = 0.2, $CHCl_3$). ^{1}H NMR ($CDCl_3$) indicated a 51:49 ratio of 2-PhBn-pseudoequatorial and 2-PhBn-pseudoaxial conformers. Assignments are based on comparison with the pure conformers (see below): δ 8.17 (apparent d, *J* = 8 Hz, 1H), δ 7.67-6.60 (m, 2H x 0.51 2-PhBn-ψeq, 2H x 0.49 2-PhBn-ψax), δ 7.47-7.29 (m, 18H), δ 7.24-7.03 (m, 9H), δ 6.84 (s, 1H x 0.49 2-PhBn-ψax), δ 6.74 (s, 1H x 0.51 2-PhBn-ψeq), δ 3.68 (s, 2H x 0.51 2-PhBn-ψeq), δ 3.25 (s, 3H x 0.49 2-PhBn-ψax), δ 3.19 (s, 3H x 0.51 2-PhBn-ψeq), δ 2.51 (s, 2H x 0.49 2-PhBn-ψax), δ 2.28-2.25 (m, 6H x 0.49 2-PhBn-ψax, 3H x 0.51 2-PhBn-ψeq), δ 2.19 (s, 3H x 0.51 2-PhBn-ψeq), δ 1.52 (s, 3H x 0.49 Bn-ψax), δ 0.29 (s, 3H x 0.51 2-PhBn-ψeq). ^{13}C NMR ($CDCl_3$) was consistent with an approximate 1:1 of 2-PhBn-pseudoequorial and 2-PhBn-pseudoaxial conformers (52 resonances found for a possible 2 x 26 unique carbons): δ 173.64, 173.27, 166.77, 166.27, 144.28, 143.10, 142.98, 141.84, 141.03, 140.97, 140.65, 136.37, 135.47, 135.34, 135.07, 134.95, 134.71, 133.61, 132.51, 132.36, 132.25, 130.58, 130.34, 130.27, 130.13, 129.87, 129.80, 129.75, 129.24, 128.33, 128.29, 128.21, 127.81, 127.70, 127.36, 126.98, 126.70, 126.48, 126.25, 126.22, 68.13, 66.88, 42.33, 39.47,

39.18, 33.94, 28.07, 21.05, 20.89, 19.91, 19.85, 16.66. HRMS (EI) calcd. for $C_{32}H_{30}N_2O$ (M^+) 458.234900, found 458.235814 (2.0 ppm, 0.9 mDa).

General Procedure for C3-Alkylation of 172a without HMPA

At -78 ºC under nitrogen, to a stirred solution of (*S*)-**172a** (30.0 mg, 0.10 mmol, 1 equiv) in anhydrous THF (1 mL) was added KHMDS (0.5 mL, 0.25 mmol, 2.5 equiv, 0.5 M in toluene). The resulting solution was stirred for a further 2 h. Electrophile (10.0 equiv) was added dropwise and then stirred for 2 h at -78 ºC. The reaction was quenched at -78 ºC with sat. NH_4Cl (aq) (1 mL), and extracted with CH_2Cl_2 (3 x 10 mL). The combined organic extracts were dried over anhydrous Na_2SO_4, filtered and concentrated under reduced pressure. The crude product was purified by flash column chromatography on silica gel.

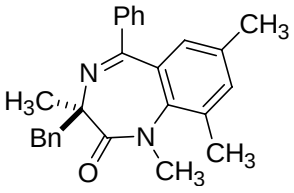

(3*R*)-(+)-3-benzyl-1,3-dihydro-1,3,7,9-tetramethyl-5-phenyl-2*H*-1,4-benzodiazepin-2-one [(*R*)-(+)-177a]

The general procedure was followed: (*S*)-(+)-**172a** (30.0 mg, 0.10 mmol, 1 equiv), KHMDS (0.5 mL, 0.25 mmol, 2.5 equiv, 0.5 M in toluene) and benzyl bromide (120 μL, 1.0 mmol, 10 equiv). Purification with flash column chromatography on silica gel (1:5 EtOAc/Hexanes) provided (*R*)-(+)-**177a** (25.2 mg, 75%) as colorless oil.

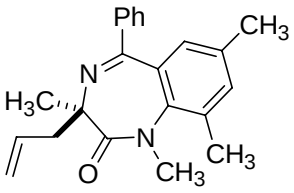

(3*R*)-(+)-3-allyl-1,3-dihydro-1,3,7,9-tetramethyl-5-phenyl-2*H*-1,4-benzodiazepin-2-one [(*R*)-(+)-179a]

The general procedure was followed: (*S*)-(+)-**172a** (30.0 mg, 0.10 mmol, 1 equiv), KHMDS (0.5 mL, 0.25 mmol, 2.5 equiv, 0.5 M in toluene) and allyl bromide (89 μL, 1.0 mmol, 10 equiv). Purification with flash column chromatography on silica gel (1:5 EtOAc/Hexanes) provided (*R*)-(+)-**179a** (26.3 mg, 77%) as colorless oil.

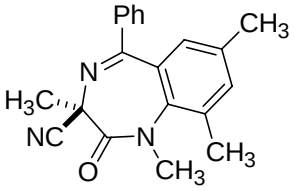

(3*R*)-(+)-3-cyano-1,3-dihydro-1,3,7,9-tetramethyl-5-phenyl-2*H*-1,4-benzodiazepin-2-one [(*R*)-(+)-178a]

The general procedure was followed: (*S*)-(+)-**172a** (30.0 mg, 0.10 mmol, 1 equiv), HMPA (110 μL, 0.62 mmol, 6 equiv), KHMDS (0.5 mL, 0.25 mmol, 2.5 equiv, 0.5 M in toluene) and *p*-toluenesulfonyl cyanide (196 mg, 1.0 mmol, 10 equiv). Purification with flash column chromatography on silica gel (1:5 EtOAc/Hexanes) provided (*R*)-(+)-**178a** (20.5 mg, 63%) as white solid.

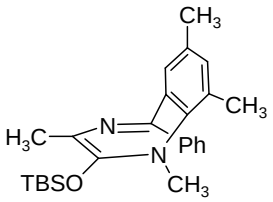

(*M*)-(+)-2-(*tert*-butyldimethylsilyloxy)-1,3,7,9-tetramethyl-5-phenyl-1*H*-1,4-benzodiazepine [(*M*)-(+)-182a]

At -78 °C under nitrogen, to a stirred solution of (*S*)-**172a** (29.8 mg, 0.11 mmol, 1.0 equiv) and HMPA (115 μL, 0.66 mmol, 6.0 equiv) in anhydrous THF (2.8 mL) was added KHMDS (0.55 mL, 0.28 mmol, 2.5 equiv, 0.5M in toluene). The resulting solution was stirred for a further 30 min before a solution of TBS-Cl (32.5 mg, 0.22 mmol, 2.0 equiv) in anhydrous THF (1.0 mL) was added via a cannula. The reaction was stirred at -78 °C for 1 hour. It was then quenched at -78 °C with 5 % $(NH_4)_2CO_3$ (aq) (2.0 mL) and extracted with CH_2Cl_2 (3 x 10 mL). The combined organic extracts were dried over anhydrous Na_2SO_4, filtered, and concentrated under reduced pressure. The crude product was purified by flash chromatography on silica gel (1:8 EtOAc/Hexanes) and followed by trituration with cold anhydrous CH_3CN. The crude crystal product was recrystallized from CH_3CN under nitrogen to give 30.8 mg (69%) of (*M*)-(+)-**182a** as yellow crystal. $[\alpha]_D^{25}$ = +959 (c = 1.85, $CHCl_3$). ^{1}H NMR ($CDCl_3$): δ 7.68-7.66 (m, 2H), 7.40-7.38 (m, 3H), 7.23 (s, 1H), 6.84 (s, 1H), 2.60 (s, 3H), 2.41 (s, 3H), 2.23 (s, 3H), 2.00 (s, 3H), 0.99 (s, 9H), 0.31 (s, 3H), 0.29 (s, 3H). ^{13}C NMR ($CDCl_3$): δ 162.3, 148.7, 141.6, 140.5, 136.2, 134.8, 134.4, 131.9, 129.20, 129.16, 129.0, 128.2, 123.4, 37.1, 25.9, 21.0, 18.9, 18.4, 18.2, -3.7, -3.9. HRMS (FAB) calcd. for $C_{25}H_{35}N_2OSi$ (M+1) 407.2519, found 407.2511 (-1.9 ppm, -0.8 mmu). Mp: 126.5–128.1 ºC. X-ray crystallography indicates

(*M*)-conformation; tetrahedralization of N1 as indicated, and concurrent slight pyramidalizations of enol carbons C2 and C3 in the same direction.

General Procedure for Cold Work-up Reactions

All glassware, except for the separatory funnel, were kept at <5 ºC during work-up. Solvent was removed at <5 ºC, and the NMR tubes were kept at <5 ºC. ^{1}H NMR data was collected at room temperature prior to chromatography. After purification and standing for around 24 hours, the mixtures of conformers at equilibrium were observed by ^{1}H NMR.

Specific procedure for in situ desilylation/benzylation experiment: At -78 ºC under nitrogen, to a stirred solution of (*M*)-(+)-**182a** (20.0 mg, 0.049 mmol, 1.0 equiv) and benzyl bromide (60 μL, 0.49 mmol, 10 equiv) in THF (2 mL) was added TASF (18.9 mg, 0.074 mmol, 1.5 equiv) in DMF/THF (1 mL/1 mL) via a cannula. The resulting solution was stirred for 1 hour at -78 ºC. The reaction was quenched at -78 ºC with sat. NH_4Cl (aq) (2 mL). The general cold work-up procedure was followed: the reaction was extracted with CH_2Cl_2 (3 x 10 mL). The combined organic extracts were dried over anhydrous Na_2SO_4, filtered and concentrated under reduced pressure. Purification with flash column chromatography on silica gel (1:5 EtOAc/Hexanes) provided 14.2 mg (76%) of (*M*)-(*R*)-**177a** as colorless oil. HPLC analysis indicated 99% ee of (R)-enantiomer.

Dynamic 1D and 2D EXSY ^{1}H NMR Measurements

Dynamic ^{1}H NMR measurements were performed on a Varian Unity 400 MHz NMR spectrometer with a recently calibrated temperature control unit with upper limit of 180 ºC. The temperature was calibrated with reference to ethylene glycol at different temperature.

2D EXSY ^{1}H NMR spectra were obtained on the Varian Unity 400 MHz NMR spectrometer with a recently calibrated temperature control unit, with ± 0.1 K uncertainty in temperature. The relaxation time T_1 of all aliphatic protons of **177a** were measured at various temperature used, and the relaxation delay was set to be 4-5 times the longest T_1 at that temperature to ensure full relaxation between consecutive pulses. Spectra were recorded at 393 K and 403 K. The mixing time t_m of each measurement was set to be around the optimized value of $1/(T_1^{-1} + k_A + k_B)$ to maximize the extent of exchange.[4]

General Protocol for Determining the Inversion Barrier of Enolate of 172a

To a stirred solution of (*S*)-**172a** (30.0 mg, 0.10 mmol, 1 equiv) and HMPA (110 μL, 0.62 mmol, 6 equiv) in anhydrous THF (1 mL) at -16 ºC under nitrogen was added KHMDS (0.5 mL, 0.25 mmol, 2.5 equiv, 0.5 M in toluene). The solution was then stirred for a time *t*. Benzyl bromide (120 μL, 1.0 mmol, 10 equiv) was added dropwise and then stirred for 2 h at -16 ºC. The reaction was quenched at -78 ºC with sat. NH_4Cl (aq) (1 mL), and extracted with CH_2Cl_2 (3 x 10 mL). The combined organic extracts were dried over anhydrous Na_2SO_4, filtered and concentrated under reduced pressure. The crude product was purified by flash column chromatography on silica gel (1:5 EtOAc/Hexanes). The enantiomeric excess was determined by HPLC t_r 28.8 min (*S*); t_r 42.7 min (*R*); t_r 44.9 min (*R*); t_r 47.5 min (*S*) [Chiralcel OD (0.46 cm x 25 cm) (from Daicel Chemical Ind., Ltd.)]

Hexane/*i*-PrOH, 99/1, 0.5 mL/min, 99% ee. The ln (% ee) was then plotted against deprotonation time *t* for determination of the racemization rate constant.

General Protocol for Determining the Inversion Barrier of 177a

Following the alkylation of (*S*)-**172a** by benzyl bromide, the Bn-ψeq and Bn-ψax conformers were separated with flash column chromatography on silica gel (1:5 EtOAc/Hexanes). R_f values: 0.26 (Bn-ψeq), 0.15 (Bn-ψax). The collected eluents were stored at <5 °C and solvent removal were performed at <5 °C, and the ^{1}H NMR tubes were kept at <5 °C. ^{1}H NMR spectroscopic data was collected at 40, 50, 60, 70 ºC by monitoring the increase of the C(3)-Me peak (either ψeq or ψax) until the ψax and ψeq concentrations had reached equilibrium. By plotting ln $(([\psi eq]_t-[\psi eq]_e)/([\psi eq]_o-[\psi eq]_e))$ vs time, where [ψeq] is arbitrarily the concentration of the Bn-ψeq conformer, ring inversion rate constants k_1 and k_{-1} were obtained at the corresponding temperature. k_1 is the equilibration from ψeq *to* ψax, while k_{-1} is the equilibration from ψax *to* ψeq. By obtaining the two rate constants at temperatures ranging over 90°C from 1D and 2D EXSY ^{1}H NMR, activation parameters $\Delta H^{\ddagger}$ and $\Delta S^{\ddagger}$ for both the forward and backward processes can be determined by plotting ln (k_1h/Tk_B) and ln $(k_{-1}h/Tk_B)$ vs $1/T$, where h is Plank constant and k_B is Boltzmann constant.

The errors in the slopes ($\Delta H^{\ddagger}/R$) and y-intercepts ($\Delta S^{\ddagger}/R$) were analyzed by Microsoft Excel using 95% confidence. The errors in $\Delta H^{\ddagger}$ and $\Delta S^{\ddagger}$ were then calculated by propagation of error according to the formula below:

$(S_c/C)^2 = (S_a/A)^2 + (S_b/B)^2$ where S_c is the error in $\Delta H^{\ddagger}$ or $\Delta S^{\ddagger}$, C is the values of $\Delta H^{\ddagger}$ or $\Delta S^{\ddagger}$; S_a is the error in the slope, A is the value of the slope; S_b is the error in the y-intercept, B is the value of y-intercept

Tabulation of Chiral Stationary Phase HPLC Conditions and Retention Times

Reported retention times were determined from racemic and enantiomerically enriched/pure samples. The HPLC columns were thermostatted at 27 °C, except for analysis of compound **179a**. Note that each enantiomer of **177a** and **179a** gives rise to two peaks in the HPLC chromatogram, due to slow conformational inversion on the HPLC timescale.

Compound	column	solvent, flow rate	fast enantiomer (config) retention time	slow enantiomer (config) retention time
171a	OD	1% isopropanol-hexanes 1 mL/min	24.6 min (3*S*)	32.5 min (3*R*)
172a	OD	1% isopropanol-hexanes 1 mL/min	28.7 min (3*S*)	34.5 min (3*R*)
177a	OD	1% isopropanol-hexanes 0.5 mL/min	28.8, 47.5 min (3*S*)	42.7, 44.9 min (3*R*)
178a	OD	1% isopropanol-hexanes 1 mL/min	16.2 min (3S)	18.1 min (3R)
179a	AD	1% isopropanol-hexanes 1 mL/min	10.9, 15.5 min (3R)	13.9, 19.9 min (3S)

Chiralpak AD (0.46 cm x 25 cm) (from Daicel Chemical Ind., Ltd.)
Chiralcel OD (0.46 cm x 25 cm) (from Daicel Chemical Ind., Ltd.)

Computational Details

Geometry optimizations and frequency calculations were performed using Gaussian03[1] at B3LYP; B3LYP electronic energies (ε_0) were calculated at the indicated basis set. Stationary points were identified as minima (nimag=0) or transition structures (nimag=1). The displacement of the imaginary frequencies corresponded to the expected molecular motion for ring inversion transition structures. Vibrational frequencies were corrected by a factor of 0.9804 to calculate zero point vibrational energy (ZPVE) and the Gibbs free energy correction G_{corr}. Gibbs free energy $G(T)$ is defined as the sum of ε_0 and $G_{corr}(T)$. Single point energies using Tomasi's polarizable continuum model (PCM) were calculated at B3LYP/6-31+G(d) and MP2/6-31+G(d) for solvent effects.

Calculated energies for equilibrium geometries and ring inversion transition structures of glycine-derived BZDs 161a and 162a.

structure	B3LYP/6-31G(d)				B3LYP/6-31+G(d) //B3LYP/6-31G(d)		MP2/6-31G(d) //B3LYP/6-31G(d)
	ε_0 (hartrees)	Corr ZPVE (hartrees)	$G_{corr}(T)$[a] (hartrees)	G(T)[a] (hartrees)	ε_0 (hartrees)	ε_0(PCM (DMSO)) (hartrees)	ε_0(PCM (DMSO)) (hartrees)
161a	-881.4968271	0.316175	0.268246	-881.22858111	-881.5252347	-881.5424624	-878.6847345
161a*	-881.457125	0.315958	0.270426	-881.18669904	-881.4862313	-881.5089882	-878.6421273
162a	-1722.0459	0.247485	0.196164	-1721.849736	-1722.074205	-1722.091368	-1718.40195
162a*	-1722.007108	0.246846	0.196402	-1721.810706	-1722.035199	-1722.057246	-1718.358848

[a]Gibbs free energy $G(T)$ is defined as the sum of ε_0 and Gcorr(T). Thermodynamic corrections were calculated at 298K.

Calculated energies for equilibrium geometries and ring inversion transition structures of silyl enol ether 181a (optimized at B3LYP/6-31G(d))

structure	ε_0 (hartrees)	Corr ZPVE (hartrees)	$G_{corr}(T)$[a] (hartrees)	G(T)[a] (hartrees)	$\Delta G(T)$[c] (kcal/mol)
(*M*)-**182a**	-1446.891339	0.525409[b]	0.460196	-1446.431143	0
(*M*)-**182a***	-1446.84656	0.526781[b]	0.465924	-1446.380636	31.7

[a]Gibbs free energy $G(T)$ is defined as the sum of ε_0 and Gcorr(T). Thermodynamic corrections were calculated at 298K

Calculated energies for equilibrium geometries of BZD precomplexes and enolates, and deprotonation transition structures 185a-202a

structure	B3LYP/6-31G(d)				B3LYP/6-31+G(d) // B3LYP/6-31G(d)	MP2/6-31G(d) // B3LYP/6-31G(d)	MP2/6-31+G(d) // B3LYP/6-31G(d)
	ε_0 (hartrees)	Corr ZPVE (hartrees)	Gcorr(T)[a] (hartrees)	G(T)[a] (hartrees)	ε_0 (hartrees)	ε_0 (hartrees)	ε_0 (hartrees)
(*M*)-(*S*)-**185a**	-1062.910383	0.419798	0.389539	-1062.101046	-1062.94144	-1059.408773	-1059.476612
(*P*)-(*S*)-**185a**	-1062.91306	0.420002	0.389311	-1062.103747	-1062.944431	-1059.408836	-1059.47622
(*M*)-(*S*)-**186a**	-1062.941572	0.424058	0.390644	-1062.12687	-1062.973626	-1059.437288	-1059.501619
(*P*)-(*S*)-**186a**	-1062.933689	0.42468	0.39176	-1062.117249	-1062.965716	-1059.431073	-1059.496826
(*M*)-(*S*)-**187a**	-1062.952784	0.425095	0.392385	-1062.135304	-1062.983793	-1059.455771	-1059.522041
(*P*)-(*S*)-**187a**	-1062.959061	0.425234	0.393848	-1062.13998	-1062.989876	-1059.462849	-1059.529894
(*M*)-(*S*)-**188a**	-1217.965698	0.500429	0.465454	-1216.999816	-1218.000762	-1213.948358	-1214.025214
(*P*)-(*S*)-**188a**	-1217.966804	0.500476	0.464652	-1217.001677	-1218.002147	-1213.945978	-1214.022072
(*M*)-(*S*)-**189a**	-1217.992389	0.504967	0.468684	-1217.018739	-1218.028313	-1213.976616	-1214.051559
(*P*)-(*S*)-**189a**	-1217.981689	0.504538	0.467289	-1217.009861	-1218.018	-1213.96417	-1214.039421
(*M*)-(*S*)-**190a**	-1218.007355	0.505678	0.468111	-1217.033566	-1218.043825	-1213.993018	-1214.070539
(*P*)-(*S*)-**190a**	-1218.01082	0.505648	0.469546	-1217.035626	-1218.045971	-1214.000108	-1214.077621
(*M*)-(*S*)-**191a**	-1205.077245	0.501143	0.466708	-1204.610537	-1205.110736	-1201.036141	-1201.111904
(*P*)-(*S*)-**191a**	-1205.066571	0.501227	0.464761	-1204.60181	-1205.100232	-1201.021206	-1201.096637
(*M*)-(*S*)-**192a**	-1205.107937	0.505742	0.467465	-1204.640472	-1205.141684	-1201.064872	-1201.135773
(*P*)-(*S*)-**192a**	-1205.10004	0.506301	0.469798	-1204.630242	-1205.133691	-1201.058506	-1201.129814
(*M*)-(*S*)-**193a**	-1205.107937	0.505742	0.467465	-1204.640472	-1205.141684	-1201.064872	-1201.135773
(*P*)-(*S*)-**193a**	-1205.123562	0.506561	0.471433	-1204.652129	-1205.154866	-1201.093683	-1201.165879
(*M*)-(*S*)-**194a**	-1515.166887	0.662126	0.618605	-1513.886157	-1515.207905	-1510.097523	-1510.193253
(*P*)-(*S*)-**194a**	-1515.156934	0.662664	0.619378	-1513.874892	-1515.19794	-1510.083576	-1510.177134
(*M*)-(*S*)-**195a**	-1515.184908	0.666143	0.621307	-1513.897458	-1515.226654	-1510.116599	-1510.210536
(*P*)-(*S*)-**195a**	-1515.192528	0.665543	0.619989	-1513.906996	-1515.234459	-1510.123454	-1510.216847
(*M*)-(*S*)-**196a**	-1515.20885	0.667441	0.62343	-1513.917979	-1515.249434	-1510.1485	-1510.245336

(*P*)-(*S*)-**196a**	-1515.203296	0.667095	0.623241	-1513.91296	-1515.244752	-1510.138526	-1510.23454
(*M*)-(*S*)-**197a**	-1655.266297	0.417287	0.385734	-1654.880563	-1655.30208	-1651.079874	-1651.160305
(*P*)-(*S*)-**197a**	-1655.259843	0.417552	0.385174	-1654.874669	-1655.295879	-1651.070189	-1651.148757
(*M*)-(*S*)-**198a**	-1655.285608	0.421422	0.387941	-1654.897667	-1655.322684	-1651.098243	-1651.174071
(*P*)-(*S*)-**198a**	-1655.272618	0.421371	0.387121	-1654.885497	-1655.309993	-1651.085722	-1651.163234
(*M*)-(*S*)-**199a**	-1655.306916	0.422597	0.389133	-1654.917783	-1655.343369	-1651.126659	-1651.208282
(*P*)-(*S*)-**199a**	-1655.313716	0.42293	0.390176	-1654.92354	-1655.349752	-1651.133583	-1651.215009
(*M*)-(*S*)-**200a**	-2120.392315	0.671008	0.612655	-2119.77966	-2120.440134	-2114.658185	-2114.772737
(*P*)-(*S*)-**200a**	-2120.382498	0.671120	0.610744	-2119.771754	-2120.431042	-2114.642406	-2114.754345
(*M*)-(*S*)-**201a**	-2120.400913	0.673897	0.612272	-2119.788641	-2120.450514	-2114.663963	-2114.774031
(*P*)-(*S*)-**201a**	-2120.394373	0.673789	0.613012	-2119.781361	-2120.443878	-2114.660845	-2114.773278
(*M*)-(*S*)-**202a**	-2120.432197	0.675745	0.614913	-2119.817284	-2120.481149	-2114.700677	-2114.81625
(*P*)-(*S*)-**202a**	-2120.436707	0.675924	0.614964	-2119.821743	-2120.485674	-2114.707055	-2114.823189

[a]Gibbs free energy *G*(*T*) is defined as the sum of ε_0 and *G*corr(*T*). Thermodynamic corrections were calculated at 195K

Calculated energies for equilibrium geometries and ring inversion transition structures of BZD enolates 203a-205a (optimized at B3LYP/6-31+G(d))

structure	ε_0 (hartrees)	Corr ZPVE (hartrees)	Gcorr(T)[a] (hartrees)	G(T)[a] (hartrees)	ΔG(T)[a] (kcal/mol)
(*M*)-**203a**	-920.2620764	0.33287	0.292455	-919.9696214	0
(*M*)-**203a***	-920.2429612	0.333686	0.296049	-919.9469122	14.3
(*P*)-**204a**	-1392.950194	0.582411	0.520323	-1392.429871	0
(*P*)-**204a***	-1392.916018	0.583216	0.524058	-1392.39196	23.8
(*P*)-**205a**	-2140.344941	0.659959	0.586074	-2139.098908	0
(*P*)-**205a***	-2140.311468	0.660433	0.586313	-2139.064721	21.5

[a]Gibbs free energy *G*(*T*) is defined as the sum of ε_0 and *G*corr(*T*). Thermodynamic corrections were calculated at 257K

Calculated energies for alkylation transition structures of BZD enolates 220-223

structure	B3LYP/6-31G(d)				B3LYP/6-31+G(d) //B3LYP/6-31G(d)
	ε_0 (hartrees)	Corr ZPVE (hartrees)	Gcorr(T)[a] (hartrees)	G(T)[a] (hartrees)	ε_0 (hartrees)
220	-3762.897103	0.445952	0.410797	-3762.040354	-3762.975328
221	-3762.889359	0.446405	0.412688	-3762.030266	-3762.965949
222	-3609.236091	0.39892	0.366734	-3608.470437	-3609.309603
223	-3609.230283	0.399535	0.367962	-3608.462786	-3609.297155

[a]Gibbs free energy $G(T)$ is defined as the sum of ε_0 and $G\text{corr}(T)$. Thermodynamic corrections were calculated at 195K

Note that all Cartesian coordinates are B3LYP/6-31G(d) geometries

Cartesian Coordinates for 161a

C	-1.217550755878	0.235849096739	-0.502662736809
C	-1.215875224968	0.234105925745	2.314081022174
C	0.001412789556	0.241355911386	0.220919594571
C	-2.418296451667	0.268817348300	0.239883395978
C	-2.429279522225	0.248763339026	1.631111522115
C	-0.011862130802	0.243015611887	1.623677990989
N	-1.231198658038	0.185379901314	-1.915476800565
C	-0.516920633920	1.075377584524	-2.709764257748
O	-0.622265343269	1.066624290221	-3.922409184858
C	0.459012855027	1.975394524185	-1.950952786530
N	1.547758056428	1.148566942057	-1.448626555675
C	1.320538747171	0.335011363199	-0.478817144803
C	-1.991204575780	-0.849940149898	-2.634190886148
C	2.454281804119	-0.511197886999	-0.003995295447
C	4.628121537633	-2.104447747483	0.791240073885
C	3.774148285556	-0.087171494475	-0.234439339604
C	2.242157813447	-1.748879018169	0.623990275927
C	3.322324685020	-2.540578246112	1.015612074948
C	4.849730179526	-0.874670354963	0.163929648067
H	-2.863314399734	-0.431334368182	-3.141193559145
H	-2.311943927894	-1.613354869468	-1.925260018443
H	-1.335707820139	-1.296619708061	-3.386008895427
H	-3.370098273112	0.272208470040	2.167570587405
H	0.924978391709	0.251845550913	2.167829885882
H	1.230513844771	-2.104828712587	0.792897363574
H	3.140755155983	-3.499720462359	1.492767826146
H	5.864680979486	-0.529289587869	-0.013273839102
H	3.933473643350	0.863876497268	-0.730862607885
H	0.856863136418	2.697496960189	-2.664519864221
H	-0.065396115638	2.515643878098	-1.147756740975
H	5.469324341876	-2.718367476632	1.101622980099

Cl	-1.217903243759	0.229075697139	4.067554384895
Cl	-3.971294309803	0.410747053563	-0.564234093999

Cartesian Coordinates for 161a*

C	-1.145217291577	0.881372621535	-0.163027079693
C	-1.438066474675	-1.907435521273	-0.575954054761
C	-0.127677876831	-0.025944946135	0.277179188624
C	-2.080201712512	0.336657087768	-1.088622868262
C	-2.266448980914	-1.032000047081	-1.261026124051
C	-0.345669039527	-1.406375679897	0.114130989726
N	-1.310058152226	2.215831372558	0.261853702746
C	-0.367996350202	3.085828300242	0.819556924693
O	-0.638793997989	4.273661526786	0.903421410431
C	0.894282775058	2.630370712241	1.548411292970
N	1.657992165212	1.452247486675	1.272104472678
C	1.235731547547	0.350029820122	0.789469581549
C	-2.679312886922	2.787706635051	0.335379293553
C	2.324749835933	-0.690434780529	0.666768897082
C	4.482641837899	-2.477819773316	0.464084612117
C	2.624841651714	-1.311042647226	-0.555339641759
C	3.127526652774	-0.968838206304	1.781416080094
C	4.191557584573	-1.864296801277	1.684175227084
C	3.700900586740	-2.192849011458	-0.656744106297
H	-2.895125510926	3.462586551443	-0.492542857438
H	-3.401879822013	1.973641543569	0.349825598459
H	-2.750943954613	3.352719509191	1.264977529093
H	-3.029344546829	-1.391395089807	-1.940925644121
H	0.374686727989	-2.097922748130	0.528338658056
H	2.913463015394	-0.469175366701	2.720955458361
H	4.797499186933	-2.078201771220	2.560526111796
H	3.928313937835	-2.655500214556	-1.613287744440
H	2.023024902918	-1.094316768189	-1.433324965080
H	0.592249636495	2.594442042163	2.608796478034
H	1.566623664597	3.490786343573	1.478829537559
H	5.315543702120	-3.171389361170	0.386387310578
Cl	-1.699098402157	-3.637310466371	-0.686454139156
Cl	-2.980263256746	1.346034850261	-2.223121346626

Cartesian Coordinates for 162

C	-1.504584105761	0.272364075203	-0.296918840108
C	-1.505274714755	0.269960448531	2.536233183504
C	-0.284658497216	0.272813760218	0.416466828436
C	-2.730163977391	0.306906456799	0.410630551513
C	-2.699981656158	0.291748911364	1.805447428869
C	-0.311014058238	0.270724112311	1.821431802554
N	-1.512119820972	0.226806177834	-1.721360137801
C	-0.801487929345	1.114795794509	-2.514493258323
O	-0.907847712794	1.113921136789	-3.729846606258
C	0.177507830248	2.008401648316	-1.752825012467
N	1.265393748165	1.178564270188	-1.253582004474
C	1.031703054556	0.368486429798	-0.280351681933
C	-4.061046003477	0.424033376217	-0.297246435849
C	-1.521258158738	0.267325950233	4.046797287383
C	-2.256919947162	-0.818663577814	-2.433102086667

C	2.170111035244	-0.477302830972	0.190284539070
C	4.348416273533	-2.072141452721	0.976577948201
C	3.489351569089	-0.057711780817	-0.050930023123
C	1.961595277316	-1.711821876062	0.825138631817
C	3.043199109417	-2.504170572173	1.212147102882
C	4.566965550538	-0.845251641838	0.342598350088
H	-4.413673287423	-0.534243415900	-0.697059815385
H	-4.825932797672	0.788328874020	0.394962145846
H	-4.003181281564	1.122889639913	-1.138339564052
H	-3.186869569381	-0.442211508406	-2.870631698728
H	-2.481283066568	-1.629525298622	-1.738171751707
H	-1.633126459984	-1.195247062468	-3.247128105727
H	-3.646469277063	0.325725490396	2.342163066521
H	-2.086060289866	1.120085811761	4.442959092436
H	-1.994554413239	-0.641448146924	4.439440377170
H	-0.507818967277	0.318167150156	4.456223892681
H	0.633308585784	0.279899311054	2.357624482290
H	0.949677053796	-2.061631083624	1.003979452695
H	2.863407341701	-3.461294867439	1.694575366009
H	5.581289386667	-0.502457239371	0.155813541435
H	3.645705874335	0.890336250653	-0.554055530553
H	0.576379922819	2.733683448594	-2.463151197953
H	-0.346654114332	2.543645946674	-0.945877122563
H	5.190955661059	-2.686648917549	1.282723320490

Cartesian Coordinates for 162*

C	-1.357811097061	0.812685994826	-0.338348249646
C	-1.751542475928	-1.955221347995	-0.896179165251
C	-0.398874925126	-0.147823086801	0.107290165047
C	-2.284620141219	0.392163736558	-1.335063471538
C	-2.480398984816	-0.972516306573	-1.562591633845
C	-0.675685172241	-1.507144752765	-0.135718853429
N	-1.476262108695	2.145593902218	0.144326909894
C	-0.536476583879	2.943110533787	0.792090560715
O	-0.769009410990	4.135405465582	0.944378297806
C	0.681402675002	2.398944978128	1.537040573605
N	1.413317572881	1.208871681563	1.222430945865
C	0.956100278027	0.148651097357	0.676221745598
C	-2.989746529056	1.349225876234	-2.283459335419
C	-2.055371466552	-3.424718831536	-1.055259221056
C	-2.826940139671	2.752670635793	0.198139651526
C	2.013663651308	-0.923488615904	0.533196730368
C	4.118964579387	-2.772775691632	0.299874991709
C	2.322811032676	-1.502129764043	-0.707032295455
C	2.782182208768	-1.276620845690	1.650674723172
C	3.818758791518	-2.202379342149	1.538520904846
C	3.372422651658	-2.413610527464	-0.823772636981
H	-3.997154205371	1.640871092599	-1.965960672926
H	-3.090821505306	0.861148735142	-3.258138012456
H	-2.411919620094	2.264552330433	-2.436055167443
H	-3.013584615407	3.453426053437	-0.617683354420
H	-3.567221579681	1.954074463101	0.181348320690
H	-2.912734213414	3.306069964014	1.133318941992
H	-3.218870573632	-1.266062052286	-2.306737866974
H	-2.802141080530	-3.759089962080	-0.322509933329

H	-1.159934399610	-4.037879683437	-0.908924454995
H	-2.458875075430	-3.645577137416	-2.049819781561
H	0.004987730652	-2.241233548489	0.278440129098
H	2.563356679642	-0.809212465856	2.605613975739
H	4.397160596848	-2.472982969087	2.418046646702
H	3.607826246622	-2.841235514251	-1.794918394625
H	1.746228493580	-1.229259938172	-1.586163809984
H	0.335970260883	2.316408182846	2.581803126650
H	1.385928468401	3.236325617353	1.542192303073
H	4.931455313702	-3.488988419748	0.210065528216

Cartesian Coordinates for 182a

C	0.955965144666	1.089510307993	-2.299050154994
C	0.907507385133	0.711372587309	-0.938487372945
C	2.139077121308	0.892268942825	-3.012780105386
C	3.282653655759	0.329951312852	-2.430003917895
C	2.059727141202	0.194307348755	-0.317661811249
H	2.172222025157	1.193196512653	-4.058449101801
N	-0.312311874350	0.925298875102	-0.198067936976
C	3.227580798185	0.000048330313	-1.079940021568
C	2.051033458094	-0.234904782465	1.105639294021
C	-0.875180248452	-0.229573970121	0.399137820755
H	4.102753608071	-0.424604772292	-0.597416892597
N	1.077180688955	-0.860426832505	1.679108770069
C	3.268502526690	-0.006269867395	1.942016532958
C	-0.182754907267	-1.118391703529	1.165157770669
O	-2.233871874987	-0.353979644906	0.322090626536
C	3.555400730210	-0.873768347156	3.010395937594
C	4.113403685344	1.096195708319	1.731375765021
C	5.213590340037	1.321110149538	2.560003763095
C	4.658472727288	-0.654334170452	3.829744417852
H	2.892744802525	-1.715176406638	3.182151375625
H	3.901162590986	1.789261236454	0.923102199329
C	5.493860577529	0.445053322738	3.608712589821
H	5.849426636238	2.185421239338	2.386027211991
H	4.869704515724	-1.342796319905	4.644072903784
H	6.354093997202	0.616786814297	4.250448483753
C	-0.819908779722	-2.368387138432	1.721459099106
H	-1.138844159874	-2.218280678936	2.761450620954
H	-1.691607463579	-2.667581540625	1.137295610903
H	-0.095409573253	-3.190461326531	1.721605509126
C	-0.222182309188	1.736764794022	-2.986203757516
H	-1.099944366469	1.085483513733	-2.993197121148
H	-0.521868984369	2.666239957692	-2.488080235602
H	0.025717648842	1.980767275015	-4.023952678647
C	-0.391745177793	2.163674839709	0.592408478200
H	-1.414590654254	2.279838713960	0.961329820119
H	0.295516407625	2.169884945457	1.450937213332
H	-0.157455979462	3.020204912619	-0.047802165471
C	4.531054707000	0.094893078831	-3.247997807415
H	5.376203830114	-0.189782678295	-2.613685408551
H	4.381805534144	-0.708043638744	-3.981407912918
H	4.817470324533	0.992489738417	-3.809154291762
Si	-3.400783634091	-0.180959282359	-0.892566539349
C	-2.884087523819	-1.192950311120	-2.403520173209

H	-2.936790043893	-2.267964209394	-2.197511503377
H	-1.852868547331	-0.971870303394	-2.699923964867
H	-3.528946415739	-0.986818923204	-3.266283550539
C	-3.659398074413	1.636702922157	-1.335117296651
H	-4.461049823259	1.748490515183	-2.075421337099
H	-2.754312354426	2.085519844301	-1.751678242239
H	-3.942817152113	2.220036109858	-0.451641003160
C	-4.993791569590	-0.880947311020	-0.089929583234
C	-4.799553308395	-2.356412700613	0.317962245970
H	-5.724539259415	-2.753289507636	0.761188261729
H	-4.003496511871	-2.467617244470	1.061580765919
H	-4.552532972349	-2.994132778663	-0.539630636179
C	-6.159625276592	-0.790322167812	-1.099972483977

Cartesian Coordinates for 182a*

C	-0.344051554348	1.179431247479	-2.909612096403
C	-0.010905958565	0.749867976425	-1.601268704516
C	0.667742627114	1.228763283192	-3.890276578511
C	1.999278447737	0.962520502066	-3.612145120282
C	1.372211905833	0.843119707371	-1.234419864907
H	0.375313574704	1.498347584867	-4.904114570686
N	-1.020337413700	0.193662249253	-0.767939369539
C	2.326688349249	0.864156681208	-2.250278831117
C	1.815135256004	1.222195241391	0.147856989855
C	-0.875220277416	-0.153765380677	0.606186115930
H	3.372951867829	0.872587975878	-1.961465919299
N	1.224187819755	0.993080275928	1.263007557160
C	3.030211641379	2.097962557980	0.277166407947
C	0.073539871009	0.253789461242	1.499782162628
O	-1.935065243589	-0.885910545168	1.071317385568
C	3.906559948817	1.882677544222	1.354260607791
C	3.287896576392	3.178715713874	-0.583456084089
C	4.386405484724	4.012733735910	-0.373512373774
C	5.013178319885	2.704616002371	1.552766646374
H	3.697658468656	1.063823193461	2.034776380434
H	2.615447154957	3.378493775334	-1.411598742012
C	5.258686502910	3.775597867912	0.689687839838
H	4.557598683172	4.852244396004	-1.042730853169
H	5.685218114969	2.510833631036	2.385109116109
H	6.120104728708	4.419726737483	0.846188444874
C	-0.128513224084	0.055964736097	2.989620545356
H	-1.152154049945	-0.216080364655	3.249763901943
H	0.549958902624	-0.698042407255	3.408909245751
H	0.117369211050	1.002998350151	3.481870611640
C	-1.706831059947	1.726632710305	-3.304994300025
H	-2.370174057981	0.999620143228	-3.788814181301
H	-2.238956018537	2.139624506659	-2.443613048343
H	-1.558071433753	2.546578962437	-4.015965014292
C	-2.136991131407	-0.437510691596	-1.490842681099
H	-1.789610515211	-0.740658772765	-2.479949574090
H	-2.478017705428	-1.318516606622	-0.967108612423
H	-2.995618806727	0.230875516524	-1.604400333299
C	3.056076457602	0.896302232416	-4.686603305212
H	2.697849316303	1.331612078887	-5.625750147308
H	3.966701708268	1.431409576212	-4.392192627710

H	3.349234261573	-0.140994740978	-4.898862833358
Si	-2.066113291252	-2.549203939372	1.444844928842
C	-0.918889115188	-3.109101779917	2.833429808365
H	-1.037362556971	-4.191320261664	2.971879271331
H	-1.120627765905	-2.622940936983	3.791645588563
H	0.130092352282	-2.925875059549	2.577622927493
C	-1.609318119512	-3.591896934913	-0.068081417306
H	-1.499140128320	-4.641504439777	0.230499629982
H	-0.645878047236	-3.271695343493	-0.483271578083
H	-2.348010591050	-3.554900899756	-0.875287461412
C	-3.905345612266	-2.726705331783	1.935723253712
C	-4.204496096053	-1.863354304128	3.181289930091
H	-5.262276825886	-1.960525036140	3.465346422530
H	-4.007229818491	-0.801996975117	2.993720277360
H	-3.606529716503	-2.169590448357	4.048206060452
C	-4.204762729314	-4.207448934228	2.259764536030

Cartesian Coordinates for (*M*)-(*S*)-185a

C	-1.168567894790	-1.661342653222	-0.109082756187
C	-1.154085148831	-1.476385044571	1.358106448255
N	0.061157296658	-1.503807074753	-0.805556828495
O	-1.994472549197	-2.076771038241	2.085835689559
N	-0.242629532219	-0.623786388941	1.954363775382
C	0.910264837872	-0.543533092262	-0.697242545020
C	0.053563736933	0.649711162830	1.353753768605
C	0.690301506878	0.693645328615	0.101717480890
C	2.157400488956	-0.661167444900	-1.515755344404
C	0.070297037092	-0.872197516536	3.364791766709
C	2.154128354658	-1.430046425779	-2.692245580131
C	3.365171878753	-0.070418583881	-1.109483527667
C	1.005993311188	1.939544796978	-0.463299900033
C	-0.317569066655	1.850994439521	2.001091357287
H	0.330988997563	-1.927311215803	3.483791403122
H	0.937892717687	-0.264908176394	3.630928618022
H	-0.754674671203	-0.649811798500	4.047196392835
C	4.531471815632	-0.238888838141	-1.857410487232
C	3.315076372555	-1.590091104993	-3.442712122043
H	1.224905971817	-1.899807100715	-2.996337388726
H	3.395984025702	0.513926733683	-0.194643863962
H	1.487467812170	1.960291263927	-1.436107137681
C	0.043383890492	3.065421182506	1.408999318358
C	0.711300481506	3.137830256460	0.183195321290
C	4.511177364971	-0.995183630233	-3.029260789024
H	5.457420431810	0.219747490598	-1.519535762940
H	3.288812984964	-2.180437766098	-4.355316288012
H	-0.234779535373	3.987828276129	1.915375214599
H	5.417704601921	-1.122237003157	-3.615330385625
C	-1.132075206339	1.889351584761	3.276506560997
H	-1.943219667001	1.154034854257	3.259915332430
H	-0.532576837341	1.692585428464	4.173221934804
H	-1.582980918282	2.878520728675	3.399444462000
C	-1.737364904601	-3.049591735109	-0.491942010393
H	-1.678369885612	-3.147298094608	-1.578576855925
H	-1.161898619368	-3.864746052452	-0.038840906579
H	-2.787665614163	-3.186613464147	-0.209654656968

C	1.092842633127	4.469716630930	-0.419201560308
H	1.223266854866	4.394964175589	-1.503472883511
H	2.038587326776	4.839690957669	-0.001011670593
H	0.331835283777	5.232734020592	-0.221160686419
H	-2.206014141360	-0.930109456731	-0.402109649112
N	-3.676568505552	-0.508078670456	-0.289970703321
C	-4.385659499250	-0.855549660585	-1.513309441757
H	-5.444815532351	-0.536063747102	-1.493350752513
H	-3.939156100024	-0.390236084302	-2.412762066674
H	-4.376283043800	-1.942281439322	-1.669902408845
C	-3.667426803680	0.938766531481	-0.123279590786
H	-4.679538743811	1.354276220031	0.040802108243
H	-3.053118511188	1.222297369505	0.742314894424
H	-3.251127928658	1.467334753185	-1.001675554302
Li	-3.614777598993	-1.652004910404	1.251547044015

Cartesian Coordinates for (*P*)-(*S*)-185a

C	1.339052029736	-0.280952992379	-1.260734298158
C	1.306248406282	-0.296720168007	0.142839374143
C	2.571701927591	-0.216839012320	-1.946106762040
N	0.106420605825	-0.308148341021	-1.998301812105
C	3.752683355671	-0.255071405600	-1.199941245793
C	2.521405348167	-0.311083030651	0.848936819963
C	-0.107294837042	-1.308101297754	-3.046868396059
C	0.037389298145	-0.105486900193	0.906800439000
C	-0.726560691163	0.783091625940	-1.947310432012
C	3.753153733053	-0.312453322190	0.197386922249
H	4.702326674205	-0.214073261705	-1.730466213251
H	2.493702411945	-0.307519954220	1.933998053421
H	-1.160588554774	-1.604581842019	-3.044646834466
N	-0.893372139916	0.720011876061	0.582723530786
C	-0.121316276040	-0.805844509830	2.222142303671
C	-1.092534739255	1.403654883593	-0.655164267851
O	-1.369101363745	1.091223573592	-3.000735179874
C	-0.912241091913	-0.231136922107	3.231375107827
C	0.448271000442	-2.067357333077	2.456953391215
C	0.239710516230	-2.732180090117	3.666617003697
C	-1.110619807610	-0.889058310803	4.441473773190
H	-1.369385760413	0.733521979408	3.039078575456
H	1.048756163948	-2.537585030093	1.683882611261
C	-0.535770226025	-2.144066026506	4.665599777942
H	0.682156430111	-3.712516025051	3.824630685419
H	-1.717203705186	-0.423408503414	5.214225743186
H	-0.694516572551	-2.658494135228	5.609853468911
C	-0.906879380156	2.918471690066	-0.523777479024
H	0.139283638283	3.183127341377	-0.321192910695
H	-1.514572365738	3.296987691173	0.304246830478
H	-1.214240511254	3.428430072538	-1.443304514993
H	0.140948168776	-0.947235188516	-4.049439043045
H	0.503967210582	-2.183136060277	-2.814536725230
C	2.656894262120	-0.062355718199	-3.448430646451
H	2.509557464765	-1.010712922035	-3.979425263451
H	3.643245947000	0.317337923619	-3.731539540576
H	1.904323537416	0.640100203809	-3.821438880087
C	5.049581973703	-0.363490668592	0.971883690859

H	5.489907199619	-1.369140370421	0.945965196853
H	4.897562289954	-0.099740451271	2.023202597689
H	5.793907124488	0.324309397545	0.554482451185
H	-2.397909909380	1.348089585989	-0.802883620956
N	-3.851322427019	1.354657668702	-1.098929787612
C	-4.312894422908	0.046653043401	-0.652654349777
C	-4.482732089770	2.401732147604	-0.310054081408
Li	-3.122214330512	1.515963539064	-2.827030988073
H	-4.122225797038	-0.127378926571	0.422303053137
H	-5.397214056060	-0.095406965077	-0.813884993748
H	-3.794692539630	-0.750293375684	-1.205884576815
H	-5.581496854694	2.416055526445	-0.435160141164
H	-4.292932341738	2.292934201825	0.774633088757
H	-4.108783398913	3.388567362064	-0.613968082651

Cartesian Coordinates for (*M*)-(*S*)-186a

C	-1.180455293018	0.538518391780	-0.919817683883
C	-1.471339580238	0.179872350848	0.537594116119
N	-0.124583957064	-0.387735644248	-1.338448586280
O	-2.467123425526	-0.463006840154	0.895822332009
N	-0.515417170750	0.528491430700	1.443020979225
C	1.072721993202	-0.228274072692	-0.888594205605
C	0.643464338814	1.294318219410	1.092035705055
C	1.463280013949	0.893072508444	0.015810666776
C	2.112144299174	-1.196716016627	-1.343738641181
C	-0.650733875681	-0.023874988335	2.802240250873
C	1.928413792881	-1.892088146250	-2.551127466035
C	3.252129433661	-1.472046595299	-0.571539124921
C	2.625298648068	1.629976541816	-0.266244855779
C	0.967936843593	2.444226296489	1.845832127938
H	-0.886003788925	-1.088422029917	2.731229516075
H	0.295886622860	0.104899945137	3.326325608506
H	-1.453095013929	0.468520071310	3.358225885118
C	4.186537840924	-2.416391938070	-0.997620998631
C	2.865866727928	-2.827280335424	-2.978193425244
H	1.040736142416	-1.685681046482	-3.139036915196
H	3.401943751520	-0.958968832610	0.373315718211
H	3.246238738483	1.320568825795	-1.101322554557
C	2.136124236641	3.137356599903	1.525648149814
C	2.984672386195	2.748999402101	0.480881276271
C	3.998950999167	-3.092758433614	-2.203206852545
H	5.058660133459	-2.625223457982	-0.384040196021
H	2.714224331827	-3.351325191221	-3.917878100066
H	2.380235103532	4.029073297508	2.099663557014
H	4.729482995411	-3.824407064583	-2.537623563270
C	0.066392091774	2.971965969831	2.938909177760
H	-0.989719937855	2.894835749040	2.660026580424
H	0.192317690475	2.432970701452	3.885496380786
H	0.287728758011	4.024992168470	3.134394460638
C	-2.400766402466	0.385990039676	-1.819626618390
H	-2.130318348927	0.658305574558	-2.844205493172
H	-2.752619858647	-0.649254563498	-1.829547633879
H	-3.220636767903	1.033307531566	-1.491735009549
C	4.235398060104	3.535992788413	0.168997089533
H	4.740005891425	3.148012253651	-0.720655165403

H	4.948028681684	3.494991277372	1.002099582664
H	4.007550410996	4.593946895548	-0.007478205647
H	-0.825922759127	1.581000999040	-0.946519384700
N	-5.826522838201	-1.756163690619	0.311370149491
C	-6.266113764159	-2.669919663998	-0.711714825196
H	-6.737184374539	-3.597160327720	-0.310848037650
H	-7.025575484770	-2.234911205527	-1.402417012477
H	-5.420237976634	-2.994664520344	-1.339295729678
C	-6.956112352235	-1.353655122579	1.109750078482
H	-7.469201793636	-2.201938185685	1.619147572416
H	-6.647623290874	-0.652000497243	1.901947445009
H	-7.755369742973	-0.840975750016	0.525277799515
Li	-4.136579192238	-1.197428447380	0.559877598164

Cartesian Coordinates for (*P*)-(*S*)-186a

C	1.412121349954	-0.277132533538	-1.153036410663
C	1.376749976921	-0.279001559168	0.255235941011
C	2.626021186107	-0.046849105984	-1.836363852617
N	0.218133953310	-0.503923269745	-1.910130355604
C	3.790204661804	0.121784805821	-1.083593504744
C	2.575926514417	-0.100326217121	0.963703024475
C	0.180533606268	-1.600410212256	-2.894121233304
C	0.092982161118	-0.334445754447	1.019371686536
C	-0.939662092912	0.183429377801	-1.717647617551
C	3.794659490217	0.089607550036	0.315422040742
H	4.723067229758	0.310279945979	-1.611240946610
H	2.540841449247	-0.091560633446	2.048538691881
H	-0.722186037291	-2.192897229766	-2.729124621331
N	-0.975795550935	0.307151452913	0.703683856991
C	0.043100952514	-1.144041023322	2.276179416418
C	-1.074214831809	1.120446554409	-0.513235258230
O	-1.907966912168	-0.036727471507	-2.471025740717
C	-0.867516028009	-0.794721306384	3.287583962535
C	0.844074569702	-2.283484588044	2.452723498530
C	0.740021111342	-3.052326600337	3.612487566624
C	-0.962341264206	-1.556678347169	4.448131185967
H	-1.495453551018	0.077253796203	3.140705144022
H	1.540912421220	-2.580074206066	1.674771446620
C	-0.158813754536	-2.688555751237	4.615355787217
H	1.360059905124	-3.937150214605	3.729009292116
H	-1.664994010634	-1.268358979398	5.225259164325
H	-0.235443927507	-3.283424902054	5.521592004838
C	-0.209495258703	2.396769872808	-0.539299433235
H	0.865571755408	2.211567173400	-0.548149481440
H	-0.451346238470	2.988417844292	0.349010041011
H	-0.472426944060	2.994771360751	-1.418427696023
H	0.159456814626	-1.223520924421	-3.919954972818
H	1.059827819919	-2.227387427039	-2.747246675241
C	2.693478904521	0.089666683992	-3.341024172613
H	2.710204746443	-0.879718702236	-3.853281164983
H	3.603474005072	0.623421207452	-3.629501216044
H	1.836452121236	0.648856363200	-3.730933268526
C	5.078406868917	0.267086821042	1.091001749588
H	5.695826062917	-0.639510843193	1.047472099531
H	4.881896455482	0.481385630580	2.145771982339

H	5.681148870098	1.087225760225	0.684897384044
H	-2.115156326217	1.467022037201	-0.559247973078
N	-4.588560017698	2.092755506296	-1.579698991853
C	-5.548826929108	1.901091350935	-0.521044026899
C	-4.609695995552	3.471026606991	-2.001007638026
Li	-3.581902181398	0.796288449701	-2.323023170186
H	-5.353255501840	2.535416359392	0.374434744119
H	-6.596569965908	2.133959137140	-0.818350906844
H	-5.545890963054	0.855857559280	-0.172865667150
H	-5.597533579801	3.807380478301	-2.390406892872
H	-4.361537894131	4.189053757228	-1.184622062700
H	-3.880242761624	3.647184499352	-2.808750850195

Cartesian Coordinates for (*M*)-(*S*)-187a

C	-1.124235795124	-1.729688121041	-0.353746150902
C	-1.349518256152	-1.472502522594	1.010204955561
N	0.101098820493	-1.647917052237	-0.965092134524
O	-2.485189881997	-1.707333489895	1.589363163101
N	-0.268476922249	-0.954031848554	1.773621166505
C	1.069108707678	-0.820200894501	-0.690883171410
C	0.153183677935	0.340611395885	1.343354554016
C	0.910959458705	0.392311386374	0.156888181700
C	2.350971127080	-1.036309836314	-1.421152501811
C	-0.157757903428	-1.382260778370	3.160671688309
C	2.372183704909	-1.771900434983	-2.620898174975
C	3.575929600028	-0.566363049902	-0.915393956576
C	1.386472343887	1.636591081973	-0.297375308277
C	-0.175704997743	1.534330892579	2.030445469587
H	-0.048715950907	-2.472264102277	3.183839609068
H	0.749377438024	-0.942238034858	3.584797713216
H	-1.015566960270	-1.120016304776	3.791522355369
C	4.773702898144	-0.810367607962	-1.588773181543
C	3.565649247782	-2.009747674523	-3.294880306787
H	1.431962087041	-2.154625644942	-3.003031559701
H	3.591738985526	-0.017507590733	0.021396090404
H	1.965540760184	1.671762195100	-1.215627007716
C	0.341756248678	2.742160799224	1.553284898551
C	1.130503661736	2.816908807961	0.396763204440
C	4.775936235691	-1.529029845826	-2.784187197245
H	5.708009674136	-0.442189107985	-1.171683646095
H	3.554526499925	-2.573139345223	-4.225096174972
H	0.113633995797	3.657159824470	2.098776605263
H	5.708187112313	-1.717769748538	-3.310422746304
C	-1.073078677543	1.544945223812	3.249390804864
H	-1.926260717127	0.870171845531	3.126078770047
H	-0.548089891536	1.229722428725	4.159564341267
H	-1.455042356602	2.555295694931	3.429617696273
C	-2.173531068486	-2.522086753352	-1.123558326132
H	-1.667908411306	-3.043870923122	-1.940873878078
H	-2.680172030333	-3.260110491640	-0.489371717209
H	-2.960857340650	-1.915035692363	-1.617685216744
C	1.682881622434	4.141868216858	-0.077472246523
H	2.053417747313	4.074897887072	-1.105458733497
H	2.519418687823	4.475007052891	0.551306909884
H	0.923519888094	4.932558895095	-0.043569531121

H	-3.591880539453	0.973988265680	-1.472375843636
N	-4.109673052983	0.872934947617	-0.597808784723
C	-5.545661173083	0.782941092988	-0.924993761100
H	-6.113242681078	0.605006113672	-0.005861505082
H	-5.929953105128	1.700808194367	-1.393736131015
H	-5.716488826981	-0.057423263863	-1.604520571798
C	-3.803494502799	2.052175763456	0.240629609438
H	-4.293203042161	1.936684418025	1.212896149408
H	-2.723714740130	2.116514335804	0.402314558252
H	-4.155251519950	2.989673190265	-0.214145474074
Li	-3.263214861799	-0.772539116794	0.257162467960

Cartesian Coordinates for (*P*)-(*S*)-187a

C	1.358128915768	-0.307465579344	-1.368625884781
C	1.336922219943	-0.359709927998	0.035292351620
C	2.565112054106	-0.471563539171	-2.076914599430
N	0.113625399598	-0.110610264042	-2.059133014690
C	3.721506367293	-0.783918204141	-1.355617712116
C	2.526248719618	-0.668209579423	0.719031606957
C	-0.334891979365	-1.068750679817	-3.063911315997
C	0.145687583698	0.108286195959	0.793532398088
C	-0.493523139343	1.135045456924	-1.995431152526
C	3.720408807030	-0.904151690349	0.039143401441
H	4.652768765990	-0.928254612035	-1.900860659431
H	2.513515964743	-0.703796340392	1.804429067252
H	-1.427297678463	-1.139716242926	-3.045002540190
N	-0.526729470951	1.177738315674	0.457357539565
C	-0.191895215407	-0.516344538421	2.101403773076
C	-0.510568990642	1.828542695257	-0.754093055000
O	-1.213373345079	1.528373401917	-2.993143585373
C	-0.793677921316	0.237719903548	3.127591378755
C	0.035135718186	-1.884316465585	2.337864488279
C	-0.324896553364	-2.475185943734	3.549621596515
C	-1.147679067059	-0.351206723787	4.337505220464
H	-0.969799088631	1.294654937626	2.955284510937
H	0.489333684279	-2.489967173445	1.558958614408
C	-0.917674008231	-1.713517549436	4.557176392697
H	-0.144412132145	-3.536448752302	3.703076457456
H	-1.599304715781	0.255815085565	5.118869724491
H	-1.195169455262	-2.172499066361	5.502507449926
C	-0.945615378197	3.281891050753	-0.726760310569
H	-0.392229176936	3.833931929760	0.040348289728
H	-2.016814706137	3.456880390452	-0.469740342563
H	-0.754127461996	3.761389184920	-1.691700803794
H	-0.040606840441	-0.802576336549	-4.085732126618
H	0.084283585959	-2.047900342262	-2.816314874508
C	2.640520555015	-0.307169037369	-3.577708312996
H	2.327243183415	-1.211984280124	-4.113994653417
H	3.668380001672	-0.088795823620	-3.884441315092
H	2.000494154955	0.511547003642	-3.921951014803
C	4.983799770754	-1.269767028044	0.784308220144
H	5.167353241234	-2.352357432051	0.753090425636
H	4.924918778600	-0.979309981695	1.838234330562
H	5.862936556086	-0.781990330911	0.347864739456
H	-2.822662448378	1.111370368227	0.411744133131

N	-3.615824193882	1.040028399730	-0.238390022366
C	-3.876958640756	-0.395333192528	-0.454676876016
C	-4.776610413364	1.727622457548	0.349162462716
Li	-2.555306056148	1.845430942358	-1.782418421265
H	-4.228371488960	-0.898560862999	0.458119100208
H	-4.640390103588	-0.517504233671	-1.231142241796
H	-2.955830913816	-0.883246411354	-0.785885412898
H	-5.605266711553	1.726035238994	-0.367673477426
H	-5.125686824447	1.248356608270	1.276320721313
H	-4.514731810882	2.766563788235	0.571789899322

Cartesian Coordinates for (*M*)-(*S*)-188a

C	-0.233947506143	-1.384966471886	-0.523211597874
C	-0.324470689243	-1.266066570335	0.951820809880
N	0.995359343379	-1.006875877751	-1.133670212253
O	-1.068993005933	-2.034690308026	1.612043108051
N	0.394052487166	-0.288029637676	1.621235555595
C	1.664811471488	0.076092846389	-0.948012758744
C	0.504700787849	1.036358556468	1.073921044658
C	1.196091676649	1.230929054173	-0.133738439407
C	2.961325331825	0.192401140482	-1.686480347298
C	0.670458098249	-0.528911701471	3.039610162925
C	3.158512807847	-0.532757600527	-2.874436432557
C	4.026244459274	0.964896353395	-1.194403024340
C	1.334341836192	2.533203559767	-0.641595727541
C	-0.097201491127	2.136066414784	1.729810935289
H	1.087560459379	-1.533817599149	3.148322765427
H	1.416935690043	0.197356099448	3.368725956984
H	-0.212340463067	-0.459686025706	3.682038974477
C	5.246552314534	1.015671022650	-1.870107935293
C	4.372407442877	-0.475232929820	-3.552405244897
H	2.341498946827	-1.142716543024	-3.244620360928
H	3.903648483658	1.520026515136	-0.269145513885
H	1.860558610795	2.670491117804	-1.581282896566
C	0.092368583699	3.414474508182	1.197962194660
C	0.809532132156	3.641107843147	0.018838700188
C	5.424259883237	0.299950553819	-3.054098005945
H	6.059956256077	1.613308550229	-1.466036826879
H	4.500557655748	-1.036134095231	-4.475010482417
H	-0.364037056604	4.259286566196	1.710790502294
H	6.372408021530	0.343147978788	-3.583916713558
C	-0.982129370794	1.988120620832	2.948783470459
H	-1.652342964443	1.127212830841	2.856078590404
H	-0.413593028006	1.861231741267	3.877807044702
H	-1.602653731341	2.881369405423	3.068104816691
C	-0.558510893175	-2.824503238987	-0.983981082974
H	-0.445117738533	-2.864577089412	-2.070377458108
H	0.123935544471	-3.557583274801	-0.538485034102
H	-1.582412657554	-3.127772451446	-0.744392195775
C	0.993565469914	5.039941317877	-0.521613701662
H	0.055668600522	5.607099379264	-0.496798539169
H	1.350145509100	5.023740731749	-1.556204445713
H	1.726457350232	5.603667120114	0.070737313666
H	-1.328799256303	-0.808379247993	-0.843058055292
N	-2.877747032304	-0.611317482002	-0.776760524530

C	-3.487143859223	-1.031677752304	-2.027235408567
H	-4.585403273438	-0.873994695186	-2.044733424553
H	-3.090926251614	-0.486625783549	-2.906999117043
H	-3.311560998688	-2.101742945807	-2.202977225433
C	-3.093174193322	0.813360090270	-0.587618840078
H	-4.162357832866	1.071994158883	-0.447502063600
H	-2.554956916200	1.169127938628	0.301545466805
H	-2.740355879117	1.422366446249	-1.443278727635
Li	-2.804157486823	-1.808103063122	0.771833052169
O	-4.127060636595	-2.801762945969	1.733683055748
C	-3.777714547814	-3.679744126950	2.802594363868
H	-2.699674630014	-3.589835258867	2.942571322530
H	-4.300776787147	-3.389819977500	3.723742824432

Cartesian Coordinates for (*P*)-(*S*)-188a

C	1.827326684381	-0.695580730155	-0.492890504128
C	1.626098217225	-0.870842295635	0.886684743456
C	3.133640435724	-0.705140340706	-1.028620602450
N	0.697170609170	-0.482094759440	-1.351568336625
C	4.205635092098	-0.976377780976	-0.173499369246
C	2.738908163509	-1.116445081620	1.708624924690
C	0.506431659105	-1.307327749444	-2.545266829744
C	0.302844304546	-0.620931154812	1.532786791117
C	-0.014380693974	0.693239516681	-1.244865080426
C	4.032631169845	-1.195371048203	1.196286265274
H	5.210830777637	-0.991207608699	-0.591055155074
H	2.581536425002	-1.235342442172	2.776067220802
H	-0.566205256902	-1.443830757484	-2.711247483569
N	-0.495576449513	0.337598719714	1.224500952724
C	-0.078460747288	-1.445971770492	2.725124260444
C	-0.474362354654	1.188470417034	0.075708756451
O	-0.478242914980	1.209394715078	-2.302298657006
C	-0.906200716417	-0.898285276392	3.719729982098
C	0.316637769762	-2.787337305563	2.849700966841
C	-0.096610119018	-3.556727015140	3.938725561176
C	-1.308577096246	-1.662045113480	4.811231328629
H	-1.228839923860	0.131449126729	3.609823977091
H	0.941871575501	-3.235930859428	2.083325954251
C	-0.906149033970	-2.996363371802	4.926671234116
H	0.213078577944	-4.596340719613	4.010919067976
H	-1.940321111253	-1.216866474522	5.575922138373
H	-1.224144426708	-3.592841234981	5.777926070476
C	-0.133323578131	2.639210021972	0.431871558262
H	0.906204766782	2.743413284242	0.769574532313
H	-0.786329429390	2.983891035988	1.239942756440
H	-0.280253510795	3.291269659200	-0.435654817660
H	0.935898703632	-0.871782659123	-3.452890691322
H	0.961436667421	-2.284001739118	-2.363370297334
C	3.419002750417	-0.383369697879	-2.478874538473
H	3.237303647255	-1.235309743406	-3.145596125397
H	4.467995558415	-0.096135929830	-2.599685407082
H	2.798532336917	0.446189189759	-2.833689760346
C	5.211355127231	-1.500760821422	2.091033100607
H	6.105506209809	-0.949338154229	1.779437007347
H	5.464883747856	-2.569115668250	2.065250716434

H	4.999736838013	-1.241676197292	3.133416031633
H	-1.715747644099	1.309560300416	-0.220484379566
N	-3.150586802911	1.531577017037	-0.688820261664
C	-3.785051716850	0.242202536124	-0.472208955006
C	-3.763440316009	2.534822221965	0.162669799705
Li	-2.236802070777	1.844133654874	-2.338127959335
H	-3.737132579679	-0.092631771415	0.582259171342
H	-4.856442485440	0.239730455632	-0.754464228072
H	-3.291519080541	-0.532523073390	-1.078151705185
H	-4.837732110517	2.687913433800	-0.064785824457
H	-3.713350060629	2.281396089221	1.240537157589
H	-3.265003850918	3.505451437445	0.031603593450
O	-2.645078985634	2.615432850651	-4.054840041954
C	-1.651305750534	2.695802196269	-5.073711264884
H	-1.452088849360	3.743501491765	-5.337061086746
H	-0.749699301320	2.235989533219	-4.666149549437

Cartesian Coordinates for (*M*)-(*S*)-189a

C	-0.534167676474	-0.533237583579	-1.654398201303
C	-0.954959280423	-0.589360896281	-0.182728918843
N	0.796842283629	-1.140484189674	-1.726542325119
O	-1.833340649039	-1.365134461067	0.229741403908
N	-0.247205381952	0.200493850879	0.666273402501
C	1.809955254353	-0.493318587515	-1.262644732063
C	0.655923077583	1.210852723114	0.206080768178
C	1.707380812231	0.871930763118	-0.671813799774
C	3.147831843222	-1.147847938108	-1.367826728060
C	-0.460159652849	0.007818958939	2.112576298027
C	3.361821472175	-2.135270835164	-2.344569623710
C	4.191892614399	-0.837659498620	-0.482170959626
C	2.614061962350	1.868376364274	-1.067809148902
C	0.490608474539	2.542548535608	0.648528958303
H	-0.398418083905	-1.061824343684	2.333822794608
H	0.331092652908	0.531107988165	2.649847025173
H	-1.444983973316	0.389502960293	2.403799811973
C	5.419213438193	-1.495365696957	-0.572557600654
C	4.588986092801	-2.784540244128	-2.438317375926
H	2.548441885810	-2.379568909070	-3.019241501994
H	4.039821029680	-0.090209892856	0.290088011113
H	3.414928537312	1.602744668583	-1.751418276906
C	1.423366278292	3.492301294319	0.224980876847
C	2.493740072132	3.183094882773	-0.623851762567
C	5.623260596934	-2.466777157845	-1.552660672015
H	6.214102738581	-1.249315496713	0.126410097007
H	4.741880690501	-3.539674591150	-3.204840329294
H	1.291864703571	4.521446807685	0.554215238233
H	6.581101720194	-2.974832527078	-1.627062347441
C	-0.672175519848	2.976037358341	1.514066199404
H	-1.569564736600	2.366532157972	1.358681750494
H	-0.425663819873	2.916121992300	2.582117577739
H	-0.921977859253	4.020436441487	1.303444828620
C	-1.501288298941	-1.286419208032	-2.560120499437
H	-1.136840172847	-1.246885953105	-3.591202750810
H	-1.575065482484	-2.333207569886	-2.256050896400
H	-2.500095625160	-0.839636084412	-2.523377913102
C	3.470995987161	4.251371929137	-1.055128351532

H	2.954008778600	5.109192100040	-1.501554618201
H	4.183005381919	3.867562534705	-1.792035913438
H	4.046751443894	4.631831380355	-0.201969040831
H	-0.497454138775	0.527959162847	-1.949034136710
N	-3.822190831400	0.927557497840	1.862229204131
C	-4.440902932344	1.915092975212	1.011873631754
H	-5.522048998270	2.086471519616	1.229362589040
H	-3.976000110357	2.928338466050	1.077750458086
H	-4.379921287990	1.615416707391	-0.047832653469
C	-3.954292668473	1.343019359197	3.235065422728
H	-5.010210067935	1.481330221467	3.570035478648
H	-3.506828660602	0.600132277603	3.916600881887
H	-3.459065218386	2.318003815362	3.464449223701
Li	-3.386153464091	-0.764941932330	1.206695672009
O	-4.511351775623	-2.333898230983	1.414181557951
C	-4.259989482386	-3.670663045377	1.006030283160
H	-3.275125936926	-3.676844489827	0.536008160602
H	-4.264870650745	-4.350578988115	1.869841533830

Cartesian Coordinates for (*P*)-(*S*)-189a

C	2.055674673104	-0.214187990937	-0.555803984199
C	1.880430300750	-0.492348627058	0.814043913805
C	3.338742789092	0.090026048218	-1.061487376043
N	0.938710847239	-0.230721804949	-1.448998958500
C	4.426072267494	0.052772386821	-0.185809311146
C	3.006441406574	-0.511137858829	1.652616409199
C	0.971315563753	-1.106474167809	-2.631239285604
C	0.524938423404	-0.641483929073	1.426506300946
C	-0.218405509572	0.462335551089	-1.231789875831
C	4.288931721854	-0.253487322771	1.172712169285
H	5.411849970702	0.297978660363	-0.576299414739
H	2.862298230620	-0.714039031941	2.709293373494
H	0.045612857742	-1.685810643470	-2.668820404565
N	-0.489488871222	0.097428160197	1.149616474695
C	0.327560879783	-1.686084671101	2.480316943157
C	-0.446749050533	1.144235298415	0.119968121482
O	-1.105744591014	0.443135311912	-2.102189926971
C	-0.673863013007	-1.508656645648	3.449693001372
C	1.078010150939	-2.872397227228	2.495274102296
C	0.835554524164	-3.855124662845	3.456042562938
C	-0.907191535432	-2.485000587765	4.413578094438
H	-1.261875340132	-0.597657601098	3.424498634507
H	1.845023290816	-3.035745654010	1.744334549504
C	-0.153538066369	-3.662633340000	4.420676795768
H	1.419155516693	-4.771935800432	3.447307389990
H	-1.679415982094	-2.328529952683	5.162045986178
H	-0.338254345273	-4.424903021055	5.173028777294
C	0.453503125391	2.355544993592	0.435189628208
H	1.520746805320	2.130706392134	0.477115847152
H	0.147264969906	2.762430001474	1.403842925974
H	0.283467267493	3.132725758165	-0.317004947474
H	1.054777938276	-0.534661228370	-3.559578474172
H	1.819759155940	-1.784627367255	-2.537779003042
C	3.560336438768	0.518574122269	-2.494874173534
H	3.596442999476	-0.329158233605	-3.189636354661

H	4.511190593095	1.051602476386	-2.585456083730
H	2.764254267347	1.186966397427	-2.839529657339
C	5.491923633025	-0.290674464920	2.085261601413
H	6.161800613610	0.556482665192	1.899470392120
H	6.078538281150	-1.205829438684	1.931448624322
H	5.195542964875	-0.263028456587	3.138202821320
H	-1.468459381359	1.544551855098	0.039640520251
N	-3.452665507314	2.617464450788	-0.803162719900
C	-4.411310397394	2.410433525621	0.251678896839
C	-3.007708613991	3.986169793581	-0.779767655764
Li	-2.820077100883	1.327813164892	-1.978209555604
H	-4.010326881626	2.609463079236	1.274529667897
H	-5.318569011117	3.056791502759	0.173954513172
H	-4.769093292344	1.367913039184	0.256757937511
H	-3.824297115608	4.732865088284	-0.927374766763
H	-2.519563747642	4.291647013998	0.178550209445
H	-2.270967377272	4.174027948223	-1.579355104942
O	-3.960275705489	0.711024572774	-3.434568867014
C	-3.797921179445	-0.317236143801	-4.395331413984
H	-3.844656053678	0.087488766020	-5.416759659162
H	-2.814806791186	-0.761117035824	-4.224480851943

Cartesian Coordinates for (*M*)-(*S*)-190a

C	-0.496896220242	-1.348309836856	-0.567809476124
C	-0.690701587996	-1.041412897974	0.786591597306
N	0.719973701883	-1.329775142476	-1.194325439308
O	-1.776964135214	-1.305194774548	1.441942338760
N	0.411721915420	-0.517474969422	1.510174463496
C	1.733694497970	-0.540635154550	-0.970041312164
C	0.909111620457	0.731842756595	1.031313882701
C	1.655694332048	0.704738485175	-0.161735192020
C	2.983722082290	-0.846238515386	-1.722480378828
C	0.593949494214	-0.940122545617	2.888471027911
C	2.936667711986	-1.623968262735	-2.895394530686
C	4.245961067078	-0.425672818065	-1.265662569326
C	2.199525840362	1.907218564947	-0.651126818242
C	0.674500783993	1.956461614731	1.698785995956
H	0.650015502946	-2.034364124187	2.921521302273
H	1.547726162858	-0.542135980291	3.247865604542
H	-0.202900479210	-0.627123409840	3.576156601399
C	5.411103948897	-0.756645691632	-1.958955775436
C	4.097668444889	-1.949088851981	-3.589038076815
H	1.967485033879	-1.968905378427	-3.239381205001
H	4.315972178063	0.153983896595	-0.350047680550
H	2.766056831574	1.886150063477	-1.577652582038
C	1.259667422735	3.119086331956	1.190194931003
C	2.028756471396	3.116782411997	0.018794808868
C	5.345269209266	-1.516450799139	-3.126949413983
H	6.374059773526	-0.423912805311	-1.578240886732
H	4.031770833344	-2.543247767929	-4.497849721317
H	1.101175427770	4.057862641217	1.719791674472
H	6.252215367257	-1.773015924183	-3.668680439884
C	-0.186274295400	2.040686289846	2.940591697924
H	-1.069106867733	1.397552788337	2.860889738841
H	0.350752953298	1.727453324249	3.844924154737

H	-0.520780001070	3.070846683226	3.103722826339
C	-1.580861110463	-2.103562753890	-1.312336091516
H	-1.103700813074	-2.727580380470	-2.074410727787
H	-2.159894873387	-2.753321849860	-0.642216899910
H	-2.299081982508	-1.459701934064	-1.847295615100
C	2.652555081378	4.393722047066	-0.497495415007
H	1.944709550351	5.230989220782	-0.465665412822
H	2.993854888870	4.281024431593	-1.531607498600
H	3.522886203012	4.687628464356	0.104693544274
H	-2.313034541272	0.706029512474	-0.741477274646
N	-3.266076066243	0.925613349832	-0.434900097876
C	-4.141054768062	0.970105677905	-1.616744943318
H	-5.175305006804	1.140298052239	-1.295935454177
H	-3.867477680470	1.773005123925	-2.318159187441
H	-4.095706683873	0.014266563894	-2.146381278782
C	-3.226569743433	2.222677513350	0.263009071317
H	-4.211558260959	2.433296548223	0.695210707761
H	-2.490998931532	2.179747790542	1.069646435642
H	-2.961473134266	3.054649475946	-0.406740306888
Li	-3.347414830188	-0.698132801320	0.847408391712
O	-4.857743040196	-1.602778070566	1.614438405666
C	-4.509455395058	-2.706317201869	2.460171861789
H	-3.420031001251	-2.764318901983	2.456756059629
H	-4.879099706061	-2.533466850206	3.479290537336

Cartesian Coordinates for (*P*)-(*S*)-190a

C	1.940546764964	-0.468449812634	-0.850126173860
C	1.940601001423	-0.468481478509	0.554711188955
C	3.150505566583	-0.468433541189	-1.572639503228
N	0.669228642617	-0.502432350122	-1.520662746647
C	4.348606645266	-0.577499171804	-0.861111636447
C	3.171797588300	-0.573107641420	1.228932319504
C	0.374951819642	-1.559377638757	-2.480088698354
C	0.701083599619	-0.132548197593	1.299026529330
C	-0.106355320350	0.651043797181	-1.521893102806
C	4.379130069785	-0.650929899918	0.537610118869
H	5.285378797558	-0.598158990091	-1.415904627616
H	3.177822084922	-0.568988580256	2.314945592539
H	-0.693656811911	-1.796729029104	-2.455054207746
N	-0.106421283364	0.826146811899	0.911705950365
C	0.455934356244	-0.714372896608	2.643891247088
C	-0.203461145548	1.403803106046	-0.323520499208
O	-0.855947920634	0.882551274587	-2.546545403538
C	-0.278539276195	-0.005860014655	3.616047270851
C	0.905157117040	-2.006000774321	2.977882376939
C	0.638629341766	-2.562379665362	4.229369300189
C	-0.540937579216	-0.560333775453	4.864562215728
H	-0.630711949888	0.990125100114	3.367960030402
H	1.460366658902	-2.581712317105	2.242864898785
C	-0.084878210492	-1.844458501940	5.182228320460
H	0.994317086694	-3.564770532530	4.456446103538
H	-1.099034881405	0.014525222138	5.600470223751
H	-0.290944888241	-2.276405254991	6.158178859262
C	-0.874285879978	2.761185914635	-0.358989207061
H	-0.370341797273	3.459654159442	0.319396202995

H	-1.934651481329	2.755586497053	-0.034202774611
H	-0.831805151444	3.187581954094	-1.366548594110
H	0.628559671799	-1.298844953764	-3.514759395385
H	0.938166503101	-2.451522133667	-2.191792650959
C	3.183544781092	-0.346366789196	-3.079298968397
H	2.997709239089	-1.304234180492	-3.582096832241
H	4.165371410173	0.007761560364	-3.409629994040
H	2.427561726530	0.359596478337	-3.438528849433
C	5.692584999845	-0.792720646759	1.272781240401
H	6.459834879504	-0.128694703712	0.857204439597
H	6.082820205681	-1.817162883985	1.202796342439
H	5.582789959912	-0.556219120354	2.336034195961
H	-2.321300929926	0.432243252758	0.629714203180
N	-3.115195486703	0.137904286596	0.049106085863
C	-3.029483920878	-1.327655879076	-0.080514861653
C	-4.359217290410	0.551333244626	0.713343437850
Li	-2.498727512614	1.078608267224	-1.722872561536
H	-3.198166371661	-1.844852144987	0.876169502870
H	-3.779301620682	-1.680148998527	-0.798639296855
H	-2.035247013864	-1.596701075984	-0.445843835688
H	-5.217460771182	0.288349212184	0.083431709716
H	-4.499647178398	0.067423828306	1.692356220318
H	-4.356177643352	1.635976620825	0.860942328646
O	-3.739554310172	1.881553329347	-2.981027145883
C	-3.155877226609	2.299098351426	-4.220708564748
H	-3.297927770834	3.378890362585	-4.361189275340
H	-2.094060226080	2.060244689809	-4.157385070194

Cartesian Coordinates for (*M*)-(*S*)-191a

C	0.721233962184	-1.134851858497	-0.611371559269
C	0.243056086967	-0.368832708145	-1.787526547281
N	-0.332397038393	-1.668529684920	0.201193519252
O	0.708043921577	-0.556341311066	-2.947361832192
N	-0.766021152832	0.550027340014	-1.644730559807
C	-1.278382296365	-0.993018054762	0.754533176476
C	-1.018688389921	1.230693445401	-0.405399355998
C	-1.359112809482	0.493677612472	0.741037328491
C	-2.295451062753	-1.768700058345	1.528663263582
C	-1.486578563248	0.951711840153	-2.858226999144
C	-1.959539883477	-3.022576987631	2.067907088357
C	-3.611467648464	-1.304955926269	1.689427111463
C	-1.655732711080	1.181314124573	1.928844204606
C	-0.928873904805	2.638732479317	-0.348187543521
H	-1.738446332635	0.058104767171	-3.434684266788
H	-2.407984510246	1.453417890098	-2.556843035175
H	-0.903675667027	1.616782343664	-3.502327807907
C	-4.560580616385	-2.067393276791	2.371930701056
C	-2.904066907483	-3.778551283229	2.755501406059
H	-0.947343761084	-3.387273271228	1.929836224573
H	-3.898613422138	-0.346762664498	1.266633369709
H	-1.906514064422	0.604549437532	2.813887811700
C	-1.255205095767	3.277762502829	0.851386497274
C	-1.628196038425	2.573310366820	2.000359091888
C	-4.210618728621	-3.305052221328	2.911630345829
H	-5.575718216264	-1.692979314469	2.477444521637

H	-2.621599182387	-4.741546705541	3.173642123443
H	-1.188468628216	4.363228179939	0.893705962018
H	-4.947575366579	-3.897253610355	3.447866904648
C	-0.446889835953	3.474789524050	-1.512986457855
H	0.394759300982	2.999087109340	-2.027699894627
H	-1.228240137731	3.650931114531	-2.262095178706
H	-0.112172923298	4.454146945969	-1.158269118857
C	1.623288334618	-2.306482653799	-1.038106467441
H	1.849616610719	-2.906401428572	-0.153096561726
H	1.142769798167	-2.957466307562	-1.778327965439
H	2.585249082041	-1.967234727348	-1.447683154758
C	-1.986433509149	3.298508505467	3.276454414438
H	-1.380260490217	4.201392569494	3.408664930697
H	-1.838941271057	2.660129617338	4.153307827284
H	-3.038960521383	3.612090896933	3.273465407669
H	1.571381920889	-0.392100898340	0.027252967947
N	2.800375316076	0.248022215173	0.639279530527
C	3.141953390412	-0.625025380372	1.756530361213
H	3.951084966033	-0.208318290039	2.385004072621
H	2.285970037283	-0.811660577116	2.433279595621
H	3.484123512189	-1.602647348399	1.390886643199
C	2.363854280474	1.541607352352	1.148706324314
H	3.159613429652	2.061746493550	1.714725951825
H	2.070258274015	2.200776623009	0.320507482947
H	1.494057270710	1.467317226685	1.828076015300
Li	3.863813575104	0.194024179604	-0.952392089437
N	4.232745691430	-0.054906026474	-2.859947723108
Li	2.470125017824	-0.647476109876	-3.348109028546
H	4.790754427379	1.113587044856	-4.583738335136
C	4.612670010533	1.206881139093	-3.492498999381

Cartesian Coordinates for (*P*)-(*S*)-191a

C	1.852395409195	-0.763438974273	-0.794082607837
C	1.852397040045	-0.763477934199	0.610865117174
C	3.072468769764	-0.763453169664	-1.505227924425
N	0.602392416619	-0.730451805485	-1.501575152717
C	4.265874067049	-0.856359313842	-0.783035460877
C	3.079680189113	-0.831512217100	1.291365537321
C	0.321928745181	-1.696193176449	-2.565805801052
C	0.610565636093	-0.516326096466	1.400115146552
C	-0.144578408315	0.426745318761	-1.448862877438
C	4.295458439646	-0.902312370145	0.613884454369
H	5.204550713657	-0.866610658665	-1.334059695330
H	3.075205927619	-0.817329176680	2.376660141790
H	-0.750401604815	-1.912796132033	-2.566458915065
N	-0.314408339693	0.317432218381	1.085621351962
C	0.468608556548	-1.187698891415	2.733217446239
C	-0.529983203696	1.012423682332	-0.147445067101
O	-0.684901335900	0.837327108117	-2.516554126749
C	-0.228155853940	-0.547696969762	3.771425354202
C	0.958638379372	-2.484171250542	2.955563994160
C	0.759768685434	-3.122475766755	4.180777759647
C	-0.415472574908	-1.179687898717	4.997592316079
H	-0.620178421965	0.447712008041	3.592433755898
H	1.486943247473	-3.001967470540	2.160414576246

C	0.076387471592	-2.471393720732	5.207915014879
H	1.137396591210	-4.130898068621	4.329533565977
H	-0.947981968219	-0.664522357554	5.793066962046
H	-0.073954641190	-2.965369438201	6.164327485811
C	-0.347544302184	2.525390142355	0.015490058511
H	0.695849235742	2.789875959954	0.228404695771
H	-0.962474991921	2.881320608850	0.848386143367
H	-0.656482630586	3.054257832750	-0.892600968363
H	0.600470607009	-1.346868378825	-3.564552642996
H	0.864578144803	-2.617415809322	-2.341183412845
C	3.139717939745	-0.616332623128	-3.009366129033
H	2.939576036424	-1.557189175369	-3.536377153518
H	4.138477184838	-0.284326685652	-3.308370692477
H	2.416515401734	0.121297038270	-3.372308182352
C	5.603187409508	-1.017421015798	1.361797782138
H	5.940959447280	-2.061095628283	1.413778550536
H	5.509123684971	-0.653736397288	2.389964854610
H	6.398283308133	-0.445129549857	0.870993648491
H	-1.792525500146	0.947194075001	-0.260876441422
N	-3.339826794344	0.841539490243	-0.215396973359
C	-3.479501936041	-0.565320251156	-0.571484568360
C	-3.641289526200	1.010757746061	1.205084581886
Li	-3.991455747568	2.115928815305	-1.466092747317
N	-3.595382807199	2.886912069623	-3.204015191140
C	-4.544064912176	2.525673402456	-4.252874482372
C	-3.431069930382	4.337297687142	-3.196884186967
Li	-1.952653094054	1.892931129938	-3.188312712476
H	-2.745145116633	-1.213459907447	-0.052877855632
H	-4.478442704751	-0.969656262824	-0.322821203883
H	-3.330102827919	-0.706005073683	-1.652040583303
H	-4.672408712412	0.692768889144	1.453912485898
H	-2.961785395758	0.435497930918	1.856893955249
H	-3.547224310485	2.068128719886	1.490646770663

Cartesian Coordinates for (*M*)-(*S*)-192a

C	1.564916608078	0.196917643042	0.641515733694
C	0.712649742069	-0.054742400481	-0.604047249662
N	0.914431660459	-0.555207090936	1.717841777161
O	1.058977674601	-0.823094268440	-1.506926072732
N	-0.513058227050	0.545501098145	-0.619423311276
C	-0.202010573629	-0.130805022430	2.201174999700
C	-0.934294047683	1.475258477918	0.384164345386
C	-0.862167653902	1.129474533454	1.750395911881
C	-0.825699306817	-0.932004681494	3.295167749834
C	-1.451562615680	0.125008082036	-1.673159529414
C	-0.021424550660	-1.773842214842	4.082039149319
C	-2.209615023551	-0.907432966955	3.530061928653
C	-1.336240690098	2.038882509010	2.710199172784
C	-1.439006057398	2.736195906312	-0.005692138907
H	-1.449778338447	-0.966662344510	-1.732398717826
H	-2.450841427298	0.469391935072	-1.406961122267
H	-1.168110728414	0.526639818172	-2.649908456418
C	-2.774700320655	-1.701800748781	4.528265239892
C	-0.585833380922	-2.559241519584	5.082348080689
H	1.045466799517	-1.799698100203	3.888689172033

H	-2.849992867022	-0.277985055721	2.920085601022
H	-1.268619181887	1.768986301919	3.759764966129
C	-1.901136191129	3.600043301352	0.988511429174
C	-1.867312129505	3.274972937469	2.350625735178
C	-1.964990279873	-2.525901129140	5.309934805705
H	-3.848867894643	-1.678264200859	4.690909575367
H	0.050184895079	-3.199663588411	5.687487710244
H	-2.279773201040	4.575090979540	0.687933988031
H	-2.404369835767	-3.140873470020	6.090781046978
C	-1.441418383473	3.194412876009	-1.446594173822
H	-0.533555240229	2.881741836824	-1.972970674374
H	-2.294115093359	2.798200782849	-2.011030604826
H	-1.501464839223	4.285535290716	-1.494225208795
C	3.003136586732	-0.274506924309	0.465481596855
H	3.552402176492	-0.115695081119	1.398526047583
H	3.032003188540	-1.338822853193	0.220417620933
H	3.501787030914	0.283544154876	-0.333743849811
C	-2.373920257511	4.246944470320	3.389925847465
H	-1.890521118715	5.226133786842	3.290455564227
H	-2.186288651629	3.881015346931	4.403737724825
H	-3.454232315756	4.409891446140	3.288542869167
H	1.547512936170	1.278252794327	0.851428792799
N	1.902516156270	0.124896661445	-4.720442895120
C	2.963481916794	1.073525373347	-4.439400062719
H	3.223857213119	1.720418977932	-5.304527211449
H	2.715400252370	1.777670378993	-3.612008568021
H	3.886657274605	0.551259557702	-4.143785946931
C	0.713522601051	0.854999830475	-5.106295059781
H	0.851648887427	1.496369969400	-6.003388731898
H	-0.114658347772	0.165044468684	-5.334884346858
H	0.343351242314	1.549049844894	-4.312865253607
Li	2.267514154429	-1.591055164815	-5.481286338940
N	1.983692438763	-3.002154151440	-4.230794031184
Li	1.612769151905	-1.272174490938	-3.248319770305
H	0.504640388821	-4.315461053112	-3.387134396303
C	0.823607055760	-3.867489361303	-4.354096393950

Cartesian Coordinates for (*P*)-(*S*)-192a

C	1.957683968201	-0.596226995464	-0.654284969761
C	1.959267541886	-0.611938650941	0.754901692495
C	3.177001930362	-0.577814774415	-1.366750409594
N	0.725276391955	-0.593855601665	-1.379761471742
C	4.370960329059	-0.632697521724	-0.644167663093
C	3.188327886197	-0.661281781230	1.432566738852
C	0.467257228947	-1.644070998920	-2.380918047685
C	0.707037510429	-0.450958457566	1.555138434615
C	-0.287816140738	0.289998262377	-1.151366592759
C	4.404903231667	-0.684872776174	0.753682872513
H	5.308956575256	-0.608412650610	-1.195365490956
H	3.182445171836	-0.661924121338	2.518055697751
H	-0.525303760827	-2.064340655615	-2.203853103954
N	-0.240137725860	0.373987885540	1.279342159937
C	0.550187109890	-1.258054454009	2.805045370910
C	-0.228232567731	1.207458953631	0.074148267211

O	-1.288081349660	0.273244010520	-1.883642738519
C	-0.243622826953	-0.763770782675	3.853464408081
C	1.130988921565	-2.529042906168	2.939387265238
C	0.925451709458	-3.285759349521	4.093595833452
C	-0.438094952904	-1.514927979058	5.008720392671
H	-0.703515707697	0.211797082775	3.739476025162
H	1.733250909164	-2.935536269659	2.132668884807
C	0.145580366970	-2.779218307722	5.133414779377
H	1.373330757953	-4.272360355643	4.177026963690
H	-1.047188348718	-1.114803102158	5.814832698377
H	-0.009137456782	-3.365474015827	6.035301449996
C	0.840937063284	2.318030749561	0.044803912037
H	1.866327127133	1.946405111292	0.022082956176
H	0.717846521850	2.936102522980	0.939544624954
H	0.678187229694	2.957926596780	-0.828962664902
H	0.492132087241	-1.249356517740	-3.399884164374
H	1.220302010845	-2.423842248345	-2.265688117604
C	3.231889161127	-0.434025224445	-2.871213387307
H	3.056141481725	-1.382098559390	-3.393136155617
H	4.217683672983	-0.073262351955	-3.178470766873
H	2.483379038313	0.278672758699	-3.233025106292
C	5.718090127657	-0.754961330452	1.496429610744
H	6.138661595205	-1.768464211341	1.462270743758
H	5.596579117593	-0.485181571620	2.549904579562
H	6.462894824325	-0.081748473003	1.057484011918
H	-1.197062271297	1.712851951290	0.053385243564
N	-3.651835542574	2.777684615522	-0.903066093565
C	-4.046948670946	2.500235938027	0.468089686748
C	-2.894524497335	4.015341111331	-0.930698457865
Li	-4.926345666152	2.434752079507	-2.300919820834
N	-4.405035748262	0.977918860740	-3.405379197359
C	-5.120329093290	-0.284735819646	-3.372887788925
C	-3.904920730931	1.199459160507	-4.750279015904
Li	-2.959215432099	1.196567309928	-1.997383900822
H	-3.185693466428	2.375464163056	1.161044047192
H	-4.672160228601	3.300584801161	0.919749578264
H	-4.630528541603	1.568119418562	0.524688575889
H	-3.460882204944	4.893043206721	-0.550462984631
H	-1.967509120778	3.983195360784	-0.313988129427
H	-2.580841233125	4.259045843313	-1.958032043257

Cartesian Coordinates for (*M*)-(*S*)-193a

C	0.229291868929	-1.399962706126	-1.372293496532
C	0.041250001625	-0.352039275363	-2.312751531097
N	-0.683283397304	-1.685974826470	-0.382476197189
O	0.599637979275	-0.336127795701	-3.467601719514
N	-0.886191108226	0.660082007568	-2.004891796121
C	-1.407537216859	-0.863633857923	0.323206275375
C	-0.730222789881	1.306678058293	-0.737468180970
C	-1.124514073803	0.593093568941	0.409596574597
C	-2.428691167285	-1.471704283742	1.222319465003
C	-1.580868036111	1.315642369261	-3.106554771069
C	-2.338384079095	-2.825220803129	1.598450452431
C	-3.540338921316	-0.737620947552	1.673561443479
C	-1.056614073252	1.230499716538	1.665118347610

C	-0.211616186429	2.617772142728	-0.621100663008
H	-2.043604919241	0.552125464424	-3.739208836407
H	-2.373046506387	1.941482384624	-2.686025156595
H	-0.937093941842	1.932604188883	-3.744511404094
C	-4.512204195682	-1.326304418390	2.483680657618
C	-3.304717993925	-3.410095987665	2.410658118468
H	-1.500482957887	-3.406674580709	1.228865208899
H	-3.652882275981	0.300213622765	1.374098868064
H	-1.372376363798	0.681550584087	2.547986920722
C	-0.181328877722	3.214988614949	0.643151473036
C	-0.610574091228	2.546247649857	1.797259934006
C	-4.398160910076	-2.663933395519	2.862176161346
H	-5.364617866814	-0.736819822638	2.812576867768
H	-3.206913725357	-4.455556740182	2.693650803112
H	0.191645493523	4.234234193501	0.728191515557
H	-5.153707560800	-3.123013545836	3.494383014755
C	0.305350354963	3.389366524674	-1.814448014826
H	0.871970867679	2.745889050602	-2.494512218347
H	-0.504918964723	3.841290774570	-2.399826987933
H	0.962591906011	4.200815729704	-1.486615123800
C	1.051435192820	-2.599514763337	-1.836580826461
H	0.855836649770	-3.436275304265	-1.160897286516
H	0.783743597882	-2.907576998548	-2.856996902860
H	2.141639723286	-2.435177864332	-1.840458609056
C	-0.602570553076	3.238842951135	3.141220105753
H	0.276203774057	3.883119512893	3.258230240099
H	-0.607440374873	2.517946770393	3.965265644427
H	-1.487771956889	3.877367457832	3.262687734594
H	1.329885660298	0.159313086182	1.648725603104
N	2.209066656372	-0.325557813599	1.456304460910
C	2.120699400871	-1.672920410719	2.048042816597
H	3.017036999621	-2.244298263564	1.781937875610
H	2.047037043204	-1.646993630734	3.146296546420
H	1.244017744224	-2.186443755982	1.645017795500
C	3.310382882673	0.462678867862	2.033128124166
H	4.266500429077	0.008377955292	1.753076626868
H	3.284257668069	1.478616884581	1.628970132278
H	3.262591004187	0.516732168532	3.132014139601
Li	2.218572169665	-0.401972327034	-0.597861711479
N	3.617638542202	-0.017165192684	-1.955764722866
Li	2.393938087337	-0.324741111124	-3.405786646314
H	4.845934333033	1.615227255265	-2.640282198628
C	4.084148026514	1.363075451855	-1.873674122770

Cartesian Coordinates for (*P*)-(*S*)-193a

C	-2.110708465244	-1.200230316740	-0.203385842255
C	-1.918686771225	0.131648919538	0.200964121538
C	-3.396268206032	-1.780336238461	-0.173663502274
N	-0.965179900800	-1.932195045457	-0.663301216063
C	-4.483317192462	-0.967294513818	0.156971695077
C	-3.043195957614	0.909972894769	0.536236834911
C	-0.979049460568	-2.597278453631	-1.961879268952
C	-0.553762830708	0.648073802845	0.455899126170
C	-0.061927579148	-2.369719473706	0.305868453758
C	-4.331848254919	0.383322278179	0.498127285869

H	-5.479633615414	-1.406565183677	0.158009350627
H	-2.897769359562	1.939308573480	0.850053612634
H	0.031897935008	-2.593691372744	-2.383390264806
N	0.389627361473	-0.061571860451	1.035355458416
C	-0.291636777980	2.102928576966	0.286049403378
C	0.395808381894	-1.422911469406	1.259485426581
O	0.447698049117	-3.543718574938	0.189863844219
C	0.493933936772	2.811385717702	1.217716782759
C	-0.815994489971	2.815525403349	-0.808352516647
C	-0.552072408985	4.175580614339	-0.976019688199
C	0.754229111256	4.171127731675	1.051529956433
H	0.882667012176	2.277106343583	2.079458579782
H	-1.432485801471	2.291869593851	-1.533638046011
C	0.236690608593	4.861146784135	-0.050263926818
H	-0.962262120996	4.699717407417	-1.835565307930
H	1.348610201624	4.699435279557	1.793321018840
H	0.438062335558	5.921261318983	-0.177821154554
C	1.204071331863	-1.875087308145	2.457309734342
H	1.149976576864	-2.963541107608	2.568879281311
H	0.807920900601	-1.437150832773	3.382515202856
H	2.267961601867	-1.585611160574	2.413738607289
H	-1.318512882664	-3.638149789028	-1.923370049619
H	-1.634398356568	-2.031006067656	-2.629456096582
C	-3.622170135406	-3.245508281330	-0.471194150382
H	-3.655250066812	-3.455451484154	-1.547790818092
H	-4.575977659334	-3.573922055060	-0.046552474204
H	-2.827208621086	-3.865429240034	-0.044391038087
C	-5.535795687001	1.232525350305	0.836213705597
H	-6.159688992414	1.412871879007	-0.049075571264
H	-5.237303622299	2.207691327252	1.233802607941
H	-6.174054530636	0.745979561490	1.583677301849
H	2.414346854632	2.312214983329	-0.218466692300
N	3.003329897868	1.614382548849	-0.674209464272
C	2.708578448637	1.652286219906	-2.116342448750
C	4.410542324044	1.938079148825	-0.393630811622
Li	2.395334249243	-0.197128207446	0.190840616967
N	3.576914912523	-1.804697604664	-0.127965383534
C	3.994749279037	-1.897327932602	-1.521046654169
C	4.770847648599	-1.831087680648	0.707487079442
Li	2.215754504958	-3.103064670299	0.275211467562
H	3.002780576696	2.605528295893	-2.583468644649
H	3.247088980954	0.842406982576	-2.618017067530
H	1.635118486560	1.509485769562	-2.269695110689
H	5.051887608425	1.153509045766	-0.805767395862
H	4.719503427359	2.902747841651	-0.827249687001
H	4.570835514846	1.974641355900	0.688647575256

Cartesian Coordinates for (*M*)-(*S*)-194a

C	0.287148433134	-0.963636027923	-0.659592770140
C	0.671496466554	-0.860418737039	0.776934228870
N	1.377497372145	-0.692147374502	-1.553265092822
O	0.413470082554	-1.764383106154	1.608800802830
N	1.375928308461	0.235768626747	1.217062630745
C	2.068425024789	0.393985702662	-1.593537896797
C	1.341392394684	1.504545306792	0.550507178708

C	1.765053406040	1.607041144228	-0.785564629618
C	3.186325436186	0.442509313156	-2.585568056180
C	2.077158338045	0.107862606781	2.498712304399
C	3.147918803372	-0.381355418641	-3.724186108191
C	4.317306507296	1.252051500883	-2.388319723911
C	1.780675607484	2.870885680535	-1.397997505587
C	0.894135330401	2.648988359531	1.246901531625
H	2.617744463955	-0.842026647896	2.516186478752
H	2.794281868084	0.926903354483	2.579854741092
H	1.402217252375	0.126588208236	3.359843053337
C	5.372755244482	1.243236163429	-3.301639284476
C	4.196946509155	-0.383996344850	-4.638373935945
H	2.281278145220	-1.017748882992	-3.867313652650
H	4.377876660760	1.884257134446	-1.507464997152
H	2.097209713645	2.941541698064	-2.434176289192
C	0.949155815460	3.886975360303	0.600190935698
C	1.394955984839	4.024718631446	-0.718419646078
C	5.316155876208	0.429127293007	-4.432790266872
H	6.241794215122	1.872127965618	-3.124537700918
H	4.142648609332	-1.021335480205	-5.517607817266
H	0.607818757870	4.768756506799	1.139720372597
H	6.135298580307	0.425516033251	-5.147309802348
C	0.314010446880	2.577443590135	2.642448662247
H	-0.330276724869	1.699949542115	2.764272573636
H	1.084169473855	2.523257135507	3.421563314983
H	-0.286637067280	3.469553029288	2.845229500714
C	-0.259467131550	-2.362979293320	-0.985522201994
H	-0.416501797383	-2.426706905616	-2.065241901016
H	0.433474433387	-3.161695529801	-0.693683926800
H	-1.231574164578	-2.537159889439	-0.509018586148
C	1.451291534231	5.380858087098	-1.382128906139
H	2.365305029291	5.923022399234	-1.104642335800
H	0.602227905190	6.007624360913	-1.087193203120
H	1.442889777454	5.291872318223	-2.473020942899
H	-0.734866648985	-0.248663122798	-0.817314924957
N	-2.189254134495	0.326930367399	-0.963415391649
C	-2.735768048647	-0.293166642229	-2.161378875365
H	-3.695364626439	0.164546832633	-2.480472525392
H	-2.061199764832	-0.218666522002	-3.039873658735
H	-2.929081201368	-1.361515437537	-1.993874847358
C	-1.995932342553	1.741862615937	-1.222565489245
H	-2.946881974891	2.275011415743	-1.433890261009
H	-1.530087314254	2.234734977036	-0.359526222683
H	-1.340828645892	1.941146224426	-2.094973153939
Li	-3.054653288752	-0.350613060770	0.689033404876
N	-3.071340875333	-2.100639611860	1.691034996071
Li	-1.198292142549	-2.717404355523	1.768107533629
H	-3.477800371620	-2.932750476055	3.641693817852
C	-3.495812260161	-1.971676610161	3.077071219098

Cartesian Coordinates for (*P*)-(*S*)-194a

C	2.571437053475	-1.214148430265	-0.175901565772
C	2.383632865026	-1.466794322381	1.193257200777
C	3.873020424166	-1.018333160827	-0.689299380072
N	1.429279431869	-1.126833660871	-1.039824302078

C	4.962186558857	-1.167915965440	0.173355164531
C	3.509841465185	-1.581938780472	2.026028082388
C	1.361726712961	-1.920718700967	-2.264326011123
C	1.027817925415	-1.446419097785	1.814641097716
C	0.598732555078	-0.025579654610	-0.909216546829
C	4.806921117813	-1.457870276489	1.532650000011
H	5.964171715273	-1.025404141886	-0.227774067367
H	3.358377096918	-1.762288247921	3.085620156833
H	0.311170050407	-2.136773880495	-2.480649563325
N	0.089079701387	-0.622885688398	1.514786689599
C	0.756472977830	-2.367694921695	2.966586069636
C	-0.000695975773	0.288299076008	0.411726778747
O	0.192323766670	0.553005758824	-1.948619943028
C	-0.162844220023	-1.993750207498	3.960942725451
C	1.348563450728	-3.638043954037	3.047894319665
C	1.035373451154	-4.507026176692	4.094428957145
C	-0.466177744546	-2.855863715052	5.010788758698
H	-0.634651164298	-1.020141487913	3.884216628255
H	2.048726714361	-3.954186627527	2.280310252339
C	0.131091818002	-4.118022637619	5.082683731490
H	1.497037557350	-5.490498138677	4.133281741936
H	-1.172517780121	-2.544349102034	5.776313979865
H	-0.109399261460	-4.792098111301	5.900810367528
C	0.085924416048	1.745808766271	0.878171662312
H	1.077717090698	1.988824036356	1.279957161715
H	-0.650159340990	1.916014050840	1.672109431191
H	-0.130986517521	2.426987955807	0.049103585126
H	1.799544598454	-1.432673008014	-3.141872776906
H	1.885107503659	-2.864348518123	-2.088606381776
C	4.126226882141	-0.604132213443	-2.121784208085
H	4.083136260231	-1.449350988984	-2.820038936101
H	5.121670471960	-0.159005453776	-2.213626284020
H	3.392281223982	0.135718132635	-2.457553278365
C	6.008303005582	-1.622857046490	2.434111919967
H	6.790966095498	-0.893016485754	2.197705805188
H	6.454224197033	-2.620599787406	2.325367139295
H	5.737509984859	-1.499311327729	3.487474232280
H	-1.201520819946	0.221612751650	0.103690549064
N	-2.773493968161	0.131638609023	-0.146449608867
C	-2.824329855844	-0.840150016471	-1.222007133079
C	-3.206739572355	-0.504604585011	1.088354098553
Li	-3.032254150757	2.015992600698	-0.522554379580
N	-2.417781551456	3.035896015412	-2.126176575668
C	-3.651591834154	3.128279890219	-2.887437021485
C	-1.879297553239	4.371137692988	-1.948677912627
Li	-1.029907971556	1.767290917939	-2.686826187926
H	-2.079429597653	-1.660929224110	-1.114330040452
H	-3.809819160599	-1.341468111251	-1.297626354227
H	-2.632072657454	-0.359842412453	-2.192500902116
H	-4.239011946123	-0.907745489369	1.016459695822
H	-2.564078105031	-1.351070965524	1.394785737553
H	-3.191056094197	0.217840869083	1.915694788194

Cartesian Coordinates for (*M*)-(*S*)-195a

C	0.045907178641	0.328677578387	-1.733187072184

C	0.002831785657	0.353019944738	-0.201703281019
N	1.468537676688	0.223049674522	-2.071218268114
O	-0.311451409623	-0.614620985304	0.490116812982
N	0.444057769908	1.515269293125	0.379881061636
C	2.233473175922	1.247477124428	-1.911764346149
C	0.813418335467	2.672523151689	-0.371718327364
C	1.740882243883	2.571756524094	-1.431871671501
C	3.673691600334	1.090184244549	-2.274616174760
C	0.638390046961	1.490810929186	1.838531628047
C	4.049627838711	0.105425506405	-3.203858854190
C	4.675786438622	1.869080713812	-1.674887512476
C	2.132904876563	3.737791086576	-2.110154615336
C	0.257177160101	3.927674840750	-0.034471416577
H	1.134665047951	0.557662026623	2.114199183632
H	1.264064170999	2.337404759552	2.123064384836
H	-0.313220141024	1.534515323364	2.374929374171
C	6.018858138402	1.669911004326	-1.997005272288
C	5.388794149195	-0.086457757425	-3.529923873333
H	3.272935265904	-0.501321759291	-3.656694445882
H	4.406526480538	2.623023113061	-0.941739592657
H	2.839629291427	3.649058559999	-2.929791327887
C	0.685493951925	5.055203715969	-0.736248532927
C	1.626554230522	4.989951716419	-1.771810201210
C	6.379230966636	0.695394975300	-2.927778500637
H	6.782851751580	2.275159206942	-1.516392768321
H	5.662706669473	-0.846473843211	-4.256907796285
H	0.247882823184	6.018499891123	-0.480849321304
H	7.424742030458	0.544036541199	-3.182959647546
C	-0.824131063674	4.069578775949	1.012503877380
H	-1.547207125395	3.249410954060	0.952150009778
H	-0.423974936048	4.074395037797	2.033375230327
H	-1.364711398102	5.010042655355	0.871256814967
C	-0.734613468497	-0.836278580227	-2.327236654268
H	-0.597136607789	-0.843144539300	-3.413452527560
H	-0.390960654884	-1.788368173391	-1.918049245579
H	-1.802309661332	-0.737575106937	-2.107390368840
C	2.059416251024	6.238724495977	-2.503208612494
H	2.649288266619	6.896697633232	-1.852264002755
H	1.196198923407	6.819312545248	-2.849444504263
H	2.674613616194	5.997644081559	-3.375339228220
H	-0.371226851748	1.280411613822	-2.097997568894
N	-3.521395885824	-1.733991508408	0.601047420032
C	-4.266156480362	-2.415688639230	-0.431305236690
H	-5.364606085623	-2.217131945239	-0.400412452405
H	-3.960304671220	-2.141831408477	-1.468407357494
H	-4.147269531079	-3.507461080660	-0.345368808608
C	-3.760750351238	-0.313208698965	0.480414559991
H	-4.837062693922	-0.029149026541	0.557410326553
H	-3.230632441237	0.240399279032	1.271926877335
H	-3.423682749326	0.123117809677	-0.490970331789
Li	-3.439396396957	-2.410588054362	2.424133001754
N	-1.587983184773	-2.676284205209	2.961636171848
Li	-1.512709819681	-2.136771317157	0.954014451014
H	0.114228840607	-1.689437687601	3.836080893350
C	-1.001297449140	-1.707878629287	3.860091478856

Cartesian Coordinates for (*P*)-(*S*)-195a

C	2.984972624904	-0.259895951221	0.479572955428
C	2.692495295100	-1.375418497122	1.291233470988
C	4.227333010645	0.402137411664	0.610425960117
N	2.036559591056	0.214056258407	-0.475426121904
C	5.163911540168	-0.106327323714	1.512569265881
C	3.668414753882	-1.843013006390	2.186798714849
C	2.425715552933	0.346729461899	-1.889373602926
C	1.339115596889	-2.007017619305	1.320257122247
C	0.727290346417	0.498832415864	-0.181339452879
C	4.914133344771	-1.231762395135	2.306100017536
H	6.114747716435	0.413052116578	1.616379758572
H	3.430408087393	-2.696458041949	2.814148807722
H	1.656292963172	-0.117707404243	-2.510439639061
N	0.225605551638	-1.363908328190	1.309440082976
C	1.251255689826	-3.497152063545	1.427751208077
C	0.165468655125	0.095994484643	1.187235432325
O	-0.000567442351	0.991167319448	-1.045991382869
C	0.145420562913	-4.083888304124	2.064878162976
C	2.223757955619	-4.333602308737	0.857691483264
C	2.092533746558	-5.721372175755	0.920262508913
C	0.021700463052	-5.468518376743	2.136839913521
H	-0.608252290650	-3.434398299073	2.497039247116
H	3.078664094866	-3.897299167233	0.350257914495
C	0.994324897138	-6.292919128468	1.563496427171
H	2.848628404687	-6.354610384701	0.463820976309
H	-0.834370483084	-5.907385006175	2.642477548296
H	0.895713518041	-7.373797406759	1.618943544366
C	0.699644886140	0.883095495753	2.400063942530
H	1.769520706909	0.757934819419	2.573779322923
H	0.162887066571	0.548267998182	3.293321005746
H	0.486048839762	1.947876611781	2.262147515025
H	2.516435096650	1.393137277284	-2.192645731766
H	3.376199910616	-0.166758275025	-2.037778215756
C	4.545604739257	1.675143651879	-0.141421581347
H	4.870531295837	1.487985489907	-1.171794858419
H	5.353549408050	2.215693154767	0.360261180365
H	3.675264360009	2.337391828660	-0.192479925533
C	5.958290457452	-1.751697671674	3.265780376498
H	6.390845138313	-0.941725450198	3.864523602262
H	6.786251771144	-2.233231706062	2.729578562706
H	5.536116223920	-2.490885462041	3.953276324390
H	-0.894072343550	0.346044466715	1.098898024585
N	-3.184223440996	1.863096962489	0.152311056405
C	-4.376442070895	1.079180001159	0.393438435596
C	-2.720810243158	2.394042300273	1.412377480063
Li	-3.327111178997	3.173824588164	-1.296013833560
N	-2.386730187328	2.551918426215	-2.882699404629
C	-3.267924634683	2.341298767627	-4.007515152947
C	-1.185724258868	3.204384253454	-3.357242973698
Li	-1.982059290739	1.157297711701	-1.395819335924
H	-4.215537558532	0.214267955223	1.077732229206
H	-5.211241340956	1.656440432467	0.859990055081
H	-4.768879007234	0.666774573393	-0.549359114532
H	-3.465561839741	3.046574452159	1.931579982357

H	-2.467085119469	1.614872408862	2.170207311287
H	-1.814518401149	3.004032664063	1.270502607643

Cartesian Coordinates for (*M*)-(*S*)-196a

C	0.709469328193	-1.574010771742	-0.616569844520
C	0.347327783634	-1.345136379421	0.728571492301
N	1.904722822925	-1.202787061440	-1.157555778536
O	-0.577431726446	-1.998857237658	1.329393993899
N	1.136428012072	-0.458755501270	1.494040670852
C	2.649967156432	-0.163602416258	-0.886801185912
C	1.312796628050	0.860378055868	0.977902815605
C	2.170422231878	1.019884157035	-0.128660085126
C	3.979693620682	-0.118419938005	-1.556957771638
C	1.338573767351	-0.755723183261	2.903517536621
C	4.218035639438	-0.875977639832	-2.720206214829
C	5.053260120219	0.622181039269	-1.028505281225
C	2.427126405063	2.323364995329	-0.599240635217
C	0.676843669767	1.980586306063	1.560191660043
H	1.705996609032	-1.782889282345	3.004383955935
H	2.107172515950	-0.079760137268	3.290071720292
H	0.438678841865	-0.662432680164	3.525830704050
C	6.305371885186	0.619635498369	-1.644777622457
C	5.465033437899	-0.874869240981	-3.336491325313
H	3.401430022119	-1.468438282683	-3.118775588811
H	4.908968936234	1.194157520339	-0.116451595316
H	3.083521453093	2.448772507329	-1.455222001514
C	0.984890110281	3.256523450121	1.074480684791
C	1.865870332491	3.449308254248	0.000759623852
C	6.519518590282	-0.124705828264	-2.805033079182
H	7.117978788379	1.196652314732	-1.209198793935
H	5.618043944790	-1.462178038471	-4.239273033140
H	0.532209355567	4.123351881785	1.555001891878
H	7.494158855717	-0.126222623245	-3.286514853361
C	-0.308300592284	1.835959841708	2.699822042730
H	-0.969473491137	0.974892826692	2.553688919765
H	0.189190049815	1.690570541793	3.666894930722
H	-0.927013618199	2.735317302445	2.789073088461
C	-0.012347528724	-2.693860338667	-1.346940740907
H	0.300569049811	-2.713387581835	-2.394829397811
H	0.208114759735	-3.681915085837	-0.913508427808
H	-1.104448966615	-2.583626439917	-1.317530736560
C	2.203306706260	4.841690567446	-0.482931341098
H	2.972288602133	5.308379700297	0.147538028465
H	1.327959574525	5.501750185054	-0.460991977507
H	2.589097363520	4.826523218283	-1.507484935525
H	-0.919173062683	-0.148072642799	-1.450720515267
N	-1.696140345309	0.448698657979	-1.762571911293
C	-2.393354349392	-0.236045962907	-2.863603859462
H	-3.253797981502	0.365349264187	-3.181116154838
H	-1.747245104588	-0.394909764209	-3.740676237610
H	-2.761002259378	-1.207378816930	-2.521933577673
C	-1.112122015502	1.723010738269	-2.212827067459
H	-1.915068687348	2.431469951637	-2.447568501179
H	-0.487803988462	2.142225913059	-1.420043748645

H	-0.488278774395	1.602508675014	-3.111665586109
Li	-2.928528906892	0.495385470490	-0.086981605917
N	-3.858982912592	-0.978065076927	0.810534652355
Li	-2.371627519582	-2.250835992776	1.226424496716
H	-4.774447050124	-1.508849010447	2.690827669910
C	-4.374047339244	-0.635122274176	2.129309659578

Cartesian Coordinates for (*P*)-(*S*)-196a

C	2.456964314780	-1.144230441394	-0.399278866640
C	2.419085299889	-0.822468980349	0.968955290118
C	3.678113057835	-1.467691770563	-1.027439988370
N	1.206512346894	-1.145611218467	-1.109151193771
C	4.820717771898	-1.595889560003	-0.232919952136
C	3.598447913165	-0.958135028307	1.727509547904
C	0.834142605858	-2.291650195811	-1.929456322334
C	1.239032554058	-0.137883666579	1.545935717251
C	0.682231395981	0.112203217727	-1.443711996607
C	4.797006714389	-1.368519775602	1.149514716541
H	5.759086420667	-1.873727224736	-0.710638478292
H	3.573521252255	-0.712488071908	2.785064083079
H	-0.257423910186	-2.374296957122	-1.966322883481
N	0.567916379498	0.802899812528	0.914542995316
C	0.927470679216	-0.318450526328	2.989735454831
C	0.555860188670	1.082233398770	-0.420247279607
O	0.221923607558	0.286977310768	-2.626945311135
C	0.460076241712	0.751444431524	3.779844611472
C	1.051019318870	-1.578865327131	3.607407867265
C	0.714716975462	-1.762965159989	4.948662739847
C	0.126837903741	0.567573464458	5.119397332232
H	0.386238816201	1.733420710777	3.324310733992
H	1.409494821864	-2.420498521127	3.021342909076
C	0.247584411919	-0.692747105756	5.713891875698
H	0.814380155427	-2.749303301612	5.395733433649
H	-0.215428692320	1.415046134498	5.709365845305
H	-0.011767091724	-0.835244856695	6.759663887722
C	0.093223779427	2.468812153909	-0.823016258163
H	0.345310241489	3.192430711048	-0.041424102673
H	-0.990885490177	2.557177574815	-1.011503724438
H	0.592355310584	2.782125251433	-1.747014484024
H	1.194909199699	-2.240932774548	-2.963367742823
H	1.234009076650	-3.193847114489	-1.457288723349
C	3.789610517184	-1.663386041410	-2.523367712514
H	3.496682659483	-2.672316883870	-2.840974920379
H	4.824404650797	-1.509913642651	-2.846385676769
H	3.155044937679	-0.955299681106	-3.065763461985
C	6.048288017779	-1.540854328118	1.980293605327
H	6.914003401277	-1.060174974282	1.508814120321
H	6.301795853451	-2.601825716144	2.108896121690
H	5.926920804527	-1.109098282850	2.978960232855
H	-1.511309013260	-0.332604629783	1.768554953399
N	-2.293177870178	-0.794039772470	1.298302658774
C	-1.824514347529	-2.131603517406	0.900978185344
C	-3.424037355407	-0.872835987576	2.233615678849
Li	-2.615531644174	0.593992426026	-0.240135539207
N	-3.187154646072	0.378517096059	-2.117332571432

C	-3.583426680812	-0.998378828439	-2.381737578954
C	-4.282956626400	1.246717905456	-2.504941801538
Li	-1.497494002686	0.716781179311	-3.105761508801
H	-1.637978113856	-2.782433058636	1.769590667882
H	-2.577834122057	-2.608320909925	0.264957538758
H	-0.893351442822	-2.026933261189	0.339651601146
H	-4.281550920497	-1.329235372724	1.725788640646
H	-3.196112858177	-1.473918056813	3.127583035933
H	-3.710554478661	0.133982967416	2.550684386728

Cartesian Coordinates for (*M*)-(*S*)-197a

C	-1.141894870952	-1.359745560422	-0.334352627845
C	-1.016821001714	-1.473148845931	1.151433013602
N	0.098197700341	-1.359716518975	-1.045430885650
O	-1.789024877084	-2.184259316797	1.827095577463
N	-0.013822231186	-0.770878904662	1.804668397099
C	1.090366160686	-0.560648804504	-0.860002134021
C	0.460683426560	0.498794004130	1.338056238827
C	1.071936391557	0.595828057507	0.075999551357
C	2.297749152497	-0.780220754733	-1.715314320548
C	0.362577645393	-1.253589360570	3.135480500622
C	2.168048403167	-1.420900040832	-2.959941748226
C	3.584574072529	-0.412737773286	-1.288131510449
C	1.570772356248	1.838336554741	-0.348942881471
C	0.312195252698	1.652839370144	2.141532128872
H	0.483165773852	-2.339095997632	3.095139304410
H	1.317905812764	-0.799549537500	3.407579840013
H	-0.377933586285	-1.029495672755	3.910285178597
C	4.703857992160	-0.670832576572	-2.081047944284
C	3.283301398242	-1.671004385058	-3.753712073063
H	1.176253481135	-1.719161741905	-3.282319852683
H	3.712491311528	0.067764060664	-0.322703943545
H	2.029812972222	1.904427063504	-1.330624434734
C	0.848397535603	2.860065597833	1.685856110432
C	1.486471700302	2.978278875071	0.446958435107
C	4.558747081495	-1.296741805407	-3.319120608037
H	5.690997986631	-0.384600395966	-1.726369929723
H	3.159115067646	-2.158509740777	-4.717655136038
H	0.735604255952	3.744593626865	2.310418717710
H	5.429329417262	-1.493210497326	-3.939669155213
C	-0.448771044926	1.650856612985	3.449926703799
H	-1.360098108934	1.045839222211	3.383558738914
H	0.138852347540	1.256143712509	4.287535316885
H	-0.743337158049	2.671607422436	3.711814547525
C	-1.987721386896	-2.518912853729	-0.901280607294
H	-1.973682856185	-2.446958172066	-1.991600561526
H	-1.591255306918	-3.497851115975	-0.609524802204
H	-3.037970776699	-2.480631911214	-0.589060069636
C	2.056622020513	4.300620456460	-0.010083368862
H	3.015133308165	4.513814750767	0.481921237421
H	1.381669848284	5.131467164230	0.225426932274
H	2.234538074868	4.306166633425	-1.089991445847
H	-1.899179452303	-0.362572398046	-0.515654728797
N	-3.171370406812	0.581037462296	-0.580544581663
C	-3.691926060832	0.485093235538	-1.931929191151

H	-4.555230927080	1.160090040049	-2.114153940220
H	-2.944288742552	0.740474587441	-2.713417068343
H	-4.037401052849	-0.537669389470	-2.145006013764
C	-2.690465384180	1.931055214311	-0.357449575343
H	-3.498918325499	2.692004598382	-0.401316855085
H	-2.223977838150	2.018508064514	0.634466989164
H	-1.928818020168	2.259151954918	-1.096443348776
K	-4.088622050885	-0.956919861766	1.362428673835

Cartesian Coordinates for (*P*)-(*S*)-197a

C	1.581427285684	-0.569441243155	-1.027384435866
C	1.563523818391	-0.526129765061	0.377114589870
C	2.812849723716	-0.601424129165	-1.720217113933
N	0.342072599433	-0.551749229916	-1.747600812533
C	3.996106057996	-0.679527545940	-0.981139647813
C	2.782513114409	-0.581005911448	1.075131844546
C	0.076347586619	-1.538918381889	-2.793228053381
C	0.314019049659	-0.241857157260	1.142658421090
C	-0.410407835937	0.612709497313	-1.746888335382
C	4.006463242652	-0.680633803607	0.417385033799
H	4.941925735957	-0.712736429297	-1.519392780241
H	2.764081021958	-0.531946264350	2.159363228203
H	-0.994355920308	-1.766301695447	-2.795522731627
N	-0.582697825048	0.612486891506	0.799374668918
C	0.134748836552	-0.888907746875	2.483534367291
C	-0.761028240192	1.275443314171	-0.457918525738
O	-0.972584356425	0.965869771043	-2.810414394205
C	-0.614104657683	-0.241046094330	3.480576329937
C	0.640173520978	-2.170183740835	2.756035388921
C	0.411648770727	-2.782531567893	3.989537490351
C	-0.831931868069	-0.846888429136	4.714451718153
H	-1.025007119818	0.738046505934	3.259166563550
H	1.205772886435	-2.697067439812	1.993270566911
C	-0.320204278788	-2.121766778764	4.976026443168
H	0.804230972904	-3.779114242579	4.175967480330
H	-1.405622540613	-0.324808806919	5.476322015520
H	-0.494447051125	-2.595355860558	5.938842477889
C	-0.442876252078	2.772517817132	-0.363856405825
H	0.617904119177	2.953917731777	-0.145762763392
H	-1.035986049041	3.230588425372	0.434035768095
H	-0.683580863358	3.271426174622	-1.309738211452
H	0.352146067917	-1.204047448631	-3.798308011999
H	0.626454516655	-2.451930740052	-2.552571587253
C	2.899228758108	-0.498428653499	-3.227171139373
H	2.694534491428	-1.451345888220	-3.730603911397
H	3.904714728782	-0.184817443354	-3.524393972838
H	2.186401222724	0.235247833129	-3.617807493577
C	5.304681577775	-0.775007906324	1.184927072104
H	5.679866134207	-1.806891175104	1.209974214825
H	5.180330710105	-0.447170830099	2.221874497709
H	6.087674569797	-0.159414645319	0.727149195722
H	-2.018953500055	1.301306354222	-0.564961163083
N	-3.577788475733	1.373096346177	-0.613310366173
C	-3.920954042656	-0.022175552637	-0.404799397021
C	-3.991279336738	2.138086783865	0.548215051482

H	-3.450904734156	-0.460182525723	0.500213166075
H	-5.012993632427	-0.191297636484	-0.297490948943
H	-3.588274805829	-0.634795768203	-1.259747274754
H	-5.090139047911	2.114096736316	0.711765717545
H	-3.535707254090	1.781665733806	1.494939311546
H	-3.711735770815	3.195897104284	0.432530134426
K	-3.256548795495	2.032417788947	-3.091736154943

Cartesian Coordinates for (*M*)-(*S*)-198a

C	-0.482094225378	-0.943634959479	-1.883548778036
C	-1.144647824806	-0.985125217789	-0.501203456242
N	0.900172358680	-1.378964781029	-1.677148725540
O	-1.936289667367	-1.878465247128	-0.173403890502
N	-0.736795107234	-0.026501625525	0.380001968961
C	1.725175747709	-0.583663559384	-1.087932505642
C	0.128767993462	1.049234152531	0.008989516568
C	1.358815208268	0.788592135668	-0.634237101835
C	3.124928468260	-1.067946020994	-0.896986756909
C	-1.169784099584	-0.167541567037	1.786237120068
C	3.637699364794	-2.061331317378	-1.748250519344
C	3.933343942249	-0.591247174678	0.147086597786
C	2.217206707325	1.860100555156	-0.932174524585
C	-0.244719903391	2.378492344040	0.315727312986
H	-0.957455372833	-1.193777576303	2.105791176466
H	-0.576985272677	0.514808158476	2.395785322113
H	-2.250314379864	0.043897472748	1.911139469174
C	5.222129854532	-1.092592178633	0.333409148793
C	4.926291097199	-2.554247336853	-1.566116485910
H	3.005297285572	-2.434865375060	-2.546399486011
H	3.548367853037	0.163913614943	0.825147125303
H	3.156378219064	1.650005334646	-1.435269710199
C	0.647836960568	3.404503845792	0.000090834019
C	1.884074639115	3.174503540318	-0.617107922037
C	5.724182119583	-2.071387757543	-0.524403169311
H	5.831485527902	-0.718991592144	1.151996196366
H	5.311886598877	-3.316144389737	-2.238460619858
H	0.354044047424	4.427756591458	0.226720494295
H	6.730217081464	-2.457520580497	-0.383144301575
C	-1.583998893292	2.724042459611	0.925958374918
H	-2.380485633998	2.058075897614	0.584099729309
H	-1.573516567915	2.655466450638	2.020169703543
H	-1.859479262980	3.751203550495	0.668302443451
C	-1.175534689584	-1.866139084062	-2.879308547792
H	-0.635437864461	-1.848868651602	-3.830892801004
H	-1.189804383064	-2.891552010861	-2.502482070146
H	-2.207280566791	-1.543782202183	-3.056757078082
C	2.811528144648	4.321992463055	-0.941357595296
H	3.173291377364	4.811477599110	-0.028299912149
H	2.304636673891	5.090240972482	-1.537646612594
H	3.685691628808	3.982191539014	-1.505024668345
H	-0.515985352079	0.094986051363	-2.249667536854
N	-4.472814271986	0.146512643014	2.255985039827
C	-5.172201908038	1.214381762408	1.590374521315

H	-6.224916551533	1.370237143653	1.934972340871
H	-4.691930044744	2.219135409513	1.710768541621
H	-5.232655366871	1.034129391741	0.501124831978
C	-4.410553042065	0.450345026447	3.660966775486
H	-5.406019004513	0.540265651572	4.162031959399
H	-3.858900006535	-0.331271882480	4.211200893643
H	-3.895478619637	1.417944220455	3.892004163235
K	-4.196786817348	-2.080871322865	1.071098763858

Cartesian Coordinates for (*P*)-(*S*)-198a

C	1.728022468233	-0.180877033978	-1.098370460371
C	1.672588242163	-0.260604474574	0.307784910891
C	2.928660721439	0.194768404289	-1.740840239458
N	0.575560823133	-0.477469044533	-1.888439376602
C	4.061017163787	0.426641497214	-0.957327314066
C	2.838705906615	-0.011675169570	1.049397550087
C	0.658065600357	-1.522646841929	-2.919809974595
C	0.386796380740	-0.479396994262	1.038350458030
C	-0.665565682733	0.068950859387	-1.675697894057
C	4.045548208245	0.321767379060	0.438195499967
H	4.981260812651	0.726089739553	-1.455402494603
H	2.785297232765	-0.063206987951	2.132526056180
H	-0.176757475378	-2.216034665344	-2.790504300524
N	-0.734204335953	0.072146145794	0.735536015750
C	0.393790259363	-1.364580883576	2.245969452094
C	-0.890138624105	0.944539748929	-0.438509520454
O	-1.597691460302	-0.237945951168	-2.431501778193
C	-0.553990750800	-1.154881840527	3.261821909078
C	1.288774682365	-2.438912532431	2.370342463680
C	1.238575378533	-3.281644142407	3.481675399106
C	-0.595837413706	-1.989874661583	4.374642996900
H	-1.251138027015	-0.330623116756	3.155844854404
H	2.019369246593	-2.625495182761	1.589061052105
C	0.300217590410	-3.057052258789	4.489196466652
H	1.932763220740	-4.114526348711	3.557409343061
H	-1.328147059063	-1.807746604187	5.156776962936
H	0.265785650842	-3.708555273126	5.358482345023
C	-0.126618857188	2.282678278610	-0.388396144269
H	0.961001824017	2.193461887030	-0.387978155273
H	-0.434126443294	2.810513421742	0.519433798835
H	-0.431764672974	2.898274804472	-1.241030020509
H	0.598735282090	-1.105364379222	-3.929295481670
H	1.598663397398	-2.060542237254	-2.798956532486
C	3.005089019151	0.418660596613	-3.234527535103
H	3.114361738899	-0.515681738298	-3.798330572572
H	3.867439887115	1.046154619512	-3.477896074937
H	2.105555921836	0.919486480808	-3.608047492790
C	5.294274486536	0.576065287590	1.249173789161
H	6.000935436503	-0.259829790960	1.164144424135
H	5.061776297968	0.704100694051	2.310713003357
H	5.817678237865	1.476080430665	0.906680921800
H	-1.955003209977	1.233034091548	-0.471978276006
N	-4.082686001524	2.202415224729	-0.577249557113
C	-4.521541753977	2.332975762972	0.785926323274
C	-3.897053869646	3.517626127465	-1.128855448973

H	-3.809002119707	2.901293237804	1.435810970887
H	-5.497974863304	2.865135908713	0.912612647873
H	-4.646654066197	1.343912890923	1.258004082746
H	-4.821328055848	4.148129971769	-1.162646006942
H	-3.156467141597	4.143641269679	-0.568167994962
H	-3.527963524431	3.464838597805	-2.169551300349
K	-4.165249167388	0.168537734469	-2.057657222836

Cartesian Coordinates for (*M*)-(*S*)-199a

C	-0.876141769214	-1.885993298063	0.091464641950
C	-0.998179651458	-1.582253496656	1.472949373334
N	0.251403878257	-1.693811352178	-0.650511610296
O	-1.984905292297	-1.923785619976	2.203018506576
N	0.102049739161	-0.891047589034	2.066368401428
C	1.166625794564	-0.764631318606	-0.530468791660
C	0.318935484913	0.408410503213	1.518248946739
C	0.979571058246	0.468770296363	0.272863383719
C	2.356152910990	-0.892852816846	-1.417106746197
C	0.410089550605	-1.191009913350	3.456542320960
C	2.300570958394	-1.685237974472	-2.580297488091
C	3.583461226184	-0.280231679236	-1.102796890094
C	1.293781515596	1.732925325626	-0.265797783341
C	-0.100288855481	1.597807642186	2.160984305155
H	0.650385872101	-2.256589720130	3.541127989278
H	1.297166425716	-0.619054256430	3.744417729406
H	-0.400894254547	-0.978339986699	4.164777109549
C	4.700707981933	-0.437113323797	-1.924076025221
C	3.413369867988	-1.838107750835	-3.400823490089
H	1.365472787206	-2.182570633970	-2.814816650318
H	3.666932066131	0.312571039013	-0.196627255466
H	1.804451045144	1.780776100614	-1.223383139238
C	0.259179621102	2.827700378433	1.600465818323
C	0.970487914372	2.916883154193	0.395257696491
C	4.623146194126	-1.212643721477	-3.081001047815
H	5.637602624147	0.043233595474	-1.651285504408
H	3.339082920258	-2.449478062333	-4.297534145372
H	-0.028490023757	3.742251924411	2.118111354381
H	5.492878101585	-1.335087419858	-3.721540324077
C	-0.925629262934	1.573508930409	3.430182901492
H	-1.658105579078	0.759168761623	3.416262247819
H	-0.312802216065	1.424668414070	4.328128323683
H	-1.458638943299	2.522495943154	3.555870012208
C	-1.883540928615	-2.846650393760	-0.516408180449
H	-1.355759392702	-3.530435851636	-1.189442172745
H	-2.390196262995	-3.435870062246	0.257035854507
H	-2.663685825712	-2.368014843107	-1.142900738882
C	1.373586863538	4.261238996686	-0.167449120097
H	2.292234634780	4.633228042755	0.306294995821
H	0.598908827104	5.019297051822	-0.001690299440
H	1.565269410465	4.203417068652	-1.244028210715
H	-1.767993105871	0.437905685851	-1.292858275116
N	-2.690422579471	0.865278898631	-1.399790489986
C	-3.196871117756	0.522432638822	-2.735371474921
H	-4.223413938649	0.893276668911	-2.844084926322
H	-2.595122596129	0.956271843690	-3.550611598526

H	-3.208050318111	-0.565104530550	-2.858989973953
C	-2.536106554141	2.318012039099	-1.234689598562
H	-3.526036645010	2.790974266161	-1.220900407055
H	-2.029911072999	2.529417383770	-0.288591132157
H	-1.952217474768	2.783397628872	-2.045241531319
K	-3.647289200523	-0.618434005347	0.829465894635

Cartesian Coordinates for (*P*)-(*S*)-199a

C	1.627285494890	-0.411066267693	-1.266687355331
C	1.556008288979	-0.506753882157	0.133698246706
C	2.853876665026	-0.588337395335	-1.938886162204
N	0.407113278179	-0.157219727072	-1.979774672828
C	3.970839706426	-0.975939446912	-1.193359403219
C	2.708624316908	-0.892107156759	0.844287186348
C	-0.006382029617	-1.043299913087	-3.058620845228
C	0.363583755192	0.002394673855	0.850168998511
C	-0.114142080953	1.143975499843	-1.953778132562
C	3.913841338723	-1.152721928354	0.195535805739
H	4.915218881415	-1.134295157382	-1.711995545336
H	2.658486047759	-0.964610182189	1.926933764374
H	-1.100776872417	-1.125354391560	-3.075099556742
N	-0.247382060210	1.113360833095	0.503006365423
C	-0.052157826928	-0.608364387475	2.139132181649
C	-0.184912990565	1.789878520137	-0.680457987007
O	-0.668267094913	1.599641342790	-3.006265982331
C	-0.675336932109	0.163003357077	3.142095094765
C	0.109608471087	-1.985875950560	2.384066555024
C	-0.332684204623	-2.565963593025	3.573541039258
C	-1.114501038467	-0.416395164190	4.328831147835
H	-0.798181455411	1.227434240676	2.969635544946
H	0.578633456912	-2.606791892173	1.626134985099
C	-0.949204515550	-1.787516890631	4.554262084565
H	-0.199024805363	-3.633900553558	3.730229856843
H	-1.579151878610	0.206524194311	5.090231254505
H	-1.292714788937	-2.238997506412	5.481370503832
C	-0.583408551813	3.247984770386	-0.616035643113
H	0.113968698763	3.828820949928	0.001328834262
H	-1.576050225695	3.415013929381	-0.148178911515
H	-0.579845524836	3.692209111518	-1.617320156327
H	0.310248512472	-0.709323174604	-4.053816302561
H	0.406469459854	-2.037070947600	-2.865308025210
C	2.990704323181	-0.357885259138	-3.427445331277
H	2.661538559851	-1.221429908125	-4.019988342280
H	4.037329814785	-0.167460091976	-3.686036562045
H	2.396335682041	0.502414555588	-3.752330972448
C	5.135312131936	-1.597612414094	0.967541898098
H	5.311836502148	-2.675863072881	0.853117309852
H	5.026115343744	-1.396264669355	2.038193249045
H	6.040419348951	-1.086185617883	0.619041969720
H	-2.352534512509	0.791658793010	0.710779414742
N	-3.300720613612	0.524683542682	0.414027927674
C	-3.288411761318	-0.931666515253	0.211061833459
C	-4.236032914837	0.910584597988	1.477142430415
H	-3.135692426929	-1.494503379394	1.145114275956
H	-4.239812979622	-1.255387272630	-0.230869085153

H	-2.475308471407	-1.194104425685	-0.473458555308
H	-5.265826737343	0.696269714297	1.164443509234
H	-4.051648576983	0.378782013952	2.424601742000
H	-4.155062565287	1.986471544037	1.667430205236
K	-2.972471780630	1.917639388722	-2.016917670660

Cartesian Coordinates for (*M*)-(*S*)-200a

C	0.697112566301	-1.113989450810	-0.786778418433
C	0.685343442615	-1.076771980117	0.710138642858
N	1.994488946147	-0.923170677348	-1.362999296511
O	0.061000445192	-1.909922854839	1.396814529375
N	1.411904742727	-0.085825636328	1.357529706689
C	2.762309242839	0.095664752689	-1.185613347882
C	1.644800596582	1.203089238693	0.778828623330
C	2.376257459314	1.309016966382	-0.416544965206
C	4.089604664044	0.063539473953	-1.874230047114
C	1.783627994380	-0.333530739207	2.750633520304
C	4.264348426750	-0.730223179274	-3.021697955122
C	5.201492907956	0.762877139058	-1.375863947406
C	2.644874696305	2.583678260237	-0.942583931697
C	1.151565656214	2.365625877549	1.414405924945
H	2.101773364735	-1.374291537074	2.850362562881
H	2.620541706682	0.321740131835	3.004566624016
H	0.969061006651	-0.162652296874	3.462139019015
C	6.444184223872	0.676866889472	-2.005661955719
C	5.501531888995	-0.810011354411	-3.653453428860
H	3.409846413295	-1.282887526173	-3.397050497836
H	5.096624035089	1.369252194063	-0.481103014010
H	3.199788534667	2.655072020641	-1.873143544453
C	1.467066846429	3.611440525947	0.865811086084
C	2.214807676266	3.746986838661	-0.309076949467
C	6.600073822635	-0.106401360601	-3.149304571408
H	7.292267585528	1.220910667938	-1.596848313906
H	5.611431317788	-1.422369040531	-4.545315939224
H	1.090948257293	4.505414883368	1.360749293905
H	7.566370870770	-0.170237414397	-3.643176475717
C	0.260953466283	2.314337473227	2.637087299892
H	-0.485021588296	1.514991024489	2.565635407171
H	0.824636878171	2.151130116850	3.564266892803
H	-0.273560542729	3.263250153433	2.747832659092
C	0.155494836889	-2.459001216376	-1.304070871313
H	0.239865419545	-2.465054124132	-2.393889919809
H	0.726305501328	-3.306454689504	-0.906776753835
H	-0.897499986957	-2.617902844059	-1.051072297537
C	2.531350713936	5.112966174541	-0.872153730848
H	3.278871453572	5.635069364923	-0.260108893462
H	1.639473903171	5.749939500660	-0.903489336184
H	2.929384690881	5.042035584111	-1.889128402404
H	-0.175239446497	-0.291882417698	-1.175424075698
N	-1.509337307966	0.448612663292	-1.627210146540
C	-1.779181427935	-0.022674596255	-2.971889082222
H	-2.649796243243	0.486232641127	-3.443488779771
H	-0.933733807538	0.125822131207	-3.678732105823
H	-2.007495170986	-1.098990592662	-2.969202630700
C	-1.186347999135	1.860092253182	-1.683753392409

H	-2.040732008778	2.486448286285	-2.028079713100
H	-0.901877524017	2.231630963736	-0.690062356157
H	-0.347530113814	2.103296203172	-2.370487965791
K	-2.527743420456	-0.946667186221	0.505383071815
O	-5.050430672628	0.153150057017	0.098072400856
O	-2.696881812208	-0.256355938754	3.157069524119
C	-4.897717242526	1.041175787241	-1.011219296049
H	-5.191372904401	2.064118857682	-0.732320981484

Cartesian Coordinates for (*P*)-(*S*)-200a

C	-0.817983495238	1.360728515037	-2.534888558306
C	-0.429083345573	2.616231995776	-2.036476563496
C	-1.838593723692	1.270906828550	-3.508541871683
N	-0.190350476105	0.177952809606	-2.025180982294
C	-2.380686215414	2.451334505240	-4.023802825679
C	-1.023180911160	3.773815638713	-2.567723621350
C	0.357787654688	-0.823565551857	-2.937003780686
C	0.462798215948	2.747323050590	-0.847412096508
C	-0.474418836679	-0.208783021907	-0.720326579664
C	-1.981996801580	3.715118890553	-3.576852602723
H	-3.160190191248	2.377218047294	-4.780383519889
H	-0.728690787185	4.739716676238	-2.169125758890
H	1.218712742839	-1.297465366373	-2.456107056928
N	0.416011850413	2.001808397948	0.197614408583
C	1.406454368685	3.911588670556	-0.788414542543
C	-0.284862014699	0.765766141025	0.398039387099
O	-0.670967980278	-1.419896779894	-0.474364184431
C	1.773601250683	4.453995382868	0.454727801335
C	1.996625303017	4.440695140705	-1.947289158896
C	2.920044048953	5.484556954612	-1.867860779190
C	2.685628806398	5.502486902955	0.532840913820
H	1.335227450337	4.027605479983	1.350528392121
H	1.741733592207	4.023933363345	-2.917241282874
C	3.264509136454	6.023740316467	-0.628417436402
H	3.372479516533	5.872661153050	-2.777164266253
H	2.949464277247	5.914630622566	1.503766020887
H	3.979650763109	6.840047043297	-0.565549816156
C	-1.481692283808	0.944617552531	1.342057229750
H	-2.263456929377	1.575394686101	0.898505799012
H	-1.146662516366	1.420182377171	2.269347197437
H	-1.921034368130	-0.027414269630	1.590024459970
H	-0.350775139669	-1.611430564817	-3.214969466804
H	0.699188647978	-0.314498244534	-3.842084591997
C	-2.402538663450	-0.054314737714	-3.972020585412
H	-1.775154587120	-0.541569743099	-4.728713300920
H	-3.390946740529	0.094067561492	-4.418081991995
H	-2.508516655974	-0.755346931076	-3.137585037303
C	-2.579016001121	4.972400373996	-4.165392466566
H	-2.103613388704	5.230429618015	-5.121328608815
H	-2.448840668047	5.828178619782	-3.495254123253
H	-3.651201439040	4.855326699893	-4.360677650038
H	0.493734660785	0.132605568450	1.115606167087
N	1.539879647069	-0.573973356663	2.132905364244
C	2.690105125210	-0.662931620920	1.255380954896
C	1.796922911626	0.439940557813	3.136609980864

H	2.916603343189	0.282322098292	0.714629734014
H	3.627364746296	-0.934912342323	1.789826951754
H	2.532003973014	-1.436595957530	0.485387036486
H	2.669884117971	0.195577253027	3.784994456612
H	2.008964075734	1.443970666730	2.714519104357
H	0.929164948891	0.546787781097	3.805022898453
K	-0.090742100272	-2.670112946017	1.840651071490
O	1.067797650166	-4.015923615260	4.003276744112
O	-2.846799646696	-2.863004756606	2.134011156892
C	2.131255128699	-3.151479121679	4.408619832044
H	2.128714567771	-2.302594544653	3.713753745886

Cartesian Coordinates for (*M*)-(*S*)-201a

C	-0.640229922491	-0.522997072369	-1.168536621416
C	-0.024608311492	-0.462871310594	0.233428396959
N	-1.790005597799	-1.424722291119	-1.033329198852
O	-0.171530512229	0.479614771681	1.016052981602
N	0.644429692193	-1.599873397177	0.616404555276
C	-1.586508760297	-2.691350057580	-0.908767867218
C	0.858824572002	-2.711880459286	-0.256405369150
C	-0.228088986206	-3.307741144259	-0.931565159781
C	-2.786587311295	-3.570423875248	-0.777090786590
C	1.057391160445	-1.686501563991	2.021555419925
C	-4.023798922678	-3.135170182359	-1.281834005792
C	-2.727157301872	-4.807387833428	-0.115554024080
C	0.002159271802	-4.444827874614	-1.723713068459
C	2.165829471603	-3.221973087675	-0.423916726527
H	0.225822811106	-1.368554439878	2.656194981546
H	1.310678685664	-2.721986434241	2.251116674981
H	1.916998765674	-1.043125002527	2.232999340120
C	-3.873006912142	-5.589420894291	0.035337289286
C	-5.164099248929	-3.919677421934	-1.137337966843
H	-4.067609373558	-2.174725659264	-1.784057168363
H	-1.783281479050	-5.153403914962	0.294266943293
H	-0.837592227393	-4.893429918480	-2.246160871505
C	2.338338587126	-4.357584144134	-1.216250348717
C	1.274265342096	-4.991459842426	-1.870992937733
C	-5.093731901463	-5.150725890373	-0.477992218048
H	-3.810154374423	-6.540746977789	0.557181205163
H	-6.111437292622	-3.572853546641	-1.541868161378
H	3.346718195097	-4.744386492788	-1.350868030630
H	-5.985022870704	-5.762543638820	-0.365943215113
C	3.373348907205	-2.530875093142	0.167217713916
H	3.302147974036	-1.444635830763	0.043316502496
H	3.497467171602	-2.734846022842	1.237756147722
H	4.284152943506	-2.868503205796	-0.335545979032
C	-1.058369850697	0.842852685212	-1.691054615872
H	-1.510267380138	0.727217329969	-2.681731586990
H	-1.801224531657	1.298954522505	-1.028660323901
H	-0.173308170393	1.495413869904	-1.769855255958
C	1.514145905436	-6.203913109803	-2.739762448954
H	2.050603980680	-6.988293781688	-2.192383246567
H	2.122105233254	-5.951099560234	-3.617577307343
H	0.572395738703	-6.629308644762	-3.099597846376
H	0.117559677133	-0.946689273732	-1.845231877498

N	1.951475871463	2.618472832715	-1.605449615549
C	1.976420356995	2.908851691721	-3.011293373387
H	2.984458360814	3.197756896438	-3.406729776285
H	1.658836926823	2.054405200749	-3.665627693786
H	1.298972954894	3.745425869696	-3.250663807215
C	2.870594916543	1.549112799462	-1.346588662514
H	3.932543259701	1.759358066922	-1.638652943757
H	2.902892094427	1.300209980738	-0.267553547138
H	2.632798218688	0.582794576445	-1.875975873082
K	0.563874399996	3.128638414266	0.548128764440
O	1.684792463114	5.747503119568	0.577801031288
O	1.654754683689	2.990681889766	3.079665295274
C	2.606009497083	5.729661338847	-0.519573219583
H	3.605369655181	6.048759904864	-0.184694406811

Cartesian Coordinates for (*P*)-(*S*)-201a

C	3.204379534006	-0.625976124990	0.390235170765
C	2.670029503149	-1.325237054199	1.492127260972
C	4.565895596406	-0.246452859767	0.388326489772
N	2.382917350111	-0.294661051745	-0.728890948733
C	5.368935382673	-0.628754030761	1.464880871159
C	3.519979891590	-1.681618163455	2.551479470494
C	2.786583184298	-0.727926605825	-2.074307932838
C	1.207747724505	-1.600389238289	1.621733032196
C	1.161181292118	0.335090404924	-0.636732175154
C	4.874037845422	-1.354617810299	2.554134507300
H	6.414055674470	-0.324717494815	1.462936852411
H	3.096881529473	-2.211116652618	3.399628431843
H	1.931327885091	-1.197844707122	-2.566302630264
N	0.270916300743	-0.773047667922	1.320786041714
C	0.779955221341	-2.919198104307	2.187695326806
C	0.546473353403	0.554617718357	0.749161901136
O	0.550246054591	0.621413615331	-1.671622086619
C	-0.423733596860	-3.006381620121	2.906997235268
C	1.524546778486	-4.090020162402	1.974928865223
C	1.075838462746	-5.317243862303	2.464886216550
C	-0.864414983772	-4.229653278801	3.405129579281
H	-0.998698097109	-2.100033226496	3.064729799996
H	2.452526188710	-4.043258563848	1.412858133848
C	-0.117192054041	-5.390439814613	3.184740945204
H	1.659338102863	-6.215820623960	2.282084897991
H	-1.791896228974	-4.278443469497	3.969678925094
H	-0.462760820963	-6.344775350028	3.573475405098
C	1.284236331756	1.541353878977	1.676574864499
H	2.305108009975	1.255440370514	1.936544431499
H	0.701746515735	1.637945146386	2.597722451931
H	1.301382145010	2.526955634678	1.200184134969
H	3.112502820538	0.111227563470	-2.696270514542
H	3.596788792974	-1.451850151682	-1.981354959325
C	5.159382789821	0.616401008642	-0.702781643973
H	5.428874530445	0.043471443904	-1.598326213598
H	6.071008242902	1.102939499044	-0.343569490640
H	4.459279235276	1.397953570194	-1.016211417996
C	5.778721557316	-1.756732950492	3.694953398993
H	6.426211864451	-2.597118940382	3.412089609592

H	5.202042863814	-2.066680835019	4.571775084344
H	6.434864078528	-0.932036805750	3.995909563512
H	-0.432540430753	1.025269804854	0.559422679212
N	-2.323950749710	2.380551581019	0.464428893753
C	-2.884651644129	2.079085071725	1.750354252929
C	-1.837510562524	3.731834091025	0.481841203710
H	-2.166558786993	2.178297881408	2.605460601158
H	-3.750498564035	2.731476912842	2.043695714845
H	-3.256759884314	1.041310614682	1.784605855419
H	-2.624005233001	4.510243579862	0.676994910803
H	-1.051734853045	3.939147490481	1.254457450541
H	-1.383202010487	4.001753150973	-0.490036781830
K	-2.100726689047	1.310027578214	-1.909188196128
O	-4.764143846655	2.166748333142	-2.446897941464
O	-1.195215971617	3.379318496176	-3.508996580255
C	-5.147038363773	2.875165669276	-1.261598774545
H	-4.291134914072	2.801109825925	-0.570320355453

Cartesian Coordinates for (*M*)-(*S*)-202a

C	-0.413611608868	-1.770238743647	0.062333437104
C	-0.817096237278	-0.846489198268	-0.940433603812
N	-1.204353339581	-2.172404964896	1.093281264680
O	-0.251572679323	-0.754554182019	-2.079699115277
N	-1.983148677483	-0.081615967310	-0.692370391810
C	-2.115015003096	-1.504127515411	1.755768741214
C	-2.022557003346	0.676868007687	0.517839942576
C	-2.227017740745	-0.026062777472	1.721815604678
C	-2.917199502474	-2.284350812774	2.736880866060
C	-2.850122810393	0.244354255995	-1.811068503305
C	-2.449962054982	-3.521535608239	3.223590920465
C	-4.187777220375	-1.855495038825	3.165953037720
C	-2.361996377060	0.709518733260	2.916911884160
C	-1.891597975609	2.085208852945	0.524580354536
H	-3.031097228296	-0.661778273391	-2.398223540537
H	-3.808556953708	0.594067799520	-1.414284403798
H	-2.457390038439	1.009308311675	-2.495835437682
C	-4.947903013387	-2.617777216804	4.053771689172
C	-3.206542978077	-4.279358665235	4.111202446201
H	-1.482804838395	-3.871717472701	2.879133167806
H	-4.590254510228	-0.920408882469	2.787188427985
H	-2.512552284242	0.169415654084	3.846943081050
C	-2.060341815247	2.771244254762	1.731544876334
C	-2.306043807644	2.101144949051	2.937762518909
C	-4.462434615261	-3.833239030226	4.536900578302
H	-5.928653400941	-2.261394762545	4.361214376922
H	-2.814826025170	-5.226347335455	4.476703581039
H	-1.993566017915	3.858661316855	1.729435239029
H	-5.053677325366	-4.427591901264	5.229078115707
C	-1.585371484713	2.871737881997	-0.731591147673
H	-0.847967566797	2.365052074096	-1.363168083249
H	-2.476759240214	3.032259460816	-1.351823843035
H	-1.190660160753	3.860418888082	-0.472183129531
C	0.701834062557	-2.735332097538	-0.303733350090
H	0.833843033907	-3.450554907394	0.512815783206
H	0.481215357726	-3.299536221632	-1.222427076395

H	1.673796422011	-2.246856472525	-0.474426226013
C	-2.504194196319	2.872741337461	4.223023923402
H	-3.510661320349	3.309788411249	4.277152058880
H	-1.790897957609	3.701193700127	4.311406037399
H	-2.381959948075	2.227406731890	5.098986532082
H	1.187771529440	-0.281739996980	1.162073186433
N	2.028179923661	0.286108526642	1.317943249643
C	3.041468993272	-0.563286331524	1.951217128276
H	3.983751028465	-0.007824908198	2.043242361573
H	2.755659625888	-0.906506803648	2.959961421500
H	3.225797548793	-1.445695542735	1.330104040677
C	1.649841706923	1.412083048866	2.179662709399
H	2.493907122039	2.108696449184	2.270530287235
H	0.803916970533	1.945199268677	1.737579312926
H	1.361289700603	1.100410907980	3.197177242883
K	2.066197709251	0.421504881010	-1.636475642979
O	4.423800719526	1.949553881236	-1.616507810871
O	1.151303079197	2.198579946799	-3.507305487525
C	4.882349491249	2.414609041368	-0.354908409229
H	5.023902296717	3.505740941419	-0.361193473079

Cartesian Coordinates for (*P*)-(*S*)-202a

C	2.984000107776	-0.682637527237	-0.246666114588
C	2.996127939801	-0.671880019728	1.158887225190
C	4.189091815431	-0.685546243179	-0.978553376076
N	1.705312616753	-0.725874239239	-0.896500662203
C	5.392766895831	-0.800141568926	-0.278035863769
C	4.233394393435	-0.782687065240	1.823336454744
C	1.412957165460	-1.783100740600	-1.850381007612
C	1.763802545341	-0.318940310318	1.896653242638
C	0.969876178875	0.469453723225	-0.962179182897
C	5.433422895843	-0.871666851537	1.121619609142
H	6.325355100166	-0.826200897324	-0.840060132116
H	4.249493355963	-0.773625252174	2.909476263134
H	0.343872171640	-2.024257602104	-1.819511635386
N	0.947731150885	0.629762815188	1.489746716906
C	1.523222554919	-0.860588874284	3.257958058282
C	0.828131060285	1.196862169178	0.257894789230
O	0.337206238205	0.742590006167	-2.035125504676
C	0.804396597686	-0.120111439301	4.219544684549
C	1.956689284617	-2.150256343917	3.623165330375
C	1.686810861921	-2.674096453573	4.887895896728
C	0.536550229644	-0.643227276167	5.480838833774
H	0.468778201959	0.876771906640	3.952658686930
H	2.501777651082	-2.749895799785	2.899749450739
C	0.974273300377	-1.926650458951	5.826710005022
H	2.030298990951	-3.675847217889	5.136359418436
H	-0.008684709069	-0.042284969553	6.205775694442
H	0.764151640275	-2.334279880772	6.812249805703
C	0.160363466641	2.553751154032	0.243961148566
H	0.769920659395	3.303895039277	0.765485686715
H	-0.814538025867	2.554410109884	0.766633971575
H	0.008593379046	2.906378997134	-0.779603425490
H	1.664724950427	-1.533789874667	-2.889964926377
H	1.974523170155	-2.675286063872	-1.558005545755

C	4.204958830287	-0.561568141417	-2.485578223610
H	4.039104981665	-1.523798427468	-2.987970566776
H	5.174208552384	-0.181882326936	-2.825448916312
H	3.426066717093	0.124126358422	-2.834933283801
C	6.751876634545	-1.022907837178	1.846377009710
H	7.129046230228	-2.052905900071	1.783665546906
H	6.654573930854	-0.774777236965	2.908361842599
H	7.524162124835	-0.372698346447	1.418043654993
H	-1.101906076411	0.104080729314	1.732810306812
N	-2.004690392176	-0.351768390230	1.551965121451
C	-1.728010211391	-1.784065683051	1.384313913518
C	-2.874537010844	-0.104522820004	2.703963656307
H	-1.370771386076	-2.268279697053	2.307788122097
H	-2.637733356275	-2.304726515404	1.056322788460
H	-0.956307791455	-1.914750057698	0.619137979728
H	-3.865018445891	-0.544561427572	2.525691665660
H	-2.483759682939	-0.531170829811	3.643003660694
H	-3.003438518848	0.974449962944	2.843502282603
K	-2.176079357752	0.802116351088	-1.150358400285
O	-5.001571470680	0.845941947199	-1.246055536262
O	-2.325032523366	3.165985384005	-2.671442912585
C	-5.883047964838	0.487119530308	-0.193362089725
H	-5.268650933390	0.122589796897	0.632428928642

Cartesian Coordinates for 203a

C	-0.862713120515	0.401992206782	-2.672112970529
C	-0.862891663385	0.400089862168	-1.264847709413
C	0.360928734780	0.403120503879	-3.359493088748
C	1.576445087701	0.412337266739	-2.657918797232
C	0.342952311633	0.178751379299	-0.534160680205
H	0.360082526302	0.435932373754	-4.449428662238
N	-2.044107098193	0.777961943472	-0.548406154986
C	1.554662076876	0.291764594475	-1.269750698355
C	0.272382139794	-0.247972657258	0.853924563505
C	-2.778940449608	-0.187576103111	0.155556167450
H	2.499695744197	0.282876745346	-0.737466252583
N	-0.762097546229	-0.895445201109	1.400536312707
C	1.481136495314	-0.241847479954	1.740856573917
C	-2.014167899924	-1.093860790281	0.991907549708
O	-4.028084432885	-0.136362306799	0.167506549635
C	2.686534346635	-0.905880195513	1.436557026811
C	1.402247778119	0.390502656902	2.998222481006
C	2.473014056681	0.384000511753	3.894254632575
C	3.763761808626	-0.914259331771	2.328334612951
H	2.767505083891	-1.461414906372	0.506722398177
H	0.472016107438	0.885273180170	3.265120094076
C	3.668946787813	-0.262358142781	3.561777751057
H	2.374471562632	0.886523540568	4.855433902751
H	4.674908941781	-1.449562870371	2.064128644880
H	4.507293767040	-0.267484696527	4.255957844010
C	-2.827365973712	-2.113799339950	1.764533517237
H	-3.528347352270	-1.641530462493	2.471955206825
H	-3.440708636306	-2.730134042889	1.093030112408
H	-2.149945589829	-2.765183003431	2.326285467594
C	-2.156577008077	0.445541487146	-3.457571709909

H	-2.972669868163	-0.036400234893	-2.910155569276
H	-2.477906879514	1.472594907983	-3.683941949269
H	-2.030053565992	-0.072093848879	-4.416808297147
C	-2.692572279177	2.045757609758	-0.842826454458
H	-3.172331116345	2.426401766167	0.066250258188
H	-1.926153407464	2.757797910381	-1.167598191171
H	-3.470482461831	1.981954822981	-1.618137142277
C	2.890036118787	0.532398459481	-3.403123566158
H	3.744763891216	0.410309090875	-2.727448849523
H	2.977791046551	-0.227585068526	-4.192398172123
H	2.991262090542	1.512791067422	-3.891179551692

Cartesian Coordinates for 203a*

C	-1.241997552489	2.382656443108	0.507319178403
C	-0.350409276886	1.318328946146	0.844920223920
C	-2.498809510659	2.079444165250	-0.058883488802
C	-2.877959985139	0.783958086880	-0.385897171217
C	-0.575235040292	0.076403406633	0.161827118552
H	-3.181057426238	2.907251419671	-0.255934315952
N	0.679174850893	1.513053750536	1.798725024152
C	-1.864874372644	-0.182314586463	-0.323740389429
C	0.490211831904	-0.907976766402	-0.177056349066
C	1.540314007393	0.481171310765	2.393141620515
H	-2.050418194697	-1.168350514085	-0.742180901930
N	1.461276430656	-1.287718813152	0.620796241101
C	0.480120196820	-1.552235916642	-1.509780303017
C	1.837887005516	-0.790506602485	1.800241142758
O	2.117126923363	0.799218166984	3.456618719714
C	1.124078648699	-2.801804610204	-1.705109063887
C	-0.085446420085	-0.953818877794	-2.664461444868
C	-0.017815697308	-1.564198416431	-3.917689528774
C	1.180310821662	-3.413006472066	-2.954276140749
H	1.587266607738	-3.271209716903	-0.843280839935
H	-0.571763525838	0.013231384727	-2.577985639155
C	0.609424397404	-2.804648628214	-4.082622344251
H	-0.456269683593	-1.058246645977	-4.777405163412
H	1.676073412535	-4.378577399441	-3.051677429349
H	0.656977641530	-3.281518807118	-5.059587201628
C	2.890118379690	-1.590899229001	2.546819897399
H	3.828382749954	-1.030972706711	2.682552130450
H	2.558878306931	-1.873184878976	3.556822710990
H	3.099150404810	-2.503830787078	1.978597484198
C	-0.870462622759	3.861954629022	0.520952631516
H	-1.091013961473	4.392103216930	1.456333518440
H	0.192361148080	4.010807968005	0.303820192512
H	-1.432391233928	4.365432359108	-0.275475247984
C	0.482624216165	2.646071302315	2.716978646476
H	1.006540017552	2.417061616234	3.641378211528
H	0.886861453271	3.581896262091	2.320765764319
H	-0.587054894480	2.776277523130	2.918166493725
C	-4.270645813053	0.443814738423	-0.863017146280
H	-4.807658430265	1.340902059700	-1.197632024442
H	-4.250631017313	-0.267329167809	-1.699367362053
H	-4.873007015954	-0.017190620100	-0.065511530002

Cartesian Coordinates for 204a

C	1.169379482332	-0.756907108369	-2.959538969034
C	1.225858684336	-0.783630551788	-1.548475584051
C	2.367358127263	-0.653953300071	-3.673606590989
C	3.608720059332	-0.527868043124	-3.029761302243
C	2.446893503257	-0.605754003130	-0.876500596510
H	2.330727780111	-0.660554921622	-4.762866393490
N	0.060307163684	-0.999906281015	-0.744477051028
C	3.628651774703	-0.486321054220	-1.636588101498
C	2.449231400133	-0.342113976999	0.583374716746
C	-0.484513232684	0.134815110292	-0.112157299968
H	4.574136577679	-0.341632487480	-1.120821325384
N	1.581717071547	0.446509700435	1.164108286696
C	3.592788176510	-0.804411598355	1.417933976463
C	0.377618248863	0.897783263925	0.700737353034
C	3.969920362860	-0.102035463337	2.580710520695
C	4.298878579896	-1.983298944551	1.108795528674
C	5.343156638390	-2.436081389137	1.919291697077
C	5.015739188572	-0.549455718609	3.385361464584
H	3.420471107425	0.798406878245	2.836121789998
H	4.016809933961	-2.559084206178	0.231511540015
C	5.712554199935	-1.721044885734	3.061497280985
H	5.865213638272	-3.354291950355	1.658050744578
H	5.292792405359	0.019248449299	4.270863533658
H	6.526976483867	-2.070562891699	3.691690502264
C	-0.108894130404	2.166718498734	1.364816752483
H	-1.182994607691	2.317701566182	1.220470633652
H	0.406708159378	3.056648806423	0.971429335829
H	0.102073151515	2.137546482434	2.442799772147
C	-0.145777158428	-0.834869833487	-3.702893442129
H	-0.926400194667	-0.268246335311	-3.184058529263
H	-0.507046439092	-1.867287252755	-3.805024883069
H	-0.036706784429	-0.426596604747	-4.713854819055
C	-0.765720317572	-2.177670712656	-0.938439503982
H	-1.213851398307	-2.471978341278	0.018542847621
H	-0.124367743393	-2.996491567028	-1.279793790838
H	-1.581206577302	-2.044887471338	-1.665169539548
C	4.884929050966	-0.417595177819	-3.835436220423
H	5.748950066720	-0.234085522041	-3.187910550488
H	4.832192052166	0.402171092325	-4.563743402756
H	5.083157840409	-1.338264668509	-4.400776450986
Li	-3.334655439313	0.860134911827	0.421290586371
O	-4.922281127326	-0.125988478079	-0.381673556737
O	-3.630025042578	0.429568834337	2.358832027753
O	-3.699959101600	2.778751771327	-0.108790605176
C	-4.829874708734	-1.544361682847	-0.247278849923
H	-4.466703789156	-1.746610362803	0.761752102513
H	-4.121180516435	-1.956283623784	-0.977034230703
H	-5.817606684127	-2.005905576611	-0.386732513051
C	-5.384321538946	0.267510585228	-1.671509956018
H	-5.414359781974	1.358310098185	-1.680921606700
H	-6.390931607655	-0.133206488679	-1.857174215702
H	-4.700480191649	-0.088081445796	-2.454575194379
C	-4.461416727923	3.759893751591	0.583468137324
H	-5.051823897890	4.363684111374	-0.120744445056

H	-3.805283297708	4.423096532397	1.164455647119
H	-5.136763675899	3.232167360874	1.260899030824

Cartesian Coordinates for 204a*

C	0.678030072181	-0.482377928321	-3.468912458268
C	0.670292420037	-0.476312156323	-2.041975085102
C	1.908233324029	-0.354384843605	-4.144657061883
C	3.133968484389	-0.318986970968	-3.490542478482
C	1.910130513819	-0.809371081653	-1.412345820821
H	1.882757892817	-0.306273731179	-5.233197152012
N	-0.509241711679	-0.141063527359	-1.323515261920
C	3.099181524644	-0.640406280196	-2.126799791209
C	2.001793150650	-1.528990817283	-0.100805609790
C	-0.592562968066	0.090089474181	0.110680962347
H	4.032112384342	-0.843029010413	-1.606875761698
N	1.318153914642	-1.268540924995	0.960100639100
C	2.948401664195	-2.681259848554	0.001797803568
C	0.296732626652	-0.363741961912	1.084667489867
C	3.537885598399	-2.994763080828	1.243809182667
C	3.240169674346	-3.523196963767	-1.089822008763
C	4.082455697443	-4.628443751611	-0.945161483832
C	4.389048454047	-4.089113035036	1.384342101974
H	3.307235056988	-2.363406219008	2.096039908495
H	2.793916232674	-3.319613485866	-2.058680958918
C	4.668449801928	-4.917332832662	0.290060511584
H	4.278408481501	-5.267094402183	-1.804009798885
H	4.838614405447	-4.298182108808	2.353039822657
H	5.330601420344	-5.772904954588	0.400111564378
C	-0.081508619425	-0.076208598114	2.524582930754
H	-1.075369110586	-0.472159773608	2.789845175268
H	-0.096257867188	0.999662490753	2.754141424207
H	0.658980887677	-0.546591554957	3.178602561846
C	-0.527351338933	-0.806244903010	-4.344391229850
H	-1.101299263948	0.065168058032	-4.683161444620
H	-1.222241555044	-1.483545768805	-3.838070761632
H	-0.173198885598	-1.325779713410	-5.241997819003
C	-1.482002506031	0.656865627233	-2.090653937587
H	-2.022407133207	1.295603189151	-1.400061951775
H	-2.208204377767	0.035878140361	-2.622523305324
H	-0.951598881767	1.279871164354	-2.818356739208
C	4.433347813511	-0.063246102001	-4.215818072757
H	4.327082160248	-0.224905965579	-5.295191472899
H	5.233949023499	-0.720344606054	-3.854170655727
H	4.777545416280	0.971266676018	-4.073496043795
Li	-2.567971334004	1.784168664090	1.608156076948
O	-4.518166671723	1.644903058829	1.023773185194
O	-2.985197502969	1.718910025246	3.615460588073
O	-1.747120657359	3.653374918995	1.491538872234
C	-5.626649306814	2.424316931886	1.450680861656
H	-5.292675740398	3.029028610182	2.296692758079
H	-6.456647421811	1.778944394731	1.773264419370
H	-5.978794765157	3.080291647963	0.641290183706
C	-4.841023498361	0.750478866278	-0.044684550848
H	-3.926439947225	0.203728131588	-0.275050142537

H	-5.178929368804	1.312869225740	-0.926434939668
H	-5.633865185431	0.056535171866	0.268439928631
C	-2.427715504446	4.899467054522	1.555590661256
H	-2.649884216988	5.276732293896	0.546943741305
H	-1.825001509507	5.646188208907	2.092468415630
H	-3.362606231178	4.734902469562	2.096445150115

Cartesian Coordinates for 205a

C	1.330672611455	-0.475989453708	-4.118131193204
C	1.330506997469	-0.476080115194	-2.706584070170
C	2.560031480514	-0.475990078964	-4.785590553147
C	3.780367303324	-0.430925340843	-4.093013161140
C	2.532130131451	-0.352717748034	-1.986031512920
H	2.565137080464	-0.500763921108	-5.875034791070
N	0.116931403289	-0.638873153716	-1.956920039810
C	3.748518398087	-0.347696939491	-2.702277589794
C	2.497998650954	0.001698200333	-0.549592319200
C	-0.427192483178	0.491613925182	-1.332530424356
H	4.681550744679	-0.251144070229	-2.153733871539
N	1.641552578720	0.872634757105	-0.057333935809
C	3.607429267757	-0.413421841103	0.346540258045
C	0.463842868064	1.310772334845	-0.572409754049
C	4.034018447996	0.406834894765	1.413316565743
C	4.244266508199	-1.662593162622	0.194994055546
C	5.259015892708	-2.071691657024	1.063221591216
C	5.049638328542	0.000638976046	2.277301584056
H	3.555293416611	1.373085431447	1.540542111052
H	3.929927303630	-2.323351009893	-0.608805836980
C	5.671483934731	-1.244166220406	2.111998303275
H	5.726110615400	-3.044203201945	0.920770779347
H	5.367808070628	0.662945794692	3.080507483141
H	6.463976290014	-1.559995084003	2.786300624077
C	-0.048297650745	2.616581930286	-0.001412166236
H	-0.998175157300	2.896929107729	-0.468103518954
H	0.668050979385	3.429516205755	-0.180641381750
H	-0.193842590679	2.582481232589	1.093584507380
C	0.045166711853	-0.472483055598	-4.916031479865
H	-0.719841300378	0.146700046783	-4.435825233747
H	-0.377267162992	-1.479437457068	-5.034383701968
H	0.225193127096	-0.076038980161	-5.921402482262
C	-0.742146483702	-1.786822849510	-2.202642448445
H	-1.232820721600	-2.084689224082	-1.267999415771
H	-0.117208338374	-2.616721179553	-2.546755504399
H	-1.530928828316	-1.602564031193	-2.944513114300
C	5.092564664497	-0.439600236365	-4.846953634427
H	5.941786131700	-0.301178526895	-4.169131618682
H	5.130329551383	0.359680579111	-5.598597111838
H	5.243578490088	-1.388732290426	-5.379011917008
O	-4.957972500433	0.689893677264	0.173128280057
O	-0.586145846218	-0.100082670746	3.430967559781
C	-6.268693299086	0.672690436343	0.712895715928
H	-6.178909654271	0.507736193867	1.790068415181
H	-6.869462498701	-0.137171158733	0.270692212222

H	-6.785188346458	1.628654770741	0.534256610413
C	-4.944908065258	0.907197522324	-1.241456444013
H	-3.901392473996	0.883259079509	-1.562093106702
H	-5.393794393429	1.882479052683	-1.482753910268
H	-5.514581244296	0.117962128199	-1.754941206389
C	0.837264737637	-0.054842732846	3.266882352188
H	1.049523790610	0.287946504457	2.251285727129
H	1.274105626399	-1.052283028892	3.416098259515
H	1.282824641122	0.642086805849	3.991520357492
C	-0.968284156229	-0.522382200240	4.729566102141
H	-2.061313715169	-0.529623495041	4.767408537040

Cartesian Coordinates for 205a*

C	1.205666175448	-0.734851434375	-4.116498486729
C	1.212488182114	-0.741873928215	-2.690106351483
C	2.434506476075	-0.737426363804	-4.807705455752
C	3.662405300934	-0.840631386705	-4.166310641664
C	2.414971245594	-1.215113707356	-2.074814707775
H	2.402382414858	-0.675588867975	-5.895378579146
N	0.081115126156	-0.284620926017	-1.960249614834
C	3.607357619657	-1.163633847866	-2.803578460727
C	2.455701056980	-1.937073573592	-0.763392504966
C	0.014989127050	-0.074165751679	-0.520862228103
H	4.520401911679	-1.460862347798	-2.294242702977
N	1.796549994119	-1.626081329752	0.304137748722
C	3.316238921906	-3.153093664535	-0.655844412837
C	0.846685477684	-0.659201779718	0.446952841243
C	3.899647853026	-3.493949717957	0.582751401115
C	3.529114207479	-4.033672890982	-1.736569287014
C	4.286129898103	-5.197799923983	-1.584901579555
C	4.665507670017	-4.648775793247	0.730573084389
H	3.731912234727	-2.833569038000	1.427778485025
H	3.087202624640	-3.811187997440	-2.703398667416
C	4.865469702526	-5.513808523480	-0.352732274414
H	4.420384771524	-5.862078422057	-2.436364805324
H	5.111757567623	-4.876147886199	1.696931794048
H	5.461414945647	-6.416149251194	-0.237322738606
C	0.472420690048	-0.384235589361	1.891629435380
H	-0.556655595743	-0.705608719923	2.136542313373
H	0.553431461476	0.681736165667	2.159234757834
H	1.156745579658	-0.941410917206	2.539178286729
C	-0.037644793347	-0.911742558889	-4.980588788761
H	-0.517160877200	0.021449276423	-5.300867127837
H	-0.797035952783	-1.516579193161	-4.474805777989
H	0.248062014738	-1.453773516315	-5.889445756051
C	-0.803314926208	0.629415216208	-2.705018058528
H	-1.280054016402	1.295882651184	-1.992809910203
H	-1.589000070089	0.100864315325	-3.251424302623
H	-0.210507786017	1.215218224381	-3.416031124935
C	4.975408768210	-0.719409394808	-4.902427171566
H	4.838783509210	-0.834652202432	-5.984405533458
H	5.696181560380	-1.477427102095	-4.571165700992
H	5.441731152435	0.262306032347	-4.735494473409
O	-4.254155575044	3.341323099599	0.814688965581
O	-4.028640337664	-0.473970145940	1.645824985479

O	-2.285022828217	1.632309478736	4.639059748044
C	-4.029060608102	4.667879554785	0.355529449844
H	-3.064015057547	4.986784357909	0.756050237273
H	-4.819873464121	5.346121032885	0.710104370928
H	-3.993553608942	4.702000307991	-0.743274430430
C	-5.463990157887	2.782884280854	0.316888663449
H	-5.517482291587	1.755596107667	0.684483683063
H	-5.468156655028	2.774882307975	-0.782924003821
H	-6.335165491155	3.351963132688	0.674942076036
C	-1.399503092462	0.743904050676	5.315334898929
H	-1.961432457373	0.032021195378	5.937495135375
H	-0.696908808567	1.301601369438	5.951506741662
H	-0.840799548542	0.196321297539	4.553508438775
C	-3.070883455055	2.403045655019	5.535714955286

Cartesian Coordinates for 215

C	-1.960153653336	-0.201145122217	-0.397274997223
C	-1.922181171078	-0.593932484616	0.893753866103
N	-0.852640905408	-0.321614211507	-1.276121278496
H	-2.871192769659	0.218802531340	-0.829210480241
C	-0.717166248065	-0.999412789287	1.605340038115
C	0.392150432038	0.340471560177	-0.966975633841
H	-2.850959630056	-0.534972450159	1.467657885909
H	-1.076783735054	-0.086134919958	-2.236640769053
N	0.483409923855	-0.503336620815	1.389806223552
C	0.936858332971	0.243871190652	0.352952193904
O	0.968128488211	0.899311446847	-1.929102183490
H	-0.846182465491	-1.535441412094	2.549455331291
C	2.333949918933	0.814452005740	0.513631589121
H	2.384186410757	1.871703279809	0.215297601679
H	2.633435796345	0.730331209875	1.564517693685
H	3.086339689568	0.290049849958	-0.102616747808

Cartesian Coordinates for 216

C	0.067140492970	0.355756425653	-2.311624531652
C	0.023259466041	0.446585492872	-0.912958598447
C	1.279542320237	0.304032788176	-3.012758274751
C	2.478343714986	0.312342256358	-2.293416882415
C	1.230060523604	0.400876167310	-0.166788604468
H	1.279018363699	0.263469132158	-4.100277375066
N	-1.217761367179	0.730459372677	-0.283896487639
C	2.438514142553	0.347591798616	-0.898466559190
C	1.274523340503	0.353197716069	1.288271869095
C	-1.736692362756	-0.158038011608	0.723424166551
H	3.370321968825	0.332623128303	-0.333362155234
N	0.362152393124	-0.215083312109	2.047411448506
C	-0.886530520286	-0.633089736252	1.770885164219
O	-2.965243280111	-0.393339865679	0.660012684385
C	-1.583145304990	-1.432045423543	2.856148119091
H	-2.363003736255	-0.852192856043	3.379003128068
H	-2.087294706995	-2.320870617131	2.450908689855
H	-0.838368064671	-1.753474415244	3.592595433972
H	2.244088821861	0.542447411258	1.755609488635
H	-0.873125468207	0.374127240143	-2.862535899345
H	-1.966096786317	0.890261957905	-0.951394408708

H	3.435573790153	0.279438678206	-2.811548311523

Cartesian Coordinates for 217

C	-0.055610432675	0.562432294721	-1.834277970136
C	-0.149222372567	0.416037697837	-0.438480787324
C	1.213316042295	0.617242474472	-2.445354084473
C	2.387775119993	0.495201987347	-1.699779722547
C	1.026029204803	0.245360941899	0.341581621525
H	1.270764063566	0.760431193942	-3.524553214922
N	-1.403200815689	0.569328454226	0.202139259723
C	2.268787658395	0.296391070164	-0.319047363026
C	0.991518444869	-0.013503416497	1.775474071097
C	-1.987724080135	-0.375896039377	1.116189966455
H	3.169143960974	0.176050224123	0.284924456692
N	0.066046350135	-0.618565238370	2.485987808795
C	-1.204667973672	-0.938200906141	2.169368783124
O	-3.219779984028	-0.561965934168	0.980036413634
C	-1.961019429658	-1.785739101175	3.172235073279
H	-2.771099446751	-1.229714072960	3.673851961616
H	-2.440090255763	-2.657515384853	2.702190114724
H	-1.258729346292	-2.140836629716	3.934737039162
C	-1.297981204291	0.728029248684	-2.683477275206
H	-2.035541585607	-0.062225365430	-2.490560255835
H	-1.805492383593	1.689822384364	-2.506525240181
H	-1.041442596123	0.693184670557	-3.748874975175
C	3.748824296664	0.568914323430	-2.359415985730
H	4.365857390772	-0.308357519277	-2.119505472052
H	3.658327629437	0.620914021484	-3.451679308910
H	4.313334965842	1.454775295859	-2.033023609119
H	1.958497463524	0.093027566362	2.277729180285
H	-2.145360373011	0.853205125715	-0.425989427210

Cartesian Coordinates for 218

C	-0.291705018017	0.315591264429	-1.794048152412
C	-0.210788501518	0.442481134011	-0.396536490230
C	0.867820678393	0.361441574543	-2.587761489340
C	2.124020864524	0.472199101589	-1.975653105979
C	1.052317536423	0.466893056248	0.232521076194
H	0.784238897490	0.336536954455	-3.674435272193
N	-1.402517927470	0.666009059396	0.353577080578
C	2.208176078670	0.502084442819	-0.584267292007
C	1.192023993702	0.328236322956	1.672424245339
C	-1.836924400431	-0.296658062270	1.305895386252
H	3.185248389348	0.526982564640	-0.100782452692
N	0.364744916315	-0.349308390883	2.445653833951
C	-0.870184594735	-0.833268846470	2.223549891205
O	-3.063633313941	-0.554357050659	1.347865427785
C	-1.427978353703	-1.763444253411	3.284185898830
H	-2.153911404723	-1.265341577874	3.949965885864
H	-1.960234491093	-2.615222526240	2.838092463897
H	-0.602628191234	-2.143150854239	3.896592986567
H	2.174651972715	0.547765648926	2.097465403981
H	-2.187025961583	1.013599041310	-0.186044066371
N	-1.571896009361	0.264083882155	-2.409896781888

N	3.297883187308	0.578681157342	-2.779657047852
H	-2.230528097306	-0.306465328264	-1.884087719717
H	-1.521405115230	-0.075019682316	-3.365308811148
H	3.231780194786	0.029868526884	-3.632330400101
H	4.130711450968	0.295709275255	-2.271650841005

Cartesian Coordinates for 219

C	-0.431450162592	0.394781846521	-1.238804219735
C	-0.474771312627	0.317636797453	0.197537578348
C	0.768644064932	0.375288853961	-1.967118653599
C	1.955675369265	0.286097505398	-1.264571979718
C	0.785804110015	0.193180085822	0.883222628927
H	0.750618354998	0.442913331279	-3.044388584874
N	-1.657634809245	0.487003752392	0.885019183058
C	1.968789602043	0.190826549536	0.131169279931
C	0.919147917718	0.119210323188	2.330459326329
C	-2.062313907459	-0.488994550861	1.908534825841
H	2.919362469567	0.136812876901	0.648659377574
N	0.081126234604	-0.500856295541	3.126978159153
C	-1.155557801516	-0.959031216204	2.900738718889
O	-3.269051921125	-0.781821317956	1.872565218042
C	-1.761063759822	-1.859798677308	3.956417450048
H	-2.601694390625	-1.380769060891	4.481602401899
H	-2.160480349769	-2.786243684614	3.521304820617
H	-0.987470266632	-2.117284447833	4.686739997043
H	1.900760322704	0.361104625419	2.739066872629
H	-2.454634437868	0.676976670113	0.280713486063
N	-1.627467018051	0.515089214837	-2.052183622189
N	3.213379245315	0.296662313774	-1.999216715135
O	-1.541049607005	0.254689122722	-3.262444830404
O	-2.700615197907	0.883176583982	-1.530617387504
O	4.266909699255	0.203668058646	-1.353873213268
O	3.180093027972	0.398539013402	-3.233553178957

Cartesian Coordinates for 220

C	0.438755541189	0.790829240949	-1.777940895053
C	0.925813455221	2.023026680156	-1.127687302776
N	-0.901615709255	0.523722807599	-1.806583158328
O	1.839574874335	2.703383940179	-1.601933052480
N	0.210523420033	2.528191589704	-0.022691170875
C	-1.783808729657	0.631199569519	-0.848497036410
C	-0.370702830014	1.674116200321	0.959094316269
C	-1.429324325329	0.821009644122	0.580656658512
C	-3.199647083624	0.398172277765	-1.233578177003
C	0.362130783936	3.955303803369	0.233276461023
C	-3.511538411546	-0.293160256951	-2.422702922781
C	-4.274573892447	0.907018787817	-0.478083148171
C	-2.033276805425	0.014146328532	1.561188958476
C	0.089416539427	1.681617583483	2.295410821695
H	0.224064418418	4.498893909664	-0.706295271387
H	-0.411255223777	4.265246285640	0.942367026913
H	1.346351017785	4.235026720401	0.627892229111
C	-5.596735020934	0.722440113162	-0.883788361269
C	-4.829655827435	-0.481278074283	-2.822547885698

H	-2.687655183554	-0.671330560702	-3.018147055107
H	-4.068081525794	1.463910636850	0.431115537549
H	-2.824917122868	-0.665081803944	1.258728776781
C	-0.557437165014	0.873351353623	3.236133824023
C	-1.615389874785	0.027280653988	2.890074647857
C	-5.886810992412	0.024074645949	-2.056420566454
H	-6.403624888344	1.133411874782	-0.279921795094
H	-5.037867682710	-1.030461842474	-3.738835750185
H	-0.197538873694	0.880861707578	4.264013903785
H	-6.917394684735	-0.123412959823	-2.371357865410
C	1.284182595882	2.500635766709	2.733937937717
H	2.087033731334	2.459983408103	1.990716798707
H	1.041177876802	3.559586913453	2.889464869726
H	1.677131806847	2.114382215367	3.680527814911
C	1.146200963908	0.500764459204	-3.089235420656
H	0.793209724222	-0.452344454210	-3.497973113011
H	0.946167088814	1.283211978964	-3.836148707772
C	5.408993624302	-0.431202967257	-0.194678740254
C	2.635341612233	-0.917275634036	-0.391895711284
C	4.542938351805	-0.001019099932	0.815803542684
C	4.889692127767	-1.113068400595	-1.298070134633
C	3.522372734452	-1.356126798001	-1.394811478835
C	3.176711931757	-0.241019524185	0.719362087132
H	4.937786677666	0.522114003170	1.684032266118
H	5.555143529075	-1.461713706895	-2.084873076946
H	3.125682223748	-1.906616318575	-2.243077177126
H	2.507069678035	0.075505147480	1.513357247591
H	2.229932078816	0.456700953536	-2.955771515410
C	1.208099447184	-1.164855864138	-0.491078831310
H	0.534832096482	-0.845879953860	0.282522954312
H	0.793629832124	-1.665394473778	-1.348293974574
H	6.477231759472	-0.241522693690	-0.119601970126
Br	1.076317440240	-3.462861556965	0.664072418026
C	-2.228440944237	-0.910329407014	3.904291530517
H	-3.299581652846	-1.055599322286	3.722146542136
H	-2.105189547414	-0.534782265211	4.926822689508
H	-1.753247369649	-1.898919701966	3.855153668467

Cartesian Coordinates for 221

C	2.510100028523	0.853619625963	0.177833893221
C	2.368608932666	-0.550070967134	0.126794870958
C	3.796497465408	1.424658384478	0.330432561696
N	1.333785564554	1.651895430079	0.101713667541
C	4.916120508139	0.589271186034	0.304045607271
C	3.527079073537	-1.350147729880	0.140149280878
C	1.270483856515	2.842310180348	-0.749236538277
C	1.033975453228	-1.197158927445	0.227365930425
C	0.536231926709	1.670258135851	1.285307542475
C	4.805807753449	-0.801577963259	0.196920309598
H	5.903645236632	1.039205791173	0.403780192875
H	3.414871729960	-2.430055396812	0.114476502879
H	0.241928696286	2.963588458976	-1.110421323573
N	0.060786703516	-0.792832272387	0.994481406073
C	0.812911995369	-2.509194658127	-0.451014151401
C	-0.136430305726	0.409228958733	1.615315908352

O	0.293985165169	2.740145239155	1.853936844227
C	-0.084637606418	-3.448962834531	0.092866924492
C	1.435047222498	-2.830111851658	-1.671652200251
C	-1.826254923459	1.151687983403	0.152822395521
C	1.180904051165	-4.042143451921	-2.315040255891
C	-0.331096483148	-4.660703708131	-0.544860748416
H	-0.588812827672	-3.193217260804	1.018609904678
H	2.112246555188	-2.113744953743	-2.126910680779
H	-1.745737913950	2.150266717242	0.549396314624
H	-1.159539092189	0.850837193683	-0.636284699141
C	0.301053374715	-4.968607342784	-1.754648805088
H	1.667935009413	-4.256842472158	-3.263944495846
H	-1.022159601855	-5.371843947260	-0.096740593692
H	0.103408708231	-5.913760242156	-2.255079054951
C	-0.852848358569	0.337341630183	2.943186402867
H	-0.166686903339	0.025062392667	3.746344742866
H	-1.663040778937	-0.396220290267	2.896726518783
H	-1.256072692975	1.315197528664	3.217433625918
C	-2.965208267303	0.329435787015	0.497752857368
C	-5.141395985041	-1.298639483128	1.248663350619
C	-3.085309298688	-0.987449348775	0.009454566828
C	-3.961911804918	0.808868090966	1.372478191243
C	-5.037169036271	0.006239696529	1.740789634601
C	-4.159683317097	-1.789797452441	0.382522811428
H	-2.322830228278	-1.371829829071	-0.659693950976
H	-3.889164147068	1.829096182155	1.739222703569
H	-5.800079764436	0.398751754955	2.409602690101
H	-4.233779121674	-2.803111690981	-0.005803598430
H	-5.982925430247	-1.925831468407	1.534771898644
Br	-2.744582354126	2.668868698277	-1.919043147115
H	1.568411141185	3.768092394040	-0.244671977234
H	1.917484063042	2.676497866437	-1.615686152941
C	3.988072946880	2.903372263836	0.586971359267
H	3.923767395888	3.507587379624	-0.326268944919
H	4.973888865485	3.082396862438	1.030261807915
H	3.226129877111	3.280623786263	1.276115697062
C	6.036895712376	-1.678714218138	0.159464799806
H	6.814820105468	-1.311580233440	0.840290312428
H	6.480818921593	-1.712200415347	-0.845717032487
H	5.800897906485	-2.710046480552	0.443720474985

Cartesian Coordinates for 222

C	-1.126553131552	-1.827652440225	0.042312150395
C	-1.161399729715	-1.846057442200	1.517446627887
N	0.073274037564	-1.833002604894	-0.608904756446
O	-1.977071760881	-2.520701606035	2.151841691578
N	-0.127409029365	-1.192993057354	2.214502826088
C	1.152435568649	-1.138016768407	-0.355345395772
C	0.430788285353	0.035136935174	1.750935623419
C	1.176974777506	0.034613719675	0.553455665687
C	2.352951573638	-1.480386343512	-1.160311186837
C	0.109261990755	-1.643411657873	3.579903996803
C	2.221829288972	-2.200391360881	-2.366276436437
C	3.658067339606	-1.168370749295	-0.730489374278
C	1.796795941620	1.229741511231	0.143757505434

C	0.261329069802	1.232318358148	2.481781673080
H	0.163143562111	-2.736318065114	3.587514751087
H	1.066100084337	-1.235484330908	3.919361560607
H	-0.676899732454	-1.352425460398	4.287578361069
C	4.775869754750	-1.543221264706	-1.476664633251
C	3.336302687119	-2.568862243748	-3.111010606796
H	1.220701865416	-2.460427068889	-2.692570468588
H	3.795839174416	-0.636522818207	0.206250610758
H	2.349386583813	1.234766839367	-0.791330753691
C	0.910438608917	2.389054088143	2.040673320073
C	1.682880444655	2.409801146531	0.874558295305
C	4.625972336578	-2.242988749418	-2.674532385333
H	5.770321028327	-1.290738739705	-1.113369579512
H	3.200656280485	-3.113265920199	-4.043665614819
H	0.779141038032	3.309385686161	2.607968301417
H	5.496849641978	-2.533218330770	-3.257970605934
C	-0.632043381180	1.309903279231	3.700168654136
H	-1.545686269099	0.723645805184	3.557417022612
H	-0.146834997487	0.933764993843	4.610240639408
H	-0.920828043018	2.349160690420	3.889841578399
C	-2.177411692066	-2.726698044476	-0.580709731652
H	-2.115452764846	-2.666339377855	-1.672253750170
H	-2.038628304174	-3.777175459223	-0.286592073526
C	-3.026287864604	0.515096811574	0.407399197079
C	-4.286423548068	0.044040065666	0.434415094157
H	-4.703487780011	-0.513728092538	-0.399925828269
H	-3.182350868393	-2.438857439772	-0.256805095062
C	-2.081946905383	0.308072412547	-0.667201858879
H	-1.079243786263	0.687324619625	-0.609244658657
H	-2.366840528942	-0.239788465106	-1.550942590210
Br	-2.469941292765	2.479353802820	-2.010635216194
C	2.300777668599	3.695495908120	0.374888445807
H	3.203831209631	3.503273799009	-0.215455192443
H	2.571288497050	4.361607675290	1.202865635571
H	1.599841358638	4.241608630358	-0.270249400766
H	-4.940563636263	0.219486301369	1.283525363528
H	-2.660473840570	1.097160885610	1.251196493691

Cartesian Coordinates for 223

C	-1.690664017937	-0.951424693204	-0.866980696309
C	-1.763836655812	0.448332522949	-0.696513703530
C	-2.763840506352	-1.641160487075	-1.482147721951
N	-0.538524103346	-1.626227908065	-0.374919435789
C	-3.823936720575	-0.905193934200	-2.016848425211
C	-2.872888241751	1.139399128854	-1.220508283110
C	0.139849099305	-2.660189337676	-1.158607438379
C	-0.784522898259	1.175220017943	0.155301228976
C	-0.495136971951	-1.771748091367	1.047226920440
C	-3.894468330104	0.488368863681	-1.907249987562
H	-4.637128735106	-1.442649326935	-2.504210023930
H	-2.934017849370	2.213982367360	-1.075006273487
H	1.208982604514	-2.643493936071	-0.914426607229
N	-0.294419544277	0.732458233544	1.278259617685
C	-0.441318231193	2.588937539290	-0.183225171515
C	-0.273684144314	-0.532629213187	1.797279561713

O	-0.452952324831	-2.897309586296	1.554323695323
C	-0.080474523635	3.495728748607	0.832658256027
C	-0.408315308698	3.050094088941	-1.512156743315
C	1.996174933041	-0.911459413174	1.406377364212
C	-0.044076742187	4.363477398008	-1.812198628666
C	0.275178730244	4.807039376950	0.533611112061
H	-0.076716226315	3.135477874092	1.855835022590
H	-0.656088458753	2.365655209264	-2.317752346585
H	1.857542835240	-1.969782956655	1.545584996908
H	1.834110149620	-0.495174888136	0.425173819219
C	0.294834823264	5.253234694090	-0.792500149944
H	-0.017148228028	4.687636322955	-2.850459538566
H	0.540542766284	5.488173997570	1.339693616342
H	0.578189294200	6.277060641649	-1.025622921358
C	-0.371198612096	-0.605988645345	3.303760205220
H	-1.403149229580	-0.426698463831	3.644416258009
H	0.263914859479	0.162926459638	3.755163795887
H	-0.071316600707	-1.594417007091	3.660004414874
C	2.666765624791	-0.137986702579	2.424429901029
C	2.848271991411	1.194632794990	2.374807743745
H	2.515877391958	1.781386615576	1.523996341498
Br	4.146394158380	-2.078464856513	0.177541657413
H	-0.235149509242	-3.674159556685	-0.980776994486
H	0.028685171341	-2.412259466043	-2.218391739994
C	-2.826120249540	-3.152530609590	-1.516454483150
H	-2.194404220993	-3.589167429112	-2.299881605336
H	-3.854545146030	-3.481543257699	-1.702172644838
H	-2.494637084372	-3.576629181160	-0.563440046055
C	-5.052069951046	1.257307091469	-2.503039033680
H	-6.005444758027	0.736848335535	-2.348083381077
H	-4.934072030755	1.392624564955	-3.587585514348
H	-5.138312600760	2.255074711957	-2.059105177564
H	3.339824969655	1.730398285507	3.183240942799
H	3.007750644825	-0.688902356928	3.299745798825

5.2 Experimental Procedures for Chapter 4

General

N-9'-(1', 2', 3', 4'-tetrahydroacridinyl)-1,n-diaminoalkanes ($AnNH_2$) were prepared according to the literature method.[3] ^1H NMR Spectra were recorded at 500 and 400 MHz; the corresponding ^{13}C NMR resonant frequencies were 125 and 100 MHz respectively. High resolution mass spectra were recorded under FAB conditions (NBA. PEG), in which the expected molecular formula (M+1, ^{35}Cl) gave the closest match among all possible formulas.

General procedure for tacrine-tethered haloacetamides and acetamide

To a stirred solution of N-9'-(1', 2', 3', 4'-tetrahydroacridinyl)-1,n-diaminoalkanes ($AnNH_2$) (1 equiv.) in 1:1 DCM/sat. Na_2CO_3 (4 mL) was added the desired haloacetic halide or iodoacetic anhydride or acetic anhydride (2 equiv.) at room temperature. The reaction mixture was stirred for 4 hours. The organic layer was separated and the aqueous layer was extracted with DCM (3 x 10 mL). The combined organic solution was dried over Na_2SO_4, and concentrated in vacuo. The crude product was purified with flash column chromatography on silica gel (9.5:0.5 DCM/Methanol with 7 mL NH_4OH per liter). The HCl or HBr salts were prepared by adding the corresponding acid into the product in methanol. The resulting solution was stirred for 30 min, followed by concentration in vacuo.

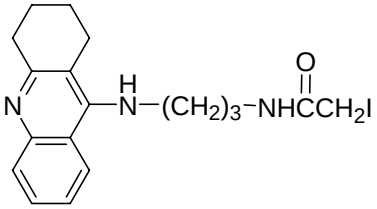

N9-(3-iodoacetamidopropyl)-tacrine [248c]

The general procedure was followed: $A3NH_2$ (0.05 g, 0.20 mmol, 1 equiv), iodoacetic anhydride (0.14 g, 0.39 mmol, 2 equiv). Purification with flash column chromatography on silica gel

(9.5:0.5 DCM/Methanol with 7 mL NH_4OH per liter) provided **248c** (50 mg, 59 %) as a yellow oil. ^1H NMR ($CDCl_3$): δ 7.98 (d, *J* = 9.6 Hz, 1H), δ 7.90 (d, *J* = 9.2 Hz, 1H), δ 7.55 (t, *J* = 8.2 Hz, 1H), δ 7.37 (t, *J* = 8.2 Hz, 1H), δ 6.47 (broad s, 1H), δ 4.60 (t, *J* = 6.8, 1H), δ 3.72 (s, 2H), δ 3.53-3.42 (m, 4H), δ 3.06 (apparent s, 2H), δ 2.78 (apparent s, 2H), δ 1.95-1.81 (m, 6H). ^{13}C NMR ($CDCl_3$): δ 168.24, 159.08, 150.87, 147.71, 129.09, 128.85, 124.44, 122.93, 120.88, 117.31, 45.90, 38.13, 34.43, 31.63, 25.55, 23.51, 23.23, -0.31. HRMS (FAB) calcd. for $C_{18}H_{23}N_3OI$ (M+1) 424.0886, found 424.0894 (+1.9 ppm, +0.8 mmu).

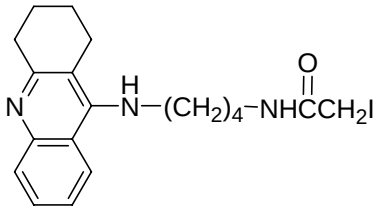

N9-(4-iodoacetamidobutyl)-tacrine [249c]

The general procedure was followed: $A4NH_2$ (0.05 g, 0.19 mmol, 1 equiv), iodoacetic anhydride (0.13 g, 0.38 mmol, 2 equiv). Purification with flash column chromatography on silica gel (9.5:0.5 DCM/Methanol with 7 mL NH_4OH per liter) provided **249c** (50 mg, 62 %) as a yellow oil. ^1H NMR ($CDCl_3$): δ 7.98-7.93 (m, 2H), δ 7.57 (t, *J* = 8.4 Hz, 1H), δ 7.37 (t, *J* = 8.4 Hz, 1H), δ 6.43 (broad s, 1H), δ 4.30 (broad s, 1H), δ 3.70 (s, 2H), δ 3.57 (q, *J* = 6.3 Hz, 2H), δ 3.32 (q, *J* = 6.5 Hz, 2H), δ 3.07 (apparent s, 2H), δ 2.71 (apparent s, 2H), δ 1.93-1.90 (m, 4H), δ 1.76-1.66 (m, 4H). ^{13}C NMR ($CDCl_3$): δ 167.31, 157.60, 151.38, 146.24, 129.14, 127.55, 124.20, 123.10, 119.80, 115.83, 48.89, 39.99, 33.33, 28.86, 26.88, 24.87, 22.98, 22.58, -0.18. HRMS (FAB) calcd. for $C_{19}H_{25}N_3OI$ (M+1) 438.1042, found 438.1037 (-1.2 ppm, -0.5 mmu).

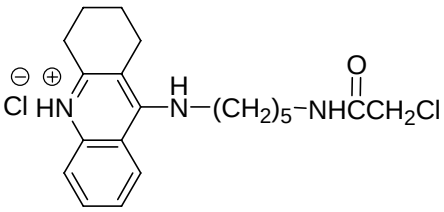

N9-(5-chloroacetamidopentyl)-tacrine, hydrochloride salt [250a]

The general procedure was followed: A5NH_2 (0.05 g, 0.18 mmol, 1 equiv), chloroacetic chloride (0.028 mL, 0.36 mmol, 2 equiv). Purification with flash column chromatography on silica gel (9.5:0.5 DCM/Methanol with 7 mL NH_4OH per liter) provided **250a** (48 mg, 59 %) as a brown oil. The HCl salt was prepared as above and was brown foam. ^{1}H NMR (CD_3OD): δ 8.35 (t, 1H), δ 7.80 (apparent d, J = 3.6 Hz, 2H), δ 7.55-7.51 (m, 1H), δ 4.00 (s, 2H), δ 3.91 (t, *J* = 7.2 Hz, 2H), δ 3.20 (t, *J* = 6.6 Hz, 2H), δ 2.99 (apparent s, 2H), δ 2.66 (apparent s, 2H), δ 1.91-1.79 (m, 6H), δ 1.59-1.50 (m, 2H), δ 1.45-1.38 (m, 2H). ^{13}C NMR (free base in $CDCl_3$): δ 166.21, 158.61, 150.89, 147.53, 128.75, 128.57, 123.90, 123.01, 120.39, 116.20, 49.43, 42.89, 39.80, 34.13, 31.51, 29.37, 25.03, 24.38, 23.22, 22.94. HRMS (FAB) calcd. for $C_{20}H_{27}N_3OCl$ (M+1) 360.1843, found 360.1822 (-5.8 ppm, -2.1 mmu).

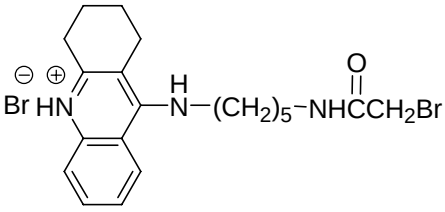

N9-(5-bromoacetamidopentyl)-tacrine, hydrobromide salt [250b]

The general procedure was followed: A5NH_2 (0.05 g, 0.18 mmol, 1 equiv), bromoacetic bromide (0.031 mL, 0.36 mmol, 2 equiv). Purification with flash column chromatography on silica gel (9.5:0.5 DCM/Methanol with 7 mL NH_4OH per liter) provided **250b** (48 mg, 66 %) as a brown oil. The HBr salt was prepared as above and was brown foam. ^{1}H NMR (CD_3OD): δ 8.39 (d, *J* =

8.8 Hz, 1H), δ 7.83-7.81 (m, 2H), δ 7.59-7.56 (m, H), δ 3.97 (t, *J* = 7.2 Hz, 2H), δ 3.85 (s, 2H), δ 3.31-3.30 (m, 2H), δ 3.23 (t, *J* = 6.6 Hz, 2H), δ 3.03 (apparent s, 2H), δ 2.72 (apparent s, 2H), δ 1.95-2.85 (m, 6H), δ 1.61-1.57 (m, 2H), δ 1.48-1.47 (m, 2H). ^{13}C NMR (free base in $CDCl_3$): δ 165.89, 158.18, 151.21, 147.03, 128.82, 128.23, 124.00, 123.16, 120.14, 115.91, 49.39, 40.10, 33.83, 31.45, 29.55, 29.31, 25.00, 24.40, 23.17, 22.83. HRMS (FAB) calcd. for $C_{20}H_{27}N_3OBr$ (M+1) 404.1337, found 404.1328 (-2.3 ppm, -0.9 mmu).

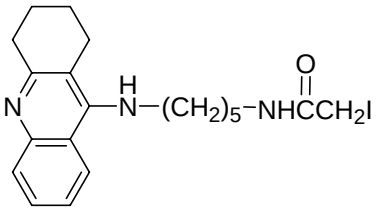

N9-(5-iodoacetamidopentyl)-tacrine [250c]

The general procedure was followed: A5NH_2 (0.05 g, 0.18 mmol, 1 equiv), iodoacetic anhydride (0.12 g, 0.36 mmol, 2 equiv). Purification with flash column chromatography on silica gel (9.5:0.5 DCM/Methanol with 7 mL NH_4OH per liter) provided **250c** (60 mg, 74 %) as a yellow oil. ^{1}H NMR ($CDCl_3$): δ 7.96-7.89 (m, 2H), δ 7.54 (t, *J* = 8.2 Hz, 1H), δ 7.34 (t, *J* = 8.2 Hz, 1H), δ 6.27 (broad s, 1H), δ 4.06 (t, *J* = 6 Hz, 1H), δ 3.68 (s, 2H), δ 3.50 (q, *J* = 6.8 Hz, 2H), δ 3.27 (q, *J* = 6.5 Hz, 2H), δ 3.05 (apparent s, 2H), δ 2.70 (apparent s, 2H), δ 1.93-1.88 (m, 4H), δ 1.73-1.65 (m, 2H), δ 1.60-1.52 (m, 2H), δ 1.50-1.43 (m, 2H). ^{13}C NMR ($CDCl_3$): δ 167.45, 157.68, 151.43, 146.46, 128.95, 127.51, 123.96, 123.18, 119.77, 115.53, 50.68, 49.23, 40.08, 33.35, 31.27, 29.08, 24.87, 24.18, 22.97, 22.59, -0.087. HRMS (FAB) calcd. for $C_{20}H_{27}N_3OI$ (M+1) 452.1199, found 452.1184 (-3.3 ppm, -1.5 mmu).

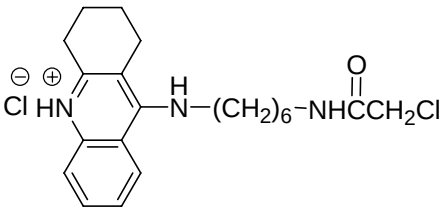

N9-(6-chloroacetamidohexyl)-tacrine, hydrochloride salt [251a]

The general procedure was followed: A6NH_2 (0.05 g, 0.17 mmol, 1 equiv), chloroacetic chloride (0.027 mL, 0.34 mmol, 2 equiv). Purification with flash column chromatography on silica gel (9.5:0.5 DCM/Methanol with 7 mL NH_4OH per liter) provided **251a** (37 mg, 58 %) as a brown oil. The HCl salt was prepared as above and was brown foam. ^{1}H NMR (CD_3OD): δ 8.39 (t, *J* = 8 Hz, 1H), δ 7.84-7.82 (m, 2H), δ 7.62-7.58 (m, 1H), δ 4.02 (s, 2H), δ 3.97-3.94 (m, 2H), δ 3.21 (t, *J* = 7.0 Hz, 2H), δ 3.04 (apparent s, 2H), δ 2.94-2.92 (m, 2H), δ 2.72 (apparent s, 2H), δ 1.95 (apparent s, 4H), δ 1.85-1.84 (m, 2H), δ 1.70 (apparent s, 2H), δ 1.54-1.38 (m, 4H). ^{13}C NMR (free base in $CDCl_3$): δ 166.05, 158.54, 151.03, 147.47, 128.79, 128.64, 123.93, 123.03, 120.36, 116.11, 49.55, 42.92, 39.89, 34.13, 31.86, 29.51, 26.76, 25.02, 23.25, 22.96. HRMS (FAB) calcd. for $C_{21}H_{29}N_3OCl$ (M+1) 374.1999, found 374.2006 (+1.8 ppm, +0.7 mmu).

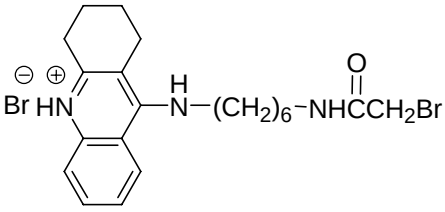

N9-(6-bromoacetamidohexyl)-tacrine, hydrobromide salt [251b]

The general procedure was followed: A6NH_2 (0.05 g, 0.17 mmol, 1 equiv), bromoacetic bromide (0.030 mL, 0.34 mmol, 2 equiv). Purification with flash column chromatography on silica gel (9.5:0.5 DCM/Methanol with 7 mL NH_4OH per liter) provided **251b** (45 mg, 63 %) as a brown oil. The HBr salt was prepared as above and was brown foam. ^{1}H NMR (CD_3OD): δ 8.38 (d, *J* =

8.4 Hz, 1H), δ 7.82-7.80 (m, 2H), δ 7.57 (apparent s, 1H), δ 3.95 (t, *J* = 7.4 Hz, 2H), δ 3.85 (s, 2H), δ 3.19 (t, *J* = 7.0 Hz, 2H), δ 3.03 (apparent s, 2H), δ 2.67 (apparent s, 2H), δ 1.94-1.82 (m, 6H), δ 1.55-1.33 (m, 6H). ^{13}C NMR (free base in $CDCl_3$): δ 165.62, 158.63, 150.96, 147.61, 128.84, 128.56, 123.87, 123.06, 120.42, 116.16, 49.53, 40.22, 34.23, 31.85, 29.58, 29.43, 26.74, 25.03, 23.26, 22.99. HRMS (FAB) calcd. for $C_{21}H_{29}N_3OBr$ (M+1) 418.1494, found 418.1471 (-5.5 ppm, -2.3 mmu).

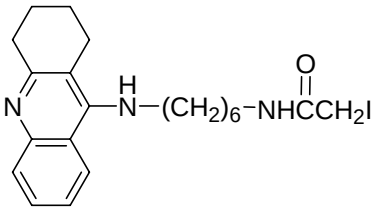

N9-(6-iodoacetamidohexyl)-tacrine [251c]

The general procedure was followed: A6NH$_2$ (0.05 g, 0.17 mmol, 1 equiv), iodoacetic anhydride (0.12 g, 0.34 mmol, 2 equiv). Purification with flash column chromatography on silica gel (9.5:0.5 DCM/Methanol with 7 mL NH_4OH per liter) provided **251c** (51 mg, 64 %) as a yellow oil. ^{1}H NMR ($CDCl_3$): δ 7.93 (d, *J* = 9.6 Hz, 2H), δ 7.86 (d, *J* = 8.4 Hz, 1H), δ 7.52 (t, *J* = 8.4 Hz, 1H), δ 7.32(t, *J* = 8.2 Hz, 1H), δ 6.68 (broad s, 1H), δ 4.00 (t, *J* = 6 Hz, 1H), δ 3.65 (s, 2H), δ 3.45 (q, *J* = 6.8 Hz, 2H), δ 3.22 (q, *J* = 6.8 Hz, 2H), δ 3.03 (apparent s, 2H), δ 2.67 (apparent s, 2H), δ 1.91-1.88 (m, 4H), δ 1.64-1.60 (m, 2H), δ 1.51-1.48 (m, 2H), δ 1.39-1.31 (m, 4H). ^{13}C NMR ($CDCl_3$): δ 167.22, 158.41, 150.88, 147.38, 128.51, 128.45, 123.71, 123.01, 120.19, 115.89, 49.33, 40.18, 34.02, 31.67, 29.21, 26.56, 26.53, 24.87, 23.08, 22.81, -0.072. HRMS (FAB) calcd. for $C_{21}H_{29}N_3OI$ (M+1) 466.1355, found 466.1343 (-2.6 ppm, -1.2 mmu).

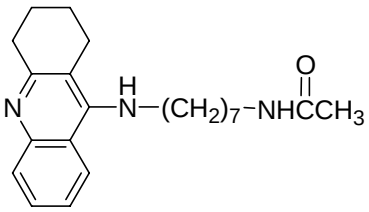

N9-(7-acetamidoheptyl)-tacrine [252]

The general procedure was followed: A7NH_2 (0.05 g, 0.16 mmol, 1 equiv), acetic anhydride (0.030 mL, 0.32 mmol, 2 equiv). Purification with flash column chromatography on silica gel (9.5:0.5 DCM/Methanol with 7 mL NH_4OH per liter) provided **252** (39 mg, 69 %) as a brown oil. ^{1}H NMR ($CDCl_3$): δ 7.94 (d, *J* = 9.2 Hz, 1H), δ 7.89 (d, *J* = 9.2 Hz, 1H), δ 7.53 (t, *J* = 8.2 Hz, 1H), δ 7.33 (t, *J* = 8.4 Hz, 1H), δ 5.69 (broad s, 1H), δ 3.97 (broad s, 1H), δ 3.46 (q, *J* = 6.4 Hz, 2H), δ 3.19 (q, *J* = 6.8 Hz, 2H), δ 3.04 (apparent s, 2H), δ 2.69 (apparent s, 2H), δ 1.95-1.89 (m, 7H), δ 1.66-1.59 (m, 2H), δ 1.47-1.26 (m, 8H). ^{13}C NMR ($CDCl_3$): δ 170.28, 158.63, 151.04, 147.63, 128.86, 128.55, 123.83, 123.11, 120.41, 116.08, 49.62, 39.75, 34.24, 31.89, 29.71, 29.16, 26.98, 26.95, 25.01, 23.57, 23.27, 23.00. HRMS (FAB) calcd. for $C_{22}H_{32}N_3O$ (M+1) 354.2545, found 354.2546 (+0.2 ppm, +0.1 mmu).

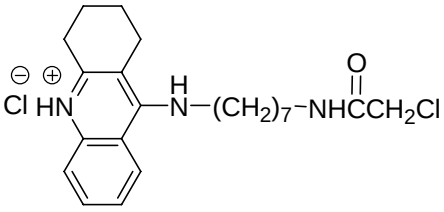

N9-(7-chloroacetamidoheptyl)-tacrine, hydrochloride salt [252a]

The general procedure was followed: A7NH_2 (0.05 g, 0.16 mmol, 1 equiv), chloroacetic chloride (0.025 mL, 0.32 mmol, 2 equiv). Purification with flash column chromatography on silica gel (9.5:0.5 DCM/Methanol with 7 mL NH_4OH per liter) provided **252a** (32 mg, 52 %) as a brown oil. The HCl salt was prepared as above and was brown foam. ^{1}H NMR (CD_3OD): δ 8.37 (d, *J* =

8.4 Hz, 1H), δ 7.82-7.80 (m, 2H), δ 7.59-7.56 (m, 1H), δ 4.02 (s, 2H), δ 3.94 (t, *J* = 7.2 Hz, 2H), δ 3.19 (t, *J* = 7.0 Hz, 2H), δ 3.02 (apparent s, 2H), δ 2.69 (apparent s, 2H), δ 1.96 (apparent s, 4H), δ 1.85-1.81 (m, 2H), 1.53-1.36 (m, 8H). ^{13}C NMR (CD_3OD): δ 168.07, 156.74, 150.44, 138.53, 132.89, 125.34, 125.16, 118.94, 115.81, 111.63, 48.71, 42.08, 39.52, 30.26, 28.88, 28.66, 28.15, 26.50, 26.42, 23.79, 21.83, 20.68. HRMS (FAB) calcd. for $C_{22}H_{31}N_3OCl$ (M+1) 388.2156, found 388.2157 (+0.3 ppm, +0.1 mmu).

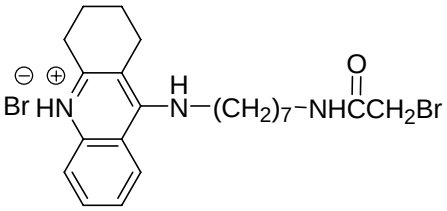

N9-(7-bromoacetamidoheptyl)-tacrine, hydrobromide salt [252b]

The general procedure was followed: A7NH_2 (0.05 g, 0.16 mmol, 1 equiv), bromoacetic bromide (0.028 mL, 0.32 mmol, 2 equiv). Purification with flash column chromatography on silica gel (9.5:0.5 DCM/Methanol with 7 mL NH_4OH per liter) provided **252b** (41 mg, 59 %) as a brown oil. The HBr salt was prepared as above and was brown foam. ^{1}H NMR (CD_3OD): δ 8.33 (d, *J* = 8 Hz, 1H), δ 7.78 (apparent s, 2H), δ 7.54 (apparent s, 1H), δ 3.92-3.87 (m, 4H), δ 3.19-3.16 (m, 2H), δ 3.01 (apparent s, 2H), δ 2.68 (apparent s, 2H), δ 1.93-1.82 (m, 6H), δ 1.50-1.35 (m, 8H). ^{13}C NMR (CD_3OD): δ 168.54, 156.51, 150.34, 138.36, 132.88, 125.42, 125.27, 118.90, 115.69, 111.62, 39.82, 30.34, 28.71, 28.69, 28.27, 27.85, 26.51, 26.46, 24.03, 21.87, 20.72. HRMS (FAB) calcd. for $C_{22}H_{31}N_3OBr$ (M+1) 432.1650, found 432.1630 (-4.8 ppm, -2.1 mmu).

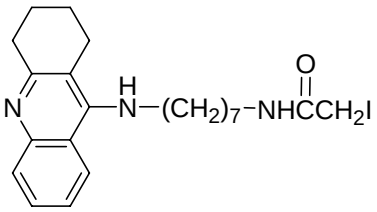

N9-(7-iodoacetamidoheptyl)-tacrine [252c]

The general procedure was followed: A7NH_2 (0.05 g, 0.16 mmol, 1 equiv), iodoacetic anhydride (0.11 g, 0.32 mmol, 2 equiv). Purification with flash column chromatography on silica gel (9.5:0.5 DCM/Methanol with 7 mL NH_4OH per liter) provided **252c** (59 mg, 77 %) as a yellow oil. ^{1}H NMR ($CDCl_3$): δ 7.93 (d, *J* = 8.4 Hz, 1H), δ 7.87 (d, *J* = 8 Hz, 1H), δ 7.52 (t, *J* = 8.2 Hz, 1H), δ 7.32 (t, *J* = 8.2 Hz, 1H), δ 6.64 (broad s, 1H), δ 4.00 (t, *J* = 6 Hz, 1H), δ 3.67 (s, 2H), δ 3.46 (q, *J* = 6.7 Hz, 2H), δ 3.21 (q, *J* = 6.7 Hz, 2H), δ 3.03 (apparent s, 2H), δ 2.68 (apparent s, 2H), δ 1.89 (apparent s, 4H), δ 1.64-1.58 (m, 2H), δ 1.47-1.44 (m, 2H), δ 1.34-1.28 (m, 6H). ^{13}C NMR ($CDCl_3$): δ 167.17, 158.41, 150.97, 147.37, 128.48, 128.46, 123.69, 123.02, 120.19, 115.85, 49.43, 40.32, 34.01, 31.71, 29.13, 28.94, 26.79, 26.66, 24.85, 23.09, 22.82, -0.049. HRMS (FAB) calcd. for $C_{22}H_{31}N_3OI$ (M+1) 480.1512, found 480.1524 (+2.5 ppm, +1.2 mmu).

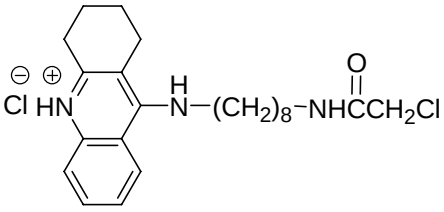

N9-(8-chloroacetamidooctyl)-tacrine, hydrochloride salt [253a]

The general procedure was followed: A8NH_2 (0.05 g, 0.15 mmol, 1 equiv), chloroacetic chloride (0.024 mL, 0.31 mmol, 2 equiv). Purification with flash column chromatography on silica gel (9.5:0.5 DCM/Methanol with 7 mL NH_4OH per liter) provided **253a** (42 mg, 69 %) as a brown oil. The HCl salt was prepared as above and was brown foam. ^{1}H NMR (CD_3OD): δ 8.35 (d, *J* =

8.8 Hz, 1H), δ 7.81 (apparent d, *J* = 3.6 Hz, 2H), δ 7.56-7.54 (m, 1H), δ 4.04 (s, 2H), δ 3.92 (t, *J* = 7.2 Hz, 2H), δ 3.18 (t, *J* = 7 Hz, 2H), δ 3.02 (apparent s, 2H), δ 2.68 (apparent s, 2H), δ 1.94 (apparent s, 4H), δ 1.83-1.80 (m, 2H), δ 1.51-1.31 (m, 10H). ^{13}C NMR (free base in $CDCl_3$): δ 165.99, 158.72, 150.96, 147.78, 129.01, 128.46, 123.78, 123.09, 120.48, 116.13, 49.70, 42.93, 40.03, 34.34, 31.97, 29.50, 29.42, 29.31, 27.05, 26.89, 25.03, 23.30, 23.05. HRMS (FAB) calcd. for $C_{23}H_{33}N_3OCl$ (M+1) 402.2312, found 402.2313 (+0.2 ppm, +0.1 mmu).

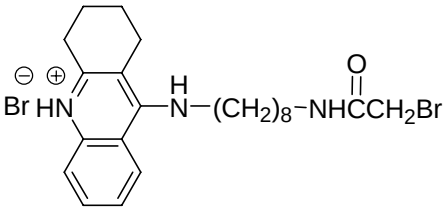

N9-(8-bromoacetamidooctyl)-tacrine, hydrobromide [253b]

The general procedure was followed: A8NH_2 (0.05 g, 0.15 mmol, 1 equiv), bromoacetic bromide (0.027 mL, 0.31 mmol, 2 equiv). Purification with flash column chromatography on silica gel (9.5:0.5 DCM/Methanol with 7 mL NH_4OH per liter) provided **253b** (67 mg, 72 %) as a brown oil. The HBr salt was prepared as above and was brown foam. ^{1}H NMR (CD_3OD): δ 8.39 (d, *J* = 8.8 Hz, 1H), δ 7.83 (apparent d, *J* = 4 Hz, 2H), δ 7.59-7.56 (m, 1H), δ 3.97-3.93 (m, 2H), δ 3.84 (s, 2H), δ 3.17 (t, *J* = 7.0 Hz, 2H), δ 3.03 (apparent s, 2H), δ 2.71 (apparent s, 2H), δ 1.95-1.81 (m, 6H), δ 1.49-1.32 (m, 10H). ^{13}C NMR (free base in $CDCl_3$): δ 165.60, 151.22, 128.67, 128.54, 123.86, 123.19, 115.86, 49.63, 40.37, 34.05, 31.92, 29.63, 29.41, 29.37, 29.27, 27.01, 26.86, 24.98, 23.23, 22.93. HRMS (FAB) calcd. for $C_{23}H_{33}N_3OBr$ (M+1) 446.1807, found 446.1765 (-9.4 ppm, -4.2 mmu).

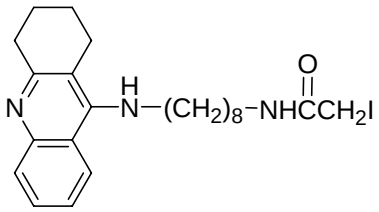

N9-(8-iodoacetamidooctyl)-tacrine [253c]

The general procedure was followed: A8NH_2 (0.05 g, 0.14 mmol, 1 equiv), iodoacetic anhydride (0.11 g, 0.31 mmol, 2 equiv). Purification with flash column chromatography on silica gel (9.5:0.5 DCM/Methanol with 7 mL NH_4OH per liter) provided **253c** (53 mg, 71 %) as a yellow oil. ^{1}H NMR ($CDCl_3$): δ 7.94 (d, *J* = 9.6 Hz, 1H), δ 7.87 (d, *J* = 9.2 Hz, 1H), δ 7.53 (t, *J* = 8.2 Hz, 1H), δ 7.32 (t, *J* = 8.2 Hz, 1H), δ 6.54 (broad s, 1H), δ 3.96 (apparent t, *J* = 5.6 Hz, 1H), δ 3.67 (s, 2H), δ 3.47 (q, *J* = 6.8 Hz, 2H), δ 3.22 (q, *J* = 6.8 Hz, 2H), δ 3.04 (apparent s, 2H), δ 2.69 (apparent s, 2H), δ 1.92-1.88 (m, 4H), δ 1.64-1.61 (m, 2H), δ 1.48-1.44 (m, 2H), δ 1.36-1.27 (m, 8H). ^{13}C NMR (free base in $CDCl_3$): δ 167.05, 158.52, 150.98, 147.52, 128.67, 128.44, 123.69, 123.04, 120.26, 115.89, 49.51, 40.43, 34.12, 31.84, 29.23, 29.21, 29.14, 26.85, 26.69, 24.89, 23.15, 22.88, -0.014. HRMS (FAB) calcd. for $C_{23}H_{33}N_3OI$ (M+1) 494.1668, found 494.1662 (-1.3 ppm, -0.6 mmu).

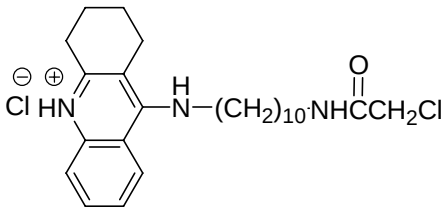

N9-(10-chloroacetamidodecyl)-tacrine, hydrochloride salt [254a]

The general procedure was followed: A10NH_2 (0.05 g, 0.14 mmol, 1 equiv), chloroacetic chloride (0.022 mL, 0.28 mmol, 2 equiv). Purification with flash column chromatography on silica gel (9.5:0.5 DCM/Methanol with 7 mL NH_4OH per liter) provided **254a** (52 mg, 87 %) as

a brown oil. The HCl salt was prepared as above and was brown foam. ^{1}H NMR (CD_3OD): δ 8.35 (d, *J* = 8.8 Hz, 1H), δ 7.80-7.76 (m, 2H), δ 7.60-7.53 (m, 1H), δ 3.99 (s, 2H), δ 3.91 (t, *J* = 7.2 Hz, 2H), δ 3.16 (t, *J* = 7.0 Hz, 2H), δ 3.00 (apparent s, 2H), δ 2.66 (apparent s, 2H), δ 1.93-1.77 (m, 6H), δ 1.48-1.26 (m, 14H). ^{13}C NMR (free base in $CDCl_3$): δ 166.01, 158.65, 151.00, 147.74, 128.92, 128.44, 123.73, 123.13, 120.44, 116.01, 49.72, 42.92, 40.07, 34.30, 31.98, 29.60, 29.55, 29.50, 29.36, 27.10, 26.98, 25.00, 23.28, 23.03. HRMS (FAB) calcd. for $C_{25}H_{37}N_3OCl$ (M+1) 430.2625, found 430.2631 (+1.3 ppm, +0.6 mmu).

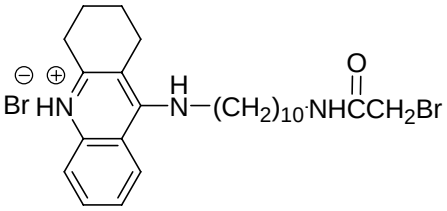

N9-(10-bromoacetamidodecyl)-tacrine, hydrobromide salt [254b]

The general procedure was followed: A10NH_2 (0.05 g, 0.14 mmol, 1 equiv), bromoacetic bromide (0.024 mL, 0.28 mmol, 2 equiv). Purification with flash column chromatography on silica gel (9.5:0.5 DCM/Methanol with 7 mL NH_4OH per liter) provided **254b** (50 mg, 76 %) as a brown oil. The HBr salt was prepared as above and was brown foam. ^{1}H NMR (CD_3OD): δ 8.40 (d, *J* = 8.8, 1H), δ 7.85 (m, 2H), δ 7.59 (t, *J* = 8 Hz, 1H), δ 3.96 (t, *J* = 7.2 Hz, 2H), δ 3.88 (s, 2H), δ 3.17 (t, *J* = 6.8 Hz, 2H), δ 3.04 (apparent s, 2H), δ 2.71 (apparent s, 2H), δ 1.94-1.80 (m, 6 H), δ 1.49-1.26 (m, 14H). ^{13}C NMR (free base in $CDCl_3$): δ 165.46, 158.57, 151.11, 147.60, 128.84, 128.56, 123.80, 123.14, 120.38, 115.97, 49.74, 40.44, 34.22, 31.99, 29.65, 29.60, 29.54, 29.50, 29.46, 29.37, 27.09, 26.98, 25.00, 23.28, 23.01. HRMS (FAB) calcd. for $C_{25}H_{37}N_3OBr$ (M+1) 474.2120, found 474.2119 (-0.2 ppm, -0.1 mmu).

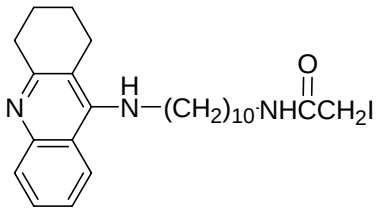

N9-(10-iodoacetamidodecyl)-tacrine [254c]

The general procedure was followed: A10NH_2 (0.05 g, 0.14 mmol, 1 equiv), iodoacetic anhydride (0.099 g, 0.28 mmol, 2 equiv). Purification with flash column chromatography on silica gel (9.5:0.5 DCM/Methanol with 7 mL NH_4OH per liter) provided **254c** (73 mg, 77 %) as a yellow oil. ^{1}H NMR ($CDCl_3$): δ 7.95 (d, *J* = 8.8 Hz, 1H), δ 7.88 (d, *J* = 8.4 Hz, 1H), δ 7.53 (t, *J* = 8.2 Hz, 1H), δ 7.33 (t, *J* = 8.2 Hz, 1H), δ 6.55 (broad s, 1H), δ 3.97 (apparent s, 1H), δ 3.69 (s, 2H), δ 3.49 (q, *J* = 6.5 Hz, 2H), δ 3.24 (q, *J* = 6.7 Hz, 2H), δ 3.04 (apparent s, 2H), δ 2.70 (apparent s, 2H), δ 1.92-1.89 (m, 4H), δ 1.65-1.59 (m, 2H), δ 1.49-1.46 (m, 2H), δ 1.36-1.23 (m, 12 H). ^{13}C NMR ($CDCl_3$): δ 166.99, 158.51, 150.96, 147.56, 128.69, 128.40, 123.65, 123.04, 120.28, 115.85, 49.55, 40.52, 34.14, 31.84, 29.42, 29.36, 29.30, 29.25, 26.89, 26.83, 24.89, 23.16, 22.89, -0.011. HRMS (FAB) calcd. for $C_{25}H_{37}N_3OI$ (M+1) 522.1987, found 522.1973 (-1.6 ppm, -0.8 mmu).

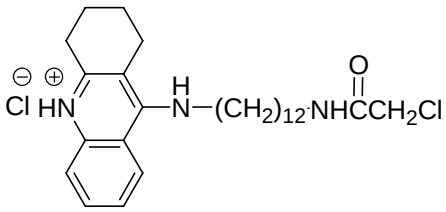

N9-(12-chloroacetamidododecyl)-tacrine, hydrochloride salt [255a]

The general procedure was followed: A12NH_2 (0.05 g, 0.13 mmol, 1 equiv), chloroacetic chloride (0.021 mL , 0.26 mmol, 2 equiv). Purification with flash column chromatography on silica gel (9.5:0.5 DCM/Methanol with 7 mL NH_4OH per liter) provided **255a** (46 mg, 78 %) as

a brown oil. The HCl salt was prepared as above and was brown foam. ^{1}H NMR (CD_3OD): δ 8.38 (d, *J* = 8.4 Hz, 1H), δ 7.84-7.82 (m, 2H), δ 7.59-7.55 (m, 1H), δ 4.05 (s, 2H), δ 3.94 (t, *J* = 7.2 Hz, 2H), δ 3.18 (t, *J* = 7.2 Hz, 2H), δ 3.03 (apparent s, 2H), δ 2.70 (apparent s, 2H), δ 1.94 (apparent s, 4H), δ 1.83-1.80 (m, 2H), δ 1.51-1.24 (m, 18H). ^{13}C NMR (CD_3OH): δ 168.29, 156.74, 150.46, 138.52, 132.89, 125.35, 125.19, 119.01, 115.82, 111.64, 42.10, 39.85, 39.72, 30.32, 29.40, 29.34, 29.33, 29.13, 29.02, 28.95, 28.20, 26.68, 26.45, 23.90, 21.85, 20.70. HRMS (FAB) calcd. for $C_{27}H_{41}N_3OCl$ (M+1) 458.2938, found 458.2957 (+4.1 ppm, +1.9 mmu).

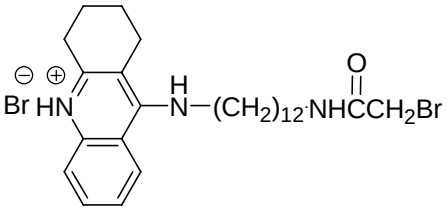

N9-(12-bromoacetamidododecyl)-tacrine, hydrobromide salt [255b]

The general procedure was followed: A12NH_2 (0.05 g, 0.13 mmol, 1 equiv), bromoacetic bromide (0.023 mL, 0.26 mmol, 2 equiv). Purification with flash column chromatography on silica gel (9.5:0.5 DCM/Methanol with 7 mL NH_4OH per liter) provided **255b** (22 mg, 33 %) as a brown oil. The HBr salt was prepared as above and was brown foam. ^{1}H NMR (CD_3OD): δ 8.39 (d, *J* = 8.5 Hz, 1H), δ 7.84-7.82 (m, 1H), δ 7.77-7.76 (m, 1H), δ 7.60-7.57 (m, 1H), δ 3.95 (t, *J* = 7.2 Hz, 2H), δ 3.80 (s, 2H), δ 3.18 (t, *J* = 7.2 Hz, 2H), δ 3.01 (apparent s, 2H), δ 2.70 (apparent s, 2H), δ 1.96 (apparent s, 4H), δ1.82 (m, 2H), δ 1.50-1.27 (m, 20H). ^{13}C NMR (free base in $CDCl_3$): 165.45, 158.59, 151.09, 147.65, 128.87, 128.53, 123.78, 123.15, 120.39, 115.97, 49.77, 40.46, 34.25, 32.01, 29.70, 29.65, 29.56, 29.47, 29.41, 27.14, 27.01, 25.00, 23.29, 23.02. HRMS (FAB) calcd. for $C_{27}H_{41}N_3OBr$ (M+1) 502.2433, found 502.2416 (-3.4 ppm, -1.7 mmu).

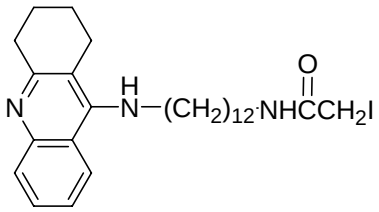

N9-(12-iodoacetamidododecyl)-tacrine, [255c]

The general procedure was followed: A12NH_2 (0.05 g, 0.13 mmol, 1 equiv), iodoacetic anhydride (0.092 g, 0.26 mmol, 2 equiv). Purification with flash column chromatography on silica gel (9.5:0.5 DCM/Methanol with 7 mL NH_4OH per liter) provided **255c** (33 mg, 46 %) as a yellow oil. ^{1}H NMR ($CDCl_3$): δ 7.96 (d, *J* = 9.2 Hz, 1H), δ 7.89 (d, *J* = 9.2, 1H), δ 7.54 (t, *J* = 8.4 Hz, 1H), δ 7.33 (t, *J* = 8.4 Hz, 1H), δ 6.43 (broad s, 1H), δ 3.99 (broad, s, 1H), δ 3.69 (s, 2H), δ 3.49 (apparent s, 2H), δ 3.25 (q, *J* = 6.3 Hz, 2H), δ 3.05 (apparent s, 2H), δ 2.70 (apparent s, 2H), δ 1.93-1.90 (m, 4H), δ 1.66-1.61 (m, 2H), δ 1.51-1.46 (m, 2H), δ 1.38-1.23 (m, 18H). ^{13}C NMR ($CDCl_3$): δ 166.88, 158.44, 151.02, 147.47, 128.64, 128.45, 123.67, 123.07, 120.24, 115.80, 49.61, 40.55, 34.09, 31.86, 29.55, 29.39, 29.30, 26.97, 26.87, 24.88, 23.16, 22.88, 0.012. HRMS (FAB) calcd. for $C_{27}H_{41}N_3OI$ (M+1) 550.2294, found 550.2300 (+1.0 ppm, +0.5 mmu).

Bioassay Procedure

Procedure for preparation of homogenate *Ag*AChE and Aphid AChE provided by Dr. Troy Anderson, Bloomquist lab (Entomology, VT)

Individual mosquitoes were homogenized in 100 μL of ice-cold 0.1 M Na_2HPO_4 buffer (pH 7.8 for *Ag*; pH 7.0 for aphid), containing Triton X-100 (0.3% for *Ag*; 0.05% for aphid), using a glass tissue homogenizer. Ten adult mosquitoes or aphids were enough for one 48-well microplate assay and could be pooled together.

Ten mosquitoes/aphids were homogenized in 1 ml of the Na_2HPO_4 buffer. The homogenate was centrifuged for 10 min in the microcentrifuge (2,200 rpm) at 4°C. While the tissue preparation was in the centrifuge, the microplate with the anticholinesterase compounds and Ellman assay[4] reagents (i.e., ATCh-DTNB mixture) were prepared.

Procedure for obtaining recombinant protein by cell lysing provided by Dr. Ranginee Choudhury, Wong lab (Animal and Poultry, VT)

Recombinant *Ag*AChE was expressed using Drosophila S2 cells. The cells were lysed in either low salt phosphate buffer (50 mM NaH_2PO_4 and 144mM NaCl) or high salt phosphate (50 mM NaH_2PO_4, pH 8.0, and 0.5 M NaCl) depending on treatment later on. The resultant was treated by PIPLC treatment, in which the protease inhibitors were composed of 1.4 mM of Pepstatin, 0.3 mM of Aprotinin, 1 mM of Leupeptin and 1mM of EDTA (optional i.e. not added when the protein was purified using Ni column).

Finally, 1% NP-40 was added to the lysis buffer (Note: non-ionising detergent was not added when the cells were to be treated with PIPLC). The cells were harvested followed by a brief wash with Phosphate Buffered Saline. Lysis buffer was then added and the cells were incubated at 4 ºC with gentle agitation for 15 minutes. This was followed by centrifugation at

5000 rpm for 15 minutes. The clear supernatant was extracted and used for Ellman Assay with or without inhibitors.

Procedure for Ellman assay

A 96-well microplate was selected and the bottom was covered with "Saran Wrap". Aluminum foil was placed on ice and the microplate was rested on the foil to chill the microplate. 10 µl of an anticholinesterase compound treatment was pipetted into the top wells of the microplate. A blank group (i.e., no anticholinesterase compound and no tissue preparation) and a control group (i.e., no anticholinesterase compound) were included. The Na_2HPO_4 buffer may be used to substitute the anticholinesterase compound and tissue preparation. 80 µl of ice-cold 0.1 M Na_2HPO_4 buffer (pH 7.8) was pipetted into each of the top wells of the microplate. The top wells should corresponded to the treatments in the bottom wells. The Ellman reagents were prepared in a 100 ml pipetting tray by combining 273.6 µl ATCh (42.4 mM for *Ag*; 0.5 mM for aphid), 1.35 ml DTNB (6.4 mM for *Ag*; 0.4 mM for aphid), and 11.34 ml 0.1 M Na_2HPO_4 buffer. 20 µl of an anticholinesterase compound treatment and 180 µl of ATCh-DTNB mixture were pipetted into the bottom wells of the microplate.

Following centrifugation, the supernatant of the tissue preparation was carefully transferred into clean 1.5-ml microcentrifuge tubes. The homogenate was kept on ice. 10 µl of homogenate was pipetted into the top wells of the microplate containing anticholinesterase compound using a "repeating" pipette. The microplate was incubated at RT for 10 min while shaking. 100 µl of Ellman assay reagents (i.e., ATCh-DTNB mixture) were transferred from the bottom wells to the corresponding top wells using a "multi-channel" pipette. The optical density of the samples were determined and recorded using a DYNEX *Triad* microplate reader at 405 nm for 30 min at 25°C.

References for Chapter 5

1. Sternbach, L. H.; Reeder, E.; Keller, O.; Metlesics, W., Quinazolines and 1,4-Benzodiazepines. III. Substituted 2-Amino-5-phenyl-3H-1,4-benzodiazepine-4-Oxides. *Journal of Organic Chemistry* **1961,** 26, 4488-4497.

2. Sternbach, L. H.; Fryer, R. I.; Metlesics, W.; Reeder, E.; Sach, G.; Saucy, G.; Stempel, A., Quinazolines and 1,4-Benzodiazepines. VI. Halo-, Methyl-, and Methoxy-substituted 1,3-Dihydro-5-phenyl-2*H*-1,4-benzodiazepin-2-ones. *Journal of Organic Chemistry* **1962,** 27, 3788-3796.

3. Carlier, P. R.; Zhao, H.; MacQuarrie-Hunter, S. L.; DeGuzman, J. C.; Hsu, D. C., Enantioselective synthesis of diversely substituted quaternary 1,4-benzodiazepin-2-ones and 1,4-benzodiazepine-2,5-diones. *Journal of the American Chemical Society* **2006,** 128, (47), 15215-15220.

4. Perrin, C. L.; Dwyer, T. J., Application of 2-Dimensional NMR to Kinetics of Chemical Exchange. *Chemical Reviews* **1990,** 90, 935-967.

5. Gaussian 03, Revision B.05, M. J. Frisch, G. W. Trucks, H. B. Schlegel, G. E. Scuseria, M. A. Robb, J. R. Cheeseman, J. A. Montgomery, Jr., T. Vreven, K. N. Kudin, J. C. Burant, J. M. Millam, S. S. Iyengar, J. Tomasi, V. Barone, B. Mennucci, M. Cossi, G. Scalmani, N. Rega, G. A. Petersson, H. Nakatsuji, M. Hada, M. Ehara, K. Toyota, R. Fukuda, J. Hasegawa, M. Ishida, T. Nakajima, Y. Honda, O. Kitao, H. Nakai, M. Klene, X. Li, J. E. Knox, H. P. Hratchian, J. B. Cross, C. Adamo, J. Jaramillo, R. Gomperts, R. E. Stratmann, O. Yazyev, A. J. Austin, R. Cammi, C. Pomelli, J. W. Ochterski, P. Y. Ayala, K. Morokuma, G. A. Voth, P. Salvador, J. J. Dannenberg, V. G. Zakrzewski, S. Dapprich, A. D. Daniels, M. C. Strain, O. Farkas, D. K. Malick, A. D. Rabuck, K. Raghavachari, J. B. Foresman, J. V. Ortiz, Q. Cui, A. G. Baboul, S. Clifford, J. Cioslowski, B. B. Stefanov, G. Liu, A. Liashenko, P. Piskorz, I. Komaromi, R. L. Martin, D. J. Fox, T. Keith, M. A. Al-Laham, C. Y. Peng, A. Nanayakkara, M. Challacombe, P. M. W. Gill, B. Johnson, W. Chen, M. W. Wong, C. Gonzalez, and J. A. Pople, Gaussian, Inc., Pittsburgh PA, 2003.

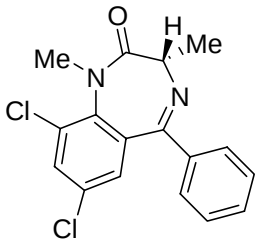
O
H
Me
Me
N
N
Cl
Cl

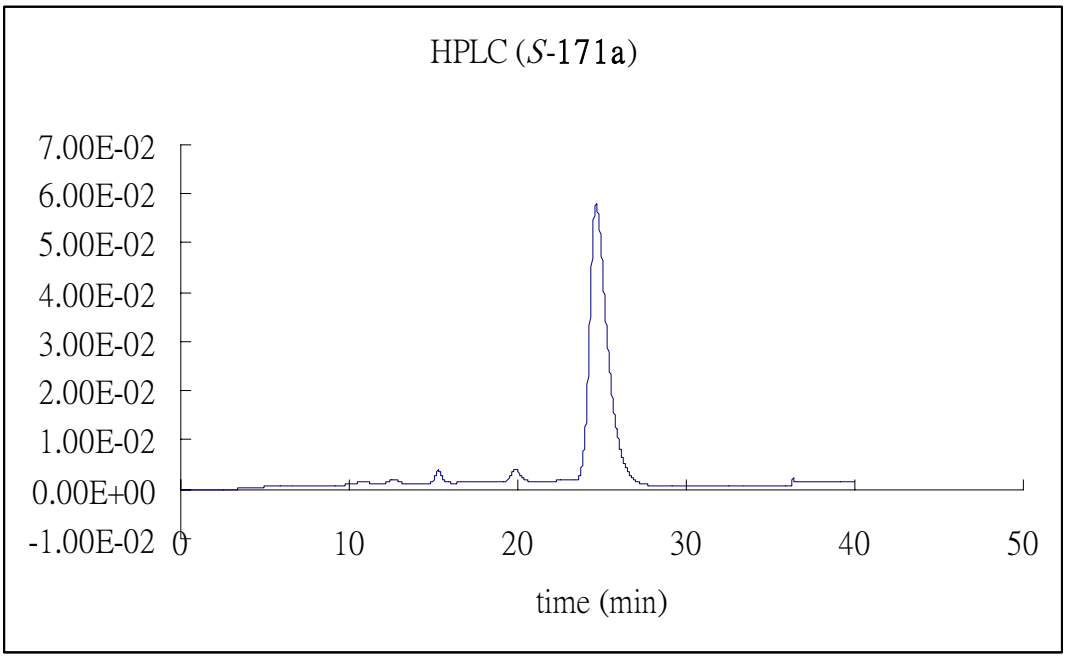
HPLC (S-171a)
7.00E-02
6.00E-02
5.00E-02
4.00E-02
3.00E-02
2.00E-02
1.00E-02
0.00E+00
-1.00E-02
0
10
20
30
40
50
time (min)

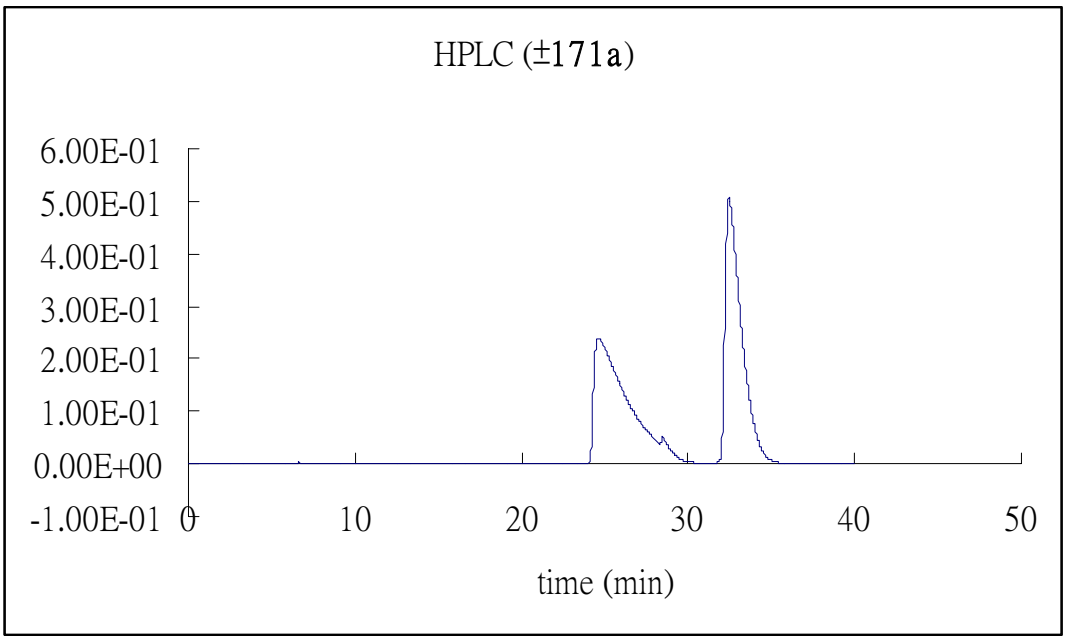
HPLC (±171a)
6.00E-01
5.00E-01
4.00E-01
3.00E-01
2.00E-01
1.00E-01
0.00E+00
-1.00E-01
0
10
20
30
40
50
time (min)

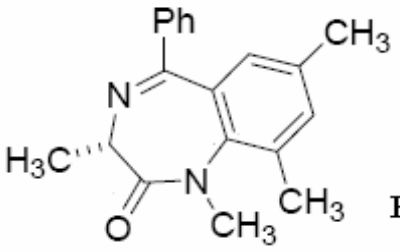

Racemic-172a

VA TECH

Project Name: Danny_Chiral
Reported by User: Danny

SAMPLE INFORMATION

Sample Name:	DH-I-80a	Acquired By:	Danny
Sample Type:	Unknown	Date Acquired:	11/29/04 7:17:42 AM
Vial:	1	Acq. Method:	1% Isopropanol
Injection #:	1	Date Processed:	11/29/04 8:06:22 AM
Injection Volume:	10.00 ul	Channel Name:	2487Channel 1
Run Time:	60.00 Minutes	Sample Set Name	

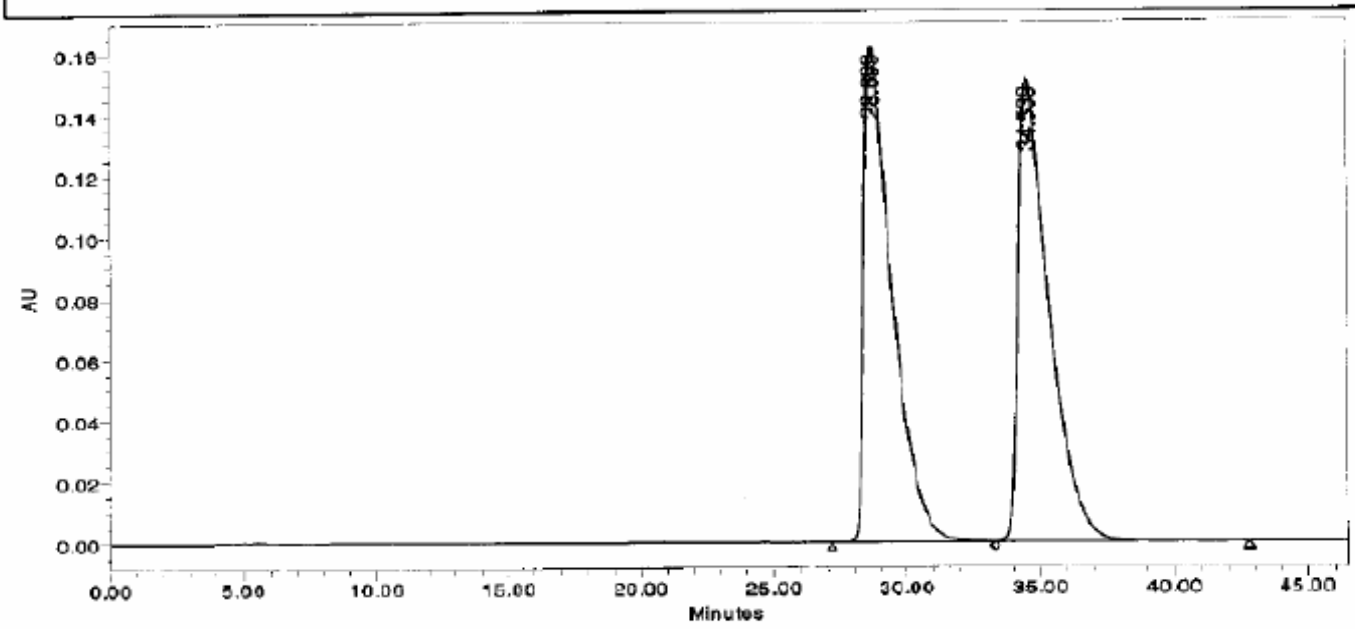

	RT (min)	Area (µV*sec)	% Area	Height (µV)	% Height
1	28.699	11888356	49.78	161908	51.73
2	34.539	11995430	50.22	151058	48.27

T = 27 °C

Report Method: Untitled | Printed 8:06:40 AM 11/29/04 | Page: 1 of 1

VA TECH

Project Name: Danny_Chiral

Reported by User: Danny

(S)-172a

Breeze

SAMPLE INFORMATION

Sample Name:	DH-I-71	Acquired By:	Danny
Sample Type:	Unknown	Date Acquired:	11/23/04 5:18:39 AM
Vial:	1	Acq. Method:	1% Isopropanol
Injection #:	1	Date Processed:	11/23/04 6:01:13 AM
Injection Volume:	10.00 ul	Channel Name:	2487Channel 1
Run Time:	60.00 Minutes	Sample Set Name	

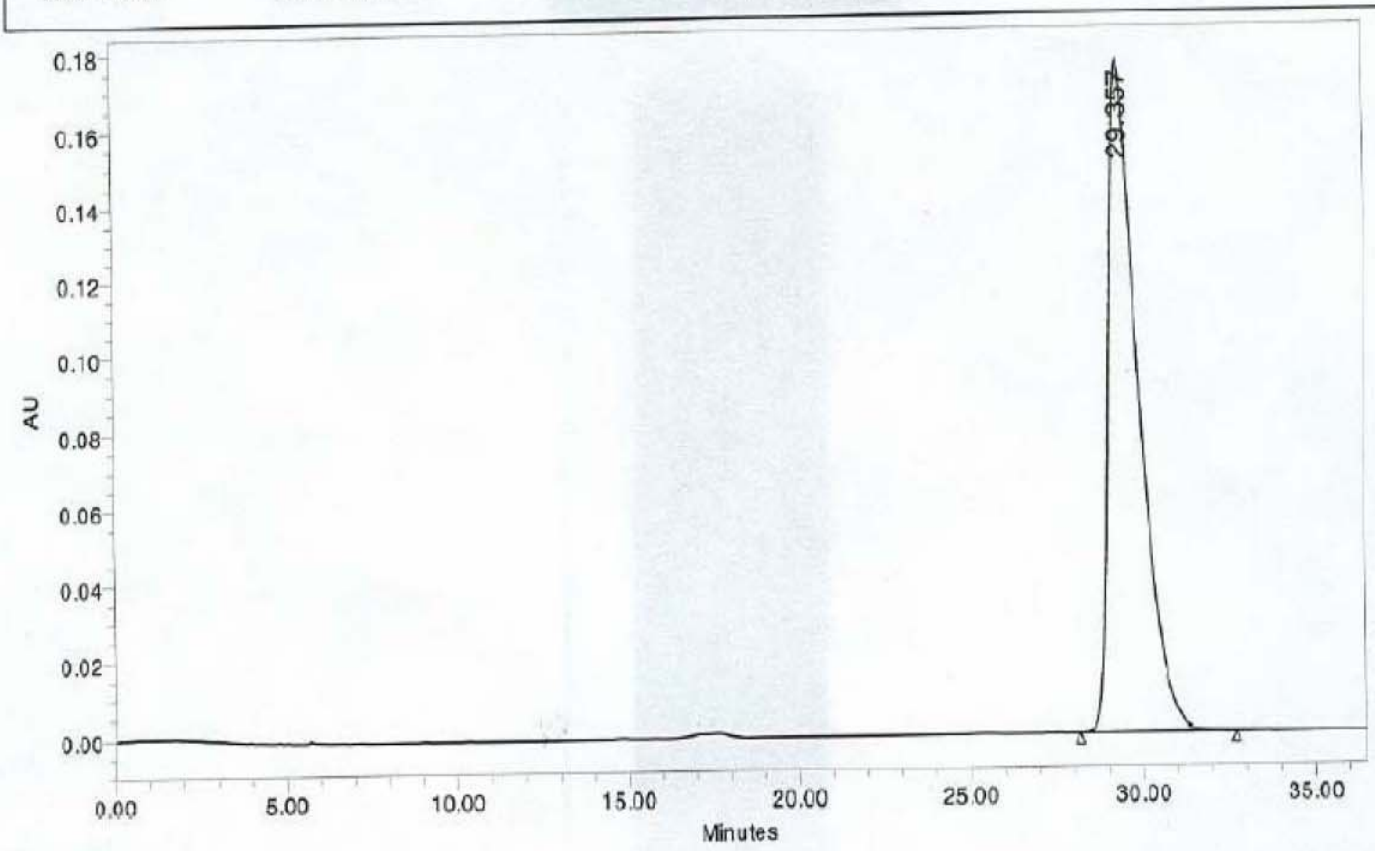

	RT (min)	Area (μV*sec)	% Area	Height (μV)	% Height
1	29.357	10611886	100.00	176677	100.00

T = 27 °C

VA TECH
Project Name: Danny_Chiral
Reported by User: Danny

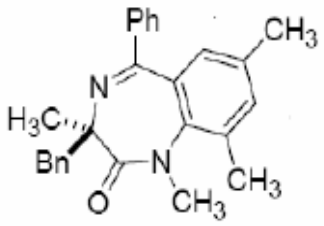

Racemic-177a

SAMPLE INFORMATION

Sample Name:	DH-I-85-OD-07211	Acquired By:	Danny
Sample Type:	Unknown	Date Acquired:	2/11/07 1:08:51 PM
Vial:	1	Acq. Method:	1%@70
Injection #:	1	Date Processed:	2/11/07 2:15:32 PM
Injection Volume:	10.00 ul	Channel Name:	2487Channel 1
Run Time:	60.00 Minutes	Sample Set Nam	85

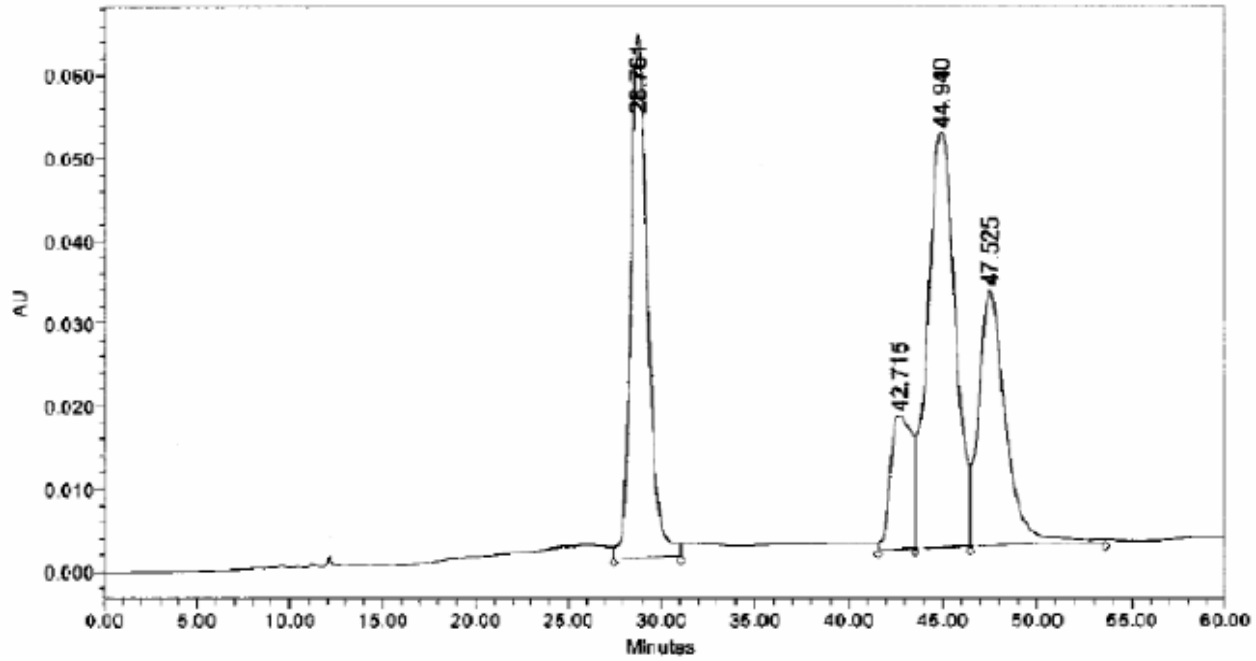

	RT (min)	Area (µV*sec)	% Area	Height (µV)	% Height
1	28.761	3940745	29.37	63242	39.46
2	42.715	1272800	9.48	15993	9.98
3	44.940	5150447	38.38	50193	31.32
4	47.525	3055505	22.77	30837	19.24

T = 27 °C

Peaks at 43 and 45 min correspond to the conformational isomers of (*R*)-**3a**; peaks at 29 and 48 min correspond to the conformational isomers of (*S*)-**3a** (see the chromatogram of (*R*)-**3a** for comparison).

VA TECH

Project Name: Danny_Chiral
Reported by User: Danny

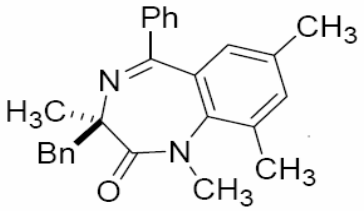

(R)-177a

SAMPLE INFORMATION

Sample Name:	DH-II-130NR-OD-07211	Acquired By:	Danny
Sample Type:	Unknown	Date Acquired:	2/11/07 9:53:45 AM
Vial:	1	Acq. Method:	1%@70
Injection #:	1	Date Processed:	2/11/07 11:30:43 AM
Injection Volume:	10.00 ul	Channel Name:	2487Channel 1
Run Time:	60.00 Minutes	Sample Set Nam	130

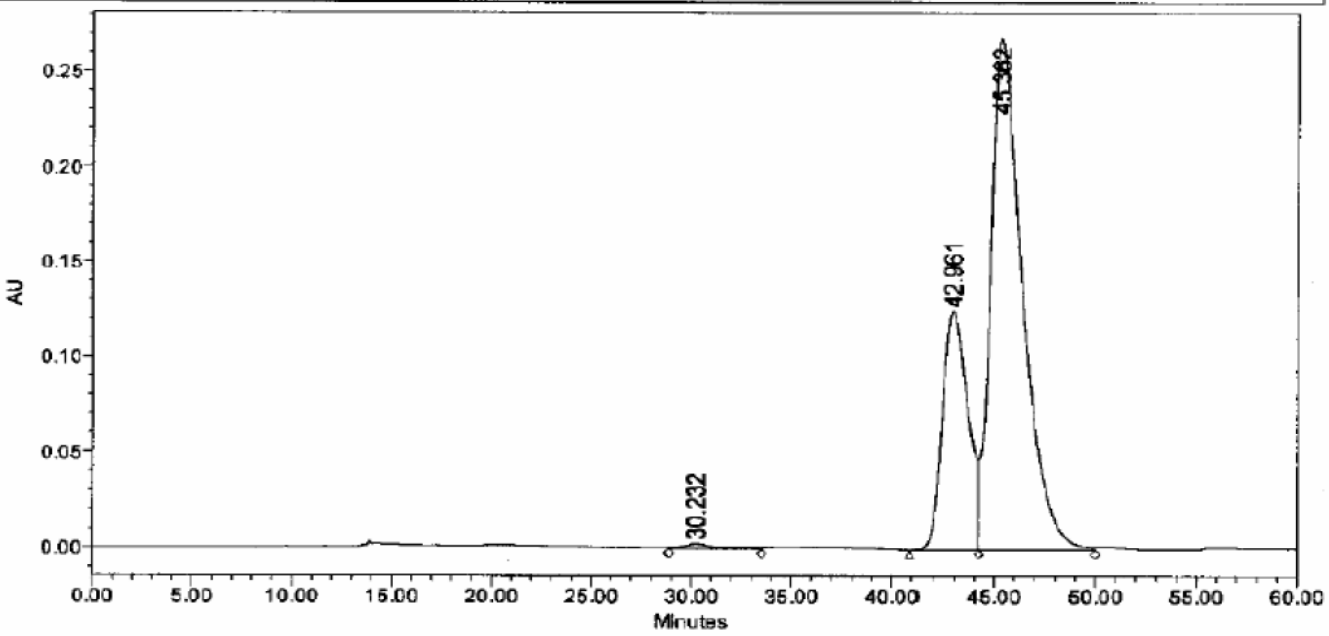

	RT (min)	Area (µV*sec)	% Area	Height (µV)	% Height
1	30.232	377915	0.92	2791	0.70
2	42.961	10994465	26.84	125536	31.58
3	45.362	29593840	72.24	269132	67.71

T = 27 °C

Report Method: Untitled | Printed 11:30:54 A 2/11/07 | Page: 1 of 1

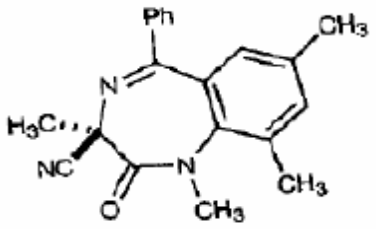

Racemic-178a

VA TECH
Project Name: Danny_Chiral
Reported by User: Danny

SAMPLE INFORMATION

Sample Name:	DH-I-81R-OD-07315	Acquired By:	Danny
Sample Type:	Unknown	Date Acquired:	3/15/07 2:53:47 AM
Vial:	1	Acq. Method:	1% Isopropanol
Injection #:	1	Date Processed:	3/15/07 3:36:23 AM
Injection Volume:	10.00 ul	Channel Name:	2487Channel 1
Run Time:	25.00 Minutes	Sample Set Nam	81

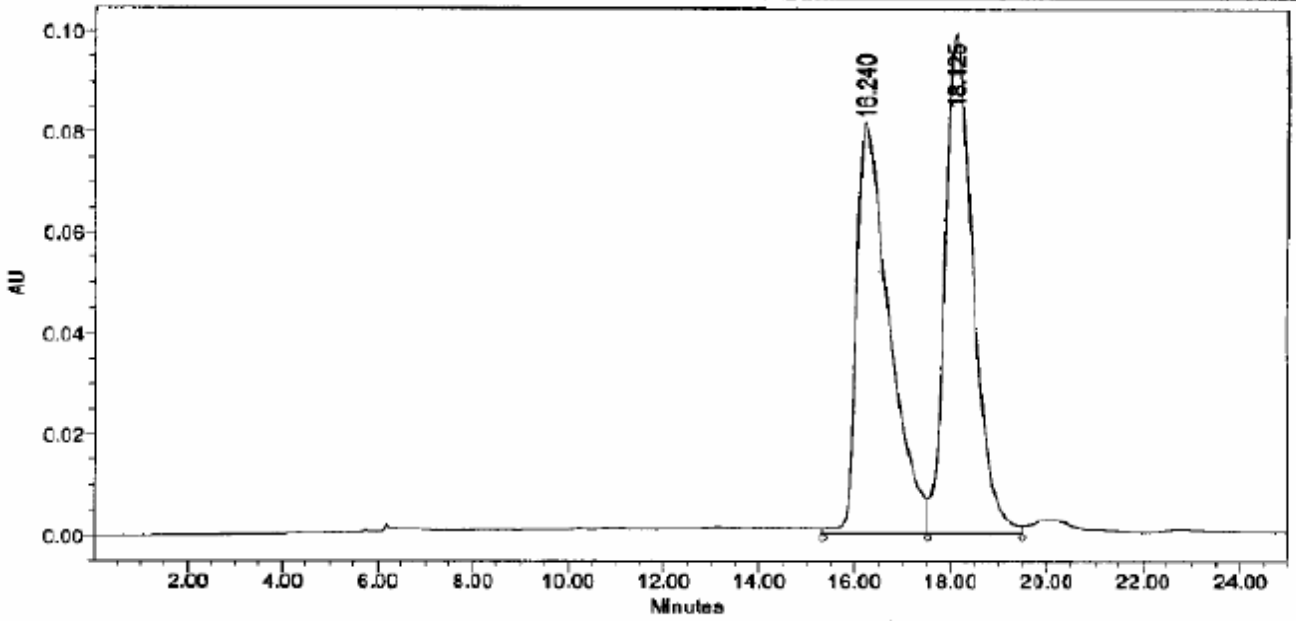

	RT (min)	Area (µV*sec)	% Area	Height (µV)	% Height
1	16.240	3861023	49.11	81487	45.12
2	18.125	4001260	50.89	99105	54.88

T =27 °C

Only one conformer exists

VA TECH

Project Name: Danny_Chiral

Reported by User: Danny

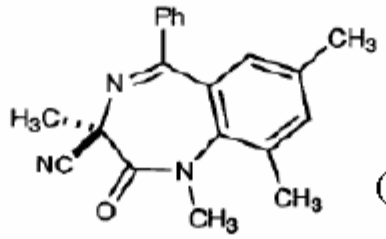

(R)-178a

Breeze

SAMPLE INFORMATION

Sample Name:	DH-I-72a	Acquired By:	Danny
Sample Type:	Unknown	Date Acquired:	12/8/04 4:27:15 AM
Vial:	1	Acq. Method:	1% Isopropanol
Injection #:	1	Date Processed:	12/8/04 4:56:39 AM
Injection Volume:	10.00 ul	Channel Name:	2487Channel 1
Run Time:	30.00 Minutes	Sample Set Name	

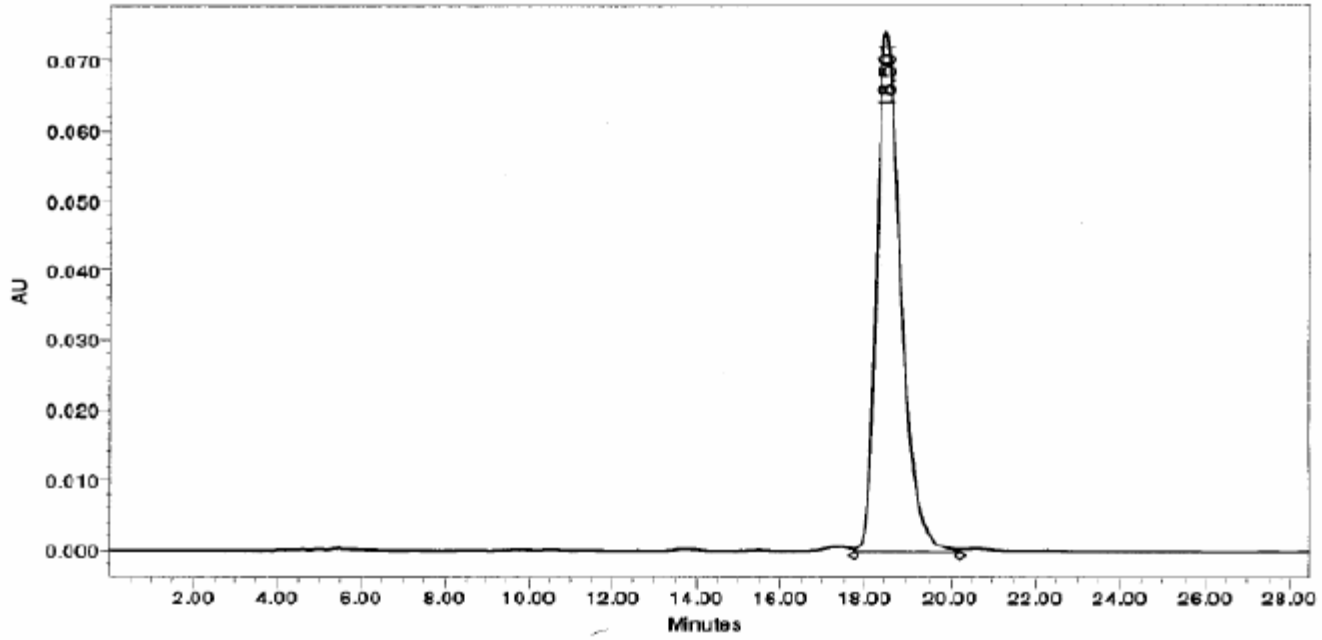

	RT (min)	Area (µV*sec)	% Area	Height (µV)	% Height
1	18.501	2949516	100.00	74155	100.00

T =27 °C

Only one conformer exists

VA TECH

Project Name: Danny_Chiral

Reported by User: Danny

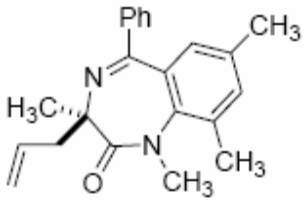

Racemic-179a

SAMPLE INFORMATION

Sample Name:	DH-I-83-AD	Acquired By:	Danny
Sample Type:	Unknown	Date Acquired:	1/26/05 12:54:35 AM
Vial:	1	Acq. Method:	1% Isopropanol
Injection #:	1	Date Processed:	1/26/05 1:32:01 AM
Injection Volume:	10.00 ul	Channel Name:	2487Channel 1
Run Time:	50.00 Minutes	Sample Set Name	

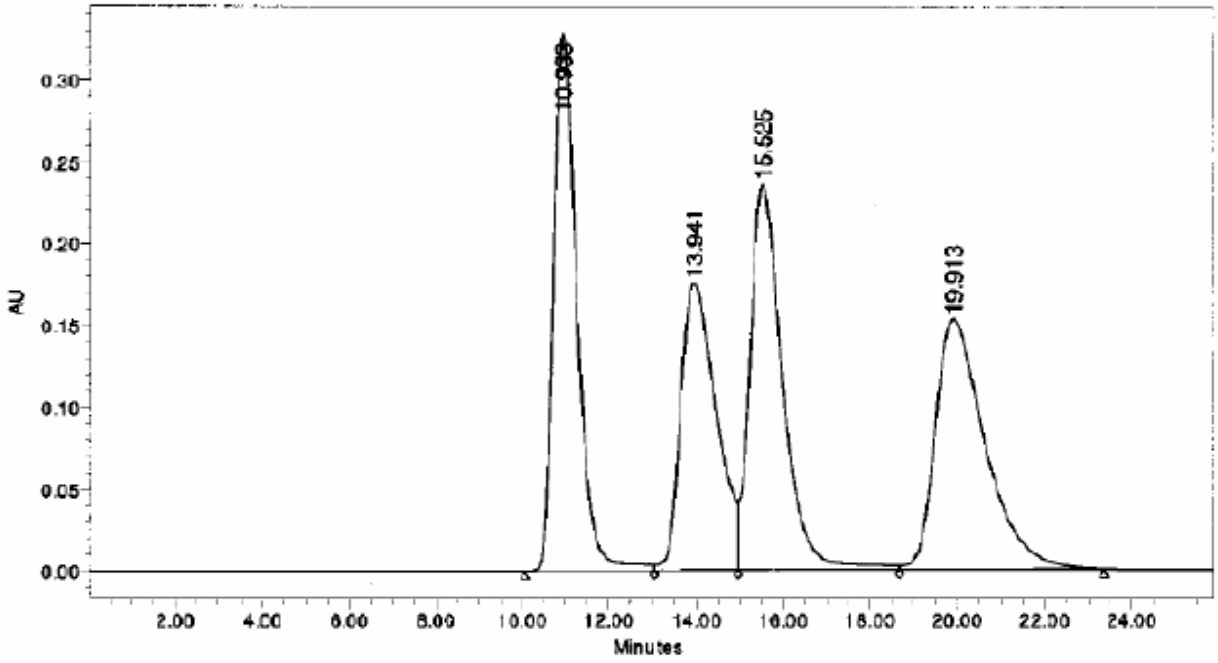

	RT (min)	Area (µV*sec)	% Area	Height (µV)	% Height
1	10.933	12424258	26.44	328355	36.76
2	13.941	10009099	21.30	175553	19.65
3	15.525	12407700	26.40	236464	26.47
4	19.913	12152320	25.86	152878	17.11

T = Ambient Temperature

Peaks at 11 and 16 min correspond to the conformational isomers of (*R*)-**4a**; peaks at 14 and 20 min correspond to the conformational isomers of (*S*)-**4a** (see the chromatogram of (*R*)-**4a** for comparison).

VA TECH
Project Name: Danny_Chiral
Reported by User: Danny

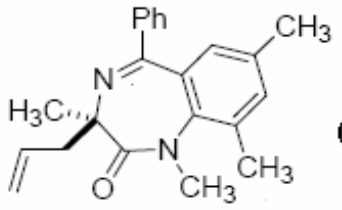

(R)-179a

SAMPLE INFORMATION

Sample Name:	DH-I-84-AD	Acquired By:	Danny
Sample Type:	Unknown	Date Acquired:	1/26/05 1:29:28 AM
Vial:	1	Acq. Method:	1% Isopropanol
Injection #:	1	Date Processed:	1/26/05 1:53:34 AM
Injection Volume:	10.00 ul	Channel Name:	2487Channel 1
Run Time:	50.00 Minutes	Sample Set Name	

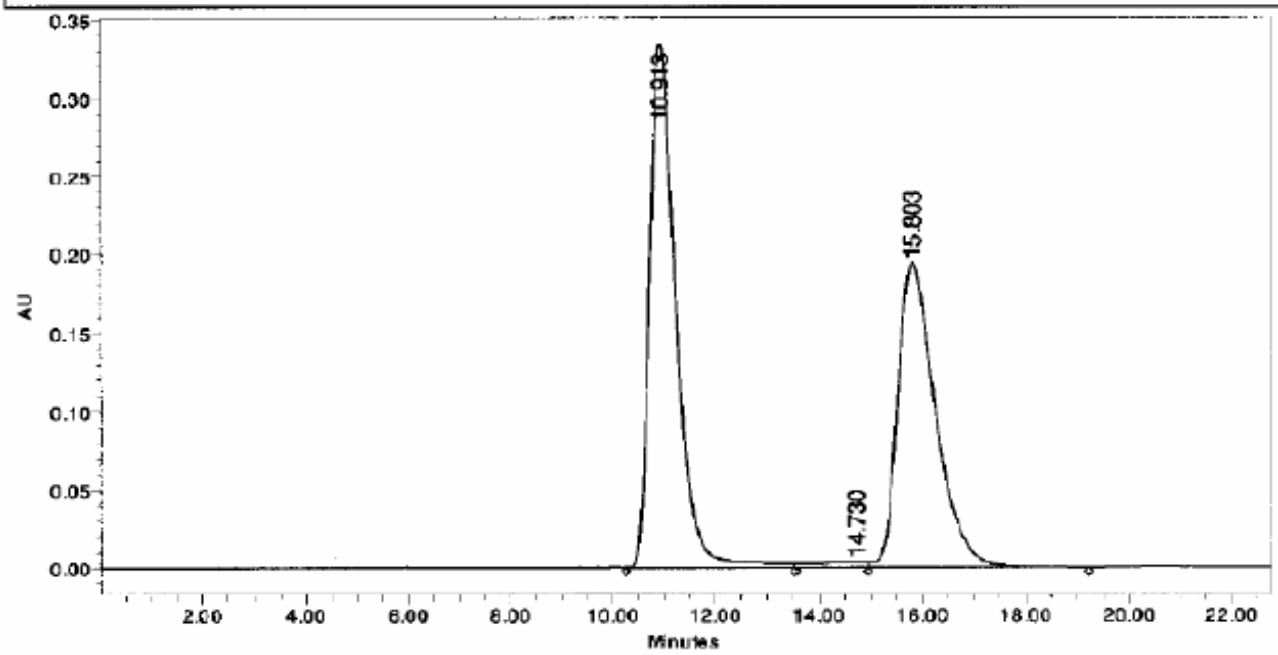

	RT (min)	Area (μV*sec)	% Area	Height (μV)	% Height
1	10.913	12084740	54.38	334382	62.82
2	14.730	274016	1.23	3619	0.68
3	15.803	9862242	44.38	194315	36.50

T = Ambient Temperature

Appendix

Data for kinetic studies in section 2.10.1

Plots of ln(([P]t-[P]e)/([P]0-[P]e)) vs time for **177a** at 50, 60, 70 °C.

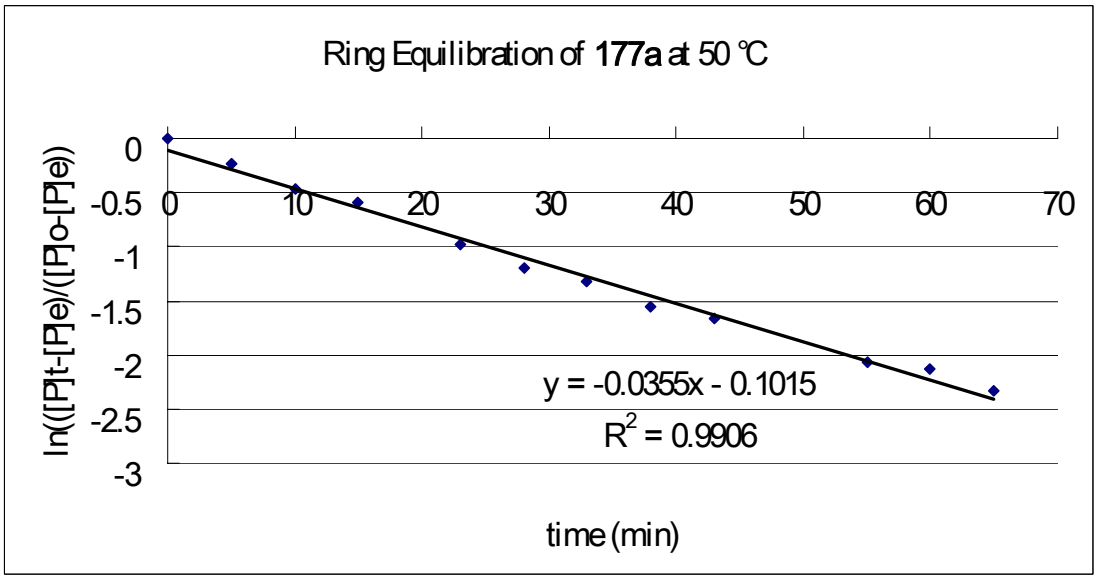

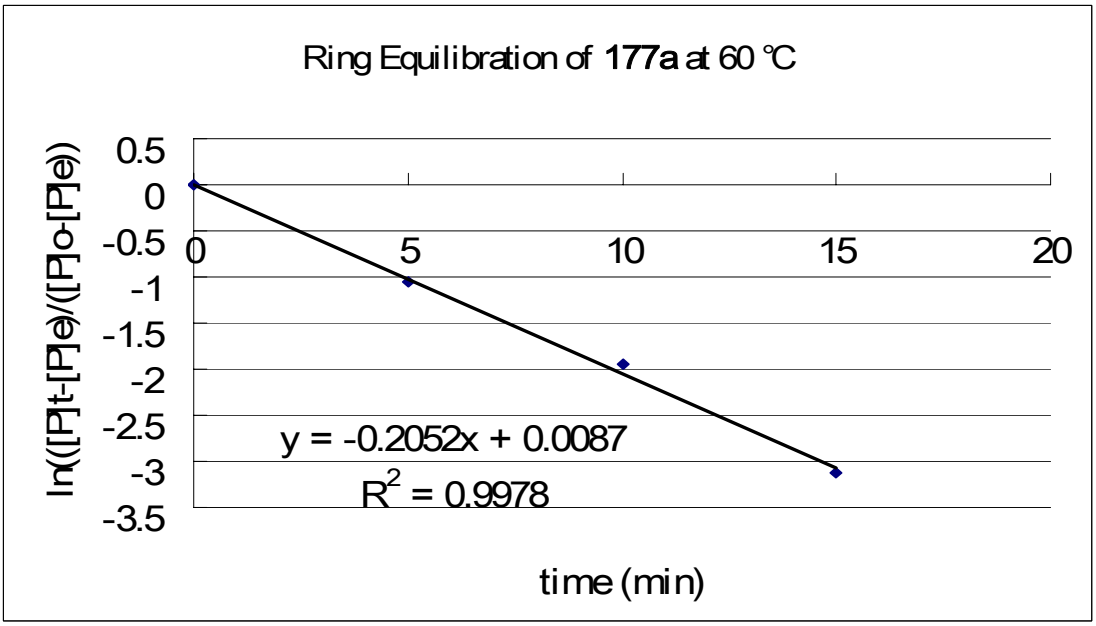

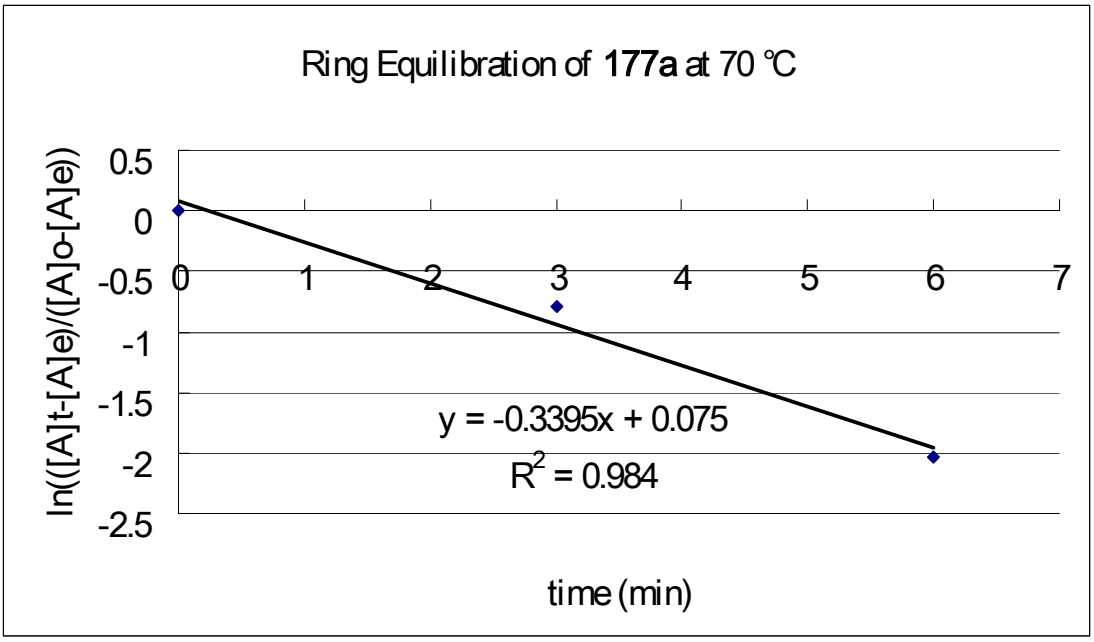

2D-EXSY obtained at 120 and 130 °C

2D-EXSY at 120°C

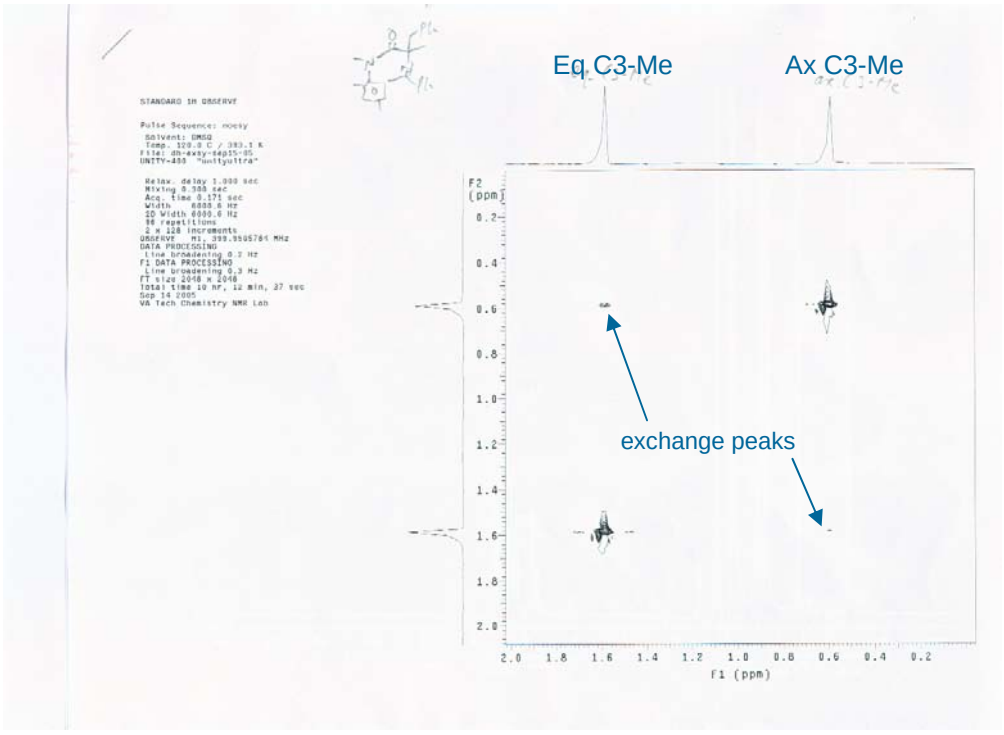

2D-EXSY at 130°C

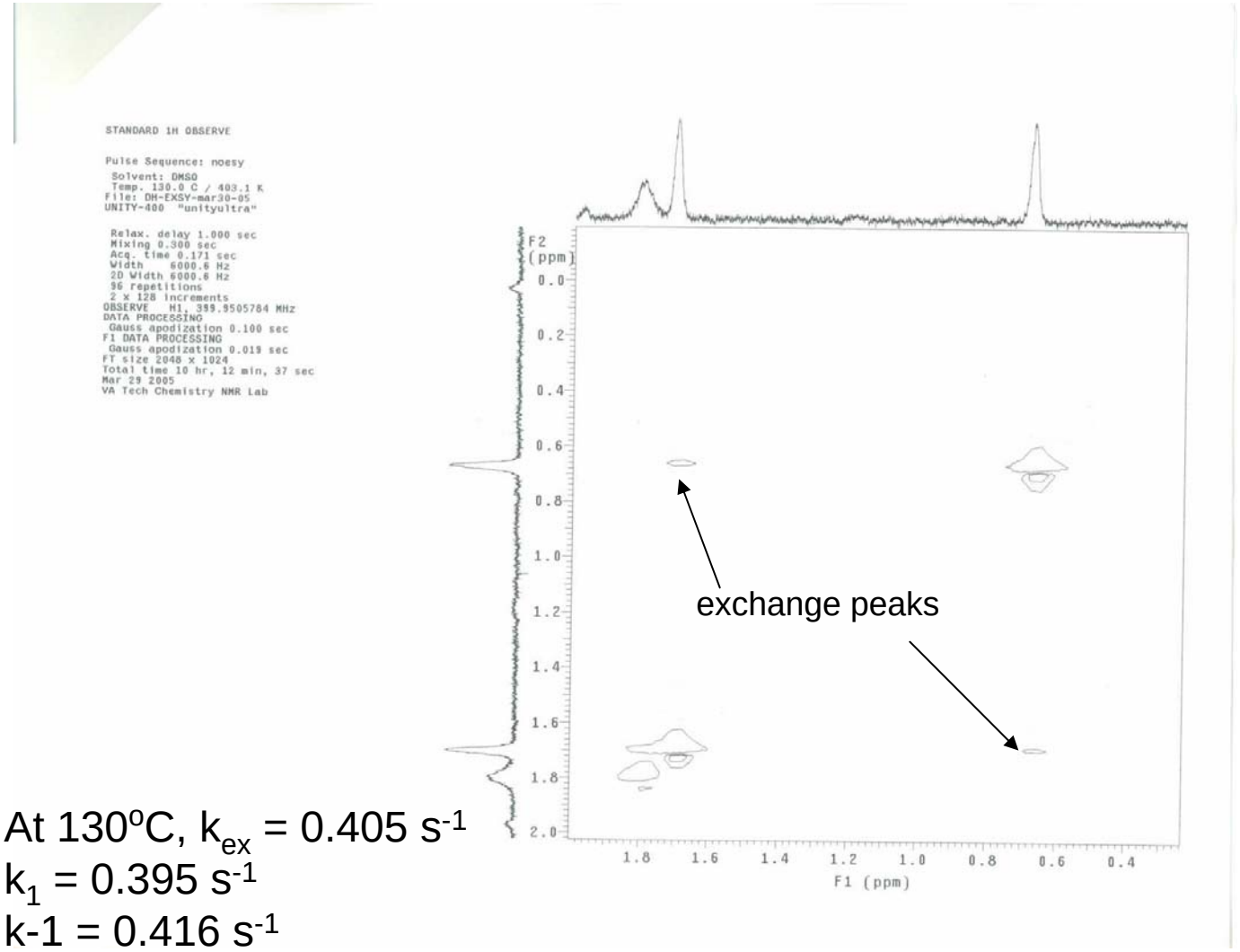

At 130°C, k_{ex} = 0.405 s^{-1}

k_1 = 0.395 s^{-1}

k-1 = 0.416 s^{-1}